Title

Removal of azo dyes in textile wastewater using microbial fuel cells and membrane technology

AUTOR

Raúl Bahamonde Soria

Supervisor:

Prof. Patricia Luis Alconero (UCLouvain)

Steering Committee:

Prof. Laurent Francis (UCLouvain)
Prof. Denis Dochain (UCLouvain)
Prof. Hervé Jeanmart (UCLouvain)
Prof. Korneel Rabaey (University of Ghent)
Prof. Anthony Szymczyk (University of Rennes)
Prof. Pablo Bonilla (Central University of Ecuador)

2022

Dedicated to my God, my Virgenita, my parents Olguita and Raúl and my sister Carmita.

Acknowledgment

Firstly, I would like to thank my supervisor Prof. Patricia Luis, who taught me that being humble makes an excellent researcher, and I would also like to thank her for every word of encouragement and help along this challenge.

I would like to thank the Universidad Central and the L'Académie de recherche et d'enseignement supérieur ARES Program for the financial and academic support throughout the doctorate, especially Dr. Rolando Saenz.

Many thanks to the members of my jury Prof. Anthony Szymczyk, Prof. Dennis Dochain, Prof. Hervé Jeanmart, Prof. Korneel Rabaey and Prof. Pablo Bonilla for their very thoughtful comments and observations, in turn, to Prof. Bart Van der Bruggen and his team for their quick and efficient help and support at the beginning of my studies in his laboratory and to Prof. Laurent Francis for his kind help in the experimental and electrochemical part.

A mi Hermosa Familia, a mi madre Olguita por todo el amor, ya que todo lo que soy lo debo a sus esfuerzos y largas horas de apoyo, sin su apoyo y su amor no podría llegar a donde he llegado, por sus hermosos, precisos y sabios consejos y por cultivar el carácter investigativo en mi, a mi padre Raúl porque no pude tener un mejor ejemplo de hombre recto y responsable, y finalmente, a mi hermana Carmita, que me ha enseñado que a pesar de todo siempre contaré con un amor y apoyo incondicional. Todos ustedes son mi razón de seguir adelante y mis logros son nuestros. A mi hermana Lili y a su bella familia por sus consejos y apoyo constante, además, por mostrarme que el amor bonito si existe. A mi Tía Marianita por cada consejo, cada regaño y cada muestra de cariño, porque contar con la misma sangre es un privilegio si la tengo como Tía.

To the best lab friends I could wish for; Mar for being my first and last best friend in Belgium, as well as for showing me once again that Mexican people are some of the best in the world and also to Julieta, to Cristhian, for his time and advice, for being a listening and non-

judgmental ear and for showing me that there is a world of people with beautiful values, to Vida for always taking care of me and showing your talent in helping every single member of the lab, to Xiao; for being so you! For showing me that the world is much more than a small thought and for letting me into your life, I know that we will always keep in touch, to Kamyll, for having opened your heart with me from the beginning and for letting me open mine with you, to Vercus, for confirming that happiness comes from a family love, to Yusak for showing me that living the passion for science makes you happy (keep going, you will be big), to Sara for having the best of two worlds, one that is the best version of me (sentimental and dreamy) and a part that I don't have, very strict, dedicated and scientific, because I always dreamed of having a daughter and seeing you grow up makes me feel part of your life, you will be very successful, to Farzane, for speaking and freeing me from the pressure of speaking in meetings and your time, to Fernando, for sharing with me his passion for the ideals of a great Latin America and for your humility. Finally, to Marie-Charlotte, for listening to me and helping me in one of the hardest moments of my life and for having the right touch to lift me up, thank you because from the first day we met, you showed me that the language barrier is not an impediment to connect with people so different but with a magnificent heart, for letting me share with you my dreams and wishes and for never having judged me, and I also thank you for opening your illusions and wishes with me, I will always wish the best for you, **enjoy and live!,** I enjoyed every moment together!.

Al Padre Ramón, por ser mi guía espiritual y demostrarme que Dios jamás me dejó solo, ¿como pude encontrar una guía de este calibre tan lejos de casa y en el momento exacto de mi vida?, solo me queda agradecer a Dios por la providencia, y a usted por su paciencia y tan sabios consejos que ahora veo que siempre vinieron de la sabiduría celestial.

A mis amigas Karlita por las interminables horas de pláticas y por tu tiempo y ser una amiga tan especial, por cuidar de mi y por tu cariño y también por el cariño de Melanita. A Irma, porque la vida nos llevó a trabajar juntos en Ecuador y después a que tu seas uno de los soportes mas grandes que tuve en Bélgica, gracias por apoyarme, escucharme y estar siempre pendiente de mi, eres mi familia ya no solo mi amiga, a Paolita y su hermosa familia, por enseñarme que puedo contar con alguien tan especial, por las largas horas de consejos y

escucha, jamás pensé que contaría con su ayuda tan lejos de casa, que Dios la bendiga siempre y sepa que siempre cuenta con mi amistad. A Marce, Paty y Jacky por su tiempo y ayuda. A mis grandes amigos Daniel A. y su familia por su incondicional amistad, gracias por que ha demostrado que mis logros también son suyos, a Billy por ser uno de los mejores amigos que tengo y a pesar de haber sido mi alumno creo que pude encontrar un amigo de verdad, gracias por tu apoyo experimental y por tu amistad.

I would like to express my sincere thanks to the 'IMAPiens': secretaries, technicians, researchers and academics. Thank you all for your great help, fun times and for making the atmosphere at the institute one of the best.

To Belgium and its people, for being the most difficult experience of my life, however, the most beautiful and for waking up in me the Raul I always dreamed to be.

In a very special way, to you, for having found me in the most difficult moment of my life, for helping me and for making real all the wishes I had since I was a child, for giving me more than what I always imagined, because now I see that having you in my life is the most beautiful thing and I only needed to desire it, To you who made me finally understand (1 John 4:8), Only who loved has known God!!!. To you my God for loving me, now I have everything, because "in the nothing I found the all" and if that wasn't enough, you gave me your mother, To you my ark of the covenant, what more can I want, I will never feel alone again.

Abstract

The use of microbial fuel cells (MFCs) as a bioelectrochemical system (BES) for the treatment of textile wastewater has attracted attention due to the ability to produce bioelectricity from wastewater treatment. However, textile wastewater is far from being an ideal electrolyte for an electrochemical process. It can generate biofouling on electrodes and separators (membranes), affecting greatly the efficiency in such systems. In recent years, different types of membranes have been explored as separators in MFCs, although to our knowledge no nanofiltration membranes have ever been used in such systems. Nanofiltration membranes share advantages with porous and non-porous membranes. In addition, the wide variety of nanofiltration membranes, high oxygen retention and lower electrical resistance compared to ion selective membranes normally used in BES, made these types of membranes potential separators.

In this work, an integrated process is proposed, including three technologies, *i.e.,* membrane technology, an advanced oxidation process and microbial fuel cells. Antifouling and self-cleaning membranes are developed as efficient separators for a new generation of osmotic systems (nanofiltration microbial fuel cells) in textile wastewater treatment.

A new method of modification of bio-inspired membranes with commercial catalysts (TiO_2 and ZnO) showed that the modified membranes acquired antibacterial, self-cleaning and antifouling properties, improved when the catalysts were combined. The application of this method on low-cost membranes exhibited a significant improvement in COD and color removal, as well as an improvement in bioelectricity production in the MFCs. In order to further improve the activation efficiency of the photocatalysts under visible light and the antifouling properties of the membranes, a new catalyst (ZnO Er/Al) was synthesized, which demonstrated high photocatalytic and antibacterial activity. The new membranes also demonstrated efficient resistance to oxygen crossover and maintained constant osmotic water fluxes during long test periods. These results combined with the wide variety of available nanofiltration membranes open up an interesting line of future research in the development of efficient separators for microbial fuel cells and other BES.

List of publications

Published chapter book 01/02/2022. **Raúl Bahamonde Soria**, Luis Patricia. Chapter 9. Current Trends and Future Developments on (Bio-) Membranes: Membrane technologies in Environmental Protection and Public Health, Elsevier, Chapter 9, Antifouling membranes for polluted solvents treatments,

Raúl Bahamonde Soria, Junyong Zhu, IrmaGonza, BartVan der Bruggen and Patricia Luis. Effect of (TiO_2: ZnO) ratio on the anti-fouling properties of bio-inspired nanofiltration membranes. *Separation and Purification Technology,* 251, (2020), 117280

Raúl Bahamonde Soria, Billy Daniel Chinchin, Daniel Arboleda, Yan Zhao, Pablo Bonilla Bart Van der Bruggen and Patricia Luis. Effect of the bio-inspired modification of low-cost membranes with TiO_2:ZnO as microbial fuel cell membranes, *Chemosphere,* 291, (2022), 132840.

Submitted research paper

Research paper in preparation: **Raúl Bahamonde Soria,** Jefferson Estupiñan, Irma Gonza, Monserrat Naranjo, Billy Chinchina, L, Patricia Luis. Research paper submitted on 03/11/2021 to Industrial & Engineering Chemistry Research Journal. Effect of Er, Al and Er/Al dopants on the photocatalytic and antibacterial properties of ZnO nanoparticles.

Research paper in preparation: **Raul. Bahamonde Soria** and Patricia Luis. Influence of Er-Al-ZnO photocatalyst in the antifouling performance of new nanofiltration Microbial fuel cells.

List of variables

h_c	Cake height (nm)
J	Permeate flux (kg $m^{-2}\cdot h^{-1}$)
J_o	Initial flux (kg $m^{-2}\cdot h^{-1}$)
J_t	Flux at a specific time (kg $m^{-2}\cdot h^{-1}$)
R_t	Total membrane resistance (m^{-1})
η	Viscosity (Pa·s)
ΔP	Transmembrane pressure (Pas, P
R	Membrane surface resistance R ($\Omega.cm^2$)
PD.	Power density ($mW\cdot m^{-2}$)
CE	Coulombic efficiency (%CE)
COD	Chemical oxygen demand ($g.L^{-1}$)
V	Power generation (Voltage) mV
CD	Current density ($mA.m^{-2}$)
CR	Color removal (%)

List of acronyms

BES	Bioelectrochemical systems
MFC	Microbial fuel cell
MEC	Microbial electrolysis cell
NF-MFC	Nanofiltration microbial fuel cell
Os-MFC	Osmotic microbial fuel cell
PDA	Polydopamine
NPs	Nanoparticles
AD	Fouling adsorption,
AFM	Atomic Force Microscopy
TiO_2	Titanium dioxide
ZnO	Zinc oxide
Er	Erbium
Al	Aluminium
CBN	Carbon-based nanomaterials
CMPs	Conjugated microporous polymers
CNT	Carbon nanotubes
COFs	Covalent organic frameworks
COs	Covalent organic structures
CPM	Cationic polymeric materials
CVD	Chemical vapor deposition

EDX	Energy-dispersive X-ray
FD	Fouling deposition
FO	Forward osmosis
FT-IR	Fourier transform infrared spectroscopy
GO	Graphene oxide
MOFs	Metal-organic frameworks
MOPs	Microporous organic polymers
MPD	M-phenylenediamine
NF	Nanofiltration
UF	Ultrafiltration
MF	Microfiltration
FO	forward osmosis
NIPS	Non-solvent induced phase separation
NOM	Natural organic matter
OSN	Organic solvent nanofiltration
OSRO	Organic solvent reverse osmosis
OSU	Organic solvent ultrafiltration
PA	Polyaniline
PAA	Polyacrylic acid
PI	Polyimide
PIMs	Polymers of intrinsic microporosity
POC	Porous organic cages
PP	Polypropylene
PS-b-PAA	Polystyrene-block polyacrylic acid
PSBMA	Polysulfobetaine methacrylate
PTFE	Polytetrafluorethylene
PV	Pervaporation
PVA	Polyvinyl alcohol
PVDF	Polyvinylidene fluoride
PVP	Polyvinyl pyrrolidone
RO	Reverse osmosis
ROS	Reactive oxygen species
SC	Segmented copolymers
SEM	Scanning electron microscopy
TEM	Transmission electron microscopy
TFC	Thin-film composite
XPS	X-ray photoelectron spectroscopy
XRD	X-Ray Diffraction

Table of contents

Abstract *1*
List of publications ..... *i*
List of variables ..... *i*
List of acronyms ..... *i*
Table of contents ..... *i*
Chapter 1. Introduction and context *2*
1.1 Textile wastewater **2**
1.2 Treatment methods of textile wastewater **3**
1.3 Chemical processes **4**
1.3.1 Advanced oxidation processes 4
1.4 Physical methods **5**
1.4.1 Membrane Technology 6
1.4.2 Membrane fouling 8
1.4.3 Fouling classification 10
1.4.4 Fouling mechanisms and interpretation 11
1.5 Anti-fouling strategies and membranes **13**
1.5.1 Membrane design and manufacturing methods. 14
1.5.2 Surface modification of membrane **16**
1.5.3 Advanced antifouling strategies 16
1.6 Bioadhesion (bioinspired adhesion chemistry) **19**
1.6.1 Polydopamine (PDA) 20
1.6.2 Adhesion of functional materials. 21
1.6.3 PDA functionalization reaction 22
1.7 Biological treatment **24**
1.7.1 Bioelectrochemical systems 25
1.7.2 Microbial electrolysis cell (MEC) 25
1.7.3 Microbial Electrosynthesis cell system (MES) 27
1.7.4 Microbial desalination cells (MDC). 28
1.7.5 Microbial fuel cells 29
1.7.6 MFC Limitations 33
1.7.7 Membranes used as MFC separators 34
1.7.8 Osmotic microbial fuel cells (OsMFCs) 38
1.7.9 Nanofiltration- microbial fuel cells (NF-MFCs). 39
1.7.10 Membrane fouling in MFC systems 39
1.8 Thesis motivation **41**

1.9 Thesis objective **42**

1.10 Thesis outline **43**

Chapter 2. Effect of (TiO_2: ZnO) ratio on the anti-fouling properties of bio-inspired nanofiltration membranes ***45***

Abstract ***46***

2.1. Introduction **46**

2.2. Experimental **51**

2.2.1 Materials 51

2.2.2 Modification of the NFX nanofiltration membrane 51

2.2.3. Membrane characterization 54

2.2.4. Antibacterial capacity of modified membranes 55

2.2.5. Photocatalytic performance of membranes for dye degradation under light conditions. 56

2.3. Results and discussion **57**

2.3.1. Polymerization time 57

2.3.2. Morphology of membrane surface 58

2.3.3. Membrane hydrophilicity 63

2.3.4. Water permeability 65

2.3.5. Separation properties of NF membranes 67

2.3.6. Anti-bacterial activity of modified membranes 68

2.3.7. Effect of solar light irradiation on membrane surface in degradation of methylene blue. 74

2.4. Conclusions **77**

Chapter 3. TiO_2:ZnO-modified low-cost membranes with mussel-inspired polydopamine binding as microbial fuel cell membranes. ***78***

3.1 Introduction **80**

3.2 Materials and Methods **83**

3.2.1 Materials 83

3.2.2 Modification of the low-cost membranes 84

3.2.3 SEM and AFM membrane characterization 84

3.2.4 Membrane surface electrical resistance 85

3.2.5 Microbial fuel cell setup 86

3.2.6 Bacteria growth, Anodic immobilization and anolyte solution 87

3.2.7 Measurement and analysis of MFC performance 88

3.2.8 Photocatalysis condition and color removal evaluation 88

3.2.9 Verification of the self-cleaning character of the membranes 89

3.3 Results and Discussion **89**

3.3.1 SEM, AFM Characterization and evaluation of membrane fouling 89

3.3.2 Morphology by AFM 92

3.3.3 Verification of the self-cleaning character of the membrane 94

3.3.4 Membrane surface area resistance 96

3.4 MFC performance **97**
3.4.1 Voltage generation 97
3.4.2 Power density 99
3.4.3 Durability of MFC 101
3.4.4 Color, COD removal and coulombic efficiency 102

3.5 Conclusions **107**

Chapter 4. Effect of Er, Al and Er/Al dopants on the photocatalytic and antibacterial properties of ZnO nanoparticles ***108***

4.1 Introduction **110**

4.2 Materials and methods **113**
4.2.1. Materials 113
4.2.2. Synthesis of catalysts 113
4.2.3. Characterization of catalyst 114
4.2.4. Photocatalytic activity 114
4.2.5. Antibacterial activity 115

4.3 Results and discussion **117**
4.3.1. Morphology of composites 117
4.3.2. XRD analysis 119
4.3.3. Optical properties 121
4.3.4. Catalyst dosage on methyl orange (MO) Degradation 121
4.3.5. Photocatalytic performance of synthesized nanoparticles 122
4.3.6. Determination of the antibacterial activity of ZnO doped and un-doped samples 125

4.4 Conclusions **127**

Chapter 5. Influence of Er-Al-ZnO photocatalyst in the antifouling performance of new nanofiltration Microbial fuel cells ***128***

5.1 Introduction **130**

5.2 Materials and method **133**
5.2.1 Materials 133
5.2.2 Synthesis of photocatalyst and membrane modification 133
5.2.3 SEM membrane characterization 134
5.2.4 Membrane surface electrical resistance and antifouling properties 134
5.2.5 Experiment setup of NF-MFC and operation 135
5.2.6 Inoculation 137
5.2.7 Measurement and analysis 137
5.2.8 Salt rejection under dark conditions 139

5.3 Results and Discussions **141**
5.3.1 MFC performances 141
5.3.2 Influence of membrane modification on water flux 144
5.3.3 Change in electrical resistance by fouling of the NF membrane 146
5.3.4 Membrane fouling in NF-MFC 148
5.3.5 Performance of membranes under light conditions and pressure 150

5.3.6 Filtration performance under Dark Conditions 151
5.4. Conclusions 153
Chapter 6. 154
General conclusions and Future work 154
6.1 Main conclusions of the thesis 155
6.2 Recommendations for future research 158
6.2.1 Surface chemistry in the formation of antifouling membranes. 158
6.2.2 Topography in surface modification and biofilm formation 159
6.2.3 Expansion of photocatalysts in membranes 159
6.2.4 Nanofiltration membranes as separator in BES 160
6.3 Perspectives 160
6.3.1 Surface modification for biofilm control 160
6.3.2 Surface modifications for other applications 161
6.3.3 Scale-up of NF-MFCs in the treatment of textile wastewater. 161
6.3.4 New approach based on BES for organic wastewater treatment 162
7. Appendices 164
Appendix 1. chapter 2 164
Appendix 2. chapter 3 172
Appendix 3. chapter 4 174
8. References 176

Chapter 1. Introduction and context

This chapter is based on the **book chapter "*Antifouling membranes for polluted solvents treatments*"** in: *Current Trends and Future Developments on (Bio-) Membranes: Membrane technologies*", published in Environmental Protection and Public Health, (2021) Elsevier, Chapter 9, and Antifouling membranes for polluted solvents treatments. Authors: **Raúl Bahamonde Soria** and Patricia Luis; and, the **published research paper "*Aramid nanofiber and modified ZIF-8 constructed porous nanocomposite membrane for organic solvent nanofiltration"*** by Yi Li, Jian Li, **Raul Bahamonde Soria,** Alexander Volodine, Bart Van der Bruggen. *Journal of Membrane Science.* 603 (2020) 118002

1.1 Textile wastewater

The textile industry produces a large amount of waste effluents due to its various wet processing operations. The primary pollutants in this wastewater are chemicals such as acids, alkalis, dyes, hydrogen peroxide, starch, surfactant dispersing agents, and metallic soaps (Holkar *et al*, 2016). The normal composition of textile wastewater is shown in Table 1.1. Among those compounds, azo dyes are considered hazardous to the ecosystem, due to their low degradability and high toxicity because of the azo group contained in their structure, which cause problems to aquatic life (Fatima *et al*, 2017; Holkar et al, 2016; Zhu et al, 2012).

Table 1.1 Common parameters of textile wastewaters.

Parameter	Value
pH	7-10
Cond /(μS/cm)	1380
TOC (mg/L)	620
Total Suspended Solids (mg/L)	160
COD (mg/L)	1650
BOD5 (mg/L)	460
Color (Hazen unids)	2900
Total phosphorus (mg/L)	1.5
Total nitrogen (mg/L)	3
Chlorides (mg/L)	1300

Dyes: synthetic dyes have a diversity of structures (Figure1.1). However, the vast majority of synthetic dyes currently used in industry are azo derivatives (Forgacs et al, 2004). Azo compounds such as Congo red (CR), methyl orange (MO) and indigo carmine (IC) have a chromophore groups (-N=N-) in their molecular structure (Zhu et al, 2012). Therefore, their discharge into surface waters can cause obstruction of light passage and oxygen transfer in the water, directly affecting aquatic life. In addition, these compounds are considered mutagenic and carcinogenic (Chen et al, 2017; Solanki *et al*, 2013a).

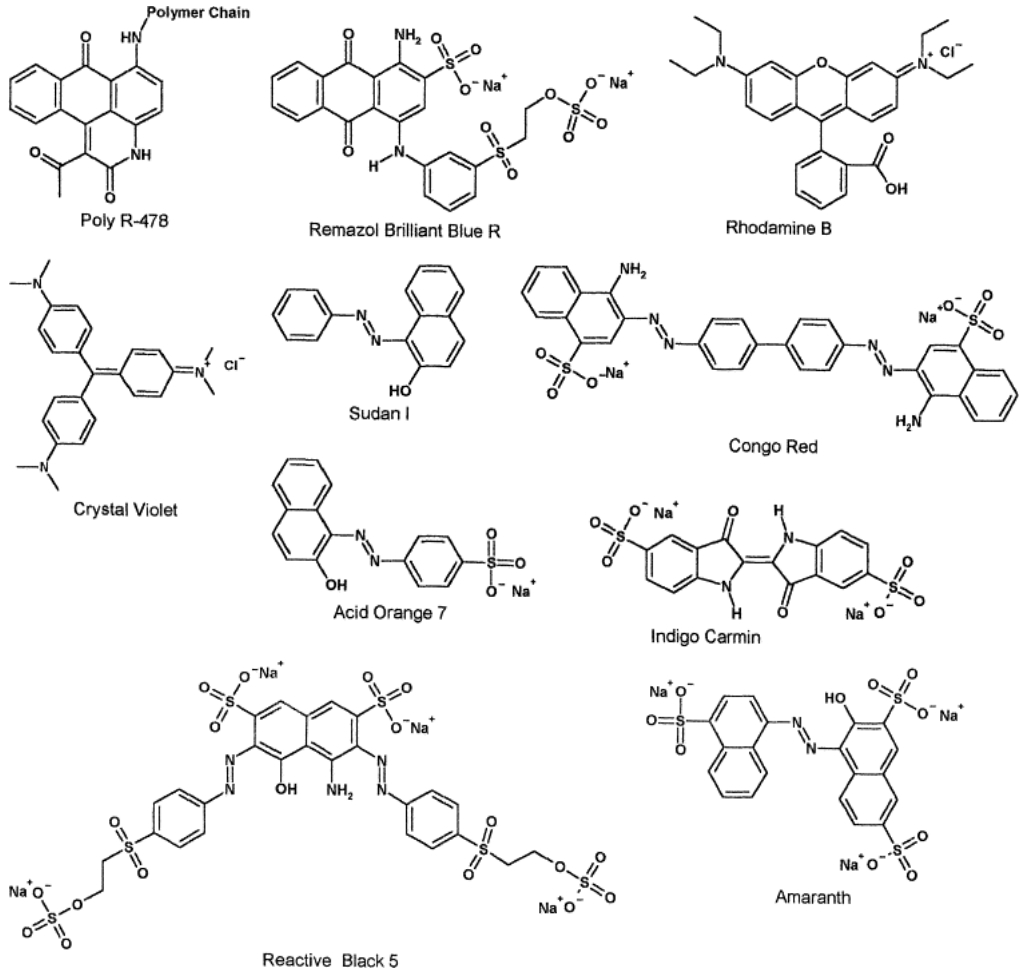


Figure 1.1 Different chemicals structure of synthetic dyes most frequently used in degradation experiments (Forgacs et al, 2004).

1.2 Treatment methods of textile wastewater

There are several treatment methods currently used to reduce the pollution caused by textile wastewater, such as: physical, chemicals, biological and hybrids methods (Table 1.2) (Holkar et al, 2016; Slokar and Majcen Le Marechal, 1998).

Table 1.2 Some dyes wastewater treatment methods.

Physical method	Oxidation method	Biological method	Hybrid method
- Filtration - Membrane technology - Flocculation - Adsorption	- Advanced oxidation (AOP) - Chemical Oxidation (COP)	- Enzymes - Microorganism	- Physicochemical - AOP/Biological - Membrane technology/AOP others

In order to better understand the methods, below they have been classified as chemical, physical and biological processes.

1.3 Chemical processes

Chemical treatments involve the use of chemicals that lead to a chemical transformation of the components in the wastewater. Examples are chemical oxidation processes, advanced oxidation processes, Fenton-related processes, neutralization and others (Xie et al, 2018).

1.3.1 Advanced oxidation processes

Advanced oxidation processes (AOPs) are those in which hydroxyl radicals (OH•) are generated. Hydroxyl radicals react with most dyes with high-rate reaction constants, which are responsible for the oxidation of organic matter. AOPs can be driven by ultrasonic irradiation (acoustic cavitation), hydrodynamic cavitation, Fenton chemistry (reaction between Fe^{3+} ions and H_2O_2) or by the use of (sun) light to produce photolysis of H_2O_2 or with the use of various semiconductor catalysts (TiO_2, ZnO, etc.) (photocatalytic oxidation) (Holkar et al, 2016; Long et al, 2017). The photocatalytic oxidation process involves many steps as shown in Scheme 1 for ZnO: (1) photoexcitation of catalyst's surface by UV or

visible light irradiation; (2)-(3) generation of electron hole-pair that produces hydroxyl radical; and (4) oxidation of organic pollutants, which produces CO_2 and H_2O as final products if the oxidation is complete (Laohaprapanon et al, 2015).

1. $ZnO + h\nu\ (UV) \rightarrow ZnO\ (e_{CB}^- + h_{VB}^+)$
2. $ZnO(h_{VB}^+) + H_2O \rightarrow ZnO + H^+ + \bullet OH$
3. $ZnO(h_{VB}^+) + OH^- \rightarrow ZnO + \bullet OH$
4. $OH\bullet + dye \rightarrow$ degradation of dye $\rightarrow CO_2 + H_2O$

Scheme 1. Photocatalytic activation of ZnO and oxidation of dyes via the formation of •OH radicals.

This technology has several advantages such as: the speed with which it degrades pollutants, the possibility of using renewable energy (solar radiation) to activate reactions (Chong et al, 2010; Laohaprapanon et al, 2015) and the ability to recycle the photocatalyst (Heggo and Ookawara, 2017). However, different factors can influence photocatalytic degradation: effect of initial dye concentration, semiconductor (catalyst) loading, pH, light intensity, irradiation time and others (Konstantinou and Albanis, 2004). The advanced oxidation processes (UV/H_2O_2, Fenton, etc.) and membrane filtration methods are quite effective for color removal, but these processes may require large amounts of energy to operate (Solanki et al, 2013a).

1.4 Physical methods

These methods are the most used and known industrially, including coagulation, flocculation, sedimentation, adsorption (on activated carbon, biological sludge, silica gel), filtration and reverse osmosis as *membrane technology*. Within the physical systems, membrane technology has attracted attention for its ability to remove contaminants without the need for large quantities of reagents. In the following, membrane technology and its potential benefits are analyzed for the development of anti-fouling membranes in microbial fuel cells.

1.4.1 Membrane Technology

In the particular case of **membrane technology,** which is a generic term that includes several membrane separation processes, membranes are used to remove contaminants and salts from surface water or wastewater (Lau et al, 2012). In pressure-driven membrane processes, the main driving force is the pressure difference at both sides of the membranes, which push the water through the membrane and allows the separation of other compounds depending of the selected membrane, as shown inFigure 1.2. The different membranes used in those processes are: reverse osmosis (RO), nanofiltration (NF), ultrafiltration (UF), and microfiltration (MF) (Alklaibi and Lior, 2005).

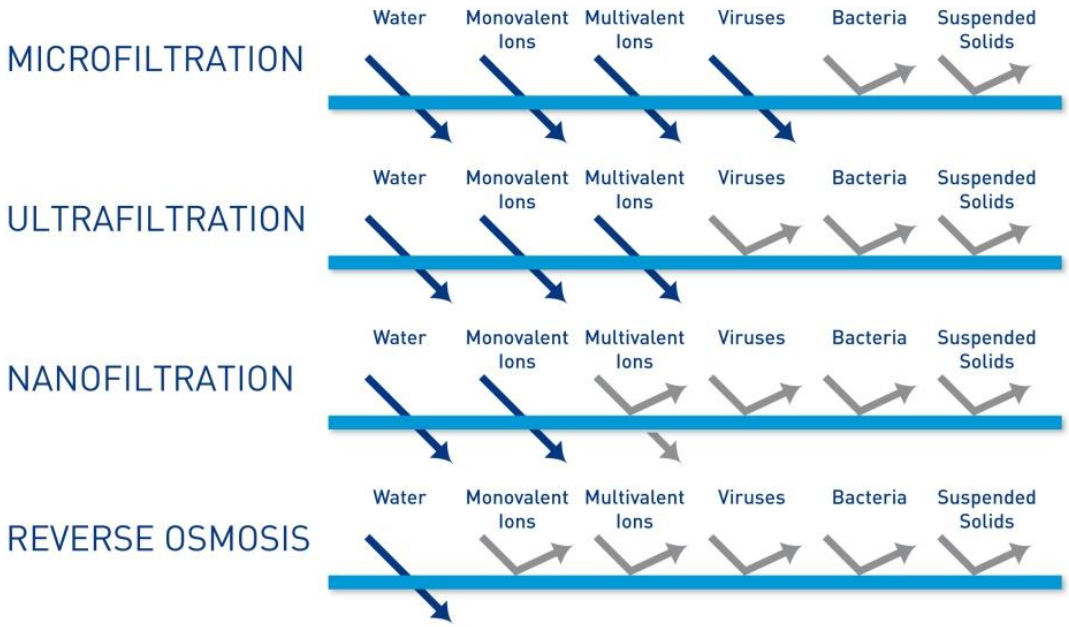


Figure 1.2. Type of membranes and characteristics (Zhang et al., 2012).

The selection of the type of membrane used (pore size and characteristics) depends on the application (desired water quality). Table 1.5 shows some common membrane processes according to the type of membrane and the pore size of the membrane (Werber et al, 2016).

As it can be seen in table 1.5, successful utilization of this kind technology (e.g., RO widely used in desalination of water from sea water) has been greatly limited by membrane

fouling. It can increases operation and maintenance costs by deteriorating membrane performance and ultimately shortening membrane lifetime (Lu et al, 2015; Vrijenhoek et al, 2001). Extensive research is currently focused on the development of fouling-resistant membranes (Alzahrani and Mohammad, 2014; R. Zhang et al, 2016), and it is one of the key aspects studied in this thesis.

Table 1.5 Characteristics, main materials and challenges in membrane technologies (Zhang et al., 2012)**.**

Type	Pore size (nm)	Applications	Species retained	Main membrane materials[a]	Challenges
MF	100-1000	- Surface waters - Fresh groundwater - Sterile filtration - Food and beverage processing	Bacteria, turbidity, particles	Ceramics and Polymeric membranes (PES, PVDF, PE, PAN PTFE)	Anti-Fouling and anti-biofouling membranes
UF	2-100	- Surface waters - Fresh groundwater- Hemodialysis - Sterile filtration - Food and beverage processing	Virus, colloids, macrosolute, Algal toxins		
NF	1-2	- Surface waters - Fresh groundwater - Food and beverage processing	Natural organic matter, sugars, divalent ions, removal oil from water	NIPS. It is an integrated porous asymmetric membrane with a selective layer on the top or a non-selective porous structure (PES, PVDF and PAN)	Membranes with high selectivity (distinction of solutes of similar size). New Materials such as polyetherketone, crosslinked polyimide and polyazoles to new applications other than water purification

Table 1.5 continued

RO	<1	- Seawater desalination - Treatment of brackish and fresh groundwater. Surface water treatment.	Monovalent ions, Low molecular weight org.	Cellulose esters TFC membranes (porous substrate usually polysulfone coated with a thin layer of polyamide)	Cost, scale up, chlorine-resistant membranes, high-boron rejection, rejection of regulated and emerging trace contaminants and anti-fouling membranes. Modified membranes and bio-membranes.
FO					Improve pore wettability (enhancing hydrophilicity) and improve flow and fouling resistance
MD	1000-6000	- Sea water desalination - Water desalination - Water purification - Removal / Concentration of ammonium - Resource concentration	Salts, ammonium	PVDF, PTFE and PP	Improve mechanical strength and membrane stability. Membrane fouling

[a] Polyacrylonitrile (PAN), polypropylene (PP), poly (ether sulfone) (PES), polyethylene (PE), polytetrafluorethylene (PTFE) and poly (vinylidene fluoride) (PVDF).

1.4.2 Membrane fouling

Membrane fouling is the accumulation of materials (contaminants) on the membrane surface or in the membrane pores, which causes a decrease over time in the transmembrane

flux. Normally, fouling can be external (contaminants deposited on the membrane surface) or internal (particles or macromolecules penetrate the internal matrix of the membrane) (Saleh and Gupta, 2016). Therefore, membrane fouling is indeed a major challenge, because in many cases this phenomenon is inevitable in membrane processes. Increased productivity in water treatment using membranes depends largely on actions taken to reduce membrane fouling, which would increase membrane lifetime and decrease cleaning and production costs (Le and Nunes, 2016). In order to better understand membrane fouling, it is important to show the most important factors that contribute to fouling. They can be classified into three main categories: operating conditions, membrane characteristics and contaminant properties (Bagheri et al, 2019) as shown inFigure 1.3.

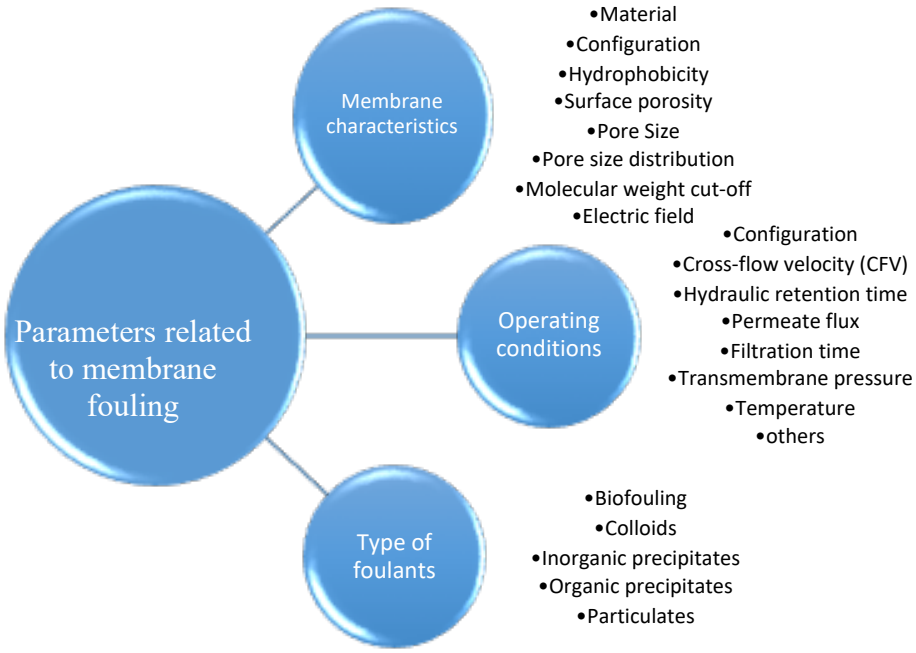


Figure. 1.3 Factors Contributing to membranes fouling

Whatever the factor is, the main effect of membrane fouling is a decrease in the permeate flux of the membranes. Darcy's law can describe the effect of fouling on membrane flow (Alventosa-Delara et al, 2014):

$$J = \frac{dV}{Adt} = \frac{\Delta P}{\eta R_t} \qquad (1)$$

$$R_t = R_m + R_c \qquad (2)$$

where **J** is the permeate flux, which can be affected by membrane fouling, η is the viscosity of the solution to be filtered, Δ**P** is the transmembrane pressure (pressure drop imposed across the fouling layer and membrane), $\mathbf{R_t}$ is the total membrane resistance which is the sum of the resistance to flow through the membrane new ($\mathbf{R_m}$), and the resistance offered by various additional resistances during the filtration process as a result of the polarization and subsequent fouling (cake' resistance, $\mathbf{R_c}$).

1.4.3 Fouling classification

For a better understanding of the membrane fouling process, it is important to know the types and nature of the fouling agent (Zhang et al, 2020). The common contaminants in membrane processes could be classified in five groups: **biofouling, colloids, inorganic precipitates, organic precipitates and particulates**

Table 1.6 Classification of common contaminants in membrane processes (Fane et al., 2006)

	Category	**Definition**	**Example of foulants**
z Parameters related to membrane fouling	Biofouling	Biofilm formation on membrane surface.	Bacteria, Viruses, and Fungi
	Colloids	Formation of cake film due to deposition of particles on the membrane surface or blockage of pores of the inner matrix of the membrane.	Metal hydroxides, colloidal silica oxyhydroxide and Clays and accumulated particles

Table 1.6 continued

Inorganic precipitates or scaling	Precipitation deposits result in bulk and membrane crystallization.	Oxides, hydroxides and calcium and inorganic salts ($CaSO_4$, $CaCO_3$, SiO_2, and $BaSO_4$)
Organic precipitates	Gel formation due to adsorption of organic compounds on the membrane.	Biological substances and macromolecules (oil, proteins, organic acids, cleaning agents, polysaccharides, etc.)

Table 1.6 summarizes the types of foulants that can be incorporated into membranes. It is not easy to reach a general conclusion about which type of fouling in membranes is more dangerous for the membrane lifetime, since there may be different interactions and fouling mechanisms for each fouling agent (Saleh and Gupta, 2016).

1.4.4 Fouling mechanisms and interpretation

Since the mechanisms of fouling are difficult to distinguish, they can be studied by classifying them into four general types (Saleh and Gupta, 2016):

Pore plugging/blocking: caused by a complete blockage of the pore, which reduces the active area of the membrane. Compounds such as colloids can block the entry or the internal way through the pores.

Pore restriction: caused by adsorption of particles on the membrane surface resulting in a reduction of the diameter or the partial blockage of pores. This produces a reduction of the active area on the membrane surface.

Cake formation/surface: caused by individual particles, aggregates and precipitates. These contaminants do not enter or seal the pores, but form a cake on the membrane surface. This phenomenon is due to a high concentration of contaminants on the membrane surface. The cake formed on the membrane surface generates a resistance to membrane permeation which is known as cake resistance.

Biofouling: caused by microorganisms, the most common type is a surface deposition due to bacterial adhesion and post-growth, resulting in a cake composed of bacterial colonies and biopolymer (biofilm).

The mechanism of biofouling is more frequent in the treatment of water with high nutrient availability, such as wastewater. As a consequence of membrane fouling, a decrease in flux under constant pressure conditions can be observed. The flux decrease can have different stages as shown in Figure 1.4.

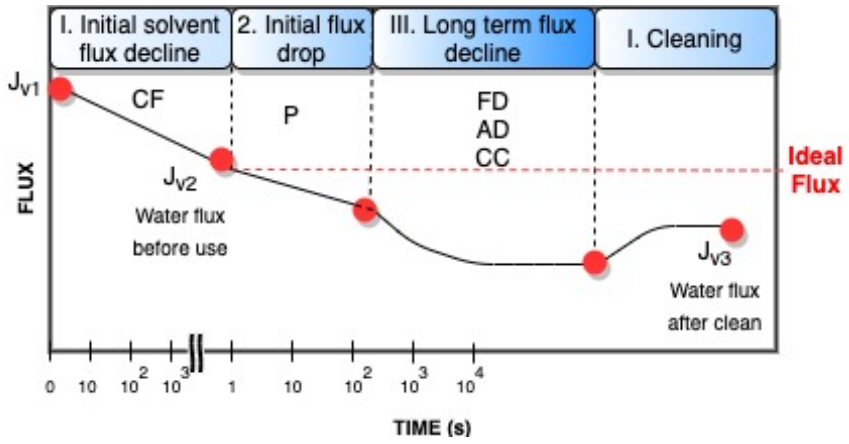


Figure 1.4 Flow stages during membrane fouling (Fane et al, 2006)

Figure 1.4 depicts four possible phases during membrane fouling. Phase I shows a flux change as a result of compaction fouling (CF) of new membranes. Phase II is a small drop in pressure generally at the start of the filtration process, this small drop may be due to polarization, pore obstruction and adsorption interactions (P). Phase III is a major decrease

in the flow rate over long operating periods, this decrease is due to fouling deposition (FD), fouling adsorption (AD) and cake consolidation (CC); and, finally, Phase IV is a small flux recovery during or after membrane cleaning (Fane et al, 2006). The ideal performance of a fouling-free membrane is also shown (ideal flux). These results suggest the necessity of antifouling membranes, capable of extending membrane lifetime and resembling ideal behavior.

1.5 Anti-fouling strategies and membranes

As we have seen in this chapter, membrane fouling is unavoidable in the vast majority of processes involving membranes (Le and Nunes, 2016).

In order to develop new membranes, it is necessary to know how the membrane fouling process occurs. This process can be studied from two approaches: a) the decrease or disequilibrium of the Gibbs free energy of the fouling-membrane interactions (thermodynamic point of view) and b) the fouling-membrane and fouling-fouling interactions (physicochemical point of view).

The fouling agent can generate membrane fouling in three consecutive stages approach-adsorption-accumulation (Figure 1.5): Phase I) approach of foulants and precursors to the membrane surface, this phase can be driven by transmembrane hydraulic pressure; phase II) adsorption of contaminants on the membrane surface due to electrostatic, hydrophobic, van der Waals, hydrogen bonding or other interactions; phase III) accumulation of contaminants on the membrane surface or in the membrane matrix, resulting in biofilms, gels, cake layers or salt scaling (Brady and Singer, 2000). Therefore, it is necessary to consider that an antifouling surface must take into account the following: 1) inhibition of direct contact or contaminant-surface interaction, which can be enhanced by hydrating the surface, if the fouling agent is hydrophobic (e.g., colloids, bacteria, proteins, etc.), 2) preventing or releasing fouling present in the medium, which could be achieved by minimizing the fouling-membrane interaction (e.g., with marked differences in the surface energy of the membrane with respect to the fouling agent), and 3) attack of the fouling prior to its adhesion to the surface (e.g., inactivation of the cells or oxidation of the fouling (Schneider et al, 2014; Zhao et al, 2018).

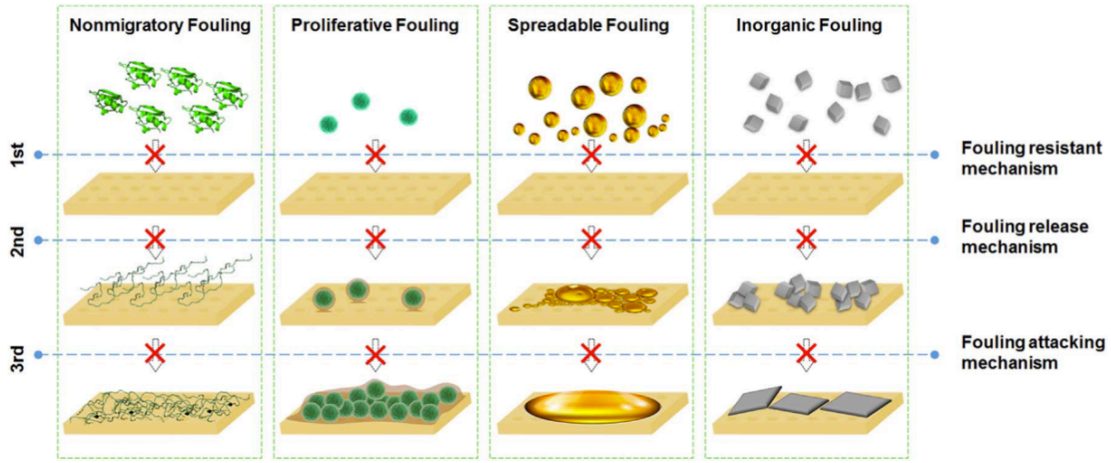


Figure. 1.5 Membrane fouling stages and antifouling mechanisms (Zhao et al, 2018).

Strategies for the development and design of antifouling membranes often consider the characteristics and properties of membranes as an important parameter. The most important properties are: a) chemical structure (functional groups, charge and hydrophilicity) and b) morphology (pore size, surface roughness). High hydrophilicity, low roughness are desirable characteristics in an antifouling membrane (Le and Nunes, 2016). Also, a combination of mechanisms can be used to enhance the overall antifouling properties of the membranes. Additionally, modification of commercial membranes has also contributed to a potentially sustainable solution to prevent fouling. Therefore, strategies to minimize membrane fouling can be divided into two groups: membrane design/manufacturing and, surface modification of membranes.

1.5.1 Membrane design and manufacturing methods.

Established water purification processes such as MF, UF, NF and RO as well as the emerging FO process use a variety of membrane materials such as polymer and inorganic membranes to produce stable membranes. However, membrane fouling can affect both inorganic and polymeric membranes.

In this section, polymeric membranes and their corresponding fabrication methods are discussed. There are two main families of membranes: made from phase inversion membranes and thin film composite membranes (Werber et al, 2016).

a) **Phase inversion membranes.** The phase inversion process was first introduced in membrane technology by Loeb and Sourirajan in the 1960's and this process represents the most widely used manufacturing technique for polymeric membranes (Hołda and Vankelecom, 2015).

   Phase inversion process refers to the process in which a polymer solution (the solvent system is the continuous phase) inverts into a swollen three-dimensional macromolecular network or gel (the polymer is the continuous phase) upon exposure to another gas/liquid phase or a temperature change. The result is a thin film designed for use as a barrier. The concept of phase inversion covers a range of different techniques such as precipitation by controlled evaporation, thermal precipitation from the vapour phase and immersion precipitation. The majority of phase inversion membranes are prepared by immersion precipitation (Kesting, 1985; Tang et al, 2021).

b) **Thin-film composite (TFC) membranes.** These membranes consist of two layers, a porous support layer (usually polysulfone) on which a highly cross-linked, non-porous layer is adhered (commonly used polyamide). Compared to cellulose acetate-based membranes, TFC polyamide membranes can provide much higher water permeability and salt rejection. The interfacial polymerization of a diamine commonly, m-phenylenediamine (MPD) can be used for the manufacture of RO, FO and NF (Lau et al, 2015; Werber et al, 2016). The use of certain synthetic polymers such as (PVDF), (PAN), polysulfone and (PES) (Cheryan, 1998) has generated many advantages in the manufacture of membranes. However, these polymers are also highly hydrophobic, which leads to a predisposition to organic and biological fouling in the membranes, both on the surface and in the inner pores of the membranes (Zhu et al, 2016).

   However, polyamide TFC membranes used in reverse osmosis, FO and NF are very susceptible to organic and biological fouling due to their high surface morphology, hydrophobicity and charge (Herzberg and Elimelech, 2007). Therefore, a major challenge is to decrease these parameters. Hence, a design of highly selective membranes could be a convenient alternative (Werber et al, 2016).

Moreover, an intelligent membrane design or modification of the chemical properties of membranes is also necessary to improve fouling resistance.

In the current work, we decided to use commercial thin-film composite (TFC) membranes as a base for the development of anti-fouling membranes.

1.5.2 Surface modification of membrane

For the design of antifouling membranes, surface engineering is a highly used tool. Normally, MF and UF antifouling membranes can be obtained by different modification methods. There are two most used methods which are the modification of commercial membranes (surface modification) and the in-situ modification or phase inversion process (3D modification).

In order to better understand the latest efforts in exploring membrane fouling mechanisms, this section will be divided into two groups: a) advanced antifouling strategies (active and passive strategies) and b) advanced methods of membrane surface modification to improve their antifouling capacity, where the "bioinspired" surface adhesion method will be addressed as the main method.

1.5.3 Advanced antifouling strategies

The mechanism of membrane fouling depends on the kind of fouling contaminant, therefore, the manufacture of antifouling membrane surfaces can be classified into two main strategies: a) passive strategy, which does not affect the characteristics of the contaminants, because it avoids the initial adsorption of the contaminants on the membrane surface, b) active strategy, in this strategy the chemical structure of the fouling contaminant on the periphery of the membrane surface is destroyed or inactivated.

a) **Passive antifouling membranes**

Passive antifouling membranes manipulate the physicochemical and/or topological structures of the membrane surface in order to weaken possible interactions between foulants and the membrane surface. This strategy can prevent the settling or adsorption of potential foulants. Passive antifouling membranes prevent contaminants arriving at the membrane surface (fouling resistance) or move adhering contaminants away from the membrane surface (fouling release) (Figure1.5) (Choudhury et al, 2018).

b) **Active antifouling strategies.** Passive antifouling strategies can show limitations, due to their low activity against microorganisms such as bacteria. An interesting alternative is the construction of antibiofouling membrane surfaces, which will have the ability to prevent microbial colonization and subsequent biofilm formation on membrane surfaces. Membranes with these active activities are known due to their ability to prevent this problem, therefore, they have been called active membranes or membrane modifications with active strategies. These modification strategies are based on the presence of antimicrobial agents, which can kill bacteria when they come in contact with the active surface and the bio-fouling can be eliminated by biochemical routes.

These strategies can be classified into two groups: off-surface and on-surface active antibiofouling strategies.

i) Off-surface

These strategies release antimicrobial agents into the medium. This promotes a leaching of antibacterial compounds from the membrane surface into the biological medium. On the other hand, it is possible to generate reactive oxygen species (ROS) into the medium.

For this purpose, nanometer-scale photocatalysts are used, which produce ROS species. ROS are produced through catalytic reactions on the surface of nanocatalysts. ROS can usually be photoinduced by external UV radiation as in the case of metal oxides such as ZnONPs or TiO_2 NPs. ROS can affect the integrity of microorganisms that come in contact with them. These nanocatalysts can be placed on the surface of the membrane, which provides active anti-biofouling character to the membrane. In addition, the release of metallic biocidal nanomaterials such as silver or copper ions are also applied as antibacterial agents (Kim and Van Der Bruggen, 2010; Soleymani Lashkenari et al, 2019; J. Zhu et al, 2016).

This effect is due to the fact that Gram-positive, Gram-negative bacteria and microalgae are affected by the antimicrobial character of these agents (Figure 1.6) (Choudhury et al, 2018).

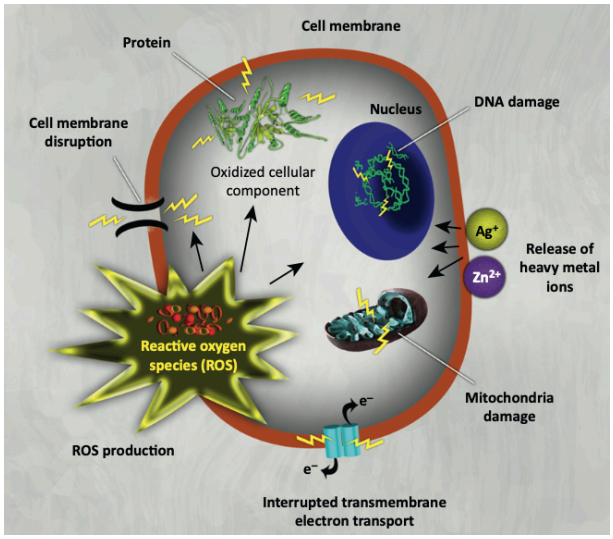


Figure 1.6 Toxicity and cytotoxicity of NPs and ions in the formation of oxidative stress ROS species (Hajipour et al, 2012).

ii) On-surface

Unlike off-surface active strategies that release antimicrobial agents, on-surface strategies do not release antibacterial agents because the antibacterial agents are introduced directly into the membrane surface structure as part of the membrane. These agents can contact cells or microorganisms adhered to the surface by different physical or chemical mechanisms. An example of non-releasable antimicrobial agents are cationic polymeric materials (CPM), which have cationic antimicrobial groups in their own structure such as phosphorus, quaternary ammonium, guanidinium and others. Among those, polycations with quaternary ammonium groups such as quaternized polyethylenimine (PEI), chitosan can be the most used for this purpose (Choudhury et al, 2018; Kolesnyk et al, 2020; Nunes et al, 2020; Susanto et al, 2020; R. Zhang et al, 2016). Furthermore, a number of carbon-based nanomaterials (CBNs) such as carbon nanotubes (CNTs) and graphene nanomaterials can exhibit cytotoxic activity to bacteria (Manawi et al, 2016; Shabani et al, 2020).

In the particular case of CNTs, the cytotoxic activity is not very well known, so, there are several hypotheses of cytotoxic mechanisms, among these the physical rupture of the

membrane, oxidative stress and disruption of intracellular metabolic pathways, which has great reception in the scientific environment. For the case of GBN, including graphene, GO and reduced GO (rGO), these hypotheses can also be considered (Figure 1.7).

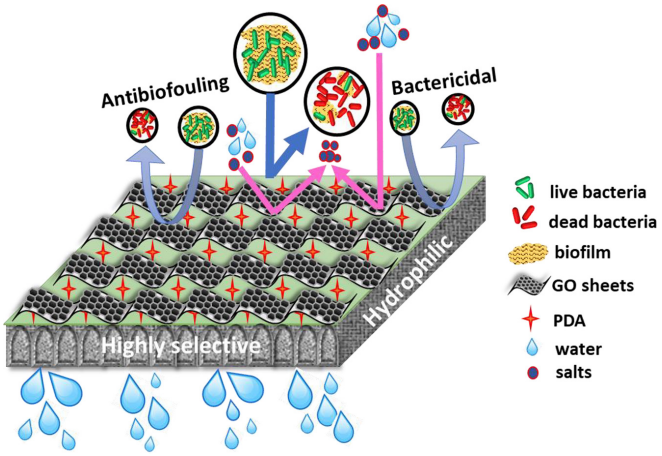


Figure 1.7 GO sheets antimicrobial activity on a membrane (Khanzada et al, 2020)

1.6 Bioadhesion (bioinspired adhesion chemistry)

Bioinspired adhesion is largely based on the replication of the way mussels adhere to a variety of wet surfaces. This bioadhesion uses mussel adhesive proteins (MAPs) to adhere to surfaces, due to the MAPs having large amounts of catechol groups, amino acids and 3,4-dihydroxyphenylalanine (DOPA), which exhibit high hydrogen bonding strength in wet conditions with different surfaces (Tang et al, 2013). The structure of dopamine (Figure 1.8) has amino and catechol groups, which present a molecular structure similar to DOPA. In recent years, dopamine has become the focus of attention, due to its capacity for effective adhesion many materials on the membrane surface (Liebscher et al, 2013).

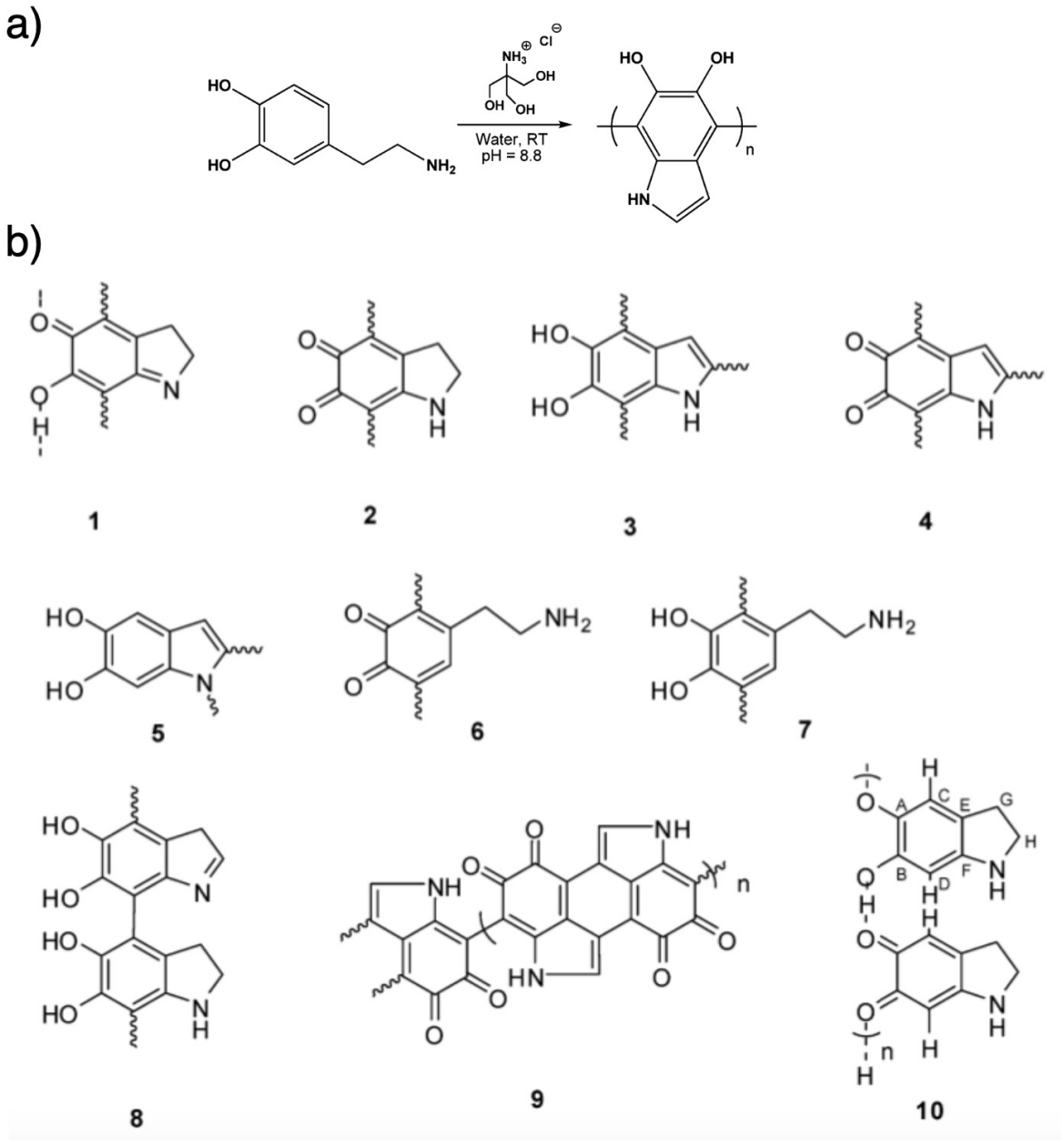


Figure 1.8 a) Dopamine and synthesis of poly(dopamine) and b) proposed structures of PDA.

1.6.1 Polydopamine (PDA)

PDA can generate an efficient multifunctional coating on membrane surfaces, which can be an efficient bio-inspired glue for the adhesion of other materials. A PDA coating can be generated via in situ oxidative self-polymerization of dopamine. This self-polymerization of

dopamine can occur on a wide range of substrates. Usually, this auto polymerization takes place in an alkaline medium and under mild conditions (Ye et al, 2011; X. Zhao et al, 2018).

PDA can firmly adhere to almost all solid surfaces, this adhesion is due to covalent bonding interactions, coordination, hydrogen bonding and stacking (Liebscher et al, 2013; Zangmeister et al, 2013). In addition, parallel reactions with other surface functional molecules can be carried out, thanks to the residual catechol, amine and quinone groups of the PDA (Ye et al, 2011).

While dopamine and its derivatives can be used as bio-glue, it is also known that dopamine and its derivatives have a hydrophilic character due to the zwitterionic groups. This hydrophilicity can also give an antifouling character when coating surfaces with dopamine or PDA (Misdan et al, 2016). Therefore, the fouling resistance of PDA can be attributed to its hydrophilicity, where the electrostatic repulsion of protonated amino groups of PDA can also play an important role in its anti-fouling characteristics (Barclay et al, 2017; Xiang et al, 2015). However, the existence of aromatic rings (hydrophobic groups) and the lack of antifouling functional groups in PDA molecules limit the antifouling characteristics of the membranes (R. Zhang et al, 2016). To increase the anti-fouling character of the PDA, catechol groups can be strongly chelated with other materials as metal ions. This chelation facilitates the adhesion of inorganic particles as nanoparticles on the PDA surfaces. The reactions necessary for this chelation can take place through co-precipitation or redox reactions. These reactions can further enhance the hydrophilic and antifouling properties of PDA-coated surfaces and thus of membranes modified with PDA and other antifouling particles. This is known as the polydopamine adhesion and reaction.

1.6.2 Adhesion of functional materials.

This method modifies a surface in a single step, using codeposition as a methodology for in situ wetting of functional materials on a PDA matrix. Hydrophilic materials such as polysulfobetaine methacrylate (PSBMA) and PEI mixed with dopamine prior to their polymerization process (Wang et al, 2015) are used as functional materials. Subsequently,

the polymerization reaction takes place, leading to a simultaneous in-situ deposition of PDA and functional materials on different types of membranes. This modification can show a significant improvement in the hydrophilicity of the membrane surface, which can improve the separation performance of membranes for solutions containing proteins or oil/water elusions, due to the high fouling resistance of both functional materials and PDA.

1.6.3 PDA functionalization reaction

This reaction can occur in two steps. First, modification of a surface with PDA, followed by bioadhesion of antifouling modifiers. Inorganic particles (e.g. Au, Cu, Si and Ag NPs or TiO_2, ZnO SiO_2, Al_2O_3, ZnO, ZrO_2, etc) (Khorshidi et al, 2018) biomacromolecules (e.g., heparin) (Jiang et al, 2010) polymers (e.g., PEG, PVA, polyvinyl pyrrolidone (PVP) and zwitterionic polymers (McCloskey et al, 2012), small organic molecules (e.g. NT, GO and graphene) and organometallic particles (metal organic frameworks) can be used as antifouling modifiers. These modifiers can be easily attached onto membrane surfaces by covalent/non-covalent bonds with the PDA layer. This surface modification can provide high antifouling characteristics against oil, proteins, platelets and microorganisms (Jun et al, 2020b; Yan et al, 2020).

In the particular case of metal oxide nanoparticles, dopamine can react through surface complexation by any of proposed routes in Figure 1.9. Surfaces modified with nanoparticles or catalysts could contribute to the degradation of pollutants such as pharmaceuticals, dyes, bio-foulants and others (Tang et al, 2013) with UV light irradiation on this modified membrane (Khorshidi et al, 2018; Nasrollahi et al, 2021).

As seen in this section, bio-inspired modification with polydopamine is a simple, fast and non-invasive alternative to avoid bacteria accumulation. In addition, PDA modification allows the functionalization of new materials such as nanoparticles on the membrane surface. The nanoparticles can oxidize organic matter that approaches the membrane surface thanks to their catalytic activity, preventing biofouling of the membrane. Therefore, this bio-inspired modification method will be used in the present work to avoid membrane fouling.

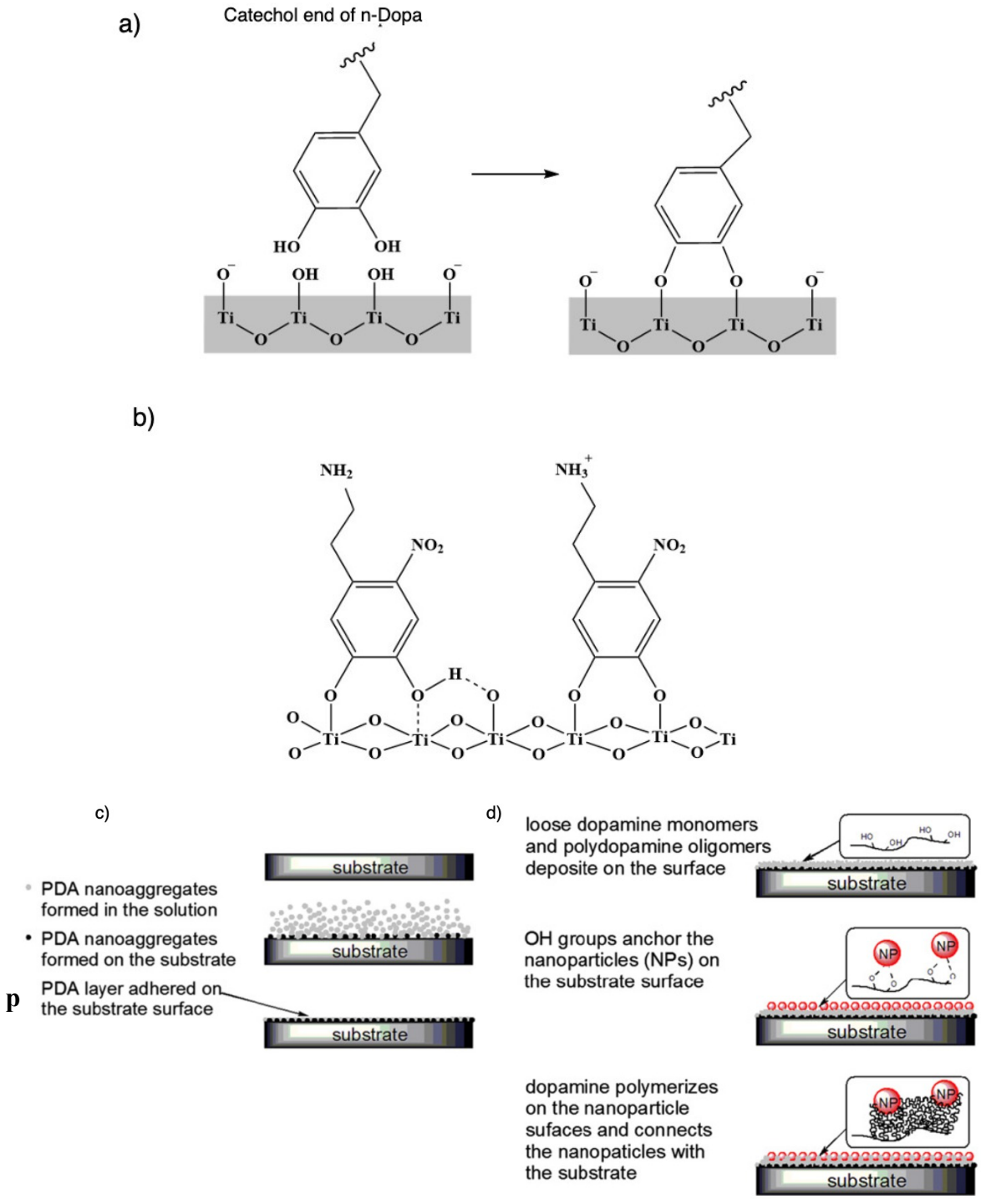


Figure 1.9 Proposed PDA adsorption configurations on TiO_2 surface: (a) probable mechanism of mPEG-DOPA binding to TiO_2 surfaces; (b) probable configurations: (I) hydrogen bridging (monodentate binding) and (II) bidentate binding (Bahamonde Soria et

al, 2020) c) deposition of polydopamine on the membrane surface and (d) binding of TiO_2 nanoparticles on the membrane surface (Zhang et al, 2013).

Furthermore, characterization techniques have a fundamental role in understanding membrane fouling and fouling mechanisms (Jhaveri and Murthy, 2016). A brief summary of the most common techniques used for the characterization of nanocomposite membranes is presented below:

a) *Scanning electron microscopy (SEM).* This technique is used to compare the surface morphology of different membranes (pristine vs. modified membranes or clean vs. fouled). This technique can evaluate both the membrane surface and the membrane cross-section.

b) *SEM - Energy-dispersive X-ray (EDX) and X-ray photoelectron spectroscopy (XPS).* These techniques provide an elemental analysis of the surface or cross-section of the membrane.

c) *Atomic Force Microscopy (AFM),* is used to know and compare the surface topology (roughness) of pristine, modified and fouled membranes. Roughness is an important factor predicting the antifouling capacity of certain surfaces, since water pollutants are less likely to adsorb on smoother surfaces (low roughness).

d) *Contact angle,* is used to determine the wetting of the membrane surface by the contact angle between the water droplet and the membrane surface. Hydrophobic: contact angle > 90°; hydrophilic: contact angle < 90°. If the membrane is hydrophilic, it can produce an antifouling effect for aqueous streams.

e) *Zeta potential***,** is a technology applied to measure the surface charge of the membrane. which will change depending on the level of membrane fouling.

1.7 Biological treatment

Different biological methods are available, depending on the presence (aerobic - recovery of biological sludge in aeration basins) or absence (anaerobic treatment) of oxygen. Among the many biological systems to treatment of textile wastewater available are: aerobic activated sludge or rotating biofilm aerobic reactors, aerobic-anaerobic packed bed reactors,

aerobic-anaerobic fluidized bed reactors, sequential batch or continuous flow aerobic and anaerobic reactors, batch anaerobic reactors. For this purpose, several cultures of microorganisms have been tested for the decolorization of textile dyes, among which the most common are: fungi, bacteria and algae (Banat et al, 1996). These methods have provided an efficient and low-cost alternative for the elimination of color and organic matter in wastewater (Banat et al, 1996; Husain, 2010). However, some dyes (e.g., orange II, CI Reactive Blue 1, among others) are non-biodegradable and cannot be eliminated via biological treatment (Suzuki et al, 2020).

1.7.1 Bioelectrochemical systems

Bioelectrochemical systems (BES) has several advantages over other conventional biological treatment technologies due to its energy recovery in various forms (e.g., electricity, hydrogen, hydrogen peroxide, methane, and ethanol) and lower sludge production (i.e., 65-71% less sludge production than activated sludge treatment) (Al-Sahari et al, 2021; Yang et al, 2019). BES are bioreactors that use electrochemically active microorganisms to catalyze oxidation and/or reduction reactions at the electrodes (Logan and Rabaey, 2013). However, treatment and energy recovery efficiencies are not sufficient to obtain high quality effluent for potential reuse and achieve energy self-sufficiency.

BES can be classified into four main types : microbial electrolysis cell (MEC); microbial electrosynthesis cell (MES); microbial desalination cell (MDC); and microbial fuel cell (MFC) (Al-Sahari et al, 2021)

1.7.2 Microbial electrolysis cell (MEC)

MEC (Fig.1.10) is considered a close system to the microbial fuel cells, which has similar anodic functions to the MFC system. However, it is widely used to produce valuable hydrogen and reduce low potential metals in the cathode chamber depending on the anodic degradation process of substrates and external power supply (Al-Sahari et al, 2021). The distinction between the MFC and MEC techniques resides in the cathodic chamber reactions, where an external voltage is applied at the MEC cathode under anaerobic conditions to

enhance the cathodic reactions (combination of electrons and protons) to produce sustainable hydrogen (H_2) in the cathodic chamber (Almatouq et al, 2020). Hydrogen is produced directly using the protons (passing through the exchange membrane) and electrons transferred from the anode chamber by increasing the electrical voltage at the MFC electrode (Logan et al, 2008). It is known that the anode open-circuit potential in the typical MFC system is about ↑-300 mV, which is can produce cathode reactions to produce water. However, to produce hydrogen, the cathode requires a higher potential of at least E_0 =-410 mV (NHE) at low pH values of 7.0, T = 25ºC, and P_{H2} = 1 atm (Sun et al, 2010). If acetate is taken as the substrate to produce hydrogen, the anodic and cathodic reactions can be described by the following equations:

Anodic reactions using acetate (CH3COO−) as substrates:

$CH_3COO^- + 4H_2O - \rightarrow 2HCO_3^- + 9H^+ + 8e^-$

Or

$CH_3COO^- + 2H_2O - \rightarrow 2CO_2 + 7H^+ + 8e^-$

Cathodic reactions (hydrogen production):

$8H^+ + 8e^- - \rightarrow 4H_2$ (Power, E_0 =↓0.41 V)

Or

$8H_2O + 8e^- - \rightarrow 4H_2 + 8OH^-$ (Power, E_0 =↓0.41 V)

In MECs, the proton exchange membrane (PEM) separates the anodic and cathodic chambers and facilitates the selective transport of protons, in addition this membrane must retain the hydrogen recovered in the cathodic chamber. Since proton migration through the PEM is the limiting factor, unfavorable competitive ion transport through the membrane results in increased resistance to proton transport and consequently reduces the hydrogen production efficiency of the cathode. Therefore, the membrane must exclusively transport protons and exclude the transport of other cations. Here, hydrocarbon-based PEMs are considered more efficient than fluorine-based PEMs (representatively Nafion) due to their relatively higher selectivity for proton transport (Park et al, 2021). However, long-term

biofouling of these membranes in MECs limits the H^+ transport capacity which is one of the key functions of PEM. Thus, biofouling is also a major obstacle to reliable and cost-effective operation of PEM membranes in MEC systems.

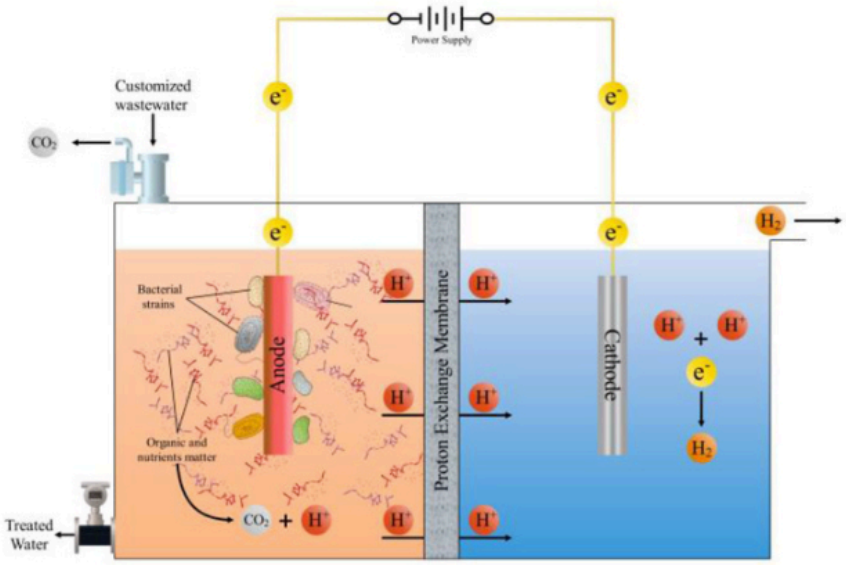


Figure 1.10. Bioelectrochemical systems: microbial electrolysis cell (MEC) (Al-Sahari et al, 2021; Santoro et al, 2017)

1.7.3 Microbial Electrosynthesis cell system (MES)

In these systems, substrates and high redox potential metals are degraded in the cathode chamber. The MES system (Figure1.11) is often supplied with higher power than the MEC system to reduce carbon dioxide, which produces industrially relevant products (Jung et al, 2020).

This bioelectrochemical system degrades organic matter to produce valuable products such as CH_4, H_2, acetate, bioalcohols, bioplastics and other by employing the cathodic biocatalysts to reduce the electron acceptor (Bajracharya et al, 2017), this process is carried out in the cathodic chamber using the energy generated by anodic oxidation. Electron transmission from the anode to the cathode and CO_2 reduction at the cathode are the most affected factors in the MES system (Christodoulou et al, 2017). MES reactions are often

dependent on the required products. However, the general and most common reaction of the MES system can be defined by the following equations:

The anodic reactions using water (H_2O) content:

$4H_2O \rightarrow 2O_2 + 8H^+ + 8e^-$

The cathodic reactions (acetate production):

$4CO_2 + 8H^+ + 8e^- \rightarrow 2CH_3COOH + 3O_2$ (Power, $E_0 = \downarrow 0.29$ V)

In MES cells the cathodic process is biological, thus the risk of membrane biofouling should be a factor to consider.

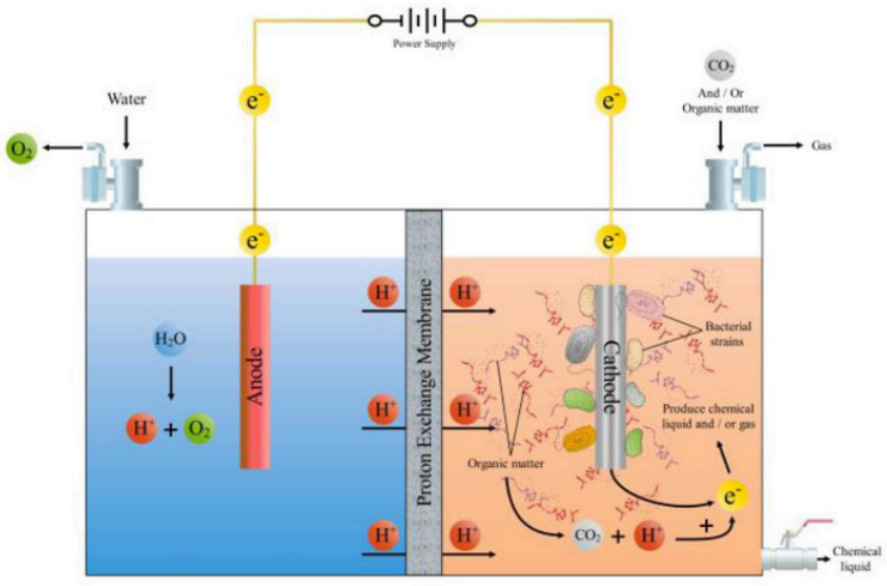


Figure 1.11. Bioelectrochemical systems: microbial electrosynthesis cell (MES) (Santoro et al, 2017).

1.7.4 Microbial desalination cells (MDC).

The MDC (Figure1.12) system is the modification of the MFC system, in which a desalination chamber is added to separate the anodic and cathodic chambers and uses the electric potential of the MFC to desalinate the saltwater. In turn, wastewater is generally provided in the anode chamber as a source of organic and inorganic substrates for microbial

metabolism processes, which ends up as clean treated water. The desalination chamber is divided by an anion exchange membrane (AEM) in the anode chamber and a cation exchange membrane (CEM) in the cathode chamber. Substrate degradation and energy generation is carried out in the anode and cathode chamber respectively. The saltwater desalination process in the middle chamber occurs when anions (Cl^-) are transferred to the anodic chamber via AEM and cations (Na^+) are transferred to the cathodic chamber via CEM preserving electroneutrality (Ragab et al, 2019).

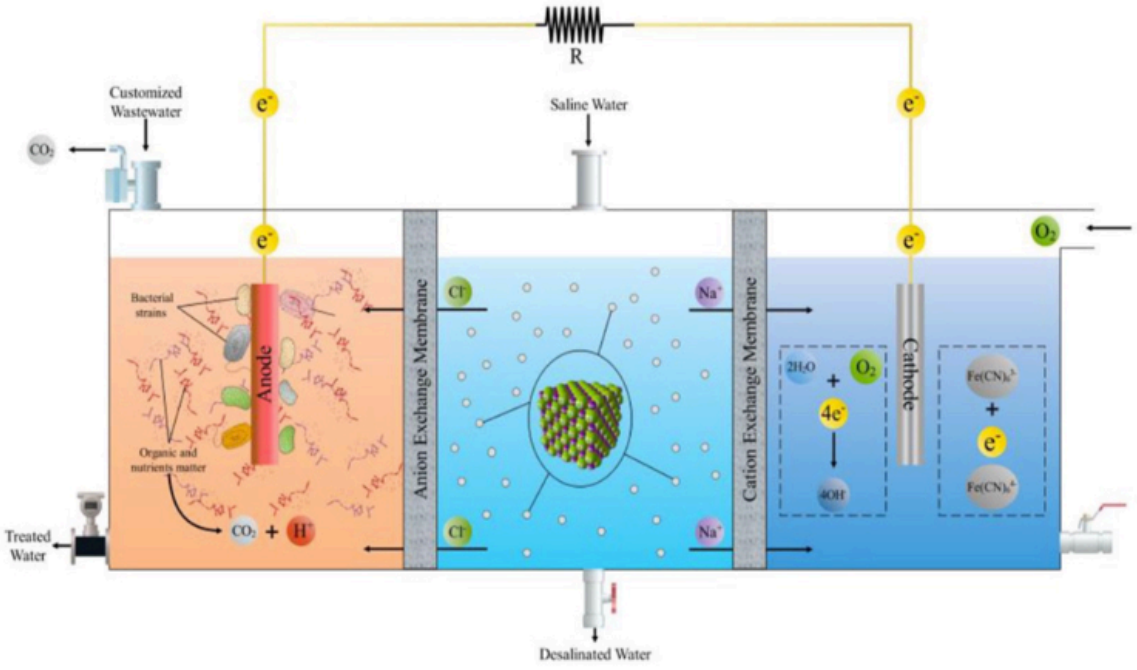


Figure 1.12. Bioelectrochemical systems: microbial desalination cell (MDC) (Santoro et al, 2017)

1.7.5 Microbial fuel cells

In 1911, Potter first observed the ability of *E. coli* to produce electricity (Potter, 1911). Microbial fuel cells (MFC) is an anaerobic process, which uses anaerobic bacteria to convert the chemical energy of a particular substrate contained in wastewater into electrical energy (Hernandez-Fernandez et al, 2015).

A MFC is composed of 4 principal components (Fig. 1.13): (1) the anodic chamber, where the organic matter (substrate) is oxidized by microorganisms (electrogenic anaerobic bacteria such as *Geobacter sulfurreducens, Shewanella*, or bacterial consortiums) (Ge et al, 2013). This chamber releases electrons produced in the oxidation process and they are deposited in a temporary electron acceptor (anode); (2) the cathodic chamber, where oxygen reduction is carried out as the final electron acceptor (cathode). The flow of electrons (from anode to cathode) is caused by the difference in electrical potential between two electrodes, (3) separator or proton exchange membrane (PEM). The majority of MFC designs require the separation of the anodic chamber with the cathode compartments by a (PEM). Separator transport the hydrogen ions (produced in oxidation process) through the membrane from the anode chamber to the cathode chamber to produce there the reduction of oxygen (Logan et al, 2006a) (4) Electrodes: the anode and cathode must be conductive, biocompatible, and chemically stable in the reactor solution. A wide variety of materials has been investigated as electrode material. However, the most commonly used material, both for anode and cathode is (modified) carbon, available as compact graphite plates, rods, or granules, as fibrous material (felt, cloth, paper, fibers, foam), and as glassy carbon.

In the metabolic energy generation process, bacteria transport electrons from a substrate at a low potential (e.g., acetate -0.296 V) through the electron transport chain to the final electron acceptor (such as oxygen or nitrate) at a higher potential. In an MFC, the anode is the final electron acceptor and its potential determines the energy gain for the bacteria. The greater the difference between the redox potential of the substrate and the anode potential, the greater the metabolic energy gain possible for the bacteria, but the lower the maximum achievable voltage of the MFC. Therefore, to maximize the MFC voltage, the anode potential should be kept as low (negative) as possible (Logan et al, 2006b)

MFC is a technology provided with the ability to clean aqueous streams loaded with organic matter (Zhao et al, 2017; Zhu et al, 2016a). Besides, MFCs are considered a eco-friendly technology that could provide sustainability for wastewater treatment in the future, they have several advantages over other wastewater treatment technologies such as: (1) they directly convert the energy present in the substrate into electricity; (2) they generate less activated sludge than conventional anaerobic treatments with activated sludge or anaerobic

digestion (3) capacity to work at different temperatures, even at low temperatures (Heidrich et al, 2018) (4) they do not produce toxic gases during their operation (although CO_2 is produced), (5) this technology could be applied in sites with insufficient electrical infrastructure (He et al, 2017).

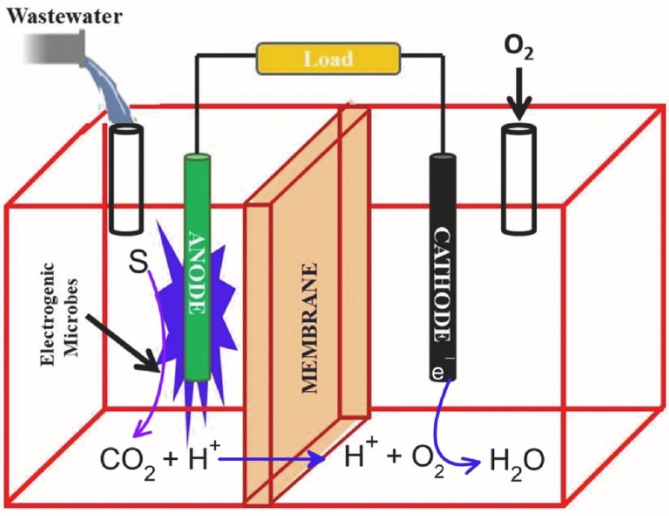


Figure 1.13. Operating scheme of a microbial fuel cell (Suresh et al, 2022).

Microbial fuel cell (MFC) system designs have varied throughout history. The main types of MFC systems can be defined as: DC; double chamber, SC; single chamber, S; stacked, MM; microalgae-microbial, SED; sediment, SB or H-type; salt bridge or H-form (Figure 1.14).

With the exception of sediment microbial fuel cells (SedMFCs), most of these bioelectrochemical systems typically use membranes as separators between the different compartments. Therefore, membranes are an extremely important component to consider. In the following sections, the function of the separators will be explained.

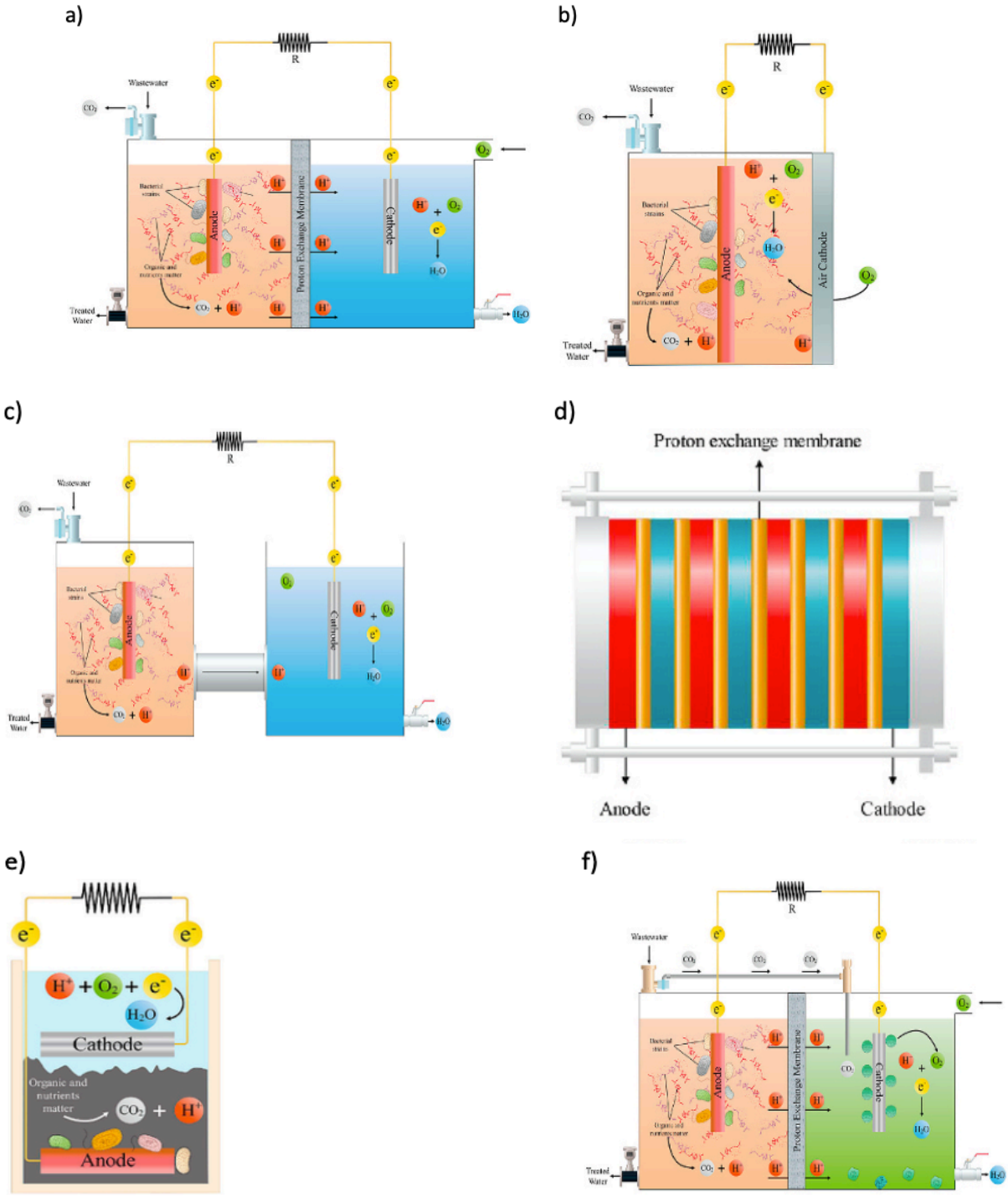


Figure 1.14 MFC designs: a) DC; double chamber, b) SC; single chamber, c) salt bridge or H-form, SB or H-type d) S; stacked, e) SED; sediment, f) MM; microalgae-microbial (Al-Sahari et al, 2021).

1.7.6 MFC Limitations

Bioelectrochemical systems may have certain limitations, such as prolonged periods of operation (around 170 hours) (Jabeen and Farooq, 2017; Kodali et al, 2017; C. E. Zhao et al, 2017), high costs of several components such as cathode (sometimes use catalytic converters Pt or Pd supported in cathode) or separators (proton exchange membrane -PEM). Table 1.3 identifies the costs of some materials used in the MFC (Manon Oliot et al, 2016; Wang and Lim, 2017a). The high cost in some materials has motivated the use of low-cost materials as separators (cellophane ultrafiltration, microfiltration or ceramic membranes), active carbon as electrodes and others (Bi et al, 2018)

Table 1.3. Cost approximate of main components in conventional MFCs (Wang et al, 2012)

Components in MFC	Mostly used in conventional MFC
Anode	Carbon cloth [E-tek 620 dollar m^{-2}]
Cathode	Platinum-coated carbon cloth [E-tek 0,5 mg cm^{-2}; 2000-dollar/m^{-2}]
Separator	Nafion membranes (2500-dollar/m^{-2})

Another important problem is the increase in the internal resistance of the cell (Zhu et al, 2015) by fouling and biofouling on the membrane surface of the separator (Kasemset et al, 2013). Fouling can decrease significantly the performance of BES. In addition, long-life fuel cell membranes applicable in real life are needed. In the following section, the most commonly used separators in MFCs will be discussed, as well as the limitations and new opportunities for anti-fouling membranes.

1.7.7 Membranes used as MFC separators

The balance of the reactions produced in electrochemical systems such as MFCs shows the formation of positive charges at the anode, while the same number of negative charges are created at the cathode. In order to maintain the electroneutrality of the system, an equivalent number of anions must be transported to the anode or cations to the cathode. Therefore, ions move through the electrolyte. The transport of ions through the electrolyte has a direct consequence on the efficiency of BES, because if the transfer rate is low, it drastically limits the rate of electron transfer at the electrodes and in turn, the electron transfer at the electrodes cannot be faster than the transport of ions through the electrolyte.

Using a membrane in between the electrodes presents the following objectives:

a) Prevention of oxygen transfer to the bioanode.

b) Avoid the transfer of substrate and other organic matter to the cathode.

c) Opposing the least possible resistance to ion transfers.

d) Allow the MFC target to be enlarged far beyond the simple production of electricity (Oliot et al, 2016).

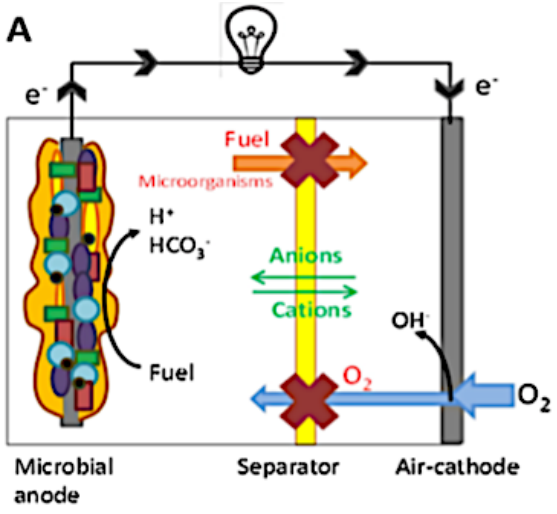


Figure 1.15. Two-compartment air-cathode MFC and the main functions of a separator (Oliot et al, 2016).

With the exception of sediment microbial fuel cells (SedMFCs), typically most bioelectrochemical systems use membranes as separators between the different compartments (Table 1.4). Different separators have been demonstrated to significantly improve the overall performance of MFCs. However, the use of separator can also cause many problems such as low electron recovery rate, unstable system performance and high costs. Recently a variety of materials, e.g., exchange membranes, size-selective separators and salt bridge, have been explored to find an efficient, cost-effective and mechanical robust separator (Li et al, 2011). Therefore, BES have recently been upgraded by integrating membrane-based treatment technologies (Yang et al, 2019).

In order to address these technological challenges, membrane-based technologies for water/wastewater treatment and energy production, such as electrodialysis, direct osmosis, reverse electrodialysis, and pressurized filtration (e.g., ultrafiltration), have been integrated into BESs. This integration has created new systems including microbial desalination cells, osmotic microbial fuel cells, pressurized filtration microbial fuel cells and reverse electrodialysis microbial cells. Depending of the use of membrane used in MFC (Osmotic UF or MF) the MFCs could generate a new kind of MFCs (Q. Zhang et al, 2016) as shown in Table 1.4. Osmotic membranes bring a new technology osmotic microbial fuel cells (Lu et al, 2015; Wang et al, 2011; E. Yang et al, 2016c; Yang et al, 2017), which generates great expectations in the future since they provide the possibility of combining great advances in membrane technology and MFCs as (Desgupta et al, 2015; Wang et al, 2012), as explained in the following section.

Moreover, NF membranes never have been tested in MFCs until now. NF membranes are in the transfer zone between porous membranes and non-porous membranes used in MFCs (Table 1.4). Therefore, these membranes have interesting characteristics to be used as separators in MFCs. Based on their very small pore size, it can be predicted that they could effectively reduce the crossover of oxygen and fuel; however, it can be expected that they create a high resistance to ion transfer compared to micro- or ultrafiltration membranes, but probably lower than ion-selective membranes, which are widely used in MFCs. Thus, NF membranes are interesting separators for MFCs that deserve to be tested.

Table 1.4. Separators used in MFC (Li et al, 2011; Oliot et al, 2016; Zhu et al, 2016a)

	Non-porous membranes				**Porous membrane**			
Type	Cation Exchange membrane (CEM)	Anion exchange membrane (AEM)	Bipolar membrane (BPM)	Reverse and Forward Osmosis (RO/FO)	Nanofiltration Membrane (NF)	Ultrafiltration membrane (UF)	Microfiltration membrane (MF)	Macrofiltration membrane (MaF)
	Ion selective			Non-Ion selective	Ion selective	Non-ion selective		
Pore diameter (Å)	/				10-50	100-1000	1000-10^4	>10^4
Merits in MFC	Nafion Normally used in MFC	Good results	The energy cost of a BPM is too high if energy production is the main objective	In FO, proton flux and anodic electrolytic conductivity are superior to the conventional proton exchange membrane (PEM),	**NOT USED**	UF membranes provided similar power densities, compared to Nafion 117	MF produced comparable power densities to Nafion 117	lower resistance than with Nafion 117

				leading to increased energy generation.				
Downsides In MFC	Expensive	In a few circumstances AEM perform less well than CEM	BPM should be reserved for specific objectives, in which pH balance is crucial	Membrane fouling led to water flux decline, but the power generation was unaffected in Osmotic-MFC (OMFC)	**PROMISING CANDIDATE**	High internal resistance due to the high interelectrode distance	Oxygen mass transfer coefficients were confirmed to be higher than that of Nafion 117 (Not good to anaerobic anodic bacteria)	Macroporous separators reject only species of very large size, such as bacteria and yeasts, or even retain only macro-particles such as granules Higher permeability to oxygen (not good to anaerobic anodic bacteria)

1.7.8 Osmotic microbial fuel cells (OsMFCs)

Osmotic microbial fuel cells represent an emerging treatment concept (Figure 1.16) by linking osmosis (Os) to microbial fuel cells (MFCs). Synergistic integration of forward osmosis (FO) into MFCs creates osmotic microbial fuel cells (OsMFCs) (Figure1.9), which possess a new function of high-quality water recovery and thus benefit water recovery to reduce the water footprint. In an FO process, water can move through a semi-permeable membrane from a high-water potential zone to a low water potential zone, due to a salt gradient that creates osmotic pressure (Qin et al, 2015).

OsMFCs create mutual benefits between the two techniques with improved performance. An OsMFC shows significantly lower internal resistance due to lower membrane resistance, higher salt accumulation, and improved ion flux, leading to higher energy generation than a conventional MFC with cation exchange membrane (Yang et al, 2017; Zhu et al, 2015; Zhu et al, 2016a). They have several advantages: reduced membrane costs, improved ion transfer and reduced susceptibility to membrane fouling compared to traditional pressure-driven membrane processes. However, as membrane fouling inevitably occurs during long-term operation, it is necessary to understand how the performance of OsMFC would be affected by membrane fouling (Zhu et al, 2016a).



Figure 1.16. Schematics of bioelectrochemical system forward osmosis (OsMFC) (Lu et al, 2015).

1.7.9 Nanofiltration- microbial fuel cells (NF-MFCs).

With pore diameters between 10 and 100 Å, NF membranes are located in a transition region between ultrafiltration and reverse osmosis membranes. Reverse osmosis and ultrafiltration membranes have a salt rejection of more than 90% and less than 5%, respectively, while NF membranes reject between 20 and 80% (Baker, 2012).

NF membranes can be classified according to the molecular weight cut-off (MWCO expressed in dal-tons (Da)), which can range from 250 to 2000 Da (Li et al, 2021). NF membranes operate with a separation mechanism based on both the size and the charge of the molecules. Thus, ions are retained by ionic charge interactions with the membrane (Jun et al, 2020b). In addition, since NF membranes have a small pore size, they can reduce oxygen and fuel crossover. However, the resistance to ion transfer may be high, but lower than ion selective membranes, which are normally used in bioelectrochemical systems. Nanofiltration membranes have not been used in MFCs or bioelectrochemical systems (Oliot et al, 2016).

Based on the above characteristics, nanofiltration membranes are an interesting candidate to be explored. However, NF membranes are known to foul especially during wastewater recovery (Mohammad and Ali, 2002), which can be considered as a serious drawback, especially for bioelectrochemical systems, which have long operating periods (M. Oliot et al., 2016).

1.7.10 Membrane fouling in MFC systems

Membrane fouling always occurs in MFC, as biofilm can be formed on PEM (CEM) surface inevitably during its long-term operation inevitably during its long-term operation (Chae et al., 2016). Intermolecular bridging by metal ions between sulfonate groups and organic foulants may play an important role in microbial adhesion and biofilm formation. The fouled PEM needs to be recovered or replaced with a new one to ensure sustainable electricity production. But the high cost of PEMs is a big barrier, especially for the scaling up and future practical application of MFCs (Xu et al., 2012a). Thus, the fouling of PEM not only deteriorates the MFC performance, but also increases the MFC operation costs. (K.-Y. Kim et al., 2014; Pellegrin et al., 2012; Xu et al., 2012a)

Zhu *et al* showed that FO could serve as a potentially tolerant separator for fouling in MFCs (X. Z. Zhu et al., 2016b). In addition, this study showed that fouling of the membrane led to an increase in the flow of ions crossing the FO membrane and better current generation in an OsMFC (lower internal resistance). Improved ion diffusion through fouling can be an important means for accelerated ion diffusion (Fig. 1.17). Fouling can increase the structure of the FO membrane and therefore its permeability for specific ions.

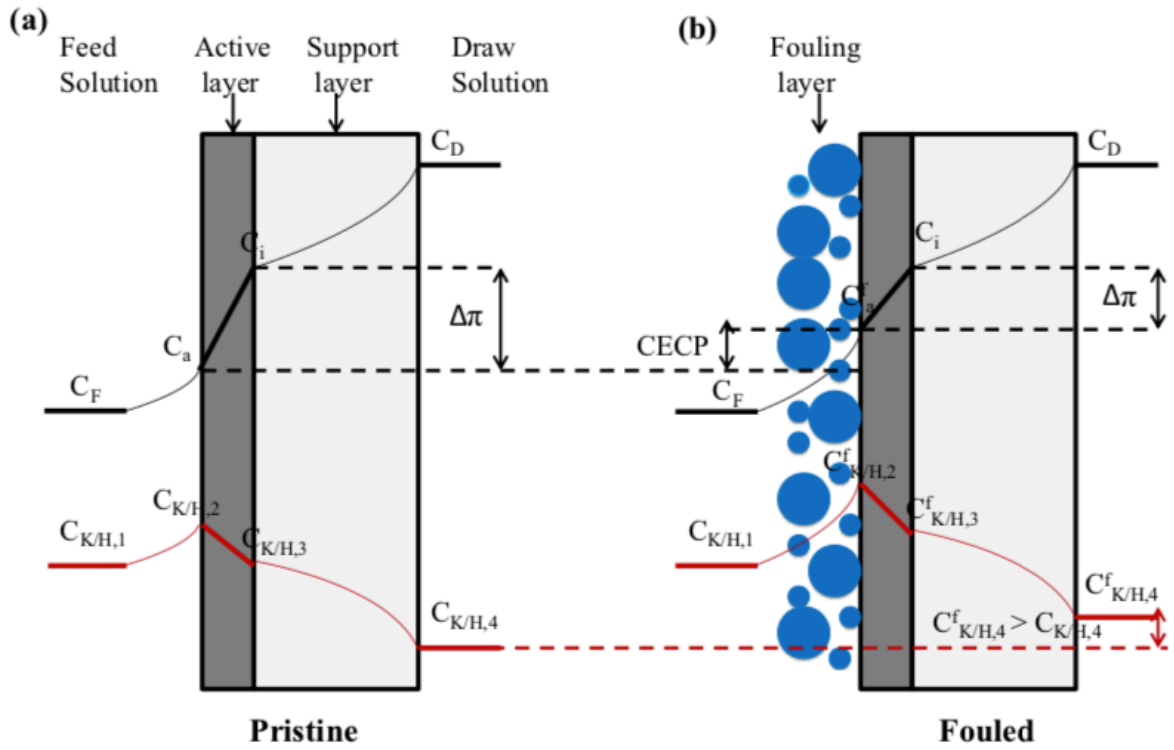


Figure 1.17. Schematic illustration of the concentration gradient of cations across (a) a pristine FO membrane and (b) a fouled FO membrane in a OsMFC (X. Z. Zhu et al., 2016a). The forward diffusion of cation (K^+, H^+, represented by red line) is improved as a result of cake-enhanced concentration polarization (CECP). The superscript f corresponds to the fouled membrane; the subscripts D and F correspond to the bulk draw and feed solution sides; a and i correspond to the active layer and the support layer-active layer interface, respectively. $\Delta\pi$ is the effective osmotic pressure.

However, fouling of the membrane can decrease the water flux, resulting in a very severe flux reduction which can lead to a non-viable process. Therefore, all efforts to have anti-fouling membranes that maintain a constant flux of water permeation are necessary, which in turn can prolong the lifetime of both the membranes and the microbial fuel cells.

1.8 Thesis motivation

As was mentioned in this chapter, azo dyes are among the most persistent pollutants in natural environments. New technologies are needed to counteract this problem. Hybrid processes such as bioelectrochemical systems (osmotic fuel cells and others) have been a novel alternative in textile wastewater treatment in recent years. However, the drawbacks generated with the fouling of separators (membranes) have led to the search for new membranes and modification methods. In order to produce antifouling membranes, both porous (MF, UF) and non-porous (FO, CEM, AEM, BPM) membranes have been used as separators, however, nanofiltration membranes have never been tested in microbial fuel cells. Nanofiltration membranes essentially share advantages with porous and non-porous membranes. With their very small pore size, the crossover of oxygen and fuel can be expected to be effectively reduced. In addition, the resistance to ion transfer could be high, but probably lower than that of ion-selective membranes, which are widely used in MFCs. All these characteristics make nanofiltration membranes excellent candidates for use as new separators in MFCs.

In turn, research on membrane technology has led to significant advances in the development of nanofiltration membranes with anti-fouling properties. One strategy to reduce membrane fouling is membrane modification by incorporating additives (e.g., nanoparticles, nanotubes, and biocidal agents). The incorporation of catalysts to membranes has produced an interesting alternative for membrane modification. Studies have shown that the mechanical properties of PEM can be improved by adding nanoparticles such as TiO_2 or SiO_2. Those catalysts can produce advanced oxidation processes (AOPs) on the membrane surface that can provide anti-fouling properties. AOPs can be activated from different sources, one of the most common being UV irradiation. However, UV lamps generate an extra cost in the operation of bioelectrochemical systems. In this thesis, AOPs based on photo-activation are an interesting alternative that is applicable in countries with high UV index, as is the case of Ecuador (Cavallos-Sierra and Ramos-Martin, 2018). This approach could decrease operating costs while using only a renewable energy source.

The present work is focused on the integration of three efficient technologies (AOPs, MFCs and membrane technology) to develop antifouling nanofiltration membranes to be used as new separators in nanofiltration microbial fuel cells for textile wastewater treatment (Figure 1.18).

1.9 Thesis objective

The overall objective of this thesis is to use the advantages of three technologies (membrane technology, advanced oxidation processes and microbial fuel cells) to develop a textile wastewater treatment process that includes antifouling and self-cleaning membranes as efficient separators. A new generation of osmotic systems, named nanofiltration microbial fuel cells, is proposed in this thesis.

The main research questions to investigate are:

- Is it technically feasible to integrate membrane technology, advanced oxidation processes and microbial fuel cells, to treat textile wastewater using anti-fouling membranes leading to a new generation of nanofiltration microbial fuel cells?

- Is it possible to develop antifouling and self-cleaning membranes from a bio-inspired membrane modification method?

- Is it possible to develop membranes with antifouling properties by using commercial catalysts (TiO_2 and ZnO) and a bio-inspired modification method?

- Are commercial nanofiltration membranes effective supports to apply the bio-inspired modification method?

- Is the novel bio-inspired membrane modification method influencing the performance of bioelectrochemical systems (BECS)?

- Is it possible to synthesize a catalyst (ZnO:Er/Al) that can be activated by visible light, effectively remove dyes from textile wastewater by solar irradiation and maintain the antibacterial activity of ZnO under visible light conditions?

- What is the performance of nanofiltration membranes modified with the new catalyst (ZnO:Er/Al) in a bioelectrochemical system Nanofiltration Fuel Cells (NF-MFC)?

1.10 Thesis outline

The content of this thesis is organized as follows: In Chapter 1, a brief review of textile wastewater treatment methodologies was presented, focusing on membrane technology, advanced oxidation processes (AOP) and Bioelectrochemical systems (BES). Mainly microbial fuel cells (MFCs), membrane fouling in membrane technology and several methodologies for the mitigation of this phenomenon are discussed. Subsequently, in Chapter 2, membrane modification was evaluated as an antifouling method, in which the effect of the ratio (TiO_2:ZnO) on the antifouling properties of bio-inspired nanofiltration membranes was evaluated, and the results obtained provide important knowledge on the efficient methodology that will be used in the next stages of evaluation of antifouling membranes in MFCs. In Chapter 3, the use of low-cost TiO_2:ZnO modified membranes with mussel-inspired polydopamine binding as microbial fuel cell membranes is analyzed. This chapter served as a preliminary evaluation of the antifouling membrane performance in textile wastewater treatment. In this part, the efficiency of the mixture of catalysts attached by bio-inspired methods to a low-cost membrane and how it influences the efficiency of a single-chamber MFC are investigated. Since the process of evaluating catalysts on membranes determined that ZnO has higher antibacterial activity compared to TiO_2, therefore, a more efficient catalyst that can be activated with visible radiation was proposed in Chapter 4. Thus, the effect of Er, Al and Er/Al dopants on the photocatalytic and antibacterial properties of ZnO nanoparticles is evaluated. In addition, this chapter assesses the improvement of the removal efficiency of the methyl orange dye under dark conditions, artificial light and solar irradiation in Quito-Ecuador. In Chapter 5, the effect of nanofiltration membranes modified with the Er-Al/ZnO photocatalyst on the efficiency of a new generation of nanofiltration microbial fuel cells is analyzed. Finally, future research prospects and technological perspectives to overcome the limitations encountered are discussed in Chapter 6.

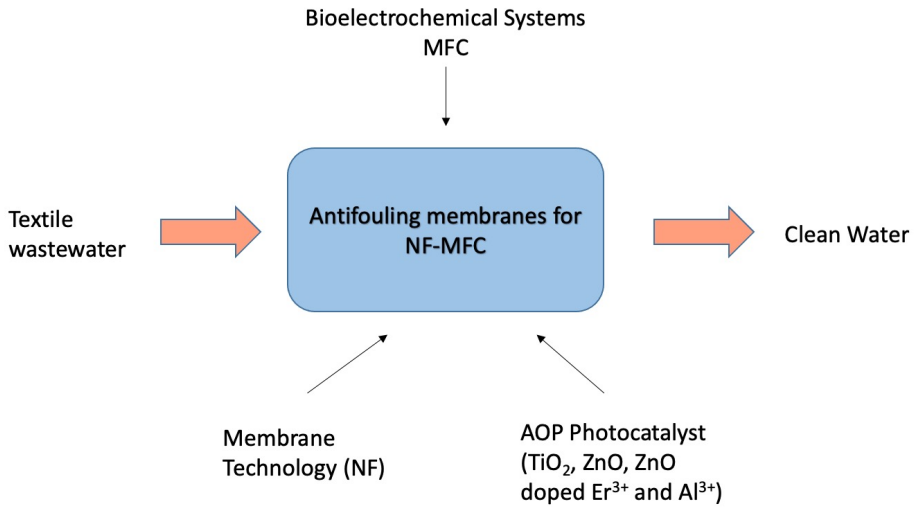


Figure 1.18. Proposed approach for wastewater treatment of the textile industry

Chapter 2. Effect of (TiO_2: ZnO) ratio on the anti-fouling properties of bio-inspired nanofiltration membranes

This chapter is based on the published research paper entitled "Effect of (TiO_2: ZnO) ratio on the anti-fouling properties of bio-inspired nanofiltration membranes" by **Raúl Bahamonde Soria**, Junyong Zhu, Irma Gonza, Bart Van der Bruggen and Patricia Luis, published in *Separation and Purification Technology*, 251, (2020), 117280.

Abstract

Membrane fouling and biofouling, which arises from the nonspecific interaction between the membrane surface and foulants, significantly impedes the efficient application of membrane technology. The addition of nanoparticles could have an impact on the properties of membranes used for nanofiltration. Nanoparticles can provide various functionalities to a membrane but, there are very few studies of the effect of mixing catalysts in PDA-modified membranes. In this study, polydopamine has been used to firmly bind a combination of nanoparticles on thin film composite (TFC) membranes. Two simple methods (a one-step and a two-step method) to assemble a multifunctional (TiO_2, ZnO) layer of nanoparticles onto a commercial NF membrane as support have been evaluated by applying fast deposition of polydopamine (PDA). The membrane performance was evaluated based on the relative water flux decline, its photocatalytic activity to remove methylene blue, and the rejection of $MgSO_4$ and NaCl.

Results showed that the modification methods did not compromise the rejection of $MgSO_4$, combined with an increase ~ 15% in the rejection of NaCl. A 25% increase in the hydrophilicity of the modified membranes compared to pristine membrane was evidenced. In addition, the two-step modification method had antimicrobial activity for an ultralow load of 0.03 wt% ZnO nanoparticles; the antimicrobial activity increased when the membrane had a combination of TiO_2:ZnO nanoparticles at 1:2 and 2:1 ratios using *Bacillus Subtilis* as model bacteria. The photocatalytic activity of the nanoparticles layer was demonstrated through the removal of methylene blue from a solution contacting the membrane when exposed to solar radiation.

Keywords: Anti-fouling; UV-photocatalysis, TiO_2 nanoparticles, ZnO nanoparticles; dopamine; nanofiltration membrane.

2.1. Introduction

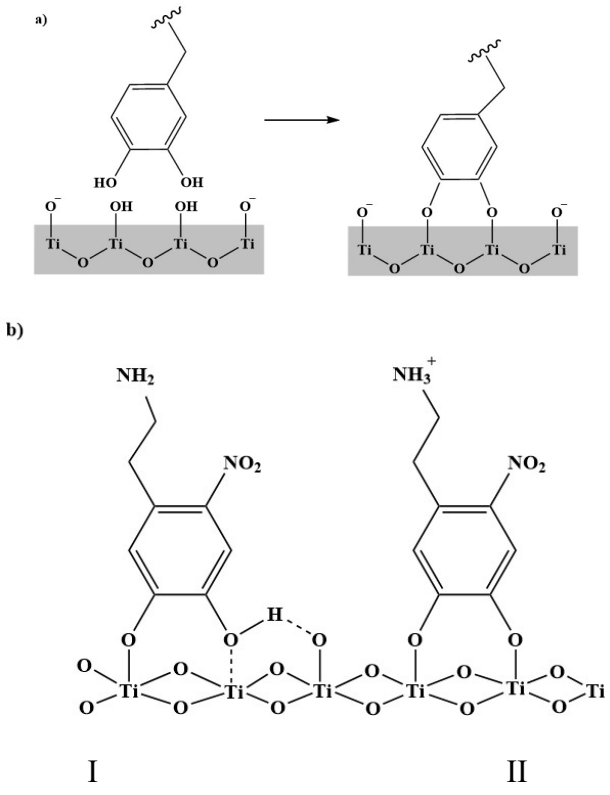
Nanofiltration (NF) is widely used for water treatment and wastewater reclamation/reuse (Bellona et al., 2004; Mohammad and Ali, 2002). NF membranes have properties in between those of ultrafiltration (UF) and reverse osmosis (RO). They are

used in a wide range of different applications, such as rejecting ions, removal of heavy metals and of organic pollutants (Fu and Wang, 2011; Mohammad and Ali, 2002).
Several studies have shown that properties such as the desalting degree, porosity, membrane morphology, charge, membrane hydrophobicity, MWCO, molecular size, charge, hydrophobicity of the solute as well as the feed water chemistry have a direct influence on the permeability, rejection, colloidal fouling and biofouling behavior of RO and NF membranes (Bellona et al., 2004; Choudhury et al., 2018; Ivnitsky et al., 2010, 2005; Khulbe and Matsuura, 2000; Vrijenhoek et al., 2001).

Membrane fouling increases operation and maintenance costs by deteriorating the membrane performance and ultimately shortening the membrane lifetime (Vrijenhoek et al., 2001). Thus, it is of utmost importance to manufacture membranes that are resistant to fouling. One of the most extended methods to produce NF membranes is via interfacial polymerization. However, conventional manufacture methods involve tedious and complicated steps. In addition, the method for manufacturing membranes may considerably affect the anti-fouling capacity of the membranes.
Recently, there has been an increasing interest in bioinspired modifications, such as the mussel-inspired chemistry of polydopamine (PDA) for membrane surface modification (Abid et al., 2017; Ding et al., 2016). Polydopamine coatings have been extensively used to change the surface properties of membranes for use in desalination (Karkhanechi et al., 2014; Kasemset et al., 2013; Wu and Hong, 2015), microbial fuel cells (K. Y. Kim et al., 2014), wastewater treatment (Kasemset et al., 2013), oil/seawater separation (Xiang et al., 2015), electrodialysis, (Vaselbehagh et al., 2014), and membrane bioreactors (L. Liu et al., 2013). These coatings have been shown to increase hydrophilicity and under water oleophobicity of many hydrophobic membrane surfaces, which can result in improved membrane performance (Kasemset et al., 2013; K. Y. Kim et al., 2014; L. Liu et al., 2013; Ryou et al., 2012; Xiang et al., 2015) and decreased microbial adhesion. (Barclay et al., 2017; K. Y. Kim et al., 2014; L. Liu et al., 2013; Miller et al., 2014, 2012).
PDA has been used due to its high material-independent adhesion and post-functionalization accessibility (Lee et al., 2007), in order to greatly accelerate the polymerization of dopamine and the deposition rate of PDA has been used $CuSO_4$ /H_2O_2 as a trigger (C. Zhang et al., 2017). $CuSO_4$ /H_2O_2 can generate reactive oxygen species (ROS) in an alkaline medium to improve the deposition rate of PDA coatings with high

uniformity and stability, which greatly expands the potential of PDA in practical applications (J. Zhu et al., 2016). Adding organic nanoparticles such as graphite oxide or inorganic nanoparticles such as TiO_2, SiO_2, Al_2O_3, Si, Ag, ZnO, ZrO_2, etc., into the thin film have had significant effects on the membrane performance (Mohammad et al., 2015) and on fouling resistance (Homayoonfal et al., 2013; Ng et al., 2013).

Dopamine can react with metal oxide nanoparticles surface through surface complexation by any of these routes: (1) via catechol as a bidentate bonding (Rajh et al., 2002); (2) bridged bidentate bonding (Dalsin et al., 2005); and (3) complex mechanism as monodentate-bidentate bonding or hydrogen bonding (Rodenstein et al., 2010; Ye et al., 2011) (Scheme 2.1). These photocatalysts deposited on the surface could help to degrade contaminants such as drugs or dyes (De Filpo et al., 2018) if the modified membranes are irradiated with UV light. The presence of nanoparticles could also have an influence on the fouling resistance of the membranes (Yang et al., 2014) .



Scheme 2.1. Possible configurations of PDA adsorbed on TiO_2: a) possible mechanism of mPEG-DOPA binding to TiO_2 surfaces; b) possible configurations: (I) monodentate binding with a hydrogen bridge to a neighboring surface hydroxide and (II) bidentate binding.

Furthermore, the anchoring of catalyst nanoparticles on membrane surfaces allows these nanomaterials to maintain maximum contact with natural organic matter, proteins and bacteria, which could reduce their adhesion and growth. The different nanoparticles on the surface of the membrane could be intimately related to an improvement in membrane performance. For this reason, some research has focused on modification of NF membranes with different nanoparticles (Table1) (R.-X. Zhang et al., 2017; Zhang et al., 2013; Zhu et al., 2018b).

Table 2.1. Comparison of the catalyst concentration on the modified surface membrane.

Support/ Membrane	**Film – Nanoparticles**	**Solution catalyst concentration (%)**	**Propriety of membrane**	**Modification method**	**Ref.**
PES	MPD/FeO	0.05-0.2	Water treatment Anti-fouling activity	Pre-seeding interfacial polymerization method	(Lakhotia et al., 2019)
RO-PSF	PDA/Ag Nano particles	1	Anti-microbial modification	PDA coating and in situ formation of AgNP	(Z. Yang et al., 2016)
FO-PA TFC	PDA- Mg_3 Al- CO_3(LDH)	0.1	Chlorine and fouling resistance	Two modification strategies as deposition and dip-coating were compared.	(Lu et al., 2017)
PU nanofibers	PDA-ZnO	0.5	Photocatalytic and antimicrobial	Combining of electrospinning, surface functionalization and hydrothermal treatment	(Kim et al., 2017)
Carboxy methyl cellulose	Chitosan-ZnO	0.5- 2	Antifungal properties	Casting method	(Noshirvani et al., 2017)

Table 2.1 Continued.

Support/ Membrane	Film – Nanoparticles	Solution catalyst concentration (%)	Propriety of membrane	Modification method	Ref.
PAN UF sheet membranes	**PDA – Cu**	**0.3**	**Elevated salt transport of antimicrobial membrane**	**Two-step deposition and co-deposition**	**(J. Zhu et al., 2016)**
UF PI	Co-polyamide TiO_2	0.05	Solvent resistant nanofil-tration membranes	In situ interfacial incorporation of TiO_2 nanoparticles along with fabrication of co-polyamide network on a polyimide (PI) support.	(Peyravi et al., 2014)
PES	PDA - TiO_2	0.1-0.5	Good hydrophilic performance	Two-step deposition	(Zhang et al., 2013)
PVD	PVDF - (TiO_2@PDA) Nanoparticles	1	Multiple antifouling capacities	Hybrid membranes fabricated by non-solvent induced phase in-version (NIPS)	(Zhao et al., 2015)
NF PA - TFC	PDA - TiO_2 PDA - ZnO PDA–TiO_2:ZnO	0.01-0.05	Photocatalytic antifouling activity	Two-step deposition and co-deposition)	This Work

In this study, we have introduced and compared two simple methods to assemble a multifunctional (TiO_2, ZnO) layer of nanoparticles onto a commercial NF membrane as support by applying the fast deposition of PDA. One of these techniques refers to a

conventional two-step deposition by the aid of a strongly adhesive PDA intermediate layer followed by nanoparticles loading. The second strategy is the simultaneous co-deposition of PDA and nanoparticles. The influence of the catalyst (TiO_2, ZnO and mixtures) and the two modification strategies are compared and studied taking into account surface morphology, selectivity for specific solutes and permeability. The antimicrobial activity of the membranes is also studied by using *Bacillus Subtilis* as model bacteria.

2.2. Experimental

2.2.1 Materials

A commercial polyamide nanofiltrationmembrane, NFX (150-300Da), was purchased from Synder filtration (USA). Dopamine hydrochloride (99 wt%) and tris(hydroxymethyl) aminomethane (Tris, 99.8% by weight) were acquired from Acros Organic-Belgium. Copper (II) sulfate ($CuSO_4$, 99 wt%), hydrogen peroxide (H_2O_2, 30wt%), hydrochloric acid (HCl, 1 M) and sodium hydroxide (NaOH, 98 wt%), titanium (IV) oxide nanopowder (anatase, <25 nm, 99.7 wt%), zinc oxide (ZnO, <50 nm 99 wt%), magnesium sulfate ($MgSO_4$, 98 wt%) and sodium chloride (NaCl, 99 wt%), were acquired from Sigma-Aldrich (Diegem, Belgium). Unless specified, all solutions were prepared in deionized (DI) water purified by a Milli-Q ultrapure unit. All reagents and solvents were commercially available and used as received.

The culture media Iso Sensitest Broth (Oxoid CM 0473) containing 0.8 wt% Agar bacteriological N° 1 (Oxoid LP0011) was used for growing *Bacillus Subtilis* (BGA) spore suspension (Merck 1.10649). The media was sterilized at 121 °C for 45 min and cooled down to 45 - 50 °C before adding 0.4 wt% of glucose and B. Subtilis strain at the required concentration.

2.2.2 Modification of the NFX nanofiltration membrane

NFX-TFC membranes (NF) were used for all surface modification procedures. The commercial NF membranes were immersed in distilled water for 12 h before surface

modification. In addition, all the membranes used in this study were stored in distilled water until use.

The methodology used to modify the membranes has been reported by Zhang et al (R.-X. Zhang et al., 2017). Two methods have been studied: 1) fast co-deposition of PDA, in which catalyst nanoparticles are added in one step with the PDA according to compositions in Table 2.1, and 2.2) binding method in two steps, in which a fast PDA deposition on the NF membrane surface is followed by binding catalyst nanoparticles at different compositions (Table 2.2) on PDA modified NF membranes. The surface modification of NF membranes was done in a membrane holder.

Table 2.2. Preparation conditions of modified membranes: i) co-deposition method (one step modification), indicated as NF-Xa membranes, and **ii)** binding method (two steps modification), indicated as NF-Xb membranes.

	Membrane	Dopamine (mg mL^{-1})	TiO_2 Content (wt%)	ZnO Content (wt%)	Deposition PDA time (h)	Catalyst co-deposition time (h)	(TiO_2:ZnO) Ratios
	NF						
	NF-PDA	2	0	0	1	0	-
NF-1	NF-1a	2	0.01	0	1	0	-
	NF-1b	2	0.01	0	1	1	-
NF-2	NF-2a	2	0.03	0	1	0	-
	NF-2b	2	0.03	0	1	1	-
NF-3	NF-3a	2	0.05	0	1	0	-
	NF-3b	2	0.05	0	1	1	-
NF-4	NF-4a	2	0	0.01	1	0	-
	NF-4b	2	0	0.01	1	1	-
NF-5	NF-5a	2	0	0.03	1	0	-
	NF-5b	2	0	0.03	1	1	-
NF-6	NF-6a	2	0	0.05	1	0	-
	NF-6b	2	0	0.05	1	1	-
NFX-1	NF-X1a	2	0.005	0.005	1	0	1:1
	NF-X1b	2	0.015	0.015	1	1	1:1

Table 2.2 continued

NFX-2	**NF-X2a**	**2**	**0.003**	**0.007**	**1**	**0**	**1:2**
	NF-X2b	2	0.010	0.020	1	1	1:2
NFX-3	NF-X3a	2	0.007	0.003	1	0	2:1
	NF-X3b	2	0.020	0.010	1	1	2:1

3.2.2.1. One step - fast co-deposition procedure

Copper sulfate (8.3 mM) was dissolved in 30 mL Tris buffer solution (50 mM, pH 8.5); then, the catalyst amounts indicated in Table 3.2 for the membranes NF-Xa were added in this suspension. The resulting suspension was agitated during 3 h at 1000 rpm and subsequently, the suspension was further treated using sonication for 1 h in a water bath (20°C). Next, 40 µL H_2O_2 solution (19.6 mM) was added into the suspension as the trigger of the rapid deposition and mixed, which was followed by the addition of dopamine hydrochloride (2 mg mL^{-1}).

The solution was then poured onto the membrane surface in the membrane holder for 1 h. Afterwards, the membrane was rinsed 5 times with distilled water to remove the excess polymerization residues and catalysts.

2.2.2.2. Two steps modification- Binding procedure

An aqueous solution of dopamine was prepared by dissolving dopamine hydrochloride (2 mg mL^{-1}) in Tris buffer solution (pH 8.5, 50 mM). In 30 mL of this fresh dopamine aqueous solution, $CuSO_4$ (8.3 mM) was dissolved with 40 µL H_2O_2 (19.6 mM). The final solution was poured onto the membrane surface placed in the membrane holder. After 60 min, the membrane was rinsed using distilled water for 5 min in order to remove most of the residual unbound polydopamine. Afterwards, the membranes were dried by compressed air for 5 min (R.-X. Zhang et al., 2017; Zhu et al., 2018a).

As the second step, different amounts of TiO_2 and ZnO nanoparticles (Table 3.2 - membranes NF-Xb) were added to a Tris buffer solution (pH 8.5, 10 mM) and agitated

for 3 h at 1000 rpm by using a magnetic stirring plate. The suspensions of TiO_2 and ZnO nanoparticles and the mixtures were further treated by sonication for 1 h in a water bath (20ºC) to obtain a well dispersed suspension of nanoparticles. The prepared catalysts suspensions (30 mL) were added over the PDA modified NF membrane in the membrane holder and placed for 1 h at room temperature to allow the deposition of nanoparticles on the membrane surface. Afterwards, the membranes were carefully removed from the membrane holder and rinsed five times with distilled water.

2.2.3. Membrane characterization

2.2.3.1 Surface morphology

The morphology of the membrane surface was evaluated by scanning electron microscopy (SEM) (Philips XL30-FEG) composed of an energy dispersive X-ray (EDX) detector. Each sample was dried before analysis in a vacuum chamber. Then, the membranes were submerged in liquid N_2 and fractionated, and afterwards they were coated with graphite.

2.2.3.2. Water contact angle

Water contact angle measurements were measured to evaluate the hydrophilicity of the modified membranes. A contact angle goniometer (OCA20, Dataphysics Instruments, Germany) was used. A drop of distilled water (2.0 μL) was placed on the membrane surface. Static contact angles were measured using a circle fitting method by the drop shape analysis software.

2.2.3.3. Filtration performance test

Water flux and salt retention were characterized using a steel dead-end cell (HP4750 High Pressure Stirred Cell Kit). Membrane samples were tested at 4 bar. The water flux (J), water permeability (P_w) and rejection (R) of prepared membranes were calculated using the following equations:

$$J = V/(A\ \Delta t) \quad (1)$$

$$P_w = J/\Delta p \quad (2)$$

$$R = (1\text{-}C_p/C_f) \times 100\% \quad (3)$$

where V is the volume of permeate (L), A is the effective membrane area (22.9 cm^2), Δt is the filtration time (h) and Δp is the applied pressure (bar). C_p and C_f are the salt concentrations of permeate and feed solutions (g L^{-1}) and were measured with an electrical conductivity meter (Thermo Scientific Orion Star A212). The dead-end cell was filled with 200 mL of solution (1 g L^{-1} NaCl and 1 g L^{-1} $MgSO_4$ in distillate water) and tested at room temperature. Once the membrane system reached a steady state, the permeate was collected. The solution into the dead cell was stirred at 800 rpm to reduce concentration polarization. The experiments were carried out in triplicate.

2.2.4. Antibacterial capacity of modified membranes

a) Iso Sensitest

The modified method proposed by Khorshidi (Khorshidi et al., 2018) was used to test the antibacterial activity of both the unmodified and modified membranes. An *Iso Sensitest* broth media containing *B. subtilis* spore suspension was incubated for 24 h at 32 °C in order to promote the bacterial growth. Either the unmodified and modified membranes were cut into pieces of 4.5cm^2 and placed at the bottom of separate petri plates. Then, 2 mL of bacterial solution was carefully poured onto the membrane surface. Two UV lamps (254 nm, 6 W) were placed at a height of 10 cm from the open surface of petri plates. After 30 minutes of UV exposition over each membrane containing the 2 mL of bacterial solution. 30 µl of the solution covering the membrane surface were taken and diluted 10:1. The resulting solution was poured onto Petri plates of 90 mm containing 8 mL of *Iso Sensitest* broth media with 0.8% of Agar Nº1 to solidification of the media. The plates were incubated for 18 hours at 30 °C, the antibacterial property of the membrane was determined by the growing radius of each bacterial colony formed on the plates.

b) Disk diffusion method

A second type of antibacterial tests was performed via the disk diffusion method. The methodology proposed by Lashkenari (Soleymani Lashkenari et al., 2019) was followed. The culture media was seeded with *B. Subtilis* strain at a final concentration of 10^4 (colony forming units) CFU mL^{-1} and 0.4% of glucose before filling the sterile Petri dishes with 8 mL of prepared media. The prepared plates were stored at 4ºC and kept one week as maximum before use. For the evaluation of the antibacterial activity, disks of 1 cm^2 of modified and pristine membranes were placed on the plates and incubated for 18 h at 32ºC in dark conditions. Antibacterial capacity of each membrane was evaluated by the presence of an inhibition zone and size of the inhibition zone around the membranes.

2.2.5. Photocatalytic performance of membranes for dye degradation under light conditions.

The photocatalytic activity of the prepared membranes was studied by degrading an aqueous solution of 10 mg L^{-1} methylene blue (99 wt%, Sigma Aldrich, supplied by Merck Ecuador). The degradation of methylene blue was tested under the influence of sunlight in Quito (Ecuador) between 10th September and 10th October 2018 (Ambient Secretary, 2018). The time period used in the evaluation was kept constant from 11:00 a.m. to 2:00 p.m. to standardize the UV irradiation (Rajamanickam and Shanthi, 2012). The tests were performed when the UV Index in Quito - Ecuador started in 10, according to the Ecuadorian National Institute of Meteorology and Hydrology. The membranes (22.9 cm^2 membrane diameter) were exposed to light irradiation for 3 h in a membrane holder; 20 mL of dye aqueous solution were added in the membrane holder without magnetic stirring. After the adequate irradiation time, 5 mL of the solution was collected and analyzed using UV-Vis spectrophotometer at a wavelength of 662 nm . All experiments were made in triplicate reporting average values, with error below 5%.
The removal efficiency was evaluated using Equation (4):

$$\%\, removal\ efficiency = \frac{C_0 - C}{C_0} x100 = \frac{A_0 - A}{A_0} x100 \qquad (4)$$

where C_o and C are initial and final concentrations of methylene blue, respectively. A_o is the initial absorption and A is the final absorption of methylene blue.

2.3. Results and discussion

2.3.1. Polymerization time

Dopamine generally forms a thin hydrophilic and adherent coating by oxidation under alkaline conditions or spontaneously by self-polymerization (Hong et al., 2012). However, the polymerization of dopamine is a slow process (Ball, 2018). In this work, a rapid deposition strategy was used to speed up the process. All solutions underwent a rapid color change due to the influence of Cu^{2+} and H_2O_2 on the self-assembly of the thin polydopamine films. Cu^{2+} and H_2O_2 generate a multitude of reactive oxygen species in an alkaline medium (pH 8.5); these reactive oxygen species are added to the aromatic rings of the polydopamine and significantly accelerate the deposition rate of PDA coatings with high uniformity and stability (Barclay et al., 2017).

A

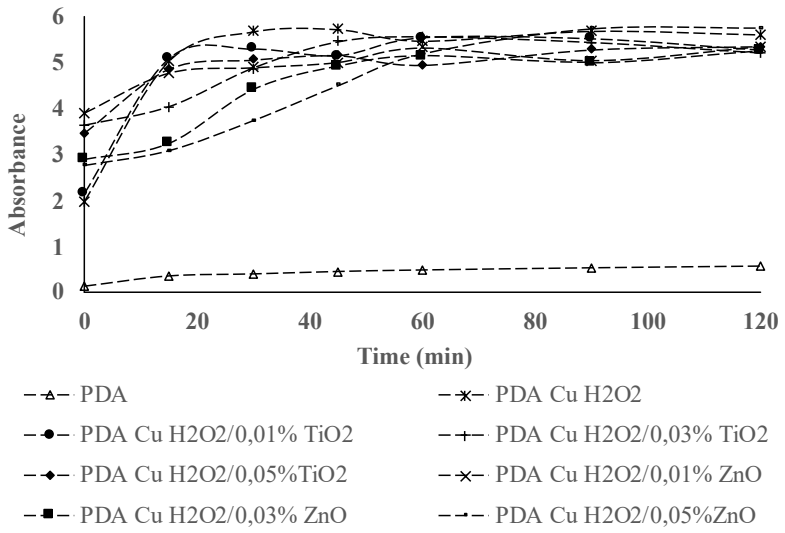


Figure 2.1. Polymerization time analysis: UV-Vis absorbance at 403 nm for dopamine solutions (a) PDA solutions without $CuSO_4/H_2O_2$ (b) PDA+$CuSO_4/H_2O_2$, (c) PDA+$CuSO_4/H_2O_2$/ 0.01%TiO_2, (d) PDA+$CuSO_4/H_2O_2$/0.03%TiO_2, (e) PDA+$CuSO_4/H_2O_2$/0.05%TiO_2, (f) PDA+$CuSO_4/H_2O_2$/0.01%ZnO, (g) PDA+$CuSO_4/H_2O_2$ /0.03%ZnO, (h) PDA+$CuSO_4/H_2O_2$/0.05%ZnO. The dashed lines are added to guide the eye.

Figure 2.1 depicts the change of UV-Vis absorbance at 403 nm for various dopamine solutions. When $CuSO_4/H_2O_2$ was not added, the absorbance increases from

0.2 to 0.5, indicating that the polymerization has started. However, this polymerization method was less efficient than the solution with $CuSO_4/H_2O_2$. The absorbance was gradually increased from 2.80 to around 5.22 for all cases using $CuSO_4/H_2O_2$ in 60 min. This result confirms a fast polymerization using $CuSO_4$ as initiator. After this time, the value was remained constant, showing that the polymerization time of dopamine is completed in 60 min. A polymerization time of PDA in membranes around 60 min to achieve a complete polymerization was also observed in previous studies (Liu et al., 2016; R.-X. Zhang et al., 2017; Zhu et al., 2018b). For this reason, the polymerization time was set at 60 minutes for all experiments. In addition, recent research have showed that this method could generate a homogeneous thickness close to 45 nm by moderate covalent polymerization of dopamine (C=C-C=O) (Bernsmann et al., 2011), and it can form a stable PDA layer on the membrane surface (Liu et al., 2016; R.-X. Zhang et al., 2017).

2.3.2. Morphology of membrane surface

The polyamide layer was modified by embedding TiO_2 and ZnO nanoparticles. Dopamine can react with metal oxide nanoparticles surface through surface complexation by any of these routes (Scheme 3.1).

a) One-step method (co-deposition)

The SEM images in Figure 2.2 confirm the change on the pristine NF surface with the one-step modification (co-deposition) method. The cross-section of the membranes can be observed in Figure A2.1 in Appendix 1 Information.

The nanoparticles are present on the surface of NF-PDA due to the reaction of the active functional groups (hydroxyl groups in catechol) of PDA with TiO_2 and ZnO nanocrystals (Guvendiren et al., 2008; Ou et al., 2010; Ran et al., 2018; Zhao et al., 2015) and homogeneous nucleation between metal oxides nanoparticles (scheme 2.2) (Ou et al., 2010). The excessive weight of the PDA coated nanoparticles is removed immediately after washing the membrane. However, the one-step method presented a limited amount of nanoparticles on the surface. The nanoparticles can be covered by PDA and form lumps on the surface of the membrane. In addition, two aspects could be also observed: i) the TiO_2 nanoparticles adhere more efficiently in comparison with ZnO nanoparticles, and

ii) the size difference of nanoparticles is more evident as the concentration of catalyst increases from 0.03 to 0.05 wt% in comparison with 0.01wt%, where the distribution and nucleation size of nanoparticles on the surface is more homogeneous (Figure 2.2c and f). Concentrations of catalyst lower than 0.03% would thus give a homogeneous distribution on the surface during the copolymerization.

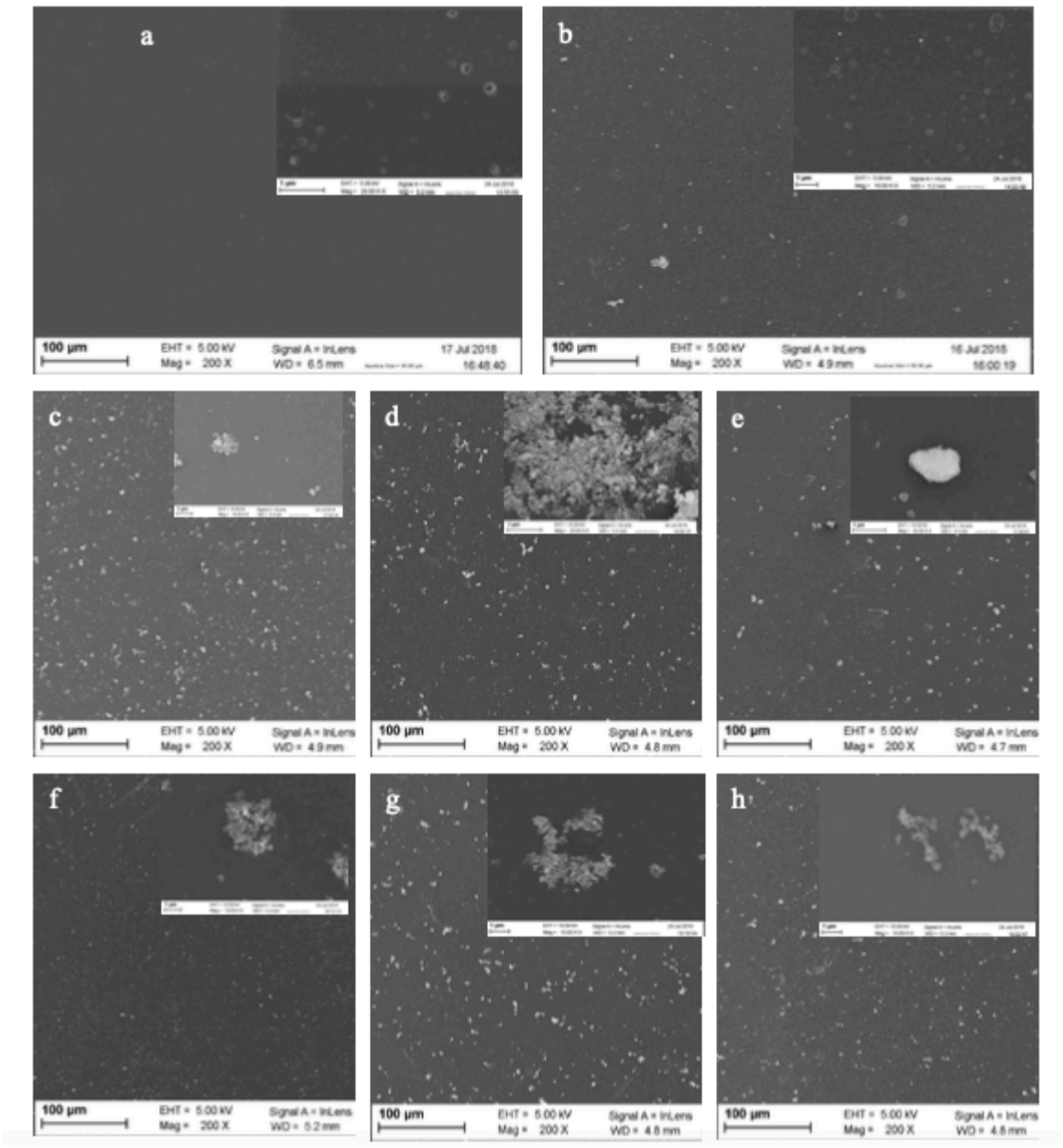
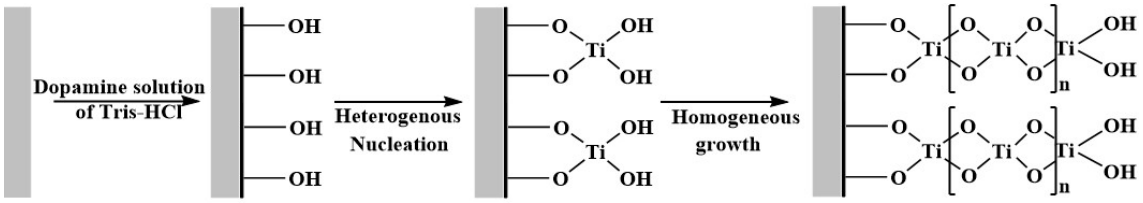


Figure 2.2. Surface SEM images of membranes using the co-deposition method (one-step): (a) Pristine, (b) NF-PDA, (c) NF-1a, (d) NF-2a, (e) NF-3a, f) NF-4a, g) NF-5a, h) NF-6a.



Scheme 2.2. A scheme of TiO_2 deposition on the polymer substrates mediated by PDA(Lee et al., 2007; Ou et al., 2010)

b) Two-step method (binding method)

The SEM images in Figure 2.3 show the membrane surface after the two–step modification (binding) method. The surface of the modified membranes showed a wide range of nanoparticle sizes. This could be due to the heterogeneous nucleation followed by homogeneous nucleation of nanoparticles (scheme 2.2) This phenomenon is more evident when the concentration of catalyst increases from 0.01% to 0.05% and with TiO_2. Previous research focused on concentrations of 0.05% TiO_2 (Noshirvani et al., 2017; R.-X. Zhang et al., 2017; Zhang et al., 2013). However, our observations prove that a load of 0.03% has a more homogeneous distribution for the two studied metal oxides (TiO_2 and ZnO).

Figure 2.3 show fewer ZnO nanoparticles on the membrane surface compared to TiO_2 nanoparticles. This can be explained by the fact that ZnO nanoparticles have only one oxygen atom in their structure and the heterogeneous nucleation with the PDA surface is not as efficient as with TiO_2 nanoparticles, which have two oxygen atoms (Kim et al., 2017).

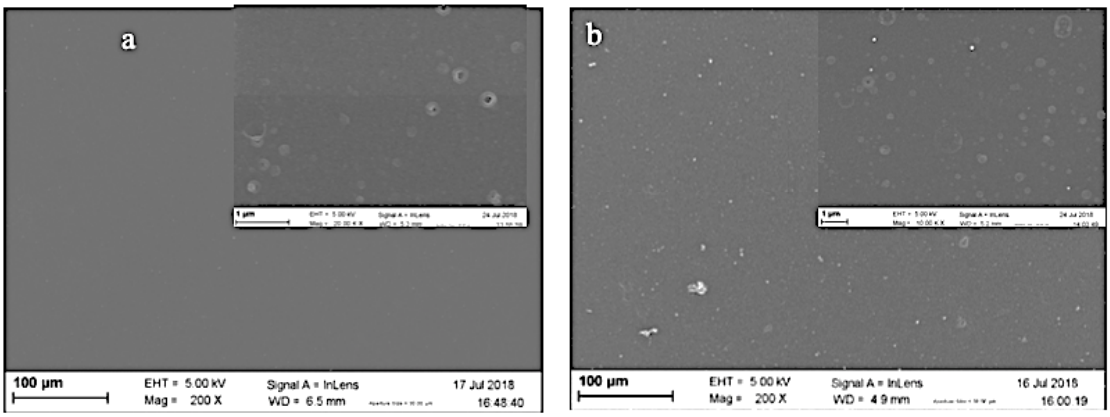


Figure 2.3. Surface SEM images of the membranes with the binding method (two steps) (a) Pristine, (b) NF-PDA, (c) NF-1b, (d) NF-2b, (e) NF-3b, f) NF-4b, g) NF-5b, h) NF-6b.

Figure 2.3 continued

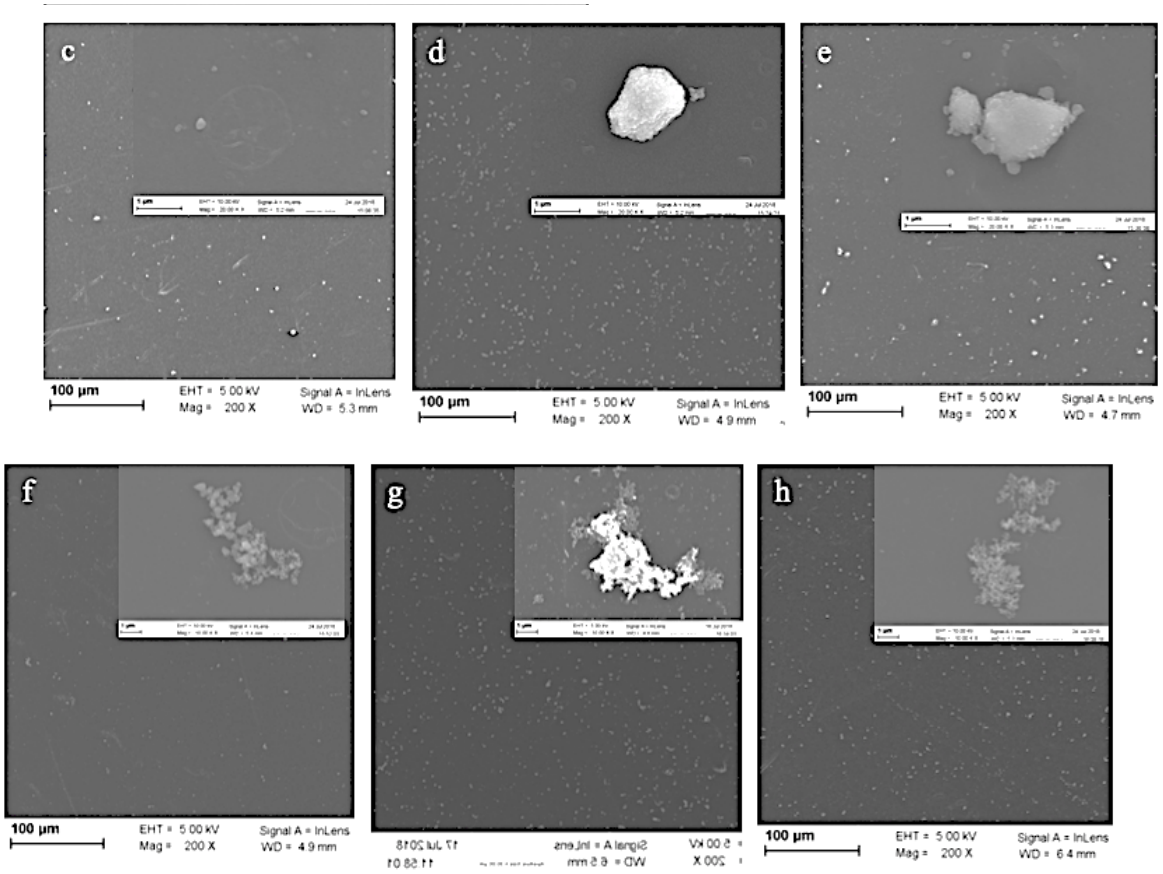
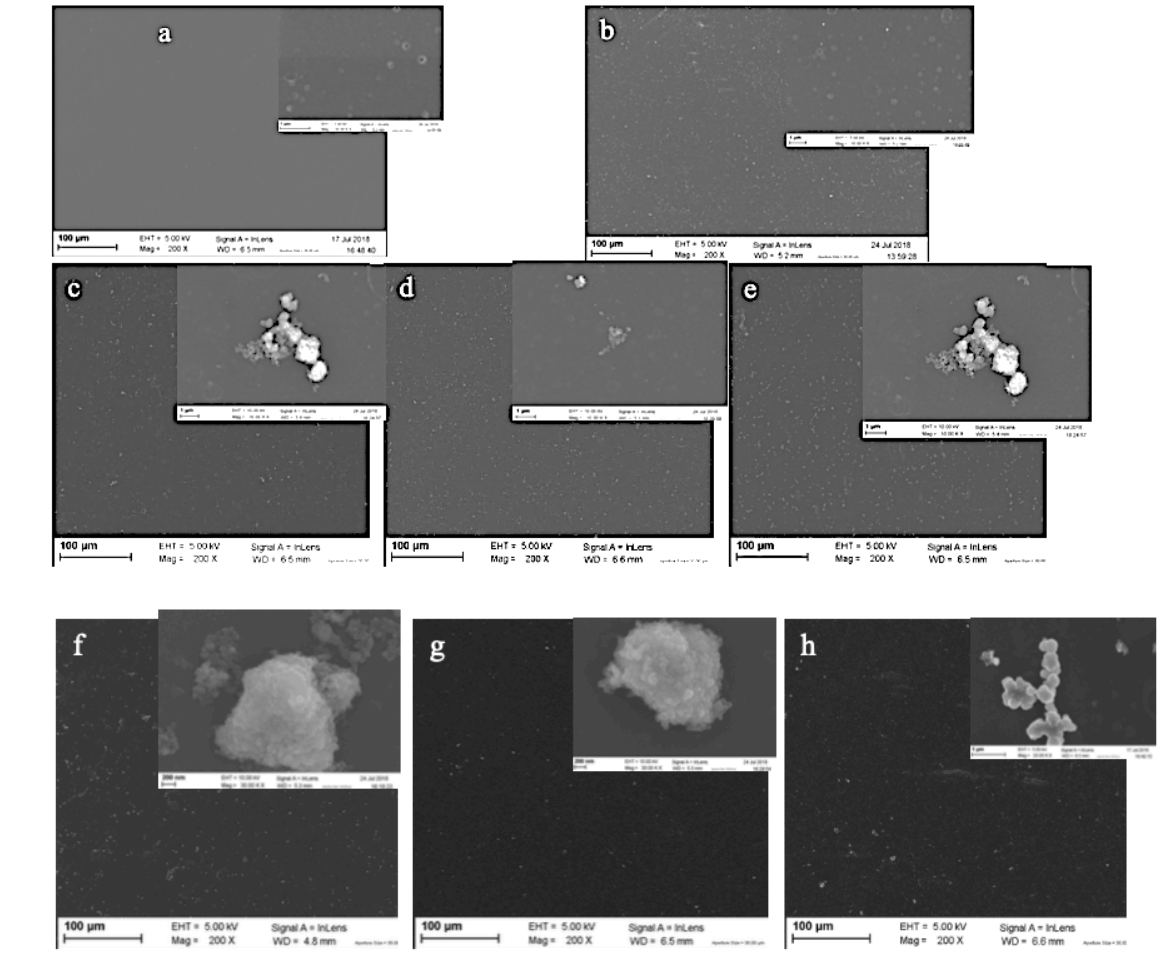


Figure 2.3. Surface SEM images of the membranes with the binding method (two steps) (c) NF-1b, (d) NF-2b, (e) NF-3b, f) NF-4b, g) NF-5b, h) NF-6b.

c) One-step and two-step methods with TiO_2:ZnO mixtures

Figure 2.4 represents images of the pristine membrane, modified membranes by co-deposition with 0.01 wt% total nanoparticles and ratios TiO_2:ZnO (1:1, 1:2, 2:1) and, modified membranes by binding with 0.03 wt% total nanoparticles and ratios TiO_2:ZnO (1:1, 1:2, 2:1). Membranes modified by the co-deposition method showed a better homogeneous nanoparticles distribution in the film in comparison with the binding method.



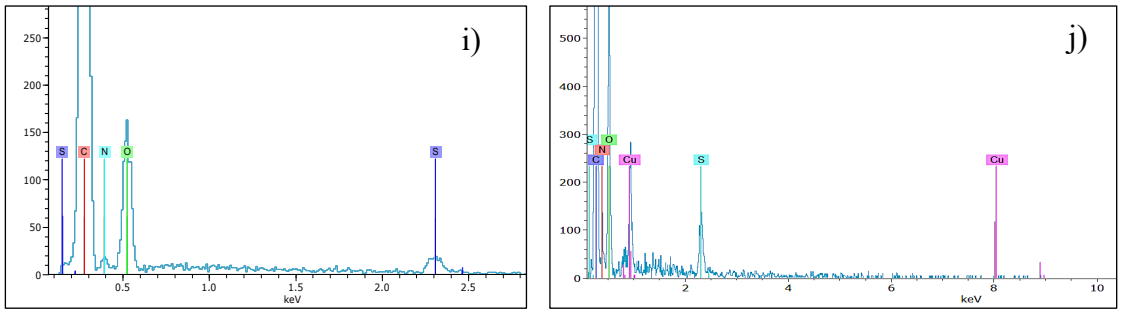


Figure 2.4. Surface morphology of the a) Pristine membrane; b) NF PDA; PDA NFX Co-deposition method 0.01 wt% total mixture Nanoparticles, with ratios (TiO_2:ZnO): c) 1:1 NFX-1a, d) 1:2 NFX-2a e), 2:1 NFX-3a. Two steeps - binding method 0.03 wt% total mixture nanoparticles, with ratios (TiO_2:ZnO) f) 1:1 NFX-1b, g) 1:2 NFX-2b, h) 2:1 NFX-3b. and EDX spectra of: i) pristine membrane; j) PDA pristine modified membrane; k) TiO_2 binding on PDA surface; l) ZnO binding on PDA surface; m) mix of both catalyst (TiO_2:ZnO).

Figure 2.4 continued

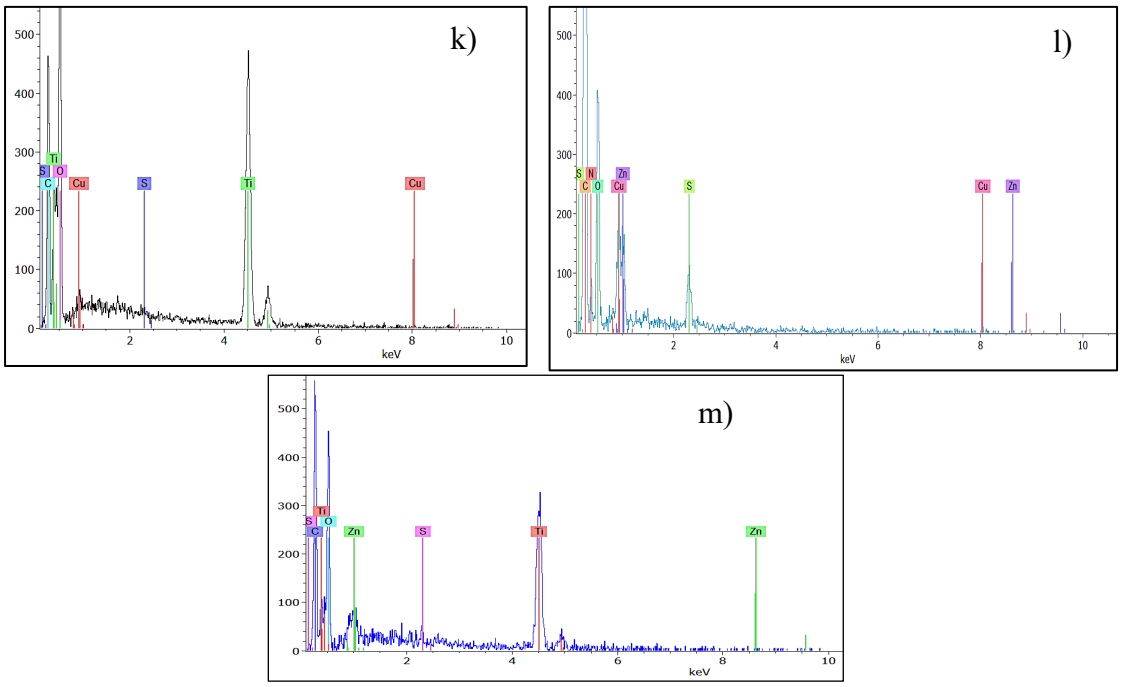


Figure 2.4. Surface morphology of the Two steeps - binding method 0.03 wt% total mixture nanoparticles, with ratios (TiO_2:ZnO) k) TiO_2 binding on PDA surface; l) ZnO binding on PDA surface; m) mix of both catalyst (TiO_2:ZnO).

Elemental analysis by EDX suggests that the membranes were covered with catalysts. EDX patterns of TiO_2, ZnO and mixtures of them are displayed in Figure. 2.4i–m. The spontaneous immobilization of catalysts can be attributed to the reducing catechol groups contained in PDA. At the same time, the O- and N-based ligand sites in PDA could serve as anchors for the resulting nanoparticles.

2.3.3. Membrane hydrophilicity

Superhydrophilic surfaces could be self-cleaning, such as *Nelumbo nucifera* (lotus leaves) and *Ruellia devosiana* (Cui et al., 2019; Koch and Barthlott, 2009). In water purification, hydrophilic surfaces are preferred, which can be achieved by changing both surface roughness and free surface energy (Yun et al., 2014; R.-X. Zhang et al., 2017). A change of surface roughness on the membrane surface can be achieved by modifying the surface with PDA or by adding metal oxide nanoparticles on the surface of the

membranes (Mansouri et al., 2010; Sotto et al., 2011) as in the section 2.3.2. Adding nanoparticles on the membrane can cause a change in the surface energy of the PDA and hence this can cause the hydrophilicity of the membrane change, because nanoparticles tend to be attracted to each other through van der Waals forces and the surface of the nanoparticles have a surface energy of their own. In addition, the contribution to the hydrophilicity of the membrane can also be caused to the fact that the oxygen in TiO_2 and ZnO can be bridging or threefold coordinated and then, this oxygen reacts causing vacancies that produce dissociative adsorption of water at the vacancy site (Lee et al., 2007; Watanabe et al., 1999).

Figure 2.5 shows the water contact angles of pristine and modified membranes. The pristine membrane had low contact angle, this showed that the membrane had hydrophilic proprieties. For the PDA membrane the contact angle of the membranes is only slightly increased in comparison with the pristine membrane, similar to the work of Zhang *et al* (R.-X. Zhang et al., 2017). In this case, PDA itself is a hydrophilic material and contains hydrophilic functional groups, such as amines and catechols (Ang et al., 2019; Zangeneh et al., 2018). However, the PDA membrane was not found more hydrophilic than the pristine membrane, this is probably related to a solid-liquid-air interface, formed between the water droplet and the polydopamine surface. The modification of the membrane surface with polydopamine can generate roughness in the membrane (ridges and valleys). When the nanoscale narrow valleys of the polydopamine layer make contact with water droplets, water may not penetrate into the surface cavities, which results in the formation of air pockets and leads to a composite interface (Bhushan, 2012).

Membranes containing nanoparticles on the PDA-modified membrane surface were more hydrophilic than the pristine and PDA coated membranes. For the one-step method, membranes modified with PDA and nanoparticles improved the hydrophilicity. This modification caused a decrease in the contact angle value because nanoparticles increased the hydrophilicity. Furthermore, the membrane could be still negatively charged even after the modification. For this reason, the rejection of ions was also high during the nanofiltration tests, as shown in the next section (Figure 2,7a).

The membranes modified by the two-step binding method showed a greater hydrophilicity compared to the membranes modified by the one-step co-deposition method, which could be explained by the coating of the surface of metal oxide nanoparticles by polymerization of polydopamine in the co-deposition method (Yun et al., 2014; R.-X. Zhang et al., 2017) whereas in the two-step method, a continuous growth of the nanoparticles that bind to the PDA layer allows for a more hydrophilic surface.

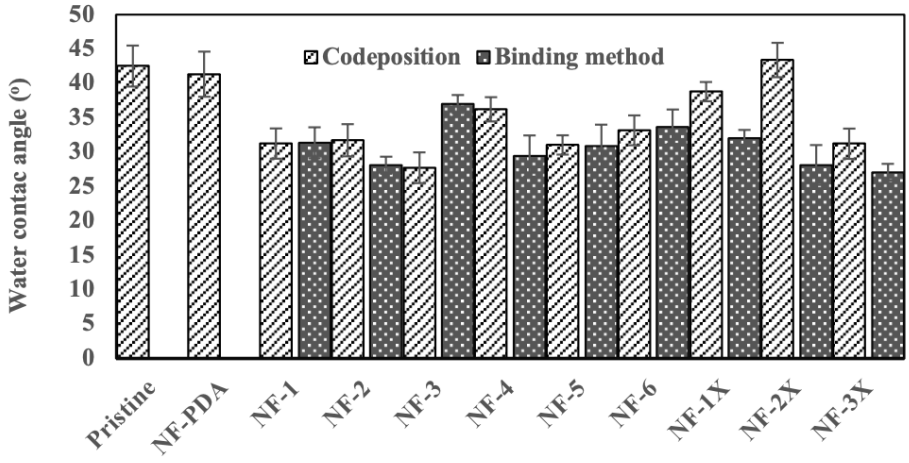


Figure 2.5 Static water contact angles of the pristine and modified membranes

2.3.4. Water permeability

Figure 2.6 shows the average water permeability of the pristine membrane and each modified membrane. The pristine membrane achieved a water permeability of 7.2 L m^{-2} h^{-1} bar^{-1}. After PDA layer deposition, the water permeability dropped to 6.1 L m^{-2} h^{-1} bar^{-1}. Interestingly, co-deposition membranes coated with TiO_2 nanoparticles achieved a higher permeability in comparison with the PDA modified membrane. However, the ZnO nanoparticle-coated membranes did not show a statistical difference in permeability decrease compared to the PDA-coated membranes. Furthermore, for the two-step coating, the water permeability decreased progressively for both the TiO_2 and ZnO nanoparticle modified membranes. This could be attributed to the strong binding of the nanoparticles through electrostatic attraction in the pores of the membrane surface for the two-step method.

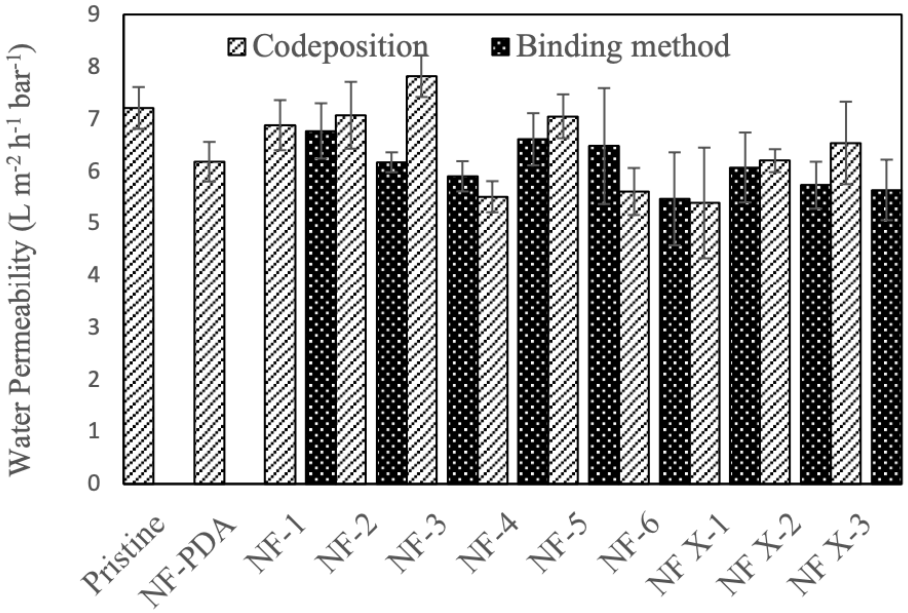


Figure 2.6. Water permeability of the modified nanofiltration membranes using PDA and various TiO_2/ZnO ratios by binding and co-deposition methods; Pristine (NF), NF-PDA 0% wt catalyst, NF-1, 2 and 3, which have 0.01, 0.03 and 0.05%wt of TiO_2 respectively and NF-4, 5 and 6 which have 0.01, 0.03 and 0.05%wt of ZnO respectively and mixtures of catalyst, using two methods; co-deposition in total composition 0.01%wt (TiO_2:ZnO) ratios 1:1, 1:2 and 2:1 for NFX-1, 2 and 3 respectively, and binding method in total composition 0.03%wt (TiO_2:ZnO) ratios 1:1, 1:2 and 2:1 for NFX-1, 2 and 3 respectively.

For the nanoparticles mixture (TiO_2:ZnO) applied in the co-deposition and binding methods, all the prepared membranes by both methods showed a lower permeability than the pristine membrane. At the same time, Figure 2.6 also shows that the water permeability improves when the concentration of ZnO nanoparticles is higher than the concentration of TiO_2 nanoparticles by the co-deposition method. This may be because the catalysts (TiO_2:ZnO) compete for binding sites on the membrane surface; ZnO does not have a very strong bond with the PDA surface because it has only one oxygen in its structure to form a complex with the PDA. Therefore, when the concentration of ZnO nanoparticles increases compared to TiO_2, the same permeability was achieved as that of the PDA-only coated membrane, as the nanoparticles did not bind strongly to the membrane surface. This is confirmed by SEM images.

For the two-step method, the increase in the ratio of ZnO nanoparticles in the nanoparticles mixture decreases the water permeability. This decrease suggests a strong

coating of TiO_2 nanoparticles and a fragile coating of ZnO nanoparticles onto the PDA layer. This could be because TiO_2 has more oxygen atoms in its molecule and these atoms are threefold coordinated with the PDA surface (Lee et al., 2007; Watanabe et al., 1999). The increased amount of TiO_2 nanoparticles on the PDA surface generates a higher roughness on the membrane surface and improves the permeability. Overall, for the catalyst-mixed membranes in both the one-step and two-step methods, TiO_2 had a more favorable effect on water permeability than ZnO.

Overall the modifications did not show to have a significant influence on water flux, which is a good omen for these membranes for use in bioelectrochemical systems due to the fact that the modifications did not significantly affect the initial flux of water from the membranes.

2.3.5. Separation properties of NF membranes

The NF performance of the membranes was systematically evaluated by individually testing the retentions of two salts ($MgSO_4$ and NaCl) at 4 bar, inlet concentrations of 1.0 g L^{-1}. Figure 2.7 compares the salt rejections of membranes with different ratios of catalysts (TiO_2 and ZnO). The membranes modified by co-deposition and binding methods exhibited a slight increase NaCl rejection, probably due to the nanoparticles and nanosized polydopamine oligomers that may block or grow in the defects or larger pores of the pristine membrane surfaces at the early stage.

Furthermore, considering the rejection range and the standard deviation, there seems to be no significant difference in salt rejections for the membranes modified by a combination of TiO_2:ZnO using both binding methods. The modification of membranes with a PDA layer and nanoparticle deposition by co-deposition and two-step method does not appear to have a significant influence on the $MgSO_4$ rejection ~95% (Figure 2.7). The membranes maintain the excellent properties of the pristine membrane.

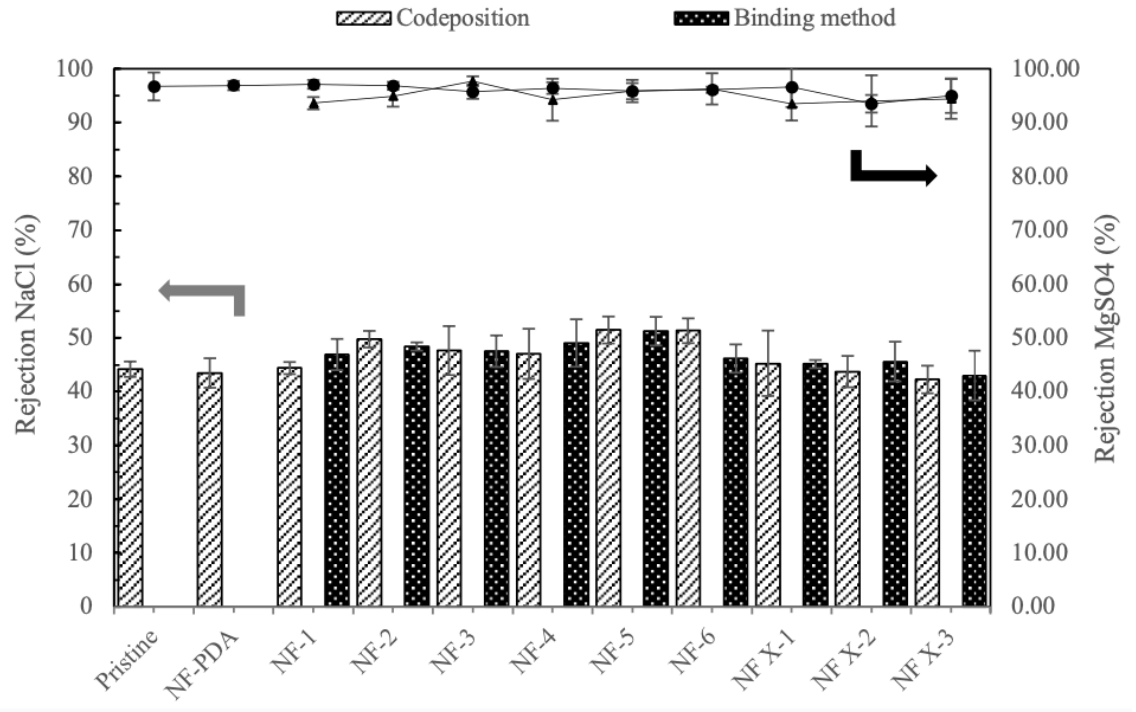


Figure 2.7. % NaCl and $MgSO_4$ rejection of the unmodified and modified membranes with co-deposition method and two steps method in different concentration of catalyst and with various ratios of catalyst (TiO_2:ZnO), 1:1, 1:2 and 2:1 for NFX-1, 2 and 3 respectively.

2.3.6. Anti-bacterial activity of modified membranes

a) Iso Sensitest

The antibacterial activity of the modified NF membranes was evaluated by observing the growth rate of nine specific seeding plates containing *Bacillus subtilis*, irradiated with UV (Khorshidi et al., 2018).

As shown in Figure 2.8 and Figure appendix A2.2 the co-deposition method showed no inhibition. This may be due to the fact that in the co-deposition method the catalyst nanoparticles may have been coated by a PDA layer.

a b

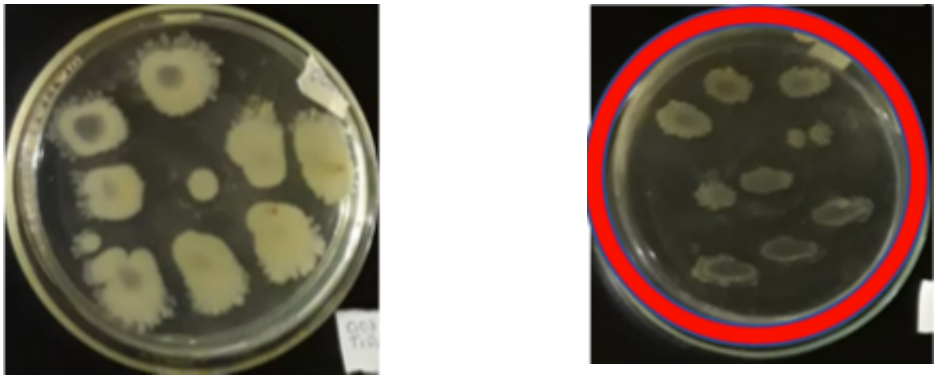


Figure 2.8. Images of the *B. Subtilis* colonies formed in the plate of UV-treated (a) NF-2b (0,03%w TiO_2), (b) NF-5b (0,03%wt ZnO), modified by two steps membranes after 30 minutes of UV irradiation

For the binding method (two steps), the exposure of the membranes to the UV light effectively decreased the viability of the *Bacillus subtilis* for the membrane with 0.03%wt (ZnO) (Figure 2.8b). The membrane with 0.03% TiO_2 exhibited no inhibition for *Bacillus subtilis.*

The antibacterial effect of ZnO nanoparticles may be due to the cell wall structure of Gram-positive bacteria. More precisely, the Gram-positive cell wall consists of a peptidoglycan layer that is bound to teichoic acids, which should be in close proximity with ZnO nanoparticles to create oxidative stress on bacteria resulting in antibacterial activity. There are reports indicating that nanomaterials as ZnO can be adsorbed on the bacterial surface, interacting with bacteria (Feris et al., 2010).

The Derjaguin-Landau-Verwey-Overbeek (DLVO) theory says that the interaction energy between bacteria and a metal oxide can be due to three components, apolar van der Waals forces, electrostatic and polar Lewis acid base component (Zhang et al., 2011). In addition, MacLean et al (MacLean et al., 2004) studied adsorption of compounds on a bacterial surface through reactive positive sites derived from amino functional groups of peptidoglycan and proteins associated with the cell wall. Therefore, materials like ZnO nanoparticles can be absorbed on the surface of the bacteria, resulting in antibacterial activity. On the other hand, the ZnO nanoparticles under UV light irradiation generate

free electrons that interact with oxygen, forming superoxides, while the holes convert hydroxyl ions into highly reactive hydroxyl radical (•OH). These reactive oxygen species (ROS) damage microbial cell walls, resulting in their inactivation (Hajipour et al., 2012). In addition to this, small amounts of ZnO nanoparticles can slowly dissociate and release Zn^{+2} ions, therefore, Zn^{+2} ions can penetrate through the cell wall of bacteria after that the reactive oxygen species (ROS) damages microbial cell walls to destroy DNA and cytoplasm of bacteria (Lakshmi Prasanna and Vijayaraghavan, 2017). In consequence, the bactericidal effect of the ZnO on *B. Subtilis* may be due to its soft cell wall as well as higher penetration and destruction capability of Zn^{+2} for Gram-positive bacteria (Hairom et al., 2014; Senthilraja et al., 2018; Sirelkhatim et al., 2015; Soleymani Lashkenari et al., 2019). The greater inhibition in the presence of light supports the notion that the higher bactericidal effect of ZnO on *B. Subtilis* could be due to the higher capacity of penetration and destruction of the Zn^{2+} ion to the cell wall of these Gram-positive bacteria, since they have a soft cell wall compared to Gram-negative ones. Although it is not clear how zinc exhibits different bacterial affinity with gram-positive, it may be ascribed to the difference in the protein constituents of their cell walls, (Sugarman, 1983). In addition, it has been suggested that zinc binds to the membranes of microorganisms, prolonging the lag phase of the growth cycle and increasing the generation time of the organisms so that it takes each of them longer to complete cell division (Atmaca et al., 2998; Hairom et al., 2014; Radke et al., 1994; Sathe et al., 2016; Sirelkhatim et al., 2015). This property could be beneficial for biofouling mitigation.

b) Disk diffusion technique

The bactericidal property of the novel membranes against *B. Subtilis* was also evaluated using the disk diffusion technique proposed by Lashkenari and co-workers (Soleymani Lashkenari et al., 2019). In this method, the inhibition zone around the disk shows the antibacterial effect of the membrane.

Figure 2.9 shows that the *B. Subtilis* grew at the edge of the modified membranes by the co-deposition method and no obvious inhibition zone are observed in their vicinity (Figure appendix A2.3). On the other hand, in membranes synthetized by the two-step method, an inhibition zone is created around the ZnO nanoparticles (0.03 wt%) membrane

disk (Figure 2.9c). Therefore, the membrane with ZnO nanoparticles has a better antibacterial effect in comparison to the membrane with TiO_2 nanoparticles. The mechanism of the biocidal action of ZnO based materials is based on the generation of surface oxygen species, killing the pathogens (Haghighi et al., 2011; Lakshmi Prasanna and Vijayaraghavan, 2017; Senthilraja et al., 2018).

The combination of TiO_2: ZnO (1:2, 2:1) (Figure 2.9 e and f) has good activity against *B. Subtilis*. The inhibition zone size is based on the ratio of catalysts. The efficiency of different catalyst ratios has been reported for solid (TiO_2:ZnO) mixtures in aqueous solutions (Adams et al., 2006; Hajipour et al., 2012; Soleymani Lashkenari et al., 2019; Yalcinkaya and Lubasova, 2017a). However, this study presents the first evidences of antibacterial activity in membranes modified with PDA and different compositions of catalysts (TiO_2:ZnO). In addition, Talebian *et al* 2013 (Talebian et al., 2013) demonstrated that the antibacterial activity of ZnO Nanoparticles also depends on the morphology of the nanoparticles. Future work will investigate how this morphology acts on the surface of modified membranes.

a

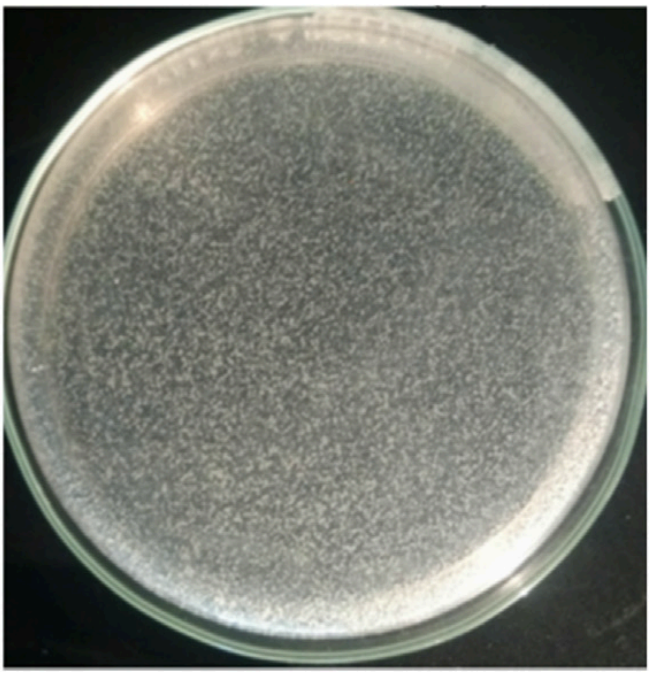
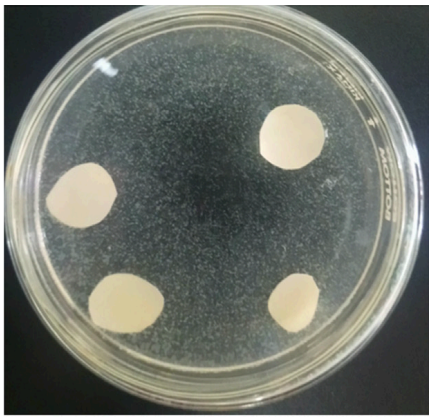


Figure 2.9. Inhibitory effect of the nanoparticles on membrane surface against *B, Subtilis* (a) blank, and modified membranes by binding method (b) NF-PDA, (c) NF-5b., (d) NFX-1b, (e) NFX-2b, (f) NFX-3b, membranes after 30 minutes of UV

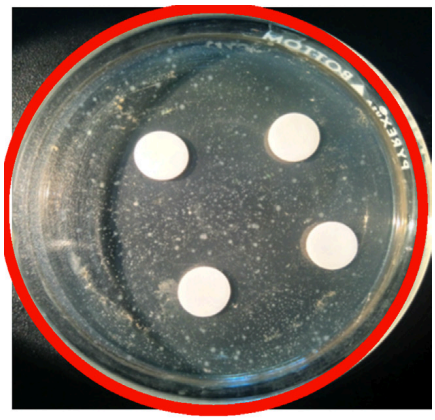
irradiation. g) quantified inhibitory effect of the control, NF-PDA, NF5b, NFX1b, NFX-2b and NFX-3b modified membranes by binding method (cell density of approximately 3000 cells/mL for *B. Subtilis*).

Figure 2.9 continued

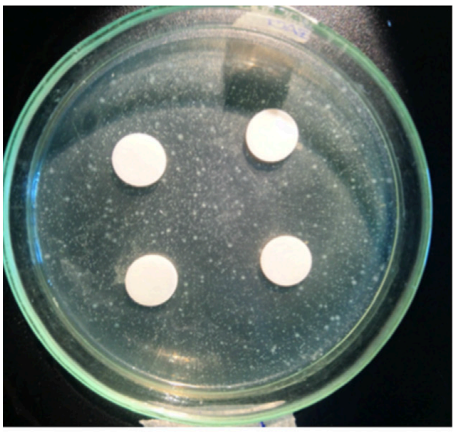
b



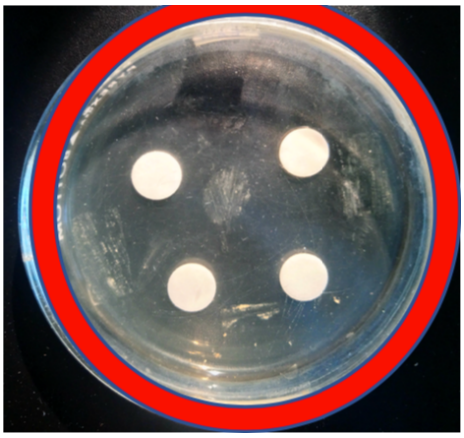
c



d



e



f

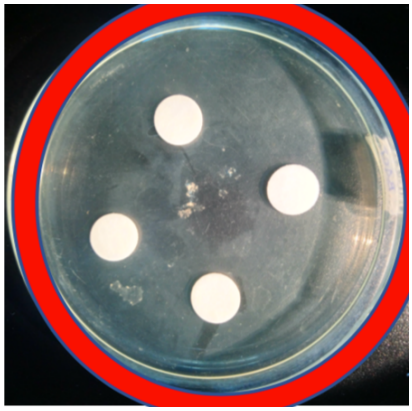


Figure 2.9 continued

g

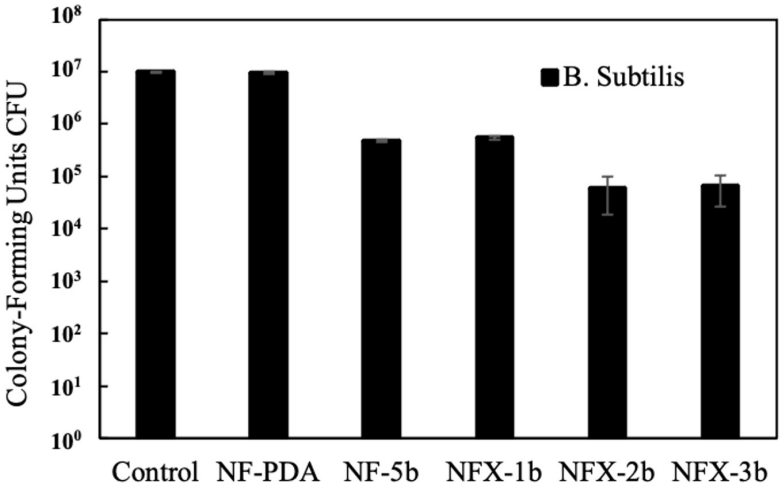


Figure 2.9. Inhibitory effect of the nanoparticles on membrane surface against *B, Subtilis* (a) blank, and modified membranes by binding method (b) NF-PDA, (c) NF-5b., (d) NFX-1b, (e) NFX-2b, (f) NFX-3b, membranes after 30 minutes of UV irradiation. g) quantified inhibitory effect of the control, NF-PDA, NF5b, NFX1b, NFX-2b and NFX-3b modified membranes by binding method (cell density of approximately 3000 cells/mL for *B. Subtilis*).

Figure. 2.9 describes the strong antimicrobial activities of the modified membranes. To quantitatively analyze the bactericidal ability, the viable cell counting technique was applied in this study. The NF-PDA membrane prepared by the fast PDA deposition exhibited a slight antibacterial ability against *B. Subtilis*. This trait may be attributed to the release of copper ions from the PDA layer (J. Zhu et al., 2016). Relative to the control sample, the modified membranes reduced 93.0%, 92.7%, 64.7% and 47.5% of *B. Subtilis* when ratios (TiO_2:ZnO 0,03%wt) 2:1, 1:2, 0,03%wt ZnO, and 1:1 binding modification method were applied, respectively (Figure2.9B). Such distinct reductions in *B. Subtilis* colonies demonstrate the excellent antimicrobial properties of the modified membranes.

2.3.7. Effect of solar light irradiation on membrane surface in degradation of methylene blue.

Figure 2.10 shows that the membranes can photocatalytically remove dyes from a bulk solution. It should be noted that the methylene blue in the unmodified membrane (pristine) has approximately 20% MB removal. This is because the MB can suffer photolysis by solar irradiation as shown in other reports (Rani and Shanker, 2018; Soltani and Entezari, 2013).

For modified membranes, the binding method (two-step modification) is more effective in removing dyes from the solution in contact with the membrane in comparison with the co-deposition method (one-step modification method). This could be because the catalysts nanoparticles in the two-step modification method are exposed on the membrane surface directly receiving sun radiation (De Filpo et al., 2018; Raizada et al., 2014; Wang et al., 2009). Furthermore, a catalyst mixture of 1:1 and 2:1 (TiO_2:ZnO) was found effective for the removal of dyes for aqueous heterogeneous photocatalytic processes (Moradi et al., 2016; Štrbac et al., 2018). This is not the case with one-step modification since co-polymerization could encapsulate the catalyst nanoparticles with a PDA layer and this would reduce the passage of light to the catalysts, decreasing their ability to remove dyes.

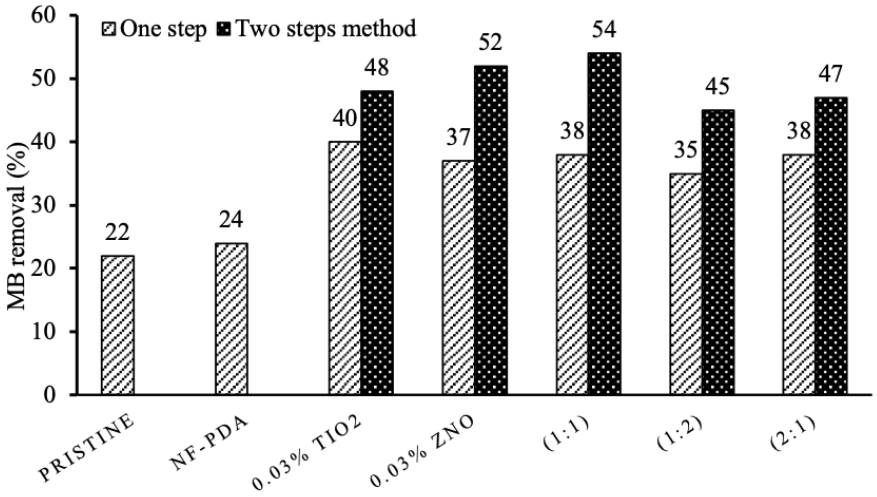


Figure 2.10. Degradation of the MB under visible light irradiation as a function of time for the various modified membranes (C_o = 10 mg L^{-1}, time of irradiation = 180 min).

Thus, nanoparticles (ZnO, TiO_2, and their mixtures) on the surface of a PDA modified membrane can be potentially used as anti-fouling agents under visible light,

following the mechanisms proposed by Prasannalakshmi and Shanmugam for mixing of powders (catalysts) (Prasannalakshmi and Shanmugam, 2017) (Figure 2.11). The observed photocatalytic activity is exactly matched with the reported results (Delsouz Khaki et al., 2018; Firdaus et al., 2012; Tian et al., 2009). It is important to note that, previous reports have shown photocatalytic activity (under solar irradiation) for the powder ratios of the two catalysts (TiO_2:ZnO), but, no data are available for catalyst ratios on PDA-modified membranes.

The mechanism of the Figure 2.11 has been proposed by Prasannalakshmi and Shanmugam for mixing of powders (Prasannalakshmi and Shanmugam, 2017). In that mechanism, under sunlight irradiation, the electrons from the conduction band (CB) of ZnO can be transferred to CB of TiO_2. In the same way, the holes are transferred from the valence band (VB) of TiO_2 to VB of ZnO. This process prevents the recombination of charge carriers and makes their availability on the surface of the photocatalysts and thus enhances the redox process. The high surface area of TiO_2:ZnO accompanies with the optimum pore size and pore volume provides much surface for the absorption of dye molecules which increases the probability of degradation. In addition to this elongated one dimension of ratios of TiO_2:ZnO helps to decrease the recombination probability of photogenerated carriers due to an increased delocalization of electrons (Prasannalakshmi and Shanmugam, 2017). In the present work, we propose this mechanism on the surface of the modified membrane.

In order to demonstrate the efficiency of our modified membranes, Figure A2.4 shows the two-step modified membranes after being in contact for 5 hours with methylene blue solution (10 mg L^{-1}) and under solar irradiation, the membranes by two steps showed much cleaner surfaces after use. This may be due to a synergy between the catalysts, as explained in the previous section. The proposed mechanism for mixing catalysts could be carried out on these modified membranes.

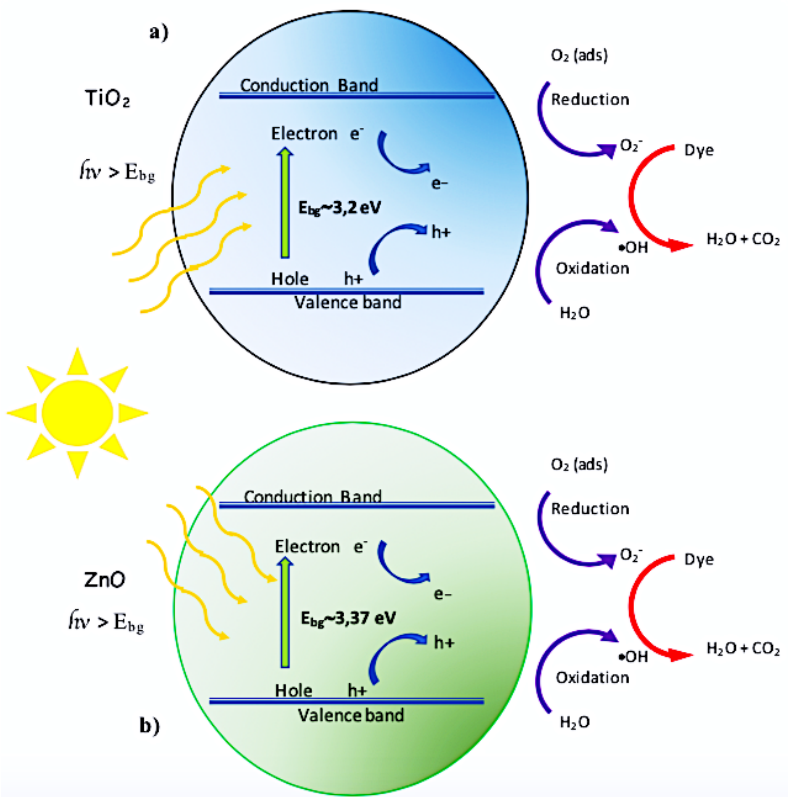


Figure 2.11. Mechanism of photodegradation of dyes using TiO_2 and ZnO (Prasannalakshmi and Shanmugam, 2017)

Two preparation techniques were tested: codeposition and two-step deposition of PDA and Catalysts (TiO_2 and ZnO). In both cases, PDA deposited rapidly onto a NF support. The two-step modified membranes showed greater antifouling properties than the one-step method when the membranes were in contact with dye solutions. The most optimal modification method for the antibacterial activity was PDA and nanoparticles by two-step deposition method. Remarkably, modified membranes with ZnO and ratios of catalysts (TiO_2: ZnO) 1:2 and 2:1 have shown high antibacterial activity achieved. The membranes used in this study provide a competitive alternative and practical solution for antifouling applications in nanofiltration. More importantly, this facile two-step deposition strategy offers possibilities in the strong binding of other ratios pf nanoparticles (i.e., Ag, and graphene oxide) with enhanced antimicrobial properties onto the membrane surface

2.4. Conclusions

In this study, nanoparticles of TiO_2, ZnO and their mixtures were successfully attached to a PDA layer surface of a nanofiltration membrane, by two methods; 1) co-deposition and 2) binding. SEM, EDX, and water contact angle measurements confirmed the formation of a thin hydrophilic PDA layer on the NF membrane surface with homogeneously dispersed structures.

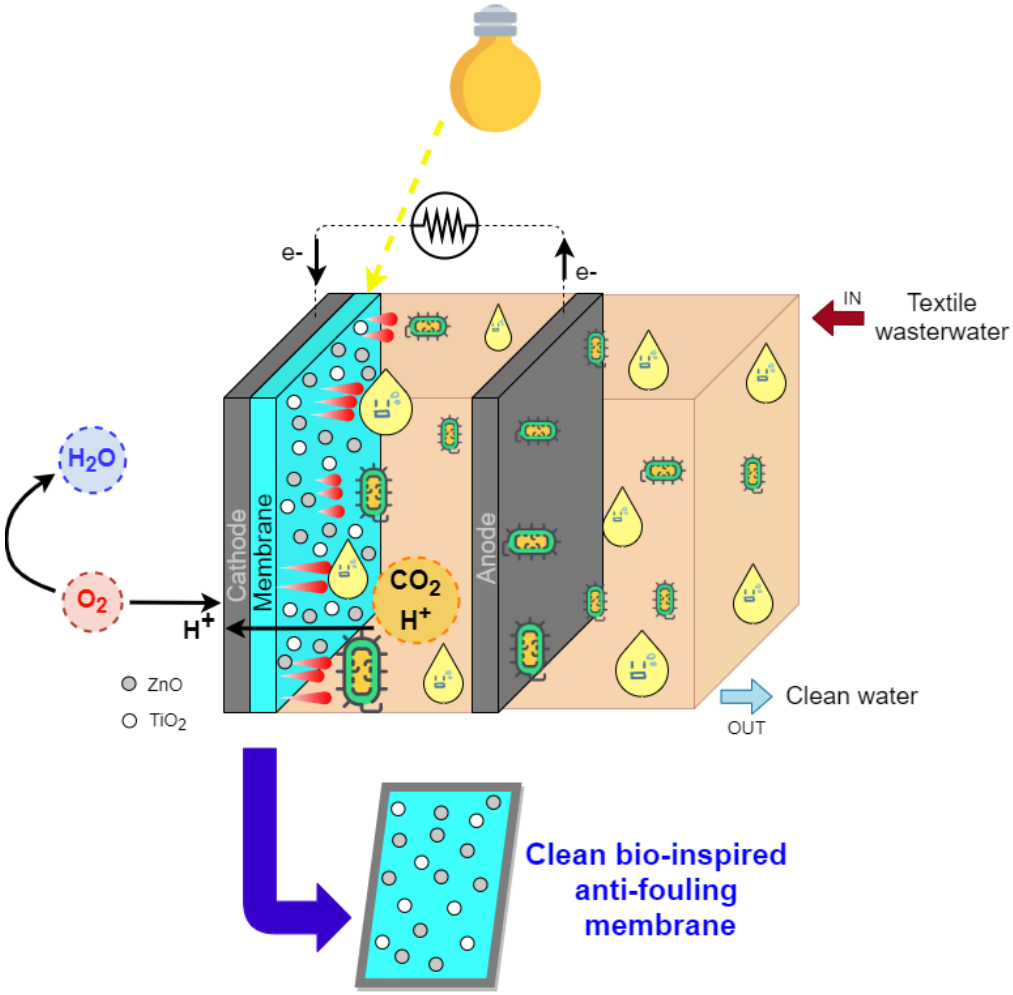
The membranes obtained by the binding method (two-step) with modifications of 0.03%wt ZnO nanoparticles and a mixture of catalyst TiO_2: ZnO (1:2 and 2:1) showed antibacterial activity against *Bacillus subtilis*. Furthermore, the combination of TiO_2:ZnO catalysts by the binding method may to be used as a practical anti-biofouling nanomaterial. Finally, the combination of TiO_2 nanoparticles with ZnO nanoparticles enhanced the photocatalytic activity of the modified membranes to remove dyes from solution.

Since the best performing method is the two-step method, this will be used as a method to modify membranes and support catalysts.

Chapter 3. TiO_2:ZnO-modified low-cost membranes with mussel-inspired polydopamine binding as microbial fuel cell membranes.

This chapter is based on the research paper published entitled "Effect of the bio-inspired modification of low-cost membranes with TiO_2:ZnO as microbial fuel cell membranes" by **Raul Bahamonde Soria**, Billy. Chinchin, Daniel. Arboleda, Yan Zhao, Pablo. Bonilla, Bart Van der Bruggen, Patricia Luis, published in *Chemosphere*, (2022),

Graphical abstract:



Abstract

To improve the fouling reduction of an ion exchange membrane (PEM) and the performance of microbial fuel cells (MFC), a novel bio-inspired modification of a low-cost membrane surface with a layer of PDA and nanoparticles (TiO_2:ZnO at 0.03 wt%, 1:1 ratio) was developed. Three identical one-compartment MFCs were operated under the same operational conditions but using different kinds of membranes (pristine, Cel-PDA and Cel-PDA/TiO_2:ZnO) in order to evaluate the effects of the modifications performed on the membrane surface and MFCs. Cellophane (pristine) membranes were modified with polydopamine and catalyst nanoparticle mixtures. The MFCs were tested with synthetic textile wastewater, and the MFC with cellophane membranes modified with PDA and catalyst was also evaluated with real textile wastewater. Results showed that using the membrane modified with PDA and a mixture of catalysts increased 2.5 times the power generation in the MFC and 5.7 times the current in comparison with pristine and Cel-PDA membranes. SEM and AFM analysis showed that the modification significantly minimized surface fouling. In addition, the modified membrane made the MFC more efficient, decreasing the operating cycle time of the MFC from 5 to 3 days and doubling the useful life of the MFCs. Finally, the MFC with Cel-PDA/TiO_2:ZnO membrane showed a superior power density (63 mW/m^2), higher COD and color removal than the others. These results showed that modification of the low-cost membrane surfaces (cellophane) with PDA and a mixture of catalysts increased the lifetime of the membranes studied and improved the electrical efficiency of the MFCs.

Keywords: TiO_2NPs; ZnONps; bio-glue; Polydopamine; bio-inspired; membranes; Microbial fuel cell.

3.1 Introduction

The textile industry processes usually use aromatic dyes. Their discharge in the surface water is undesirable because azo dyes and their breakdown products could have toxic and/or mutagenic properties in aquatic environments (De Aragão Umbuzeiro et al., 2005; Solanki et al., 2013b).

In recent decades, numerous techniques have been adopted to find greener, economically feasible, and efficient ways to treat textile dyeing wastewater, including physicochemical, biochemical, combined treatment processes, and other technologies (Mathew et al., 2019). In recent years, microbial fuel cell (MFC) has been widely explored for its innovative environmental benefits (Solanki et al., 2013b). MFCs are devices that use virtually any source of biodegradable organic matter, including simple molecules (e.g., carbohydrates, proteins), as well as complex mixtures of organic matter present in human, animal, and industrial wastewaters to produce electricity electrochemically in anaerobic conditions (L. C. Wu et al., 2020). An MFC uses bacteria to oxidize organic and inorganic matter and generate current (Potter, 1911). The flexibility of microorganisms to use a range of "fuels" makes the MFC an ideal technology for renewable bioelectricity generation from biomass (Logan, 2009; Saratale et al., 2017).

As a reminder, an MFC consists of an anode (anaerobic oxidation) chamber and a cathode (aerobic or aerated reduction of O_2) chamber separated by a separator (normally proton exchange membrane-PEM). In MFCs, protons and a current of electrons are produced by microbial oxidation of organic substrates (fuel) in the anodic chamber. (Kondaveeti et al., 2014). Electrons produced by the oxidation processes of MFCs are deposited at the anode (negative terminal) then flow to the positive terminal or cathode through a conductive material (e.g., a metal wire) as a result of an electrical potential difference (Logan et al., 2006c). The protons also generated in this process cross (diffusion) through the anolyte and the separator (usually PEM) toward the cathode compartment to compensate the charge (for each electron produced at the anode, a positive ionic charge needs to move to the cathode or a negative charge to the anode) (Fig. 3.1). Finally, in the cathodic chamber, a combination of electrons, protons, and oxygen from water (Kondaveeti et al., 2014). The separator or ion/proton exchange membrane (PEM) is an important component of MFC (Xu et al., 2012b). In addition, the

membrane is also important because it can also prevent the transfer of bacteria from the anode to the cathode and maintain anaerobic conditions in the anode chamber. (Ghasemi et al., 2013).Figure. 3.1. shows the concept of an MFC in the treatment of wastewater.

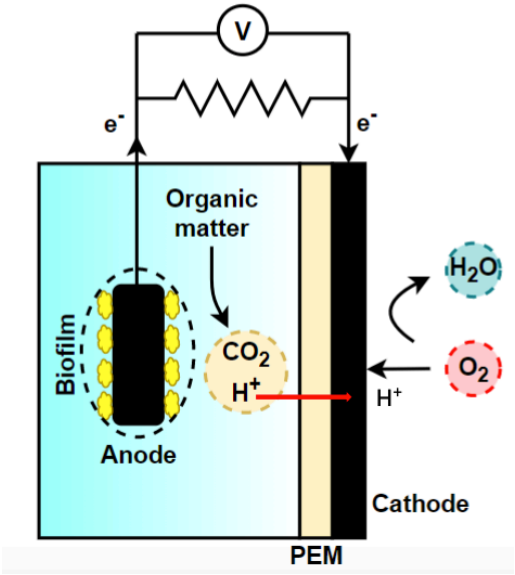


Figure 3.1. Single-chamber MFC with the open-air cathode (Q. Zhao et al., 2017)

However, MFCs present an important limitation. The high cost associated to some components of MFCs, such as membranes and electrodes, and the low power density achieved due to the high ion transport resistance through the ion exchange membrane (internal resistance) could limit their application in wastewater treatment. In order to reduce costs, some low-cost cellulose-derived membranes such as cellophane have been used as a PEM in MFCs (Freguia et al., 2010, 2009; Logroño et al., 2017; Moqsud et al., 2013; Sakai et al., 2009; Wang and Lim, 2017b). Cellophane is a well-known material with good mechanical and hydrophilic properties. It has found applications in two main areas: as semipermeable membranes for hemodialysis and in the packaging industry (Tomé et al., 2011). Besides, cellophane is a very economical material compared to other separators used in MFCs, such as Nafion 117. However, cellulose is a polyol compound and its operational lifetime is short due to oxidative and hydrolytic cleavage (Vakili et al., 2020); hence, these membranes can be used to study the MFC performance only for short periods of operation (G. Zhao et al., 2019).

Additionally, another drawback of membranes, and more specifically, cellophane membranes, is the irreversible membrane biofouling caused by organic foulants and biofoulants such as extracellular polymeric substances, which participate in the formation

of microbial aggregates and soluble microbial products. Besides, cations, present in large quantities in textile wastewater can also cause fouling, which increases the electrical resistance of a PEM (Choi et al., 2011). This accumulation of cations and bacteria present anodic chamber can increase the electrical resistance of PEM significantly due to the formation of a dense biofilm on the PEM surface (Lee et al., 2002). In addition, membrane fouling increases operation and maintenance costs by deteriorating the membrane performance and ultimately shortening the membrane lifetime (Vrijenhoek et al., 2001). Thus, it is important to manufacture anti-biofouling membranes. Chemical modification of membranes is an attractive alternative for tailoring important properties for specific applications.

Recently, bio-inspired modifications have been explored as a method of forming anti-fouling surfaces. Among these, mussel-inspired modification has shown great potential in surface modification (Abid et al., 2017; Ding et al., 2016). It is known that mussels can adhere and remain strongly adhered to different surfaces, including under adverse conditions. This adhesion ability of mussels can be associated with proteins containing 3,4-dihydroxy-L-phenylalanine (DOPA) or lysine amino acids since the catechol or amine groups of these proteins have shown effective functionalization with even hydrophobic surfaces (Ding et al., 2016). The coating of surfaces with polydopamine (PDA) (rich in catechol and amine groups) from the oxidation of dopamine has opened a way of surface modification in recent years. While hydrophobic surfaces are more susceptible to biofouling, coating surfaces with PDA could increase the surface hydrophilicity of materials (catechol groups), which could improve the antifouling properties of certain surfaces. To greatly accelerate the polymerization of dopamine, $CuSO_4$ /H_2O_2 has been used as a trigger (Zhang et al, 2017). $CuSO_4$ /H_2O_2 is used for the rapid formation of reactive oxygen species (ROS) in alkaline media, which accelerates a uniform and stable deposition of PDA (J. Zhu et al., 2016). Besides, adding 2D nanosheets such as graphite oxide or inorganic nanoparticles such as TiO_2, SiO_2, Al_2O_3, Si, Ag, ZnO, ZrO_2, etc. into the thin film can show significant effects on membrane performance, hydrophilicity (Mohammad et al., 2015), and on the fouling resistance (Homayoonfal et al., 2013; Ng et al., 2013). However, the benefits of these modifications have been extensively explored in water treatment processes using membrane technology,

but these modifications have not been largely explored in the development of antifouling or self-cleaning membranes in MFCs.

The ability of PDA for self-polymerizing on the membrane surface and the interesting properties that metal oxide nanoparticles (and mixtures of NPs) could provide will allow the development of a new generation of bioinspired ion/proton exchange MFCs membranes.

In this study, a simple chamber MFC system equipped with a modified membrane with a mixture of ZnO and TiO_2 nanoparticles using polydopamine as a bio-inspired "glue" was constructed for textile wastewater treatment. It was explored how these modifications, far from compromising the operation of the MFCs, contribute to the enhancement of the electrical performance and the removal of color and COD in the MFC. It is assumed that the binding method can keep the good hydrophilicity and photocatalytic properties of metal oxides on membrane surfaces (Zhang et al., 2013). Furthermore, the impact of bioinspired modification of low-cost membranes on the anti-fouling properties of the membrane and the electrochemical parameters of MFC was investigated. Several studies to provide anti-fouling properties in membrane technology for water treatment have been published. However, to the best of our knowledge, anti-fouling membranes using a bio-inspired modification of membrane surface with PDA layer and (TiO_2:ZnO) nanoparticles as separators in MFCs have not been previously described, indicating the novelty of this research.

3.2 Materials and Methods

3.2.1 Materials

The commercial cellophane membrane was purchased from Papelesa Co., Ltd. Cod. 15273 (Ecuador). The commercially available TiO_2-anatase (99.7 wt%, <25nm) and ZnO (99 wt%, <50nm) were acquired from Sigma Aldrich (Diegen, Belgium), 3-Hydroxytyramine hydrochloride, (Dopamine hydrochloride 98 wt%), and Triss base (tris(hydroxymethyl) aminomethane, 99.8 wt%) were acquired from Acros Organic (Belgium). Copper (II) sulfate anhydrous, powder, ≥99.99 wt%, hydrogen peroxide (30

wt%), hydrochloric acid, sodium hydroxide (98 wt%) and sodium chloride (99 wt%) were acquired from VWR (Belgium). Acetone, ammonium peroxydisulfate (Fisher), and sulfuric acid were acquired from (Novachem-Ecuador). Deionized water purified by a Milli-Q ultrapure unit was used for all experiments.

3.2.2 Modification of the low-cost membranes

The cellophane membranes were immersed in deionized water for 12 hours before modification.

The two-step membrane modification methodology was based on our previously reported study of modification membranes (Bahamonde Soria et al., 2020). The surface of the cellophane membrane was coated with a layer of PDA by accelerated oxidation of dopamine with $CuSO_4$ and H_2O_2 in an alkaline medium (pH =8.5) as triggers (1hr). Then, a 1:1 ratio (0.03 wt%) of TiO2 and ZnO nanoparticles suspended in Tris buffer (pH 8.5, 10 mM) was deposited on the PDA layer (1hr). The catalyst suspension was previously stirred for 3 hr at 1000 rpm using a magnetic stir plate and subsequently sonicated for 1 hr (25°C) before use. Afterward, the modified membranes were carefully rinsed five times with distilled water prior to use in MFCs. In the following sections, three different membranes used in single-chamber microbial fuel cells will be named Pristine, Cel-PDA and Cel-PDA/TiO_2:ZnO for cellophane membrane, cellophane with PDA and cellophane plus PDA, and catalysts respectively. All the membranes used here were kept in a sodium chloride solution (0.5 $g \cdot L^{-1}$) before being used.

3.2.3 SEM and AFM membrane characterization

Scanning electron microscopy (SEM) was used to study the surface membrane morphology by SEM (JEOL IT300 equipped with an EDX-MAN1-Oxford Instrument). All samples were dried before analysis at room temperature.

In order to determine the increase in height and surface roughness of the membranes. Atomic force microscopy (AFM -Park System model NX10.) was used as an analytical tool. The scanning areas were 2.5 x 2.5 um^2. AFM images were taken in contact mode. As an indication of membrane surface fouling, the maximum vertical

distance (Rm) of membrane surfaces was investigated before and after application to the MFCs.

3.2.4 Membrane surface electrical resistance

The membrane surface resistance was measured in a cell ofFigure.3.2 (Zhao et al, 2019; Zhao et al, 2020, 2018) where compartments 1 and 4 were filled with 0.2 M Na_2SO_4 solution and compartments 2 and 3 were filled with 0.1 M sodium chloride solution. The modified membranes were clamped between 2 and 3 compartments for evaluation. Anion exchange membranes (AEM) were clamped between 1 and 2 compartments and between 3 and 4 compartments. In order to determine the voltage change due to membrane resistance, two Ag/AgCl reference electrodes were placed on both sides of the membrane. The membrane surface resistance R ($\Omega \cdot cm^2$) was calculated with $R = (V - Vo)/I \times A$, where V and Vo is the voltage of the membranes and blank respectively (V), I is the constant current through the membranes, which was 0.004 A and A is the effective area of the membrane (7.1cm^2). Normally, this resistance is influenced by modification on the surface membrane (Jin et al., 2018).

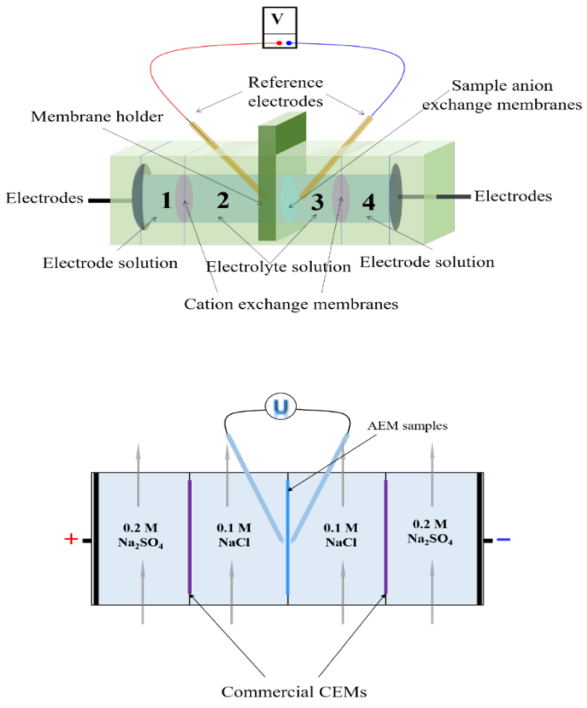


Figure 3.2 Schematic diagram of the device for the determination of the change in pristine and modified membranes resistance, a)The membrane surface electric resistance measurement device and b) scheme of the solution for every compartment in the resistance measurement (Zhao et al, 2019; Zhao et al, 2020, 2018).

3.2.5 Microbial fuel cell setup

Cubic air-exposed batch MFCs (volume 100 mL) were made of plexiglass (Fig. 3.3). Carbon cloth (ELAT- Hydrophilic, Fuel Cell Store., USA) was used as anode electrode with 25 cm^2 of apparent surface area, while in the air-cathode chamber, carbon cloth (0.5 mg $Pt \cdot cm^{-2}$, 60% Platinum on Vulcan Fuel Cells Store, USA) was used as cathode (25 cm^2). Both electrodes were connected through Ni-Ti wires (0.016, Fresmile). In order to obtain favorable conditions for inoculation, the anodes electrodes were pre-treated as follows: 1) immersed in acetone (12h). 2) washed with deionized water 6 times; 3) immersed in ammonium peroxydisulfate (0,5 moles L^{-1}) (15 min) followed by sulfuric acid treatment (1.5 mol L^{-1}) for 15 min; 4) heated in a furnace 450 °C (30 min) (Feng et al, 2010); and finally, 5) washed 5 times with distilled water.

The cathodic electrodes were in contact with cellophane membranes by 25 cm^2, which was considered as membrane surface area in an MFC. All MFCs were placed under visible light conditions as shown in section 4.2.8 and maintained at a temperature range of 20 -25ºC.

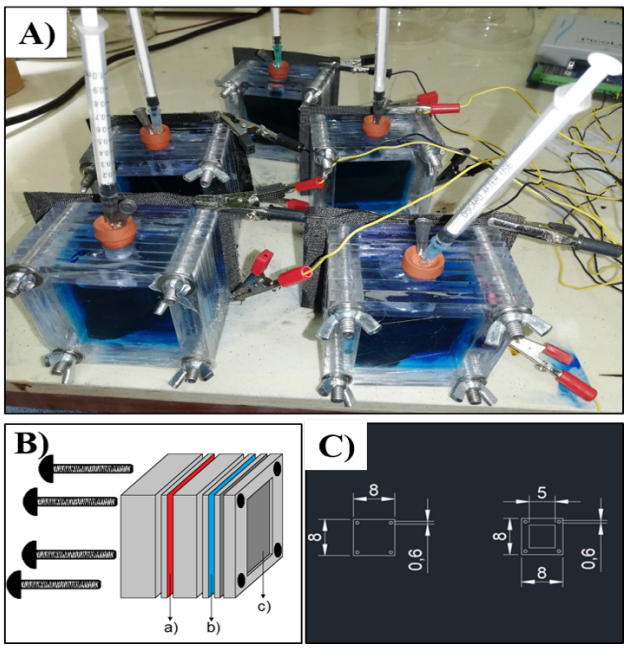


Figure 3.3. A) Photographs of the MFCs used in this study; B) Configuration of the MFC: a) anode, b) membrane and c) cathode; and B) dimensions in cm of the MFCs used in this work.

3.2.6 Bacteria growth, Anodic immobilization and anolyte solution

In this study, real textile wastewater samples from local industry (JP Jerse Quito-Ecuador) were used as microbial inoculum. The real textile wastewater had the following chemical composition: chemical oxygen demand (374 mgO_2 L^{-1}), biochemical oxygen demand (117 mgO_2 L^{-1}), color (163 Hazen), phenols (0.057 mg L^{-1}), total phosphorus (6.5 mg L^{-1}).

Then, a bacterial growth medium was prepared according to Kim et al (2005). Per 20 ml of the growth medium, 1 mL of primary textile wastewater was added as inoculum in anaerobic conditions.

Subsequently, a bioelectrochemical fed-batch reactor was built as growth maintenance place, which a reference electrode (RE) (Ag/AgCl, sat. KCl, 0.197 V vs SHE) and graphite rod and Pt were used as working electrode (WE) and the counter electrode (CE) respectively. A chronoamperometric method was used to the growth and maintenance of bacteria. This method of chronoamperometric bacteria growth, maintenance, and basic characterization of the electroactive microbial biofilms was done according to the methodology described by Gimkiewicz and Harnisch (Gimkiewicz and Harnisch, 2013). Which showed that biofilms obtained by the specific conditions of this protocol could be highly dominated by *Geobacter* species (not demonstrated here) (Gimkiewicz and Harnisch, 2013; Torres et al., 2009).

Afterwards, the biofilm of a mixed consortium composed of electrogenic bacteria present in work electrode was collected and transferred to a BHI broth and preserved to 37ºC until it reached a concentration of $1x10^7$ CFU (colony forming units), then 0.30 mL of this solution was transferred to 10 mL of fresh BHI broth and used as inoculum for the formation of a biofilm on the carbon cloth (anodes). The carbon cloth and the solution were incubated at 32°C for 5 days before the use on the MFCs.

Two types of anolytes were used for this study: 1) synthetic wastewater (STW) containing sodium acetate (1.0 g), NH_4Cl (0.31 g), KCl (0.13 g), $Na_2HPO_4 \cdot 12H_2O$ (10.32 g), $NaH_2PO_4.H_2O$ (2.94 g), methylene blue (10 mg) and vitamin solution (20 mL) in a

liter of deionized water; and 2) real textile wastewater (COD_o = 374 mg·L^{-1}). In order to remove the dissolved oxygen, the anode chamber was purged with nitrogen gas, and then capped with a rubber stopper. The anolyte in the reactor was refilled every 3 days.

3.2.7 Measurement and analysis of MFC performance

The voltage was registered by data logger device ADC-24 (Pico® technology, UK). A computer with PicoLog 6 software recorded all measurements. External resistors (1.5 to 222KΩ) were used to perform the bias curve at stable OCV. Next, the current (I) was calculated using Ohm's law, the ratio of voltage (V) to resistance (R), I = V/R. 25 cm^2 was considered the electrode area (A) for the development of current and power density curves and these were calculated as I (mA·m^{-2}) = V/(R × A) and P (mW·m^{-2}) = (I^2 × R)/A, respectively.

The coulombic efficiency was calculated according to $CE = (M\int Idt)/(\Delta COD\ F\ V\ b)$, where the molar mass of oxygen is in g·mol^{-1}(M), the change in chemical oxygen demand in g·$L^{-1}$is ΔCOD. F is 96485 C·mol^{-1} electron or Faraday's constant, V is the total volume of the anolyte (L) and b is the number of electrons exchanged per 1 mol of O_2; for this study b= 4.

The initial chemical characterization of the real textile wastewater (RTW) was realized in the accredited Laboratory OSP of the Chemical Science Faculty-UCE. COD and color removal efficiencies were calculated using Eq. (1).

$$R_E(\%) = \left[\frac{(Y_i - Y_f)}{Y_i}\right] \times 100 \qquad (1)$$

where Yi is the initial concentration in the fuel of MFCs and Yf represents the final concentration in the MFCs effluent.

3.2.8 Photocatalysis condition and color removal evaluation

The photocatalytic and antifouling activity of the unmodified and modified membranes was tested by removal of color and COD present in the anolyte under a bulb of visible light, this kind of light to prevent damage on the membrane (using a poor source of UV light) (Zhang et al, 2017a). A 20 W visible light source (Sylvania®) was used for the

current studies, the light intensity was measured by digital lux-meter (6211± 10 lx). The space between the MFCs reactor and light source was kept constant at 30 cm in all cases. In order to eliminate external light sources, all experiments were conducted in a dark isolation box.

After 24 h as time interval of irradiation, an amount of 5 mL was withdrawn and centrifuged in order to separate the biomass. Then, the UV absorption spectra of the samples were taken to analyze the degradation. This was repeated until the complete degradation of dye. The removal of color concentration with time was recorded by monitoring the optical absorption of MB at 664 nm for synthetic wastewaters and running a spectral sweep from 400 to 750 nm for real textile wastewater, using UV–vis spectrophotometer.

3.2.9 Verification of the self-cleaning character of the membranes

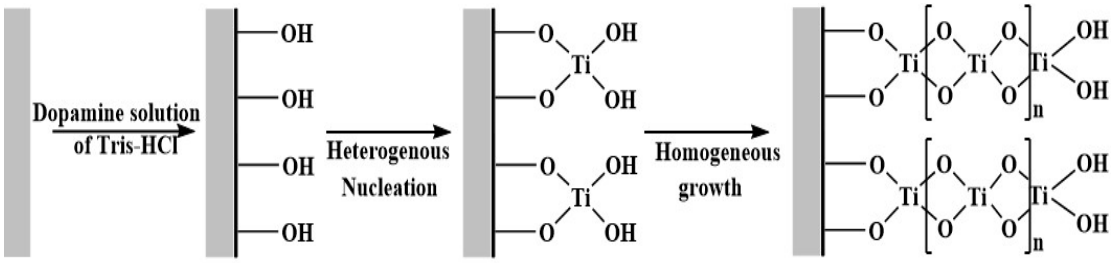
The self-cleaning activity of studied membranes could be verified by the color change of the membranes, which remained in contact with an aqueous solution of 10 mg L^{-1} MB for 96 hours. After 96 hours of contact of one side of the membrane with the MB solution, the membranes were placed under the influence of sunlight. The self-cleaning activity of membranes was evaluated under sunlight in Quito (Ecuador) between 4th no August and 4th November 2019. The evaluation hours were from 11:00 a.m. to 13:00 to harmonize the UV-irradiation (Rajamanickam and Shanthi, 2012). The UV Index in Quito - Ecuador was around 10, according to the INAMI-Ecuadorian National Institute of Meteorology and Hydrology. The membranes were exposed to this irradiation for 90 min.

3.3 Results and Discussion

3.3.1 SEM, AFM Characterization and evaluation of membrane fouling.

Fig. 3.4A shows the change of a cellophane membrane surface before and after modification with PDA and the addition of TiO_2:ZnO (1:1). Remarkable color and surface morphology changes were obtained after PDA coating: the cellophane membrane became brown and the surface of the membranes showed residual molecular structures from PDA polymerization in SEM images. (Fig. 3.4B) (Lu et al., 2018).

A PDA coating layer can provide a negative charge on the surface of the membranes, this negative charge could be due to deprotonation of the phenolic hydroxyl groups (K. Y. Kim et al., 2014; Yu et al., 2010). In turn, this negative charge could affect the hydrophilicity of the PDA-coated surfaces at neutral pH conditions. This effect could help the passage of positive ions through the membrane. In addition,Figure. 3.4A shows the modified cellophane membrane surface with PDA + TiO_2:ZnO in ratio 1:1 (0.03%wt), the cellophane membrane changed to a clear color and this surface membrane showed a wide range of nanoparticle sizes (Fig. 4B c and d). Apparently, heterogeneous nucleation followed by homogeneous nucleation of nanoparticles could produce a large number of NP aggregate sizes bonded to the PDA layer (Scheme 1). It has been reported that the hydroxyl (OH^-) groups in catechol derivatives (polydopamine) can react with metal oxides as TiO_2 and ZnO (heterogeneous nucleation) (Guvendiren et al., 2008). In addition, the process of aggregation between metal oxide nanoparticles is known as homogeneous nucleation. For example, in this work, the homogeneous growth could be induced by the heterogeneously nucleated TiO_2 and ZnO nanoparticles layer on the substrate PDA, which could serve as the seed layer to boost the homogeneous nucleation of both TiO_2 nanoparticles (Scheme 4.1), and ZnO nanoparticles (Ou et al., 2010).



Scheme 3.1. A scheme of heterogeneous and homogeneous TiO_2 deposition on polydopamine as substrate (Lee et al., 2007; Ou et al., 2010).

Ion exchange membranes (IEM) in MFCs can suffer fouling, both colloidal contamination (e.g. cell fragments, humic substances, biopolymers, and bacterial biofilm known as biofouling) and inorganic contamination (chelation of metal ions or inorganic salts with organic matter) (Li et al., 2020). Therefore, biofouling may occur and layers of biofilm can form on the membrane surface after operating the MFCs for 10 cycles for synthetic textile wastewater and 2 cycles for real textile wastewater. In Figure 3.4 is

possible to observe SEM images of surface membranes before evaluation (Zone I) and after use on MFCs (Zone II).

A)

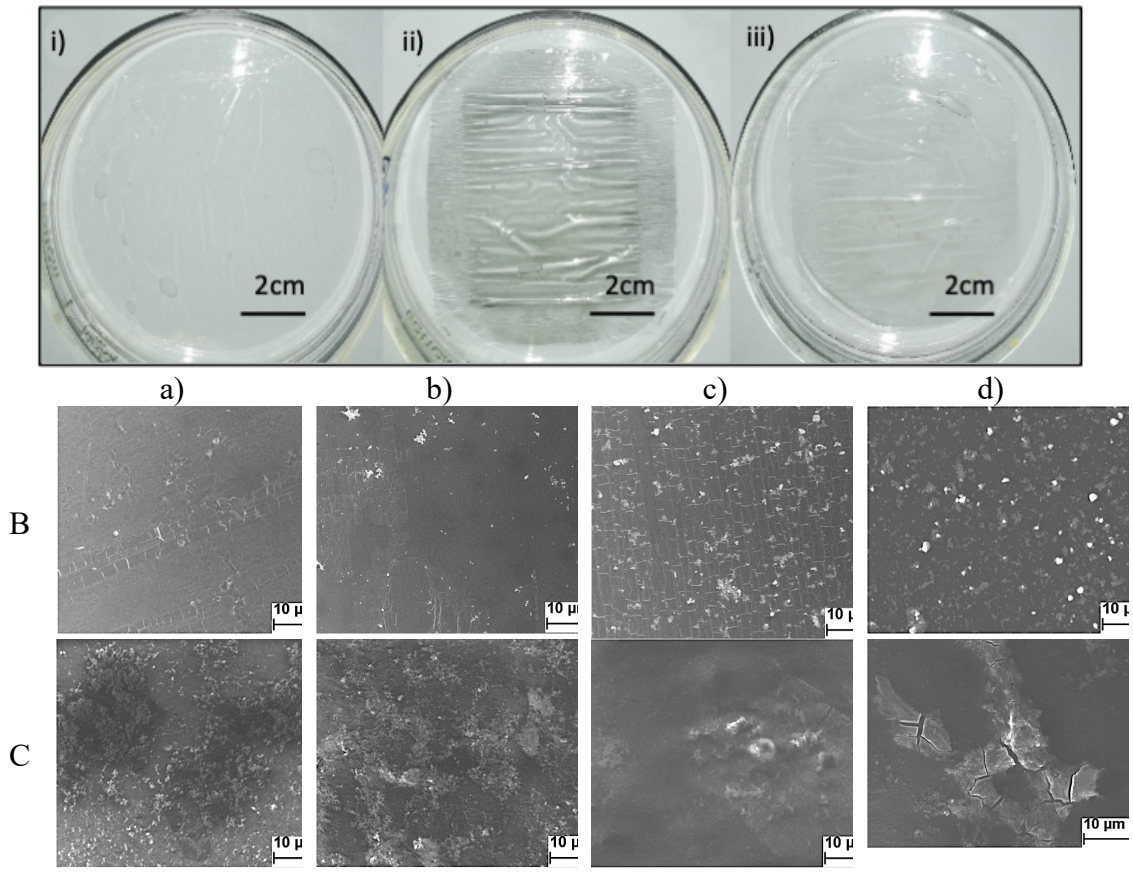


Figure 3.4. A) Images of membranes before and after modification of i) pristine, ii) Cel-PDA and iii) Cel-PDA/TiO_2:ZnO and B) SEM images of surface membranes before evaluation (Zone B) and after evaluation (Zone C) on MFCs with synthetic textile wastewater for (a) pristine membrane (b) Cel-PDA, (c) Cel-PDA/TiO_2:ZnO, and MFCs with real textile wastewater for d) Cel-PDA/TiO_2:ZnO

Compared with the pristine and Cel-PDA membranes, fewer mixed culture bacterial communities presented on the surface Cel-PDATiO_2:ZnO membrane for synthetic and real textile wastewater (Fig. 3.4B c and d). In addition, the accumulation of extracellular and intracellular polymeric substances from bacteria can be adhered to the surface of pristine and Cel-PDA membranes, forming a dense and thick biofouling layer, as shown

inFigure. 3.4B a and b. Usually, a biofilm could obstruct ion transport, increasing the internal resistance of the system and reducing the membrane mechanical stability, ultimately leading to a decrease in the power density of MFC.(Li et al., 2020; Miskan et al., 2016).

These results showed that Cel-PDA-TiO_2:ZnO membranes could have good anti-fouling properties. AFM images can support this description, due to the fact that the formation of a biofilm layer in Cel-PDA/TiO_2:ZnO is relatively thinner compared to other membranes (pristine and Cel-PDA). Membranes with low fouling could maintain good ion transport capacity, thus avoiding the increase of internal resistance, which improves the power density and efficiency in MFC (Xu et al., 2012b).

3.3.2 Morphology by AFM,

Fig. 3.5 shows the 3-dimensional (3D) micrograph, indicating the surface topology of the pristine, Cel-PDA and Cel-PDA/(TiO_2:ZnO) before evaluation (Zone I) and after evaluation (Zone II) on MFCs with synthetic and real textile wastewater. From the three-dimensional AFM images inFigure. 4.5, it can be observed that Cellophane membranes coated by PDA and Cel-PDA with catalysts have different top maximum heights. Table 1 summarizes the maximum height (Rm) for different membranes, before and after treatment of synthetic and real textile wastewater using MFCs.

The commercial cellophane membrane exhibited the lowest maximum height with Rm = 7.2 nm (Fig. 3.5a). After the PDA layer was introduced, much higher thickness was observed (Rm 30.6 nm) (Fig. 3.5b). This change in height could be due to the incorporation of PDA on the membrane surface, as well as nodular PDA structures in the dopamine polymerization process. Comparatively, a more marked increase in Rm (up to 43.1 nm) was observed when the TiO_2:ZnO (1:1) ratio of 0.03 wt% was binding to the surface of the PDA (Fig. 3.5c toFigure. 3.5d). This major change shows the important role of nanoparticles in the membrane modification process. Thus, the morphology of the surface and the height of the modified membranes are influenced by the type of modification (Zhu et al., 2018c).

In order to evaluate the biofouling on the membrane, Figure. 3.5 and Table 3.1 show the thickness of the membranes after being used in the MFCs. Based on these observations, the catalyst-modified membranes showed photocatalytic activity under visible light radiation. For synthetic textile wastewater treatment, after evaluation, the membrane heights increased 600%, 50%, and 0.3% for pristine, Cel-PDA, and Cel-PDA/TiO_2:ZnO membranes respectively after evaluation.

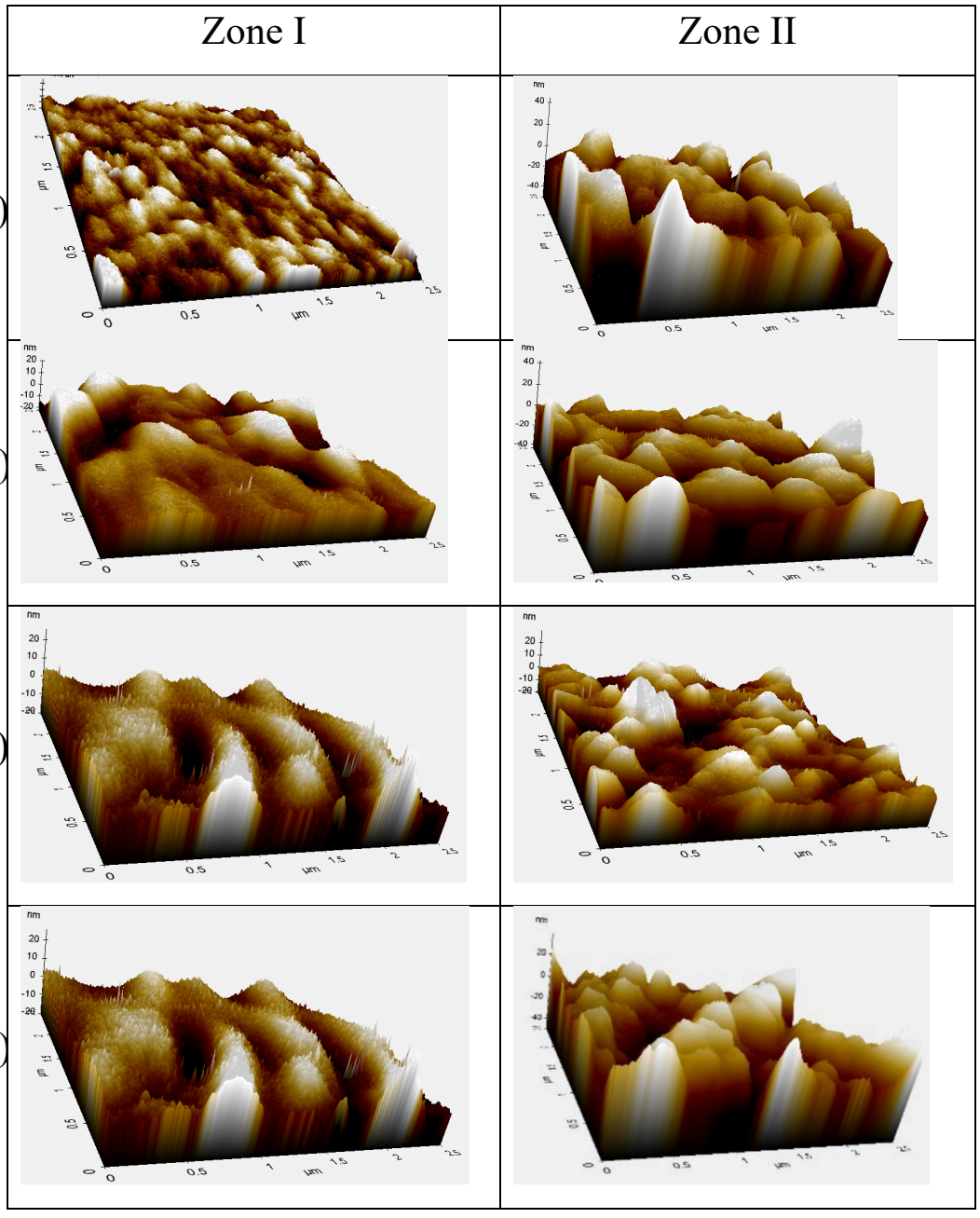


Figure 3.5. AFM 3D image morphology of membranes before evaluation (Zone I) and after evaluation (Zone II) on MFCs with synthetic textile wastewater for (a) pristine membrane (b) Cel-PDA, (c) Cel-PDA/TiO_2:ZnO, and MFCs with real textile wastewater for d) Cel-PDA/TiO_2:ZnO

These results show that the pristine membrane has a large amount of biofouling on the surface of the membrane compared with the PDA-coated membrane, which has undergone less biofouling. This effect may be due to the high hydrophilic effect of polydopamine (Barclay et al., 2017; K. Y. Kim et al., 2014; E. Yang et al., 2016b). The membrane modified with PDA and catalysts did not undergo biofouling because the height did not increase in comparison to the initial conditions. These results show that Cel-PDA/TiO_2:ZnO membrane could have anti-biofouling characteristics.

Additionally, Figure. 3.5. shows the AFM micrographs of the Cel-PDA/TiO_2:ZnO membrane before and after treatment of real wastewater in MFCs. The result shows that the membrane did not increase its thickness after two treatment cycles. This result shows that the modified membranes maintain their anti-biofouling properties when used for the treatment of real textile wastewater. As observed, the bio-inspired modification of membranes with polydopamine and catalysts (TiO_2:ZnO) in ratios 1:1 at 0.03 wt% can be a good method of membrane modification to obtain self-cleaning membranes and an ideal alternative for modification of other PEMs such as Nafion. In addition, this modification could be tested for the long-term stable performance of MFCs.

Table 3.1. AFM parameters of pristine and modified membrane surface heights. Surface scanning area values (2.5×2.5 μm^2) represented as Rm (maximum height).

Membrane	Pristine	Cel-PDA	Cel-PDA/TiO_2:ZnO	
			Synthetic TWW	Real TWW
Before Evaluation / (nm)	7.18± 1.23	30.64±2.11	43.10±2.32	43.10±3.97
After Evaluation /(nm)	43.68± 4.21	45.79± 4.52	43.21± 3.56	49.29± 4.30

3.3.3 Verification of the self-cleaning character of the membrane

In order to prove the effectivity of our modified membranes,Figure. 3.6 shows dirty membranes before and after being under 90 minutes of solar irradiation. The Cel-PDA membrane showed much cleaner surfaces after testing in contrast with the pristine membrane, which showed no self-cleaning of the surface. This effect could be because PDA does not allow the adhesion of methylene blue molecules, due to its hydrophilicity (Barclay et al., 2017). Methylene blue in pristine membrane could have methylene blue removal. This could be because the methylene blue could have photolysis under solar irradiation, as shown in other reports (Rani and Shanker, 2018; Soltani and Entezari, 2013).

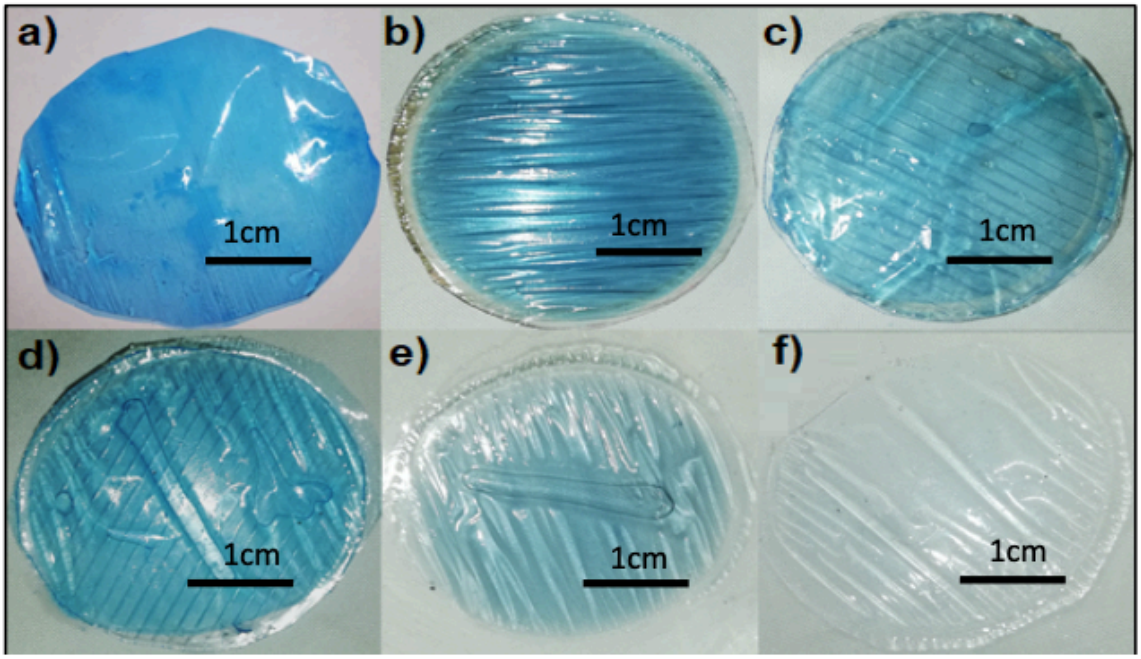


Figure 3.6. Membrane self-cleaning. a) Pristine, b) Cel-PDA and c) Cel-PDA/TiO_2:ZnO membranes contaminated with methylene blue and the effect of 90 minutes of solar irradiation on d) pristine, e) Cel-PDA and f) Cel-PDA/TiO_2:ZnO membranes

Additionally, the Cel-PDA/TiO_2:ZnO membrane showed a totally clean surface after the solar exposition. This effect could be because the catalysts nanoparticles are directly exposed to the membrane surface that receives direct sunlight (De Filpo et al., 2018; Raizada et al., 2014). The mechanism suggested by Prasannalakshmi and Shanmugam for a mix of catalysts (Prasannalakshmi and Shanmugam, 2017) could be applicable on these modified membranes. In this proposed mechanism (under sunlight irradiation), electrons present in the conduction band (CB) of ZnO can be transferred to the CB of

TiO_2. Similarly, the holes in the valence band (VB) of TiO_2 are transferred to the VB of ZnO. This process could prevent the recombination of charge carriers and their availability on the surface of the photocatalysts, thus improving the redox process. The high effective surface area of the catalysts (TiO_2:ZnO) is due to the effective pore size and volume of the catalysts, which provides a large surface area for adsorption of the dye molecules, increasing the probability of degradation.

3.3.4 Membrane surface area resistance

After modification, the membrane resistance of the pristine was 16.9 Ω cm^2. After the PDA modification layer, the resistance increased to 69.3 Ω cm^2. When the PDA layer increases, the membrane area resistance also increases, and it reflects the thickness of the modified layer, as shown in Section 3.3.2. The membrane resistance increase value corroborated the difference of the modified membrane with respect to the unmodified membrane.

For the Cel-PDA /TiO_2:ZnO membrane, the resistance dramatically decreased to 5.9 Ω cm^2. This is lower than for the two previous membranes. The significant drop in internal resistance could be attributed to two possible causes. First, the improved hydrophilicity of catalysts present on membrane surface can increase the ionic conductivity, as also reported in our previous work (Bahamonde Soria et al., 2020) and other modified membranes (Ang et al., 2019; Zangeneh et al., 2018; Zhang et al., 2013) and secondly, a surface that is highly negatively charged can enhance the bidirectional transport of cationic ions or protons throughout the membrane, leading to a decrease in resistance to mass transport (Li et al., 2018; Lu et al., 2014). This negative charge could be due to the PDA negative charge by the deprotonation of phenolic hydroxyl groups at neutral pH, and the large increase of OH groups caused by the presence of TiO_2 and ZnO NPs on the PDA layer (Heinlaan et al., 2008; Ou et al., 2010; X. Wang et al., 2019) (scheme 3.1). Moreover, Vakili et al (Vakili et al., 2020) proved that the silver nanoparticle penetration into the cellulose chains can generate spaces that enhance the permeability of ions through the membrane which could be occurring with the TiO_2 and ZnO nanoparticles in this work.

3.4 MFC performance

3.4.1 Voltage generation

The effect of membrane modification on MFC performance was evaluated by using different membranes. Both Cel-PDA and Cel-PDA/TiO_2:ZnO membranes were compared with cellophane pristine membrane. After 72 h (time of operation/cycle), the color removal percentage showed a maximum, and the anolyte was replaced. The electrochemical performance measurement of all the systems was started after the maximum voltage was stabilized. As can be seen fromFigure. 3.7, two MFCs (pristine and Cel-PDA) produced similar open-circuit voltages (OCV), approximately 740 mV, while the MFC with Cel-PDA/TiO_2:ZnO membrane produced maximum OCV, approximately 1000 mV. It is worth noting that the Cel-PDA/TiO_2:ZnO and Cel PDA achieved a longer operating time (720 h) than the pristine membrane (360 h), which might be ascribed to the severe biofouling of the pristine membrane. Additionally, MFCs with pristine membranes lasted five cycles until the membranes broke while two others lasted several more cycles. These results show that the modifications increased the lifetime of the MFCs. Within the period of over ten cycles of inducing synthetic textile wastewater, similar peak voltages were generated following the periodical addition of substrate every 3 days. In the case of the Cel-PDA/TiO_2:ZnO, the stable OCVs were 15 - 30% and 28 - 78% higher than those of the Cel-PDA and pristine membranes respectively for every batch experiments.

These results show that the modified membranes were twice as durable as the cellophane pristine membranes, most probably due to the fact that PDA can increase the hydrophilicity of the surface, which prevents the adhesion of biofouling (Kasemset et al., 2013; Ye et al., 2011). In addition, Cel-PDA/TiO_2:ZnO membranes can further improve the anti-biofouling character of the membranes owing to the elevated surface area and hydrophilicity of the TiO2:ZnO NPs, which prevents the absorption of the bacteria, increasing bactericidal activity. Additionally, bothTiO_2 and ZnO NPs are exposed on the membrane surface enables adsorption in the visible light spectrum, and they could be slightly excited by visible light 3.2 eV (~387.5 nm) (Zhang et al, 2017a), generating (•OH) radicals, which oxidize organic matter that approaches the modified membrane surface (Bahamonde Soria et al., 2020). In turn, catalyst mixtures such as TiO_2:ZnO can

increase the photogeneration probability of radicals. The exchange of electrons and holes in the conduction and valence band between these catalysts may prevent the recombination of charge carriers on the surface of the photocatalysts, which favors the formation of hydroxyl radicals (•OH) (Prasannalakshmi and Shanmugam, 2017). This statement could be further supported by verification of the self-cleaning character of the membrane Cel-PDA/TiO_2:ZnO in section 3.3.2, which shows a self-cleaning surface after solar exposition compared to other membranes (pristine and Cel-PDA).

In addition, after nine cycles, the voltage started to decrease gradually. Despite the decrease, the Cel-PDA/TiO_2:ZnO membrane showed a better performance than the others. The voltage decrease on the MFC equipped with Ce-PDA/TiO_2:ZnO membrane could be due to two factors. First, cellophane membranes used in electrochemical systems (free of biofouling) usually exhibit a relatively low lifetime (Duay et al., 2018; Li et al., 1996) due to oxidative and hydrolytic cleavage (Vakili et al., 2020), which could be even more affected in bioelectrochemical processes since these membranes can be susceptible to biofouling. Secondly, although the PDA modified membrane with catalysts doubled the lifetime compared to the pristine membrane, it is also important to mention that ROS species generated by the catalysts can also affect the membranes, suggesting that more resistant membranes may be used for future studies.

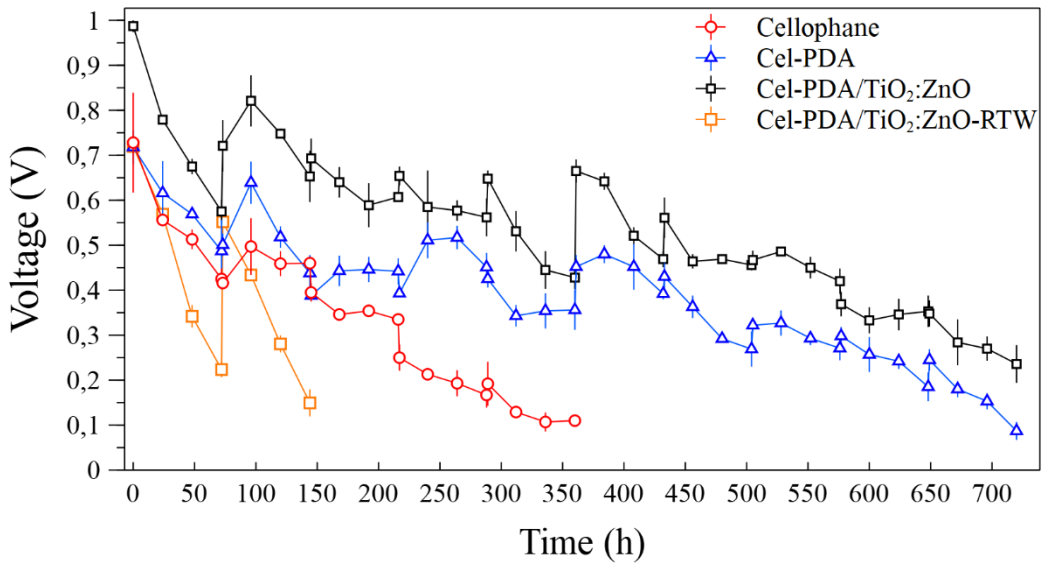


Figure 3.7. Power generation (Voltage) of MFC with cellophane, Cel-PDA and Cel-PDA/TiO_2:ZnO membrane using synthetic textile wastewater and power generation of MFC with Cel-PDA/TiO_2:ZnO membrane with real textile wastewater (RTW).

In order to evaluate the efficiency of the Cel-PDA/TiO_2:ZnO membrane, the membrane was also evaluated in the treatment of real textile wastewater.Figure. 3.7. also shows the power generation of MFC with Cel-PDA/TiO_2:ZnO membrane. As can be seen, MFC with Cel-PDA/TiO_2:ZnO generated a maximum power of 740 mV for first and second batch work. While this power is lower than the power generated with our synthetic textile wastewater, it is higher than the maximum power generated in previous works (Han et al., 2013). The difference in power generation of these studied membranes shows the advantage of this bioinspired modification on the membrane properties and the MFC performance. In addition, this higher potency could be caused by the O-H groups on the membrane surface that ease the passage of ions across the membrane, or by the fact that the membrane pores are still not blocked, which delay or inhibit the formation of biofouling (Ghasemi et al., 2013).

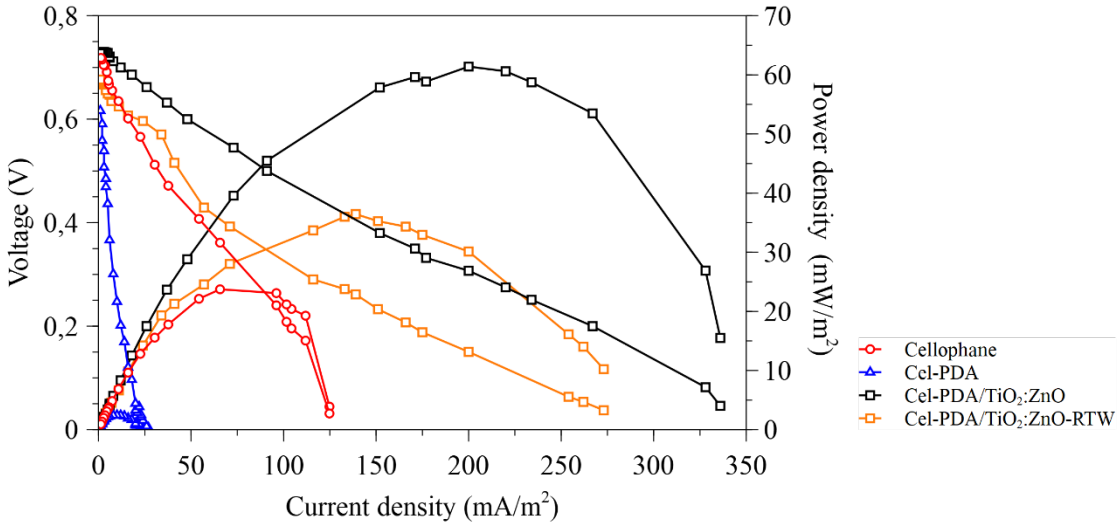
3.4.2 Power density

As shown inFigure4.8a, The PDA-coated cellophane membrane had a maximum power and current density of 3 mW/m^2 and 15 mA/m^2 respectively. These results are significantly lower than those generated by the pristine membrane, and the cellophane membrane treated with PDA and catalysts before use. which generated a peak power and power density of 24 mW/m^2 at 60 mA/m^2 respectively. This difference shows the disadvantage of coated PDA on the membrane properties. This result is contrary to previous work (K. Y. Kim et al., 2014). This difference may be due to the fact that ultrafiltration membranes were used in Kim *et al*'s work, which has larger pores than cellophane membranes. This suggests that a PDA coating can be efficient on membranes with larger pore sizes.

The Cel-PDA/TiO_2:ZnO membrane generated the highest maximum power and current density of 63 mW/m^2 at 200 mA/m^2 respectively. The current generation improvement could be credited to the reduction of internal resistance (Fig. 3.8b) of the MFC as a consequence of significant changes in membrane characteristics. First, the improvement of hydrophilicity in the membrane by catalysts and PDA can increase the ionic conductivity. Secondly, the decrease in the ohmic resistance of the MFCs may be linked to the reduction of the electrical resistance of the membrane. Finally, the OH^-

groups present on the membrane surface could negatively charge the membrane and enhance the bidirectional transport of ion/protons or cationic ions through the membrane (E. Yang et al., 2016b).

a)



b)

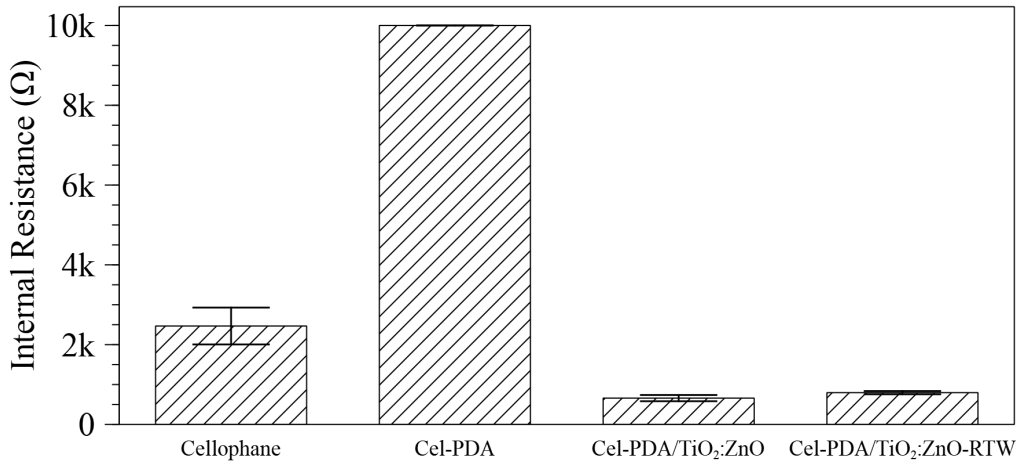


Figure 3.8. a) Polarization curves of MFCs with cellophane membrane and Cel-PDA and Cel-PDA/TiO_2:ZnO composite membranes, b) comparison of internal resistances of MFCs.

Moreover, the power density of MFC with Cel-PDA/TiO_2:ZnO was higher than that of the other membranes in all operating cycles (Appendix- informationFigure. 3.3a), while the MFC's internal resistance was kept lower in all the cycles for the MFCs with Cel-PDA/TiO_2:ZnO, showing the anti-fouling capacity of this membrane (Appendix informationFigure. A3.3b). These results are consistent with the conclusions on the power

generation, which shows that Cel-PDA/TiO_2:ZnO membrane possesses an improved anti-fouling property, while, Cellophane and Cel-PDA membranes in MFC could suffer both biofouling and inorganic pollution. Therefore, this fouling can hinder the transport of protons and ions, increasing the internal resistance of the system and reducing the mechanical stability (integrity) of the membrane (Flimban et al., 2018; Li et al., 2020).

In turn, when the membrane Cel-PDA/TiO_2:ZnO was confronted with real textile wastewater, it maintains its properties, the Cel-PDA/TiO_2:ZnO membrane maintained its good antifouling property in all cycles, which prevented high internal resistance and ensured a better energy generation density compared to the other membranes tested in this work (Fig. 3.8a and 3.8b).

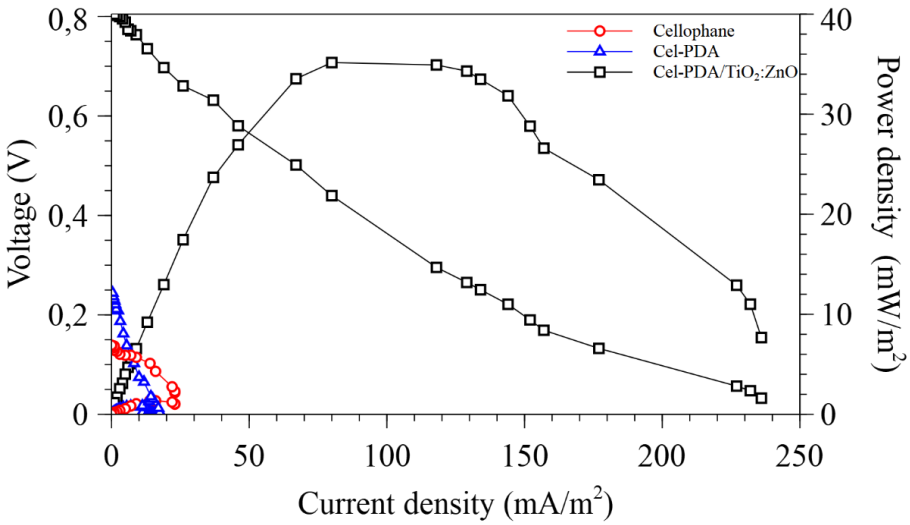
3.4.3 Durability of MFC

In order to assess the durability of studied membranes, polarization and power density curves were obtained last operating cycle of the MFC for each membrane (Fig. 3.9). On the other hand, it is important to note that the pristine membrane (cellophane) only lasted 5 cycles until it broke, while the modified membranes (Cel-PDA and Cel-PDA/TiO_2:ZnO) lasted 10 cycles (support informationFigureA3.1). These results showed that the oxidative and hydrolytic cleavage was retarded by a further 5 cycles.

Similar to the previous results the power and current density obtained by the MFC equipped with the Cel-PDA/TiO_2:ZnO membrane was always higher in all cycles. In addition, there was an increase in the internal resistance of 127.2%, 135.0%, and 0.8% for MFC with cellophane, Cel-PDA, and Cel-PDA/TiO_2:ZnO membrane respectively. These results show that MFC systems equipped with PDA/TiO_2:ZnO membranes kept a low internal MFC resistance relative to the others. Both the low resistance exhibited by the Cel-PDA/TiO_2:ZnO membrane and the increase in lifetime could be due to two reasons: firstly, membranes have a better anti-biofouling property than other candidates, which helps in enhancing the performance of the MFC. Metal oxide nanoparticles are believed to have the ability to reduce biofilm growth because both TiO_2 and ZnO nanoparticles under visible light irradiation could generate highly reactive hydroxyl radicals (•OH). (Hajipour et al., 2012), which can damage microbial cell walls, causing their inactivation (Adams et al., 2006; Yalcinkaya and Lubasova, 2017b). In addition to

this, small amounts of Zn^{2+} from the dissociation of ZnO nanoparticles can penetrate through the cell wall of bacteria previously damaged by reactive oxygen species, destroying the DNA and cytoplasm of bacteria (Lakshmi Prasanna and Vijayaraghavan, 2017; Sirelkhatim et al., 2015). Secondly, the low internal resistance of the MFC could be because both TiO_2 and ZnO nanoparticles were able to enter the cellulose chains (membrane matrix), which may enhance the permeability of ions through the membrane by the increasing spaces (Khorshidi et al., 2018; Wei et al., 2013).

Therefore, the major benefit of this modification was the improved lifetime, membrane fouling resistance, and decreased internal resistance of the MFC compared to the others studied in this work.



Figur 3.9. Polarization and power density curves obtained after 5 cycles of MFC operation for pristine membrane, Cel-PDA, and Cel-PDA/TiO_2:ZnO membranes

3.4.4 Color, COD removal and coulombic efficiency.

The efficiencies of color removal (%) in the course of sequential batch cells of synthetic textile wastewater are shown in Figure. 3.10. Wastewater color removal was observed in the MFC effluent, which suggests the practicability of wastewater treatment.

The MFC containing the Cel-PDA/TiO_2:ZnO membrane showed 90% dye removal in the first and second batch cycles, while the cells with the Cel-PDA membrane showed 79 and 75%, respectively. In turn, the cells with cellophane membrane showed lower color removal compared to the others (70%) (Fig. 3.10a). The high color removal of Cel-PDA/TiO_2:ZnO could be because the membrane with catalysts layer could

probably oxidize the dyes coming from the solution near the membrane, which is not the case for the other membranes because the catalyst particles are exposed on the surface of the membrane and receive directly the visible light radiation (Delsouz Khaki et al., 2018; Tian et al., 2009). In addition, our previous work (Bahamonde Soria et al, 2020) demonstrated that a 1:1 (TiO_2:ZnO) catalyst mixture can remove dyes close to the membrane, as shown also by other authors (Bahamonde Soria et al., 2020; Moradi et al., 2016; Štrbac et al., 2018). This result shows that the simultaneous use of membrane modification with PDA and metal oxides in MFCs would be an advantage for wastewater treatment. On the other hand, in comparison with Cel-MFCs, the major color removal of Cel-PDA MFCs could be tied to the fact that the biologically degradable/oxidizable organic fraction of the PDA could provide favorable bacterial conditions.

Fig. 4.10b. shows the bioelectricity produced, COD removal and coulombic efficiency from artificial wastewater. The Cel-PDA/TiO_2:ZnO membrane showed higher COD 59% and EC (49%) removal efficiency. As previously mentioned, more functional groups from catalysts (TiO_2:ZnO) binding to the surface of the membrane could produce these benefits (Bazrgar Bajestani and Mousavi, 2016; Di Palma et al., 2018). On the other hand, untreated cellophane with a COD (58%) and EC (28%) removal were next. Finally, Cel-PDA with 53% COD removal and only 8% EC had the lowest results.

For real textile wastewater, the performance of the Cel-PDA/TiO_2:ZnO membrane in the color removal from real textile wastewater (RTW) (COD = 374 mg L^{-1}) was evaluated for two continuous operating cycles.Figure. 3.10c represents the time-dependent UV–vis absorption spectra of color removal from real textile wastewater treated by MFC with pristine and Cel-PDA/TiO_2ZnO membranes. The MFC with pristine membrane removed around 30 % of color in RTW while MFC with modified membrane degraded 80% of the color within 72 h. This result was replicated for the second cycle. It shows that the modified membrane allows the removal of the color from the matrix wastewater. At the same time, this result suggests that ratios of TiO_2:ZnO (1:1) allow removing color and other contaminants present in this wastewater (Bahamonde Soria et al., 2020; Brooms et al., 2018; Delsouz Khaki et al., 2018; Moradi et al., 2016; Tobajas et al., 2017).

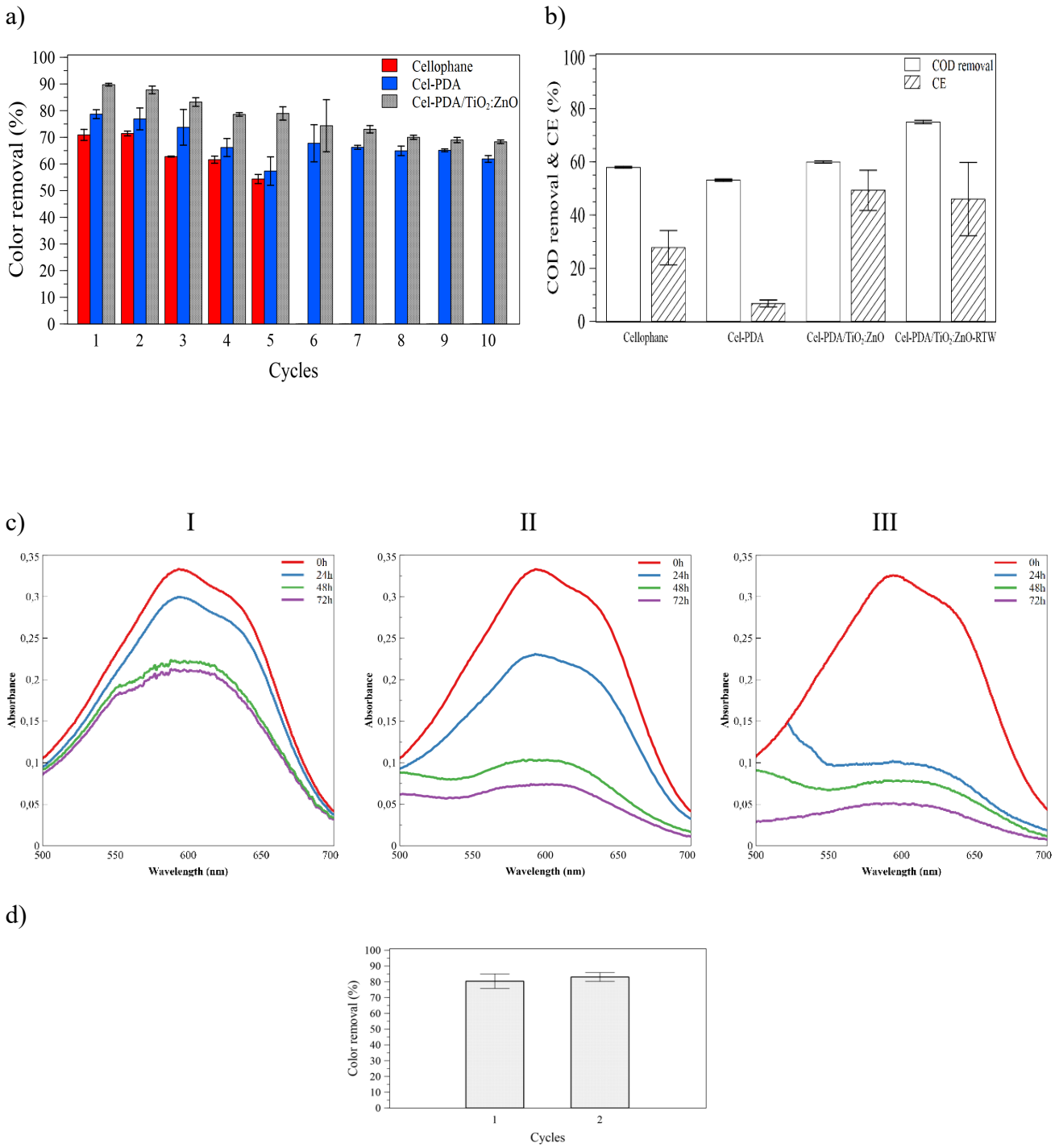


Figure 3.10. a) Color removal and b) Coulombic efficiency and (%) COD removal. c) Time-dependent UV–vis absorption spectra of the degradation of color by MFCs with (I) pristine membrane, (II) Cel-PDA/TiO_2:ZnO membranes, first and (III) second cycle, d) COD removal test of MFC with pristine and Cel-PDA/TiO_2:ZnO membranes for the first and second cycle.

In order to test the practical applicability of the MFC with a modified membrane, COD removal was measured for real textile wastewater.Figure. 3.10d shows the COD removal, which shows that the degradation efficiency in the MFC with Cel-PDA/TiO_2:ZnO dramatically increases in comparison with the MFC with a pristine membrane. The MFC with the modified membrane is able to remove COD by 81.7% on average for the first and second cycles.

COD removal is more evident for real textile wastewater than for synthetic wastewater. This may be because RTW has a greater amount of organic matter that can serve as a substrate for the bacteria present in MFCs, which creates a more favorable environment for bacterial growth and the concomitant removal of COD. On the other hand, the coulombic efficiency of the CFM-Cell-PDA TiO_2:ZnO was 46% for the actual wastewater. This indicates that the prepared membranes and the modification of membranes could help to remove COD from real textile wastewater and this procedure could be applied to modify membranes normally used in MFCs.

Results of this newly developed Cel-PDA/TiO_2:ZnO system show a superior power density compared to recent studies (Table 3.2). It is worth mentioning that the modified membranes in the S-TiO_2/PPSSA-5.0 and SPEEK+7.5%TiO_2 dual-chamber systems obtained slightly higher potency. However, our system is a single chamber and low-cost membrane, which could be further improved by enhancing the membrane quality. In addition, the membrane characteristics such as membrane resistance and open-circuit voltage indicate that the Cel-PDA/TiO_2:ZnO membrane has remarkably better membrane properties in comparison to other membranes and it is also comparable with the Nafion membrane. A fundamental advantage of this study was the photocatalyst bioinspired attached to the surface of the cellophane with PDA as a bio glue and this could help to remove contaminants using visible light in situ, i.e., the photocatalyst could be activated in the presence of sunlight on the surface of the membrane.

Table 3.2. Comparison of properties of modified membranes and performance of MFCs.

Type of reactor	Anode Volume (mL)	PEM/separator	Anolite	Maximum power density (mW m^{-2})	COD Removal (%)	OCV (mV)	Membrane surface electric resistance (Ω)	Internal resistance MFC (Ω)	Reference
Double chamber	150	Nafion 117	Artificial domestic WW	132.0	74	450	-	210.57	(Li et al., 2020)
		S-TiO_2/PPSSA-5.0		130.5	91	460	-	224.24	
Double chamber	1250	Nafion 112	K_2HPO_4, HCl and mixed culture sludge	-	-	321	-	-	(Bazrgar Bajestani and Mousavi, 2016)
		Nafion/DMF (1%TiO_2)		-	-	302	-	-	
		Nafion/DMAc (1%TiO_2)		-	-	325	-	-	
Double chamber	160	[bmim][PF_6] ionic liquid	Acetate	179	-	700	-	268	(Koók et al., 2019)
Double chamber	250	Nafion 117	Sodium acetate	17.6		612.5	5.79	-	(Di Palma et al., 2018)
		20%Fe_3O_4/PES		9.5		552.5	8.8	-	
Single chamber	28	SPEEK+7.5%TiO_2	E coli nutrient medium	98	-	800	108	-	(Narayanaswamy Venkatesan and Dharmalingam, 2015)
Single chamber	125	Cellophane (biocathode *C. vulgaris*)	Textile wastewater	2.25-6.4	92-98	420	-	-	(Logroño et al., 2017)
Single chamber	100	Cellophane-PDA/TiO_2:ZnO	Textile wastewater	61	60	1000	5.9	660	**This work**

3.5 Conclusions

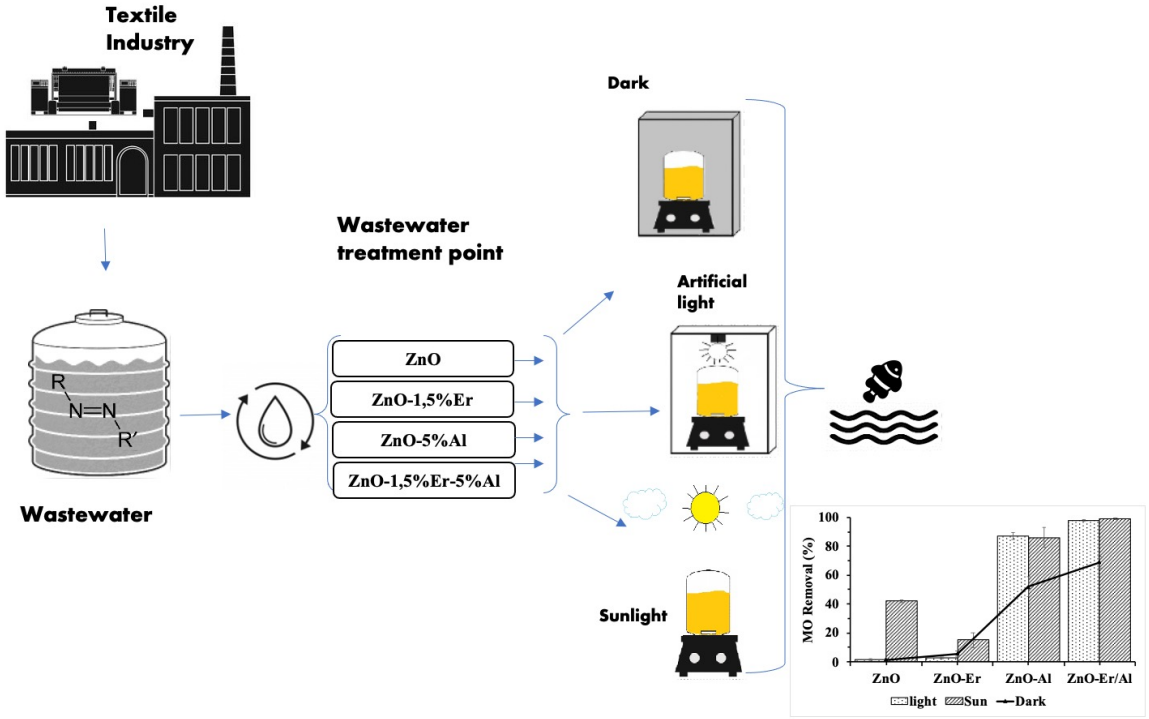
In this chapter, the mixing of catalysts TiO_2:ZnO (1:1) at 0.03 wt% was successfully bonded to the PDA layer by a bio-inspired method. In this way, Cel-PDA/TiO_2:ZnO composite cation exchange membranes with higher physical stability than the original ones were obtained. The TiO_2:ZnO composite membrane had higher hydrophilicity and cation-proton conductivity than the pristine (cellophane) and PDA coated cellophane membranes, it could be to the introduction of more negative charges (OH- groups) on the surface membrane which boosting proton transmittance. Furthermore, SEM and AFM analysis confirmed the hypothesis that the modification could minimize surface fouling. In addition, the modified membrane made the MFC more efficient, decreasing the operating cycle time of the MFC from 5 to 3 days and doubled the useful life of the MFCs. Finally, the microbial fuel cell with Cel-PDA/TiO_2:ZnO membrane increased 2.5 times the power generation in the MFC and 5.7 times the current and exhibited a maximum power density far superior to other membranes. In addition, the highest COD removal of 60% and 75% were obtained for synthetic and real textile wastewater, respectively, and in turn, a color removal of 90%. Considering its physicochemical and electrochemical properties, its good antifouling property, and its simple preparation process and lower cost, this membrane, and method of modification is a promising alternative to the new generation of modified membranes for microbial fuel cells. Also, visible light (artificial and natural) was used to activate the membrane catalysts and not ultraviolet light, which decreases operating costs and avoids violent activation of the catalysts and prevents undesirable damage to the membrane.

In order to further improve the characteristics for a new nanofiltration fuel cell system and knowing that ZnO produced better antibacterial results in chapter 2, the next chapter will synthesize a new photocatalyst which will be active with both artificial and natural visible light (sunlight), in order to support on nanofiltration fuel cells for a new nanofiltration membrane for a system (NF-MFC) and provide better antifouling characteristics.

Chapter 4. Effect of Er, Al and Er/Al dopants on the photocatalytic and antibacterial properties of ZnO nanoparticles

This chapter is based on the research paper submitted on 03/11/2021 to *Industrial & Engineering Chemistry Research Journal*: "*Effect of Er, Al and Er/Al dopants on the photocatalytic and antibacterial properties of ZnO nanoparticles*", by **Raúl Bahamonde Soria,** Jefferson Estupiñan, Irma Gonza, Monserrat Naranjo, Billy Chinchin, Patricia. Luis.

Graphical abstract:



Abstract.

Improving the absorption of photons from the visible region in catalysts could facilitate photocatalytic reactions, decreasing the consumption of electrical energy, especially in countries where the amount of sunlight is considerable. This kind of photocatalysts could become an interesting alternative for the removal of aquatic pollutants. This work reports the synthesis of ZnO and ZnO doped with 1,5 at.%Er, 5 at.% Al and 1,5 at.% Er : 5 at.%Al nanoparticles by sol-gel method. The effect of dopants on the structure, morphology, absorption spectra and photocatalytic properties were investigated by XRD, SEM, EDS and UV–Vis spectrophotometry. The results showed the existence of wurtzite ZnO structure. UV–vis diffuse reflection spectra showed that doped ZnO samples exhibited a red-shift of the band-edge as compared to the pristine ZnO. Photocatalytic activity of nanoparticles was measured by degradation of methyl orange (MO) as a model component under artificial visible light and natural (sunlight) in Quito-Ecuador. It was observed that doped ZnO with Er/Al nanoparticles showed a significant enhancement of the photocatalytic activity in the degradation of MO under solar light. These results show that solar light could realistically replace artificial light if ZnO-Er/Al catalysts are used, which could significantly reduce the operating costs of the photocatalytic process. In addition, all dopants preserved the remarkable anti-bacterial properties of ZnO against *B. subtilis,* and the presence of Er and Al co-doping of ZnO showed better inhibitory property for E. *coli* compared to the ZnO.

Keywords

Rare earths, photocatalysis, ZnO, Erbium, Aluminum, nanoparticles, Sol-gel, anti-bacterial properties.

4.1 Introduction

The removal of organic pollutants in wastewater is an important measure in environmental protection. Synthetic organic dyes are specifically used in the textile, paper, plastic leather, food, and other industries (Anandan et al., 2020). Textile wastewater contains a large amount of azo dyes, which are considered as non-biodegradable, persistent and highly stable pollutants in the environment, causing acute hazard to aquatic life (Zhu et al., 2012).

Advanced oxidation processes (AOPs) have been considered as important, promising, efficient and environmentally friendly methods for the removal of persistent organic pollutants (POPs) such as dyes from water and wastewater. Generally, AOPs are based on the in situ generation of a powerful oxidizing agent, such as hydroxyl radicals (•OH), obtained at a sufficient concentration to effectively decontaminate water (Oturan and Aaron, 2014). In situ formation of •OH radicals can occur by various chemical, photochemical (heterogeneous photocatalysis), sonochemical or electrochemical reactions (Štrbac et al., 2018). In photochemical processes, heterogeneous photocatalysis involves a process in which a semiconductor (e.g., TiO_2, ZnO, ZrO_2, SiO_2) is excited by photons from a light source with energy (*hv*) greater than or equal to the forbidden energy gap (Eg) of the catalyst; electrons from the valence band (VB) are excited and pass into the conduction band (CB) region, leaving holes in the VB. This creates an electron-hole pair (e^- /h^+). Then, diffusion of the photoexcited electrons onto the catalyst surface occurs and they react with the adsorbed oxygen, reducing it to a superoxide radical ion ($O_2^{-\bullet}$). In turn, the holes move towards the surface and react with neighboring adsorbed H_2O or dye molecules, oxidizing them to hydroxyl radicals (•OH) and oxidized dye radical cation ($Dye^{+\bullet}$) (Weldegebrieal, 2020). The most typical catalysts used for photo-electrocatalytic degradation of pollutants are titanium dioxide (TiO_2) and zinc oxide (ZnO). Both are semiconductors with a wide band gap: Eg = 3.2 and 3.4 eV for TiO_2 anatase and ZnO, respectively (Tekin et al., 2020). Titanium dioxide (TiO_2) has been used primarily for decolorizing and decomposing organic dyes (Rajeshwar et al., 2008). Nevertheless, ZnO presents a clear advantage in comparison to TiO_2 under illumination conditions regarding the inhibition of bacterial growth (even at the lowest tested dose of 10 ppm) (Adams et al., 2006). Also, ZnO is one of the multifunctional

semiconductors with exceptional antibacterial capability due to its excellent optical, electrical, mechanical and chemical properties. Typically, ZnO has a lower cost and high surface-to-volume ratio at the nanometer scale (Balta et al., 2012). These characteristics make ZnO a potential alternative that can meet the demand for an efficient and low-cost catalyst. Furthermore, it makes it a very promising catalyst for the removal of dyes from wastewater (Yoon and Oh, 2021).

ZnO can be activated under UV irradiation with a wavelength below 387 nm due to their large band spacing (3.2-3.4 eV). However, these oxides absorb only a small fraction of sunlight (less than 5% of solar energy is emitted as UV radiation) (Weldegebrieal, 2020). This aspect limits the application of these oxides on a large scale (Daghrir et al., 2013). Additionally, the recombination of the photo-generated carrier, hole and electron is also a disadvantage in semiconductor photocatalysis (Gomez-Solís et al., 2015). Preparing new photocatalysts by incorporating other elements is a major challenge in the development of the ZnO-based photocatalysts but it is a promising strategy to motivate the application of ZnO.

Several dopants are available for ZnO, such as anionic, cationic, rare earths, co-dopants and couple semiconductors (Munawar et al., 2020; Zhang et al., 2015). Cationic doping is essentially carried out by the addition of transition metals, group I and group V elements. The insertion of dopant cations such as Ce, Mn, Cu, Mg, Al, and so forth, into the crystal lattice of ZnO enables interesting modifications to its properties, adding additional energy levels to the new photocatalyst (Andrade et al., 2017). This reduces the activation energy required to initiate the photocatalytic activity and increases the catalytic efficiency of the new photocatalyst. Thus, cation-doped ZnO has a lower band gap energy value, compared to the undoped ZnO. In addition, the built-in elements act as electron traps, which suppress the recombination of photogenerated electrons and holes. This slows down the speed of electron-hole pair formation. Dopants can widen the range of light absorption and improve the photoresponse of cation-laden ZnO in the visible light range (Lee et al., 2016).
Recently, rare earths such as Erbium (Er^{3+}) have been used as dopants, due to the fact that pristine ZnO cannot directly utilize visible light to achieve photocatalysis because of its wide

band gap. Doping rare earths into the ZnO structure could enhance the visible light absorption, improving the photocatalytic activity of ZnO under visible light. This effect could improve the photocatalytic degradation of dyes in the visible light region, which could be attributed to the enhanced adsorption and 4f electron transition of the rare earth ions (Zhang et al., 2015).

In turn, rare earth metals can also reduce the work function of adsorbed oxygen species, which could enhance the oxygen adsorption capacity, forming more superoxide anions on the catalyst (ZnO) surface. This improves the amount of oxidizing species (hydroxyls, peroxyls and superoxides), increasing the rate of photodegradation of organic pollutants (Lee et al., 2016).

In addition, the co-doping of Al/Er in ZnO could further enhance the response to visible light. The doped catalysts could provide an efficient alternative for the degradation of aquatic pollutants under visible light (sunlight), especially, in countries with high solar incidence such as Ecuador.

In the present work, Er^{3+} Al^{3+} doped ZnO nanoparticles were synthesized by sol-gel method, which is one of the most efficient methods to synthesize nanoparticles. This method has precise control of the material´s structure until its final form and the homogeneity of the solution, generating exclusive properties of the nanoparticles synthesized by the sol-gel method (Mahdavi and Talesh, 2017). Nevertheless, little is known about how co-doping affects the antibacterial properties of the catalyst. The doped ZnO nanoparticles were used for the removal of dyes in synthetic textile wastewater. The photocatalytic activity was studied by degrading methyl orange in water under visible light irradiation and natural light conditions (solar radiation) in Quito, Ecuador. The optimal operating conditions were applied for the treatment of real textile wastewater from a textile company in Quito, Ecuador. In addition, the effect of the dopant on the antibacterial activity against Gram-positive (*Bacillus subtilis*) and Gram negative (*E. coli*) bacteria was also evaluated in the present study.

4.2 Materials and methods.

4.2.1. Materials

Zinc nitrate hexahydrate, 99% (metals basis) and erbium nitrate hydrate (99,9%) were purchased from Alfa Aesar (Belgium). Oxalic acid dihydrate (99,5%) and aluminum nitrate nonahydrate (95,5%) were supplied by Sigma Aldrich (Belgium). Ethanol (EtOH) (absolute alcohol) was provided by VWR Chemical Co., Ltd (Belgium). Methyl orange (MO) was obtained from Sigma Aldrich (Fisher scientific®, Reactive Grade: ACS Certified). All reagents were of analytical grade and used without further purification.

4.2.2. Synthesis of catalysts

ZnO was synthesized by the conventional sol–gel method (Chen et al., 2017). Briefly, 1,503 g (0.005 mol) of zinc nitrate were dissolved in 30 mL of EtOH and stirred at 60 °C for 30 min. After that, based on Zhang's work (Zhang et al., 2015), the most efficient concentrations of the dopants were taken, for this $Er(NO_3)_3$ and $Al(NO_3)_3$ with different Er and Al doping amounts (Table 4.1) were dissolved in this suspension with continuous stirring for 30 min to obtain solution A. Solution B was prepared by dissolving 2.507 g (0.02 mol) of oxalic acid dihydrate in 80 mL of EtOH and stirred at 50 °C for 30 min. Solution B was added to the warm solution A dropwise and continuously stirred for 1 h. A white sol was obtained and aged to form a gel, which was dried at 80 °C for 24 h. Finally, ZnO doped an undoped were obtained by thermal treatment at calcination temperatures of 400 °C for 1 hour.

Table 4.1. Composition of catalyst with different dopant ratios.

Catalyst name	Atomic% Er^{3+}	Atomic % Al^{3+}
ZnO	0	0
ZnO-Er	1,5	0
ZnO-Al	0	5
ZnO-Er/Al	1,5	5

4.2.3. Characterization of catalyst

Surface morphology of the samples was examined using SEM (JEOL, IT300) composed of an energy dispersive X-ray (EDX) detector, and analysis at accelerating voltages of 15 kV. The structure of doped and undoped ZnO powders were analyzed by X-ray diffraction (XRD) using a Bruker AXS - D8 Advance diffractometer with a Cu Kα1 source (λ = 1.5406 Å) in the 2θ range from 20º to 80º with a scan rate of 2 min^{-1} and a step of 0.02.

The average crystallite size was estimated using the Scherrer equation $D = K\lambda/\beta \cos\theta$, where *K* is a constant (0,92) reflecting the shape factor, λ= 0.154 nm, mean wavelength of $CuK\alpha_1$ radiation, β is the FWHM of the Bragg peak, and θ is Bragg's angle in radians.
Diffuse reflectance UV-Vis (DRUV) spectra were recorded on a Shimadzu UV-Vis-NIR spectrometer (Shimadzu Benelux, The Netherlands) equipped with a Praying Mantis in a spectral range from 200 to 600 nm using the Shimadzu UV software package. A Spectralon pellet was used to measure the background spectrum, and the Kubelka–Munk function F(R) was calculated based on the reflectance (R). The band gap energy value (Eg) was calculated from the optical absorption edge in the DRUV spectra using the Tauc method. $(FR\ h\nu) = A(h\nu\text{-}Eg)^n$, where FR is the Kubelka−Munk function, A is a constant, h is Planck's constant, *v* is the photon frequency, Eg is the optical band gap and n is 2 for a direct semiconductor (Andrade et al., 2017). Finally, BET surface area was measured using the Micromeritics AutoChem II apparatus.

4.2.4. Photocatalytic activity

The photocatalytic activity of pristine ZnO and Er, Al co-doped ZnO was evaluated by the degradation of MO. 0.01, 0.03 and 0.05 g of the photocatalyst were added to 100 mL of 10, 25 and 50 mg/L MO solution in a 200 mL beaker under continuous stirring.
Under artificial visible light, the suspension was irradiated by three different commercial lamps 20W UV Blacklight lamp Sylvania MLX 20W BL368, 18 W LED lamp (4000K) 2000

lumens (Philips CorePro LED bulb A67 18W 840 Mat), and 9W led (4000K) 987 lumens Osram Parathom Classic A 9W 840 Matt. All bulbs were provided by Budgetlight (Belgium), and were placed 15 cm above the liquid level for 24 hours.

Under solar light, the photocatalytic activity of the prepared catalysts was also studied by degrading an aqueous solution of Methyl orange at the previously mentioned concentrations. The degradation of MO was tested under the influence of sunlight in Quito (Ecuador) between September 10th and October 10th, 2020. The time period used in the evaluation was kept constant from 11:00 a.m. to 2:00 p.m. to standardize the UV irradiation (Rajamanickam and Shanthi, 2012). The tests were performed when the UV Index in Quito - Ecuador started in 10, according to the Ecuadorian National Institute of Meteorology and Hydrology (Ambient secretary government of Quito Ecuador, 2020).
During the experiment, several solution samples (2 mL) were collected at various treatment times, centrifuged for 15 min at 13000 rpm and then analyzed in a UV-Vis spectrophotometer to determine the concentration of MO at 464 nm.

All experiments were also performed inside a dark chamber to avoid interference from ambient light and were done in triplicate reporting the average values.
The removal rate (η) of MO can be calculated as follows:

$$\eta = \frac{C_0 - C_t}{C_0} x100\% \qquad (1)$$

$$\eta = \frac{A_0 - A_t}{A_0} x100\% \qquad (2)$$

Where Co, and Ct, are the concentrations of MO at t=0 and after an irradiation time *t*, respectively and, Ao and At are the absorbance of MO at t=0 and after an irradiation time *t*, respectively.

4.2.5. Antibacterial activity

The antibacterial activity of four catalyst suspensions was evaluated using culture turbidity as the estimation of cell growth in test tubes. The test tubes with each sample were placed in a thermostatic bath with agitation. Experiments were carried out under dark and

light conditions in order to evaluate the influence of visible light into the antibacterial activity of synthetized nanoparticles. To simulate dark conditions, the test tubes were wrapped in aluminum foil, whereas for light conditions, an artificial light bulb of 18W 2000 lumens was placed 30 cm above the liquid level.

Bacillus subtilis (Gram positive) and *Escherichia coli* (Gram negative) bacteria were employed to test the antibacterial activity of nanoparticles. The bacterial suspensions were freshly prepared, being the initial concentration of bacteria 10^2 UFC/ mL into the test tubes. For this, aqueous catalyst stock suspensions (10000 mg/L) were prepared under constant stirring. Then, test tubes containing 10 mL of Iso Sensitest broth medium were supplemented with the corresponding µL of stock suspensions of each catalyst to obtain a final concentration of 300 mg/L catalyst and finally 100 µL of bacterial suspension were added to each test tube. Blanks were also prepared for each sample.

To evaluate the bacterial growth behavior, the optical density (OD) at 600 nm was measured, using an UV-vis spectrophotometer Hach DR1900. Blank readings were taken, measuring the OD due to the culture media and nanoparticles suspensions. A tube containing only 10 mL of culture media and 10^2 UFC/ mL of bacteria was used as positive control. These test tubes were placed in a shaker and were allowed to growth overnight at 35 ºC, for *B. subitilis* and *E. coli* respectively. The OD at 600 nm of suspension (containing the bacteria and catalysts) was periodically monitored and the OD of test tubes after 24 hours was measured. The percentage of growth inhibition compared to the positive control was used as indicator of the antibacterial activity of nanoparticles. Cultures of nanoparticle-free medium under the same growth conditions were used as a negative control. To avoid potential optical interference during optical measurements of the growing cultures caused by the light-scattering properties of the nanoparticles, the same culture liquid medium without microorganisms, but containing the same concentration of nanoparticles cultured under the same conditions was used as blank control. After 24 h, cultures were diluted to 10^{-6} and placed onto tryptic soy agar (TSA) plates in triplicates and incubated at 37 ºC to determine the presence of viable bacteria. Colonies were counted and the percentage of growth

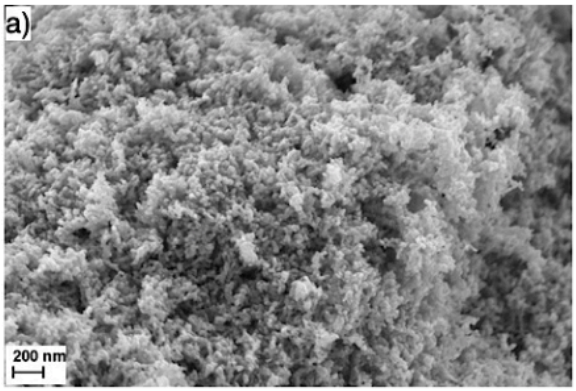
inhibition was calculated and plotted for each catalyst. The experiments were repeated at least three times.

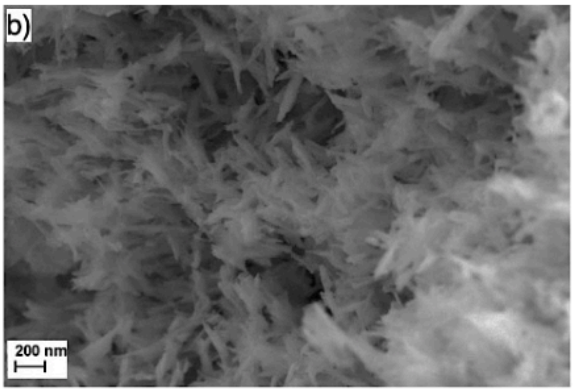
4.3 Results and discussion

4.3.1. Morphology of composites

The morphology of synthesized pristine ZnO and doped ZnO samples was investigated using SEM technique.Figure. 4.1 shows some aggregations of nanoparticles. Er-Al co-doped ZnO synthesized by the sol-gel method has the typical morphology of ZnO nanoparticles, as observed inFigure4.1a-d. The pristine ZnO structures in Figure 4.1a are in agreement with the reported literature, observing a granular form (Chen et al., 2017). However, ZnO-Er, ZnO-Al and ZnO-Er/Al nanoparticles exhibited a mixed structure of rod-like and flake shapes and the flake shape increased when erbium and aluminum were used as dopants. The incorporation of both Er^{+} and Al^{+} ions replacing the ZnO lattice could influence the formation of nano-sized rods.

In addition, an increase in particle size in Er-Al co-doped ZnO showed that the grain growth of ZnO particles can be hindered by the presence of doping elements (Er and Al) (Divya and Pradyumnan, 2016). Furthermore, the particles with small size have very large specific surface area so that strong local aggregation can be found in the images. Few bigger particles are also seen in the micrograph, which may be due to the aggregation or overlapping of smaller particles (Bououdina et al., 2017).





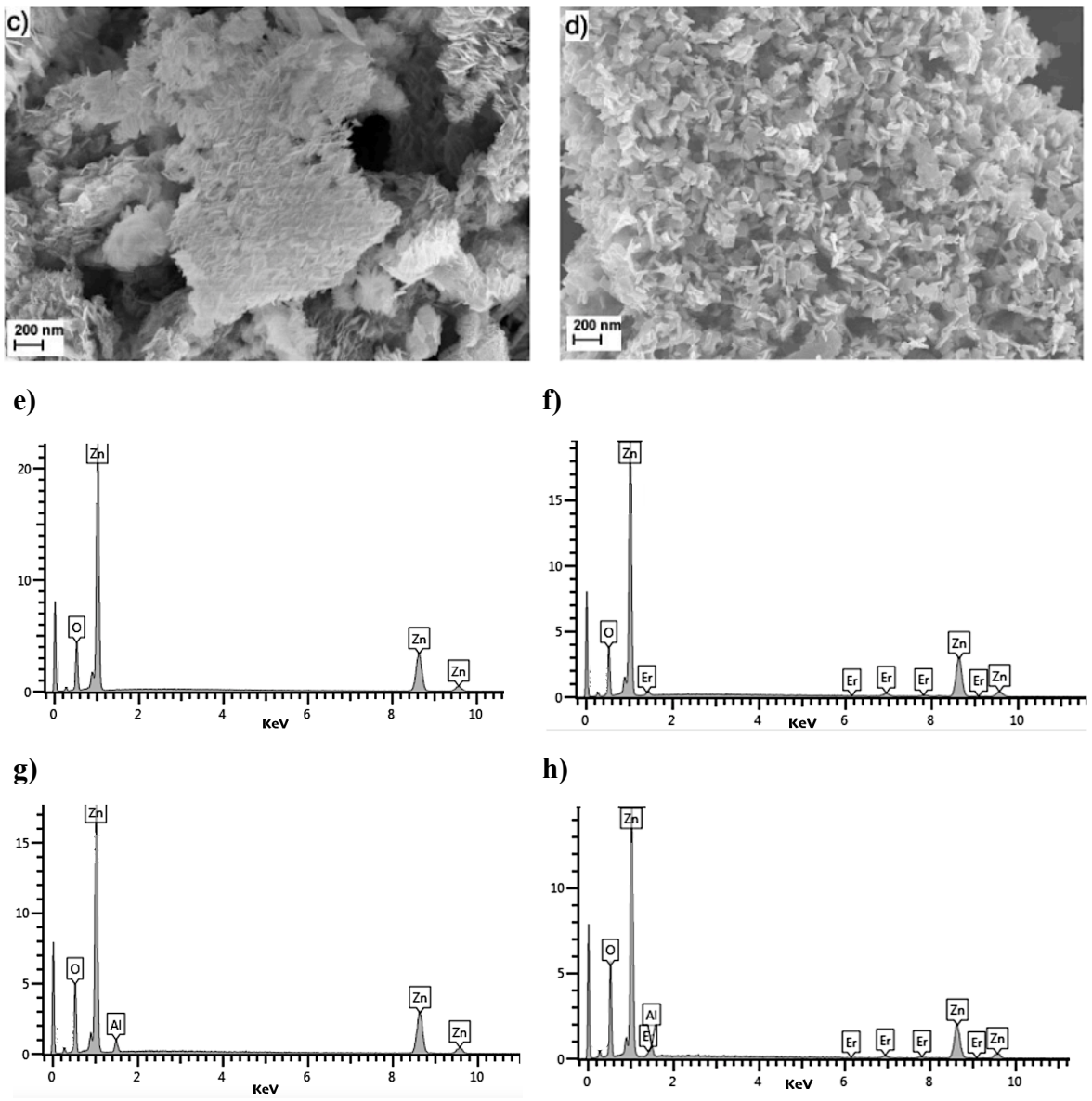


Figure 4.1. SEM images of pristine ZnO (a), ZnO-Er (b), ZnO-Al (c) and ZnO-Er/Al (d), As well as EDX spectrum of pristine ZnO (e), ZnO-Er (f), ZnO-Al (g) and ZnO-Er/Al (h),

The EDX spectra of the pristine ZnO (Figure4.1e) was compared whit doped ZnO (Fig.4.1f-h), which show the presence of Al, Er and Al/Er ratio. The weight percentage of oxygen content decreased in co-doped nanopowders, which confirmed the incorporation of the Al and Er into the ZnO matrix. The atomic percentages in all samples were verified and were as expected regarding the synthesis (Table 4.2). All doped samples contain only O, Zn,

Al and Er. Therefore, no other impurity-related peaks were observed, which reveals the high compositional purity of the samples.

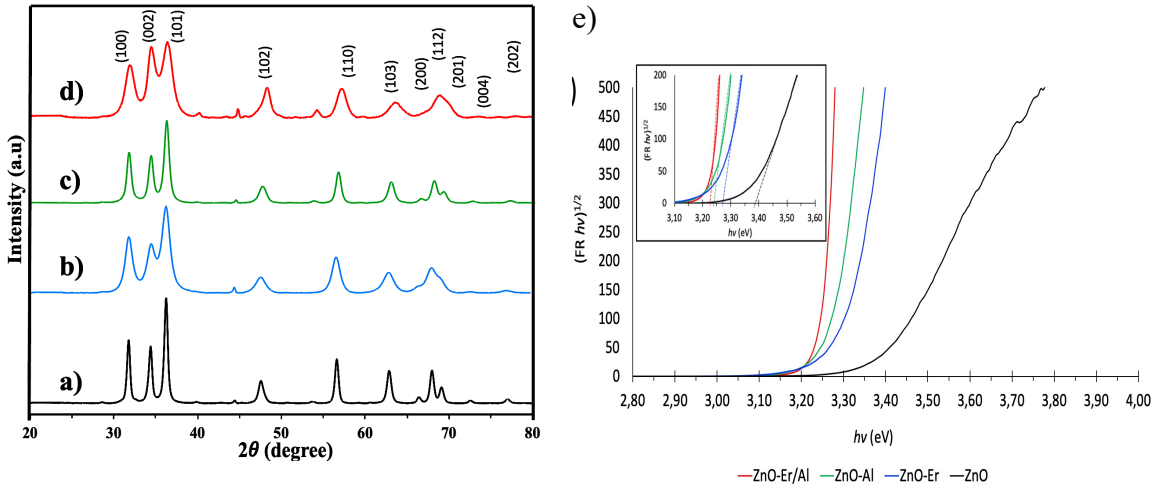
Table 4.2 Elemental composition of synthesized pristine ZnO and doped ZnO samples.

Sample	**atomic%**			
	Zn	**O**	**Er**	**Al**
ZnO	56.61	43.24	0	0
ZnO-Er	50.42	47.32	1.52	0
ZnO-Al	50.10	44.8	0	5.06
ZnO-Er/Al	44.74	48.51	1,46	5.15

4.3.2. XRD analysis

The crystal structure of the prepared nanopowders was investigated by powder X-ray diffraction. Figure 4.2 showed the XRD patterns of pure ZnO (Fig. 4.2a: ZnO) and doped ZnO (Fig. 4.2b: 0% Al, 1,5% Er,Figure. 4.2c: 5% Al, 0% Er andFigure. 4.2d: 5% Al, 1,5% Er). The XRD peaks at 2θ were 31.8°, 34.4°, 36.3°, 47.6°, 56.6°, 62.9°, 66.5°, 68.0°, 69.1°, and 77.0° and were indexed to the (100), (002), (101), (102), (110), (103), (200), (112), (201), and (202) planes of the ZnO crystal given by the standard data file. All observed peaks can be indexed within the wurtzite type structure, in agreement with the data JCPDS card No. 36-1451. No additional peaks corresponding to any form of oxides of Al or Er were observed (Fig. 4.2b–d). This indicated the complete dissolution of (Er, Al) dopants within ZnO crystal lattice by occupying Zn sites (Ghomri et al., 2018). Interestingly, the presence of Er and Al caused a decrease in all ZnO peak intensities (Fig. 4.2d) which resulted in a FWHM increase also implying that Er–Al co-doping inhibited the growth of crystal size. Thus, it is understood that Al^{3+} and Er^{3+} ions substituted Zn^{2+} ions sites within the ZnO crystal, suggesting a change in the lattice parameters. However, all samples show a preferred orientation along the (101) direction of the ZnO phase.

The calculated crystallite sizes of ZnO-Er, ZnO-Al, ZnO-Er/Al and pristine ZnO were 17.46 nm 13.90nm, 10.28nm and 21.84 nm, respectively, according to the Scherrer's equation (Andrade et al., 2017).



f)

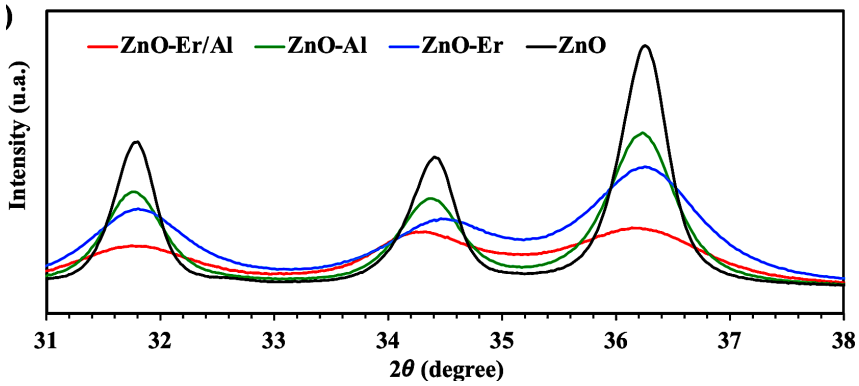


Figure 4.2.- XRD patterns of a) un-doped ZnO, b) ZnO-Er, c) ZnO-Al and d) ZnO-Er/Al and f) zoom-in for the range 31-38º; (FR $h\nu$)$^{1/2}$ versus $h\nu$ curves for band gap determination of the ZnO and the doped ZnO nanoparticles**.**

In addition, the ZnO-Er/Al photocatalyst showed the highest specific surface area (119.48 m^2 g^{-1}) compared to (92.59 m^2 g^{-1}) for ZnO. The BET surface area of the ZnO-Er/Al catalyst is 22.5% higher compared to the area of pure ZnO. The surface area increase could be due to the alteration of the crystal structure of the host ZnO by the addition of dopants (Er

and Al), which could lead to the inhibition of crystal growth through the introduction of these elements into the ZnO lattice. Therefore, the ZnO-Er/Al photocatalyst is more probable to show optimum dye removal rate due to the availability of higher textural properties.

4.3.3. Optical properties

Optical properties of pure and co-doped ZnO nanopowders were studied by DRS. The bandgap energy (Eg) was determined by using Tauc's plot by applying equation: $(FR\ h\nu)^{1/2} = A(h\nu - Eg)$ (Makuła et al., 2018). The bandgap energy estimated from the intercept of the linear portion from Figure. 4.2f, was found to be 3.22, 3.23, 3.24 and 3.32 eV for ZnO-Er/Al, ZnO-Al, ZnO-Er and pure ZnO respectively by the extrapolation of the $(FR\ h\nu)^{1/2}$ versus $h\nu$ plots (Viezbicke et al., 2015).

The data showed that the co-doping (Er, Al) slightly reduced the band gap energy (Eg) in comparison with the pristine ZnO (Figure4.2f). This could be attributed to the defects created by dopants along with the changes of lattice parameters due to incorporation of Er and Al in ZnO crystal lattice. Besides, these dopants can result in the formation of oxygen vacancies and additional energy levels, which increases the average atomic distances and decreases the energy gap, which can harvest more photons to excite the electron from the valence (Ghomri et al., 2018). The smallest Eg leads to the highest photocatalytic efficiency under visible light illumination (Zhang et al, 2017), which correspond to the sample with both Er and Al.

4.3.4. Catalyst dosage on methyl orange (MO) Degradation

In order to determine the optimum catalyst concentration, experiments were carried out at three different concentrations (0.01, 0.03, 0.05%wt) under an 18W LED lamp with solutions of 25 mg MO/L in presence of a ZnO-Er/Al. The concentrations 0.01, 0.03 and 0.05%wt of catalyst showed 85.8, 98.7, and 97.5 % MO removal, respectively. This behavior could be due to the fact that when the photocatalyst amount is increased more active sites can be found on the photocatalyst surface, which increases radicals formation (Chen et al., 2017).

However, there is a slightly higher value for the 0.03 %wt (0.3g/L) concentration compared to the following concentration 0.05 %wt (0.5g/L), which could be due to the probability that at higher catalyst concentration the probability of aggregation of catalyst molecules also increases, decreasing the amount of available active sites where photocatalysis takes place. Thus, 0,3g/L (0,03%wt) of catalyst was chosen as the optimal amount to continue the study.

4.3.5. Photocatalytic performance of synthesized nanoparticles

After comparison of different light sources (Appendix Figure A4.1), it was concluded that there is not significant difference among the different lamps. Thus, only the results obtained using the 18W LED lamp are shown in this section, since its energy consumption level is lower than the other lamps used.

Since the photocatalytic reaction occurs on the surface of the catalysts, and recombination of the photogenerated electron and hole is very fast (nanosecond timescale), interfacial charge carrier transfer is possible only when the donor or acceptor is pre-adsorbed before the photocatalytic reaction (Xu et al., 2002). Thus, the adsorption equilibrium of MO was studied. Suspensions were stirred for 30 min in the dark condition to ensure equilibration of MO over the oxide surface, and the amount of MO adsorbed on the oxides was tested by comparing the concentration before and after stirring.

The preliminary adsorption of the substrates and the amount of adsorption are very important pre-requisites for highly efficient degradation. The results summarized in Figure 3a showed that the order of decreasing adsorption capacity was ZnO-Er/Al>ZnO-Al>ZnO-Er>ZnO. Thus, ZnO had the smallest adsorption amount of MO and the ZnO-Er/Al sample had the largest one. All doped samples showed stronger adsorption capacities than pure ZnO, thus it is expected to reach high reactivity in samples with strong adsorption capacities. The photocatalytic activity shows thus a positive correlation with the amount of adsorption over the catalysts. The results indicate that the amount of substrate adsorbed on the catalyst is an important factor affecting the photocatalytic activity.

In addition, Er and Al co-doped ZnO showed clearly an enhanced removal, followed by Al doped ZnO. In this study, Al^{3+} ion plays the trap role, preventing recombination of electron and holes, and improvement of photocatalytic activity (Mahdavi and Talesh, 2017).

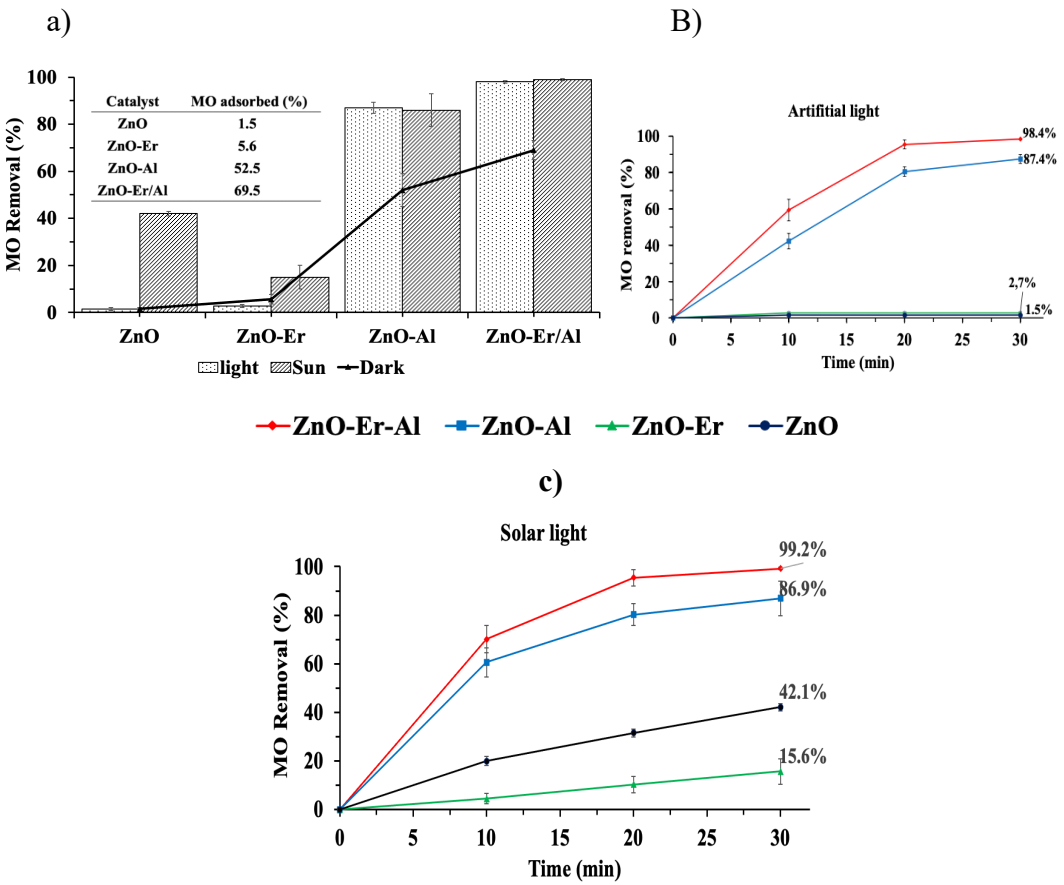


Figure 4.3. Photocatalytic degradation curves of methyl orange (25 mg/L) using ZnO, ZnO-Er, ZnO-Al and ZnO-Er/Al under a) Comparison of photodegradation rate of MO using different catalysts after 30 min, b) artificial white light (18W) and c) solar light irradiation.

This fact is attributed to Al^{3+} and its release on the surface of catalyst because the placement of Al^{3+} at donor level prevents the recombination of excited electrons and holes of valance band. Also, Al doping can decrease band gap quantities (section 4.3.3) as a

sideway band, creating an excessive energy surface between two conduction and valence bands which reduces band gap (Dong et al., 2011; Fu et al., 2011; Mahdavi and Talesh, 2017). The following equations describe the proposed mechanism:

$$ZnO + UV \rightarrow e^- + h^+ \quad (3)$$

$$Al^{3+} + e^- \rightarrow Al^{2+}\ (trap\ of\ electron) \quad (4)$$

$$Al^{3+} + h^+ \rightarrow Al^{4+}\ (trap\ of\ hole) \quad (5)$$

$$Al^{2+} + O_2 \rightarrow Al^{3+} + O_2^-\ (release\ of\ electron) \quad (6)$$

$$Al^{4+} + OH^- \rightarrow Al^{3+} + \cdot OH\ (release\ of\ electron) \quad (7)$$

As shown in Eqs. (4) and (5), the Al^{3+} ion can react with electron and holes and creates Al^{2+} and Al^{4+} ions, which are unstable in comparison with Al^{3+} and, in order to achieve stability, they react with oxygen and hydroxyl ion on the surface of the catalyst, producing radicals of superoxide and hydroxyl (Mahdavi and Talesh, 2017). Thus, Al^{3+} entraps electrons and holes due to preventing of couple and releases them by reaching to the catalyst surface (Eqs. (6) and (7)).

In addition, Er doping in ZnO-Al benefited to visible-to-UV up conversion followed by photocatalytic oxidation of MO, as it can easily accommodate discrete 4f levels of light emitting rare earths ions in their broad forbidden gap to tune the excitation and emission ranges (Layek et al., 2016). Er^{3+} has luminescence efficiency in the green region and low UV absorption ability, but its doping with ZnO enhances absorption and thus luminescence efficiency. Furthermore Er doping could reduce the crystal size of ZnO, resulting in maximum photocatalytic activity (Divya and Pradyumnan, 2016). In this regard, ZnO-Er/Al could represent a new class of luminescent materials.

Interestingly, the Er-doped ZnO showed an inefficient photocatalytic activity under artificial light (figure 4.3b). This result could be due to the band-gap energies of the rare earth oxides used in the experiments are not sufficient for initiating photocatalytic reaction after UV irradiation (Layek et al., 2016; Xu et al., 2002). In contrast, ZnO-Er had slight

improvement under sunlight radiation (figure 4.3c). It could be due to the fact that the level of UV radiation in Quito Ecuador was high during the evaluation time, which improved the photocatalytic capacity of ZnO-Er. This result can be verified since the pure ZnO also increased its photocatalytic activity in under sunlight.

4.3.6. Determination of the antibacterial activity of ZnO doped and un-doped samples**.**

The catalyst concentration 0.03%wt has shown to be a good minimum inhibitory concentration (MIC) against *B.subtilis* and *E.Coli* in both dark and light conditions, as shown in Figure 4.4.

For *B. subtilis*, all catalysts showed outstanding bacterial growth inhibition (~ 93%). Interestingly, this work has shown no negative effect of dopants on the inhibition of bacterial growth for *B.subtillis* (Figure 4.4a). In the case of *E. coli*, the inhibitory activity of ZnO (78%) was lower compared to the inhibitory activity of doped samples. Apparently, the doping contributed to the improvement of the inhibitory activity, the ZnO-Er/Al sample showed better inhibitory activity among the doped samples (94%) (Figure 4.4b).
It is known that ZnO can be photo-catalytist under UV light, which could be a reason for the production of reactive oxygen species (ROS). However, the antibacterial tests of this work were also carried out under the dark conditions showing good results too. These results show that ZnO could maintain its antibacterial properties even if the ZnO nanoparticles are in dark conditions, which is in agreement with previous work (Zhang et al., 2007).

The antibacterial activity of ZnO nanoparticles, against Gram-positive and Gram-negative bacteria could be related to its capacity to produce reactive oxygen species (ROS) and the formation of coordination bonds between metal ions with N, O or S atoms presents in biomolecules (Prasert et al., 2020; Raghupathi et al., 2011). The greater inhibition on *B. subtilis* could be attributed to the higher capacity of penetration and destruction of the Zn^{2+} ion to the cell wall of these Gram-positive bacteria, since they have a soft cell wall compared to Gram-negative ones as *E. coli*. Although it is not clear why zinc exhibits different bacterial affinity with gram-positive, it may be ascribed to the difference in the protein constituents of their cell walls (Bahamonde Soria et al., 2020).

ROS species, also ease the mass transport and dispersion of reactant molecules which are being generated by the mitochondria. The ROS species can basis the devastation of DNA and cellular proteins by direct diffusion or through endocytic vesicle formation. The incorporation of particles in the cytoplasm or nucleus can cause damage to the plasma membrane or DNA (Munawar et al., 2020). Besides, the use of dopants of ions could lead to enhance the antibacterial activity. Saxena & Pandey (2019) demonstrated that Al doped ZnO nanoparticles had greater antibacterial activity against *E. coli* and *E. hirae* than ZnO nanoparticles attributing this enhanced activity to the electrostatic interactions between bacterial cell and positively charged Al doped ZnO nanoparticles (Saxena and Pandey, 2019). In the same context, the antibacterial activity of lanthanide oxides nanoparticles has been studied, it was observed that Er oxide nanoparticles were effective against *E. coli* and *P. aeruginosa* under dark and light conditions (Dědková et al., 2017).

This work presents evidence that the Er and Al co-doping of ZnO showed an increase in antibacterial activity for *E. coli* compared to synthesized ZnO. Also, co-doping apparently did not affect the good antibacterial activity shown by pure ZnO against *B. subtillis.*

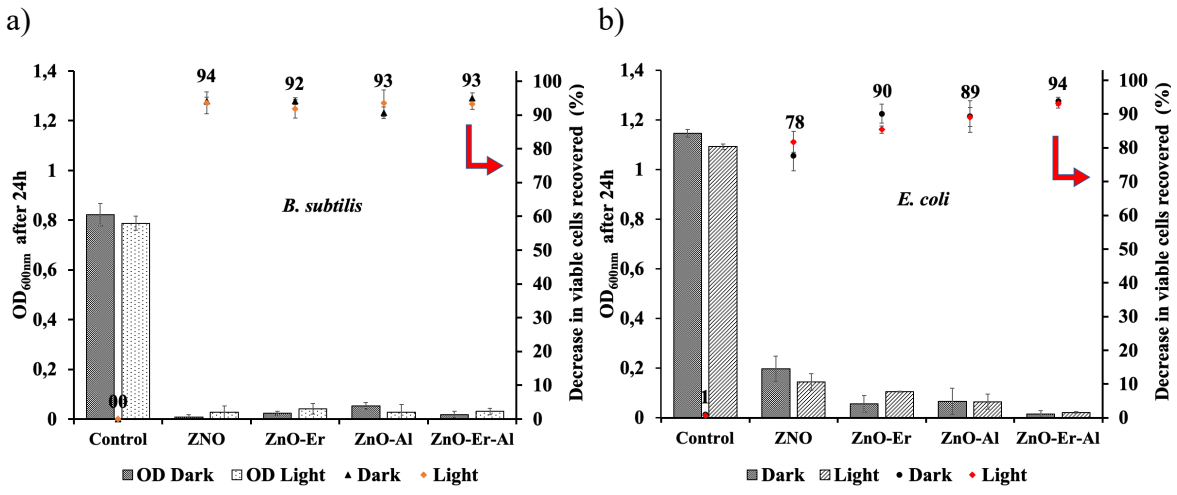


Figure. 4.4. Effect of dopant on ZnO nanoparticles on the growth of *B. subtilis* and *E. coli* strain. The growth analysis was measured by optical density (OD) at 600 nm after 24h, and

the growth inhibition measured by viable bacteria recovered from TSA plates after 24 h of incubation at 37 °C for a) *B. subtilis* and b) *E. Coli.*

4.4 Conclusions

The photocatalyst ZnO-Er/Al prepared by sol–gel method exhibits simple operation, flexibility, and high photocatalytic efficiency. The SEM-EDX results revealed that Er and Al ions were successfully doped into ZnO. The insertion of Er ions into the crystalline structure of the ZnO nanoparticles decreased their photocatalytic activity in comparison with other samples. The Al ion into ZnO structure enhanced the photocatalytic activity but the co-doping Er/Al obtained the highest MO removal results, compared to the other catalysts. Both artificial and natural light source (sunlight) present the same effect on MO removal for ZnO-Er/Al, with a slight increase for sunlight. It could be due to the fact that all dopants exhibited a broad absorption band slightly shifted to the visible region, leading to reduction in the band gap energy. These results show that the sun (free source) could replace the artificial source used for MO removal for ZnO-Er/Al catalysts, which could reduce the operating costs of the catalyst.

Respect to cytotoxicity, Er and Al co-doping of ZnO showed an increase in antibacterial activity for *E. coli* compared to synthesized ZnO. Furthermore, all dopants apparently did not affect the good antibacterial activity shown by pure ZnO against *B. subtillis*, which generates positive perspectives on the inhibitory properties of these catalysts.

According to these results, we can say that the synthesized catalyst is efficiently activated by visible light and possesses antibacterial characteristics, thus, it is an excellent candidate for modifying nanofiltration membranes for nanofiltration fuel cells.

Chapter 5. Influence of Er-Al-ZnO photocatalyst in the antifouling performance of new nanofiltration Microbial fuel cells

This chapter is based on the research paper (under preparation): "*Influence of Er-Al-ZnO photocatalyst in the antifouling performance of new nanofiltration microbial fuel cells*" by **Raúl Bahamonde Soria** and Patricia. Luis.

Abstract

Textile industry processes often use aromatic dyes. Their discharge into surface waters is undesirable since azo dyes and their decomposition products could have toxic and/or mutagenic properties in aquatic environments.

Some Bioelectrochemical systems (BES), such as microbial fuel cells (MFCs), are capable of producing energy by treating wastewater, these systems are considered promising sustainable waste-to-energy platforms and part of the circular bioeconomy. However, the high cost of some materials, such as membranes, has led researchers to explore alternatives. Membranes applied so far in BES can be divided into two groups: porous-loaded membranes (macro, micro and ultrafiltration), and non-porous-charged membranes, which are osmotic membranes (uncharged) and ion exchange membranes (cation and anion exchange, and bipolar). However, nanofiltration (NF) membranes have never been tested in MFCs. NF membranes are in a transition region between ultrafiltration (porous) and reverse osmosis membranes (non-porous). In addition, membrane fouling is also a problem in all the configurations and membranes studied. Therefore, nature-inspired modifications using polydopamine (PDA) and semiconductors such as TiO_2 and ZnO could provide the membrane with the ability to oxidize organic matter that tries to adhere to the surface, providing self-cleaning and antifouling performances.

In the present work, the technical feasibility of nanofiltration membranes as a new membrane for microbial fuel cell (NF-MFC) was investigated. Additionally, the modification of nanofiltration membranes with PDA as a support for an Er^{3+} and Al^{3+} doped ZnO photocatalyst activated by visible light is proposed, evaluating the impact on water recovery, COD removal, energy production and membrane antifouling properties during long periods of operation of the NF-MFC in the treatment of textile wastewater as a feed solution.

The results showed that the Er-Al/ZnO composite membrane presented a high antifouling capacity and maintained almost constant water permeability during long periods of operation. However, the modified membrane presented lower energy production efficiency compared to the pristine membrane, even so, the achieved power densities were higher than those of recently published osmotic fuel cells. Finally, since the catalyst used in

the present work can be activated by visible (solar) light, the energy efficiency for catalyst activation can be even higher.

Keywords
Biofouling, photocatalysts, polydopamine, microbial fuel cell, osmosis.

5.1 Introduction

Textile wastewater contains a large number of toxic substances such as azo dyes, which are potentially carcinogenic and threaten the health of humans and aquatic life. Typically, the methods for dye removal in wastewater are adsorption, flocculation, biological treatment and photocatalysis techniques. However, high cost, high time demand and high energy consumption give these methods relative ineffectiveness (Wu et al, 2020).
Bioelectrochemical systems (BES) have the ability to recover nutrients and/or recover energy from various sources of organic waste, such as wastewater (Logan and Rabaey, 2012; Rittmann, 2008). An electrochemical system consists of an anodic and a cathodic electrode, usually separated by an ion-selective membrane to create two separate compartments in which a current can be applied (electrolytic system) or occur spontaneously (galvanic system), usually in these systems at least one of the reactions at the electrodes (oxidation and/or reduction) can be catalyzed by microorganisms (De Vrieze et al., 2018). When an abiotically catalyzed reaction at the cathode occurs at a higher potential compared to a biotically catalyzed reaction at the anode, the result is a cell potential, which means that energy can be obtained from the combination of both reactions (De Vrieze et al., 2018; Rabaey and Verstraete, 2005). This configuration is referred to as a microbial fuel cell (MFC) (Logan et al., 2006c)

This kind of bioelectrochemical systems are based on successive processes (a) electron transfer from the cathode to the dissolved species, (b) ion transport through the electrolyte and (c) electron transfer from the dissolved species to the anode (Oliot et al, 2016). For each electron that is released from the cathode and collected at the anode, a positive ionic charge must move to the cathode or a negative ionic charge must move to the anode. The speed of

this chain controls the performance of the system since, if the transport of ions in the electrolyte is not fast enough, it can severely limit the rate of electron transfer at the electrodes. Ion transport through the electrolyte causes a loss of power in the cell, which can be reduced by decreasing the distance the ions must travel (anode-to-cathode distance) (Oliot et al, 2016; Zhang et al, 2009). However, in MFCs the chemical composition within the electrolyte at the anode and cathode must be different. Therefore, the use of a separator between the anode and cathode has been standardized (Zhang et al., 2009).

Membrane-based separators used in BES can be divided into two groups: porous-loaded membranes (micro- and ultrafiltration), which are size-selective polymeric membranes, and non-porous-loaded membranes made of non-porous ionomers, which are osmotic membranes (unloaded) and ion exchange membranes (cation and anion exchange, and bipolar, called CEM, AEM and BPM, respectively), the latter being the most commonly used (M. Oliot et al., 2016; E. Yang et al., 2016a). MFCs have been combined with forward osmosis (FO) membrane technologies, which recover water from wastewater using an osmotically driven force generated by the concentration difference across a semi-permeable membrane. Which have shown increased energy generation and reduction of the pH gradient between the anodic and cathodic chambers due to the active proton/ion transport incurred by the water flux generated by the osmotic pressure difference across the FO membrane (E. Yang et al., 2016a). Nevertheless, FO membranes have many similar characteristics to nanofiltration (NF) membranes (Liu et al, 2013).

As far as is known, nanofiltration membranes have not been used in bioelectrochemical systems. NF membranes are in a transition region between ultrafiltration (porous) and reverse osmosis membranes (non-porous). NF membranes have the ability to retain solutes both by the size and charge of the molecules, due to the fact that, ions can be retained by ionic charge interactions with the membrane, moreover, multivalent ions are known to have even higher rejection than monovalent ions for their higher charge interaction (Van Der Bruggen et al., 2004). In addition, it is known that NF membranes are generally negatively charged (Darbi et al., 2003), which contributes to the high rejection of anions such as sulfates, nitrates (Deepti et al., 2020; Labarca and Bórquez, 2020) or ions with high toxicity such as arsenic

in the form of arsenate(Fang and Deng, 2014). However, the removal of cations has also been proposed. In turn, due to their small pore size (10 and 100Å) they can be considered as a good candidate to reduce the oxygen and fuel crossover through the compartments (Oliot et al, 2016). These advantages make NF membranes interesting candidates as separator in Bioelectrochemical systems. However, the treatment of waste with high solids and organic matter content can be problematic for the performance of the BES, generating problems of clogging and fouling of both the electrodes and the membranes (Bakonyi et al., 2018). The incorporation of some inorganic nanomaterials, such as, zeolites, TiO_2, MgO_3Ti, SiO_2, ZnO, silver, zirconia and others into membranes have shown enhance in the performance of various filtration membranes (Anand et al., 2018; Bahamonde Soria et al., 2020). The nanomaterials could exhibit a major hydrophilicity, charge, anti-fouling/biofouling, salt rejection and anti-scaling and antibacterial properties (Anand et al., 2018).

However, many of these inorganic oxides need to be activated with a UV light source, which leads an extra expenditure of energy. ZnO is known to exhibit considerable antibacterial activity, due to photocatalysis and dissociation of ions Zn^+ (Bahamonde Soria et al., 2020). However, this catalyst also must be photoactivated by UV light. Studies show that the doping of rare earths such as Erbium (Er) or transition metals produces an improvement in the absorption of visible light and production of hydroxyl radicals, these last ones in charge of the organic matter degradation (Bahamonde Soria and Luis, 2021; Bououdina et al., 2017; Ghomri et al., 2018; Zhang et al., 2015).

Recently, mussel-inspired polydopamine (PDA) deposition has been considered a promising modification method of surface membranes, due to the adhesive capacity of PDA, which is used as a method of incorporating nanoparticles on membrane surfaces (Zhu et al., 2018a).

Therefore, in this chapter, the technical feasibility of nanofiltration membranes as a new membrane for microbial fuel cell (NF-MFC) is investigated. In addition, the modification of nanofiltration membranes with PDA as a support for a visible light activated Er^{3+} and Al^{3+} doped ZnO photocatalyst is proposed, evaluating the impact on water recovery, COD

removal, energy production and anti-fouling properties of the membrane over long periods of NF-MFC operation from textile wastewater as a feed solution.

5.2 Materials and method

5.2.1 Materials

Commercial polyamide nanofiltration membrane, NFX (150-300Da) manufactured by Synder filtration (USA) was used for all experiments. Tris(hydroxymethyl) aminomethane (Tris, 99.8% by weight) and dopamine hydrochloride (99% by weight) were purchased from Acros Organic-Belgium. Copper (II) sulfate (CuSO4, 99 wt.%), hydrogen peroxide (H_2O_2, 30 wt.%), hydrochloric acid (HCl) and sodium hydroxide (NaOH, 98 wt.%) were purchased from Sigma-Aldrich (Diegem, Belgium). Erbium nitrate hydrate (99.9%) and 99% zinc nitrate hexahydrate (metal base) were purchased from Alfa Aesar (Belgium). Aluminum nitrate not dehydrated (95.5%) and oxalic acid dihydrate (99.5%) were purchased from Sigma Aldrich (Belgium). Ethanol (EtOH) (absolute alcohol) was supplied by VWR Chemical Co., Ltd (Belgium). Methyl orange (MO) was obtained from Sigma Aldrich (Fisher scientific®, Reactive Grade: ACS Certified). All reagents were used as received. Deionized (DI) water purified by a Milli-Q ultrapure unit was used to prepare the solutions.

5.2.2 Synthesis of photocatalyst and membrane modification

The synthesis of the Er-Al/ZnO catalyst was carried out according to the procedure described in Section 4.2.2 in Chapter 4. The NFX nanofiltration commercial membranes were immersed in deionized water for 12 hours before modification. The membrane modification methodology was performed as indicated in Section 2.2.2 in Chapter 2. Nanofiltration microbial fuel cells will be designated Pristine NF-MFC and Er-Al/ZnO MFC, according to the membranes used: pristine nanofiltration membrane and modified membrane, respectively. The NF membrane used in the Er-Al/ZnO MFC was precoated with a layer of polydopamine (PDA) in an alkaline medium (pH =8.5); the coating time was 1h. Then, a suspension of Er-Al/ZnO nanoparticles (0,03 wt%) in Tris buffer (pH 8.5, 10 mM) was

deposited on the PDA layer (1hr). In order to obtain good disaggregation of the nanoparticles, the photocatalyst suspension was previously stirred for 3hr at 1000 rpm by magnetic stirring and then sonicated in an ultrasonic bath for 1hr (25°C). After modification, the membranes were carefully rinsed five times with distilled water before use. Prior to use, the membranes were kept in sodium chloride solution (0.5 g L^{-1}).

5.2.3 SEM membrane characterization

Scanning electron microscopy (SEM) was used to study the surface membrane morphology by SEM (JEOL IT300 equipped with an EDX-MAN1-Oxford Instrument). The membranes were dried and cut into small pieces and immersed in liquid nitrogen for around 1 min. The frozen fragments of the membranes were broken and taped onto holder with carbon type. The samples were sputtered with gold before the measurement.

5.2.4 Membrane surface electrical resistance and antifouling properties

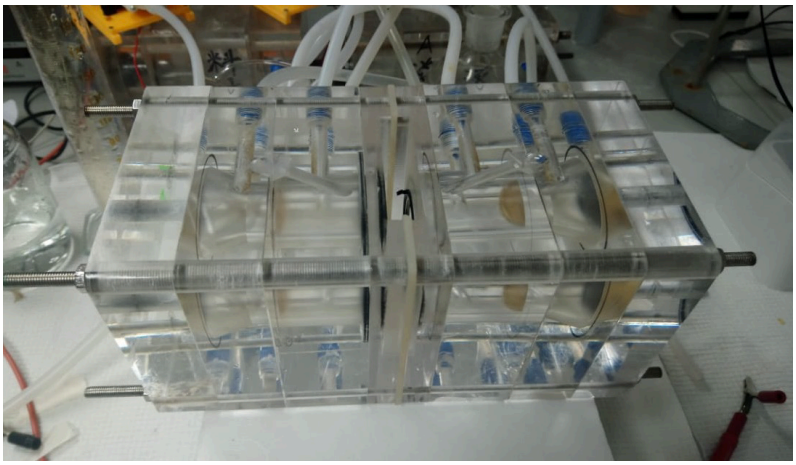
The surface electrical resistance and antifouling properties of membranes were measured in the device (Figure 5.1) (Zhao et al, 2019; Zhao et al, 2020, 2018). The R_{mem} (Ω cm^2) was calculated as section 3.2.4 in the chapter 4(Soria et al., 2021):

$$R_{mem} = \frac{U-U_o}{I} \times S$$

where U and Uo are the voltage (V) of the membrane and target, respectively, I is the constant current through the membranes (4 mA) and S is the effective area of the membrane (7.065 cm^2).

The separators used in MFCs are typically fouled by organic and inorganic foulants. Here, Bovine Serum Albumin (BSA) was used as organic fouling material, the BSA solution was placed in the diluted solution compartment of the Figure 5.1. The increase in the R_{mem} at determinate time was used to evaluate the overall antifouling property of membranes. The membrane resistance was measured with a Metrohm Electrochemical System by electrochemical impedance spectroscopy (EIS) over a frequency range from 1 kHz to 1 MHz. The conductivity cell was filled with 0.5M NaCl solution in each compartment with an effective area of 0,25 cm^2.

a)



b)

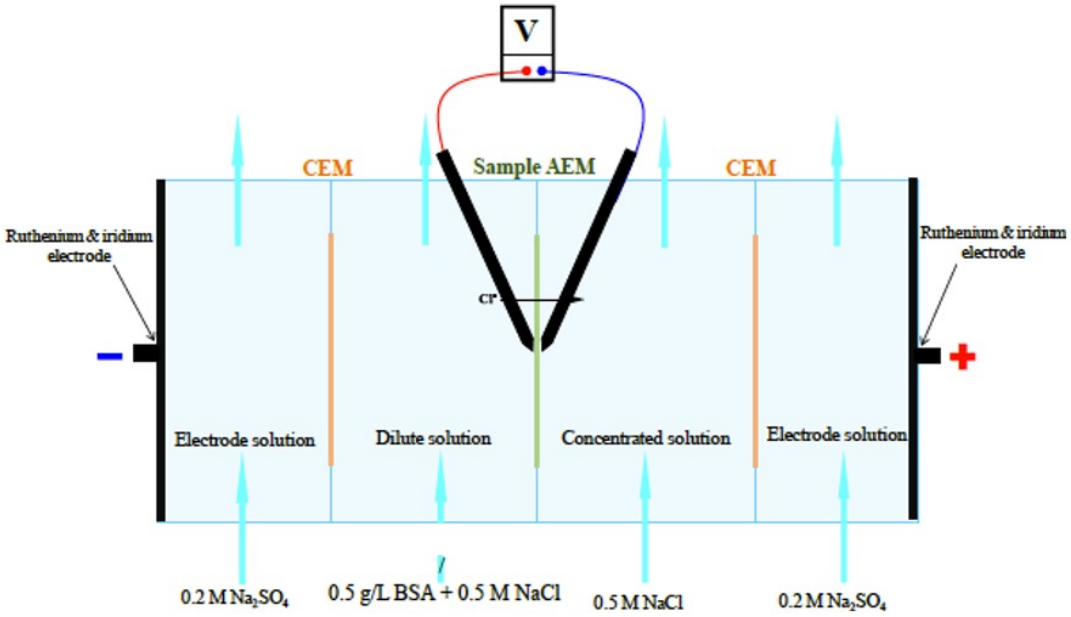


Figure 5.1. Membrane surface electrical resistance and antifouling properties of a) real device and b) device schematic.

5.2.5 Experiment setup of NF-MFC and operation

Plexiglass double-chamber NF-MFC cells with 0.1 L volume were fabricated for the anode and cathode. 25 cm^2 was the effective surface area of the NF membrane. The anode was a carbon fiber brush of 9cm^2 of area, purchased from Ecscell and 0.5mg cm-2 Pt 60%

carbon cloth (15cm^2) was used as cathode, which was purchased from fuel cell store USA. The electrodes were connected by Ni-Ti wires (0.016, Fresmile) to an external resistor of 10 Ω. The anode electrodes were pretreated following this procedure, 1) immersed in acetone (12h). 2) washed six times with deionized water; 3) immersed in ammonium peroxydisulfate (0.5 mol L-1) (15 min) and followed in sulfuric acid (1.5 mol L-1) for 15 min; and finally, 4) heated in an oven at 450 °C (30 min).

In order to activate the photocatalyst, the experiments were realized under artificial visible light. A commercial lamps 18 W LED lamp (4000K) 2000 lumens (Philips CorePro LED bulb A67 18W 840 Mat) was placed 15 cm above the anode chamber (figure 5.2). The activation process was based on our previously work (Chapter 4).

a) b)

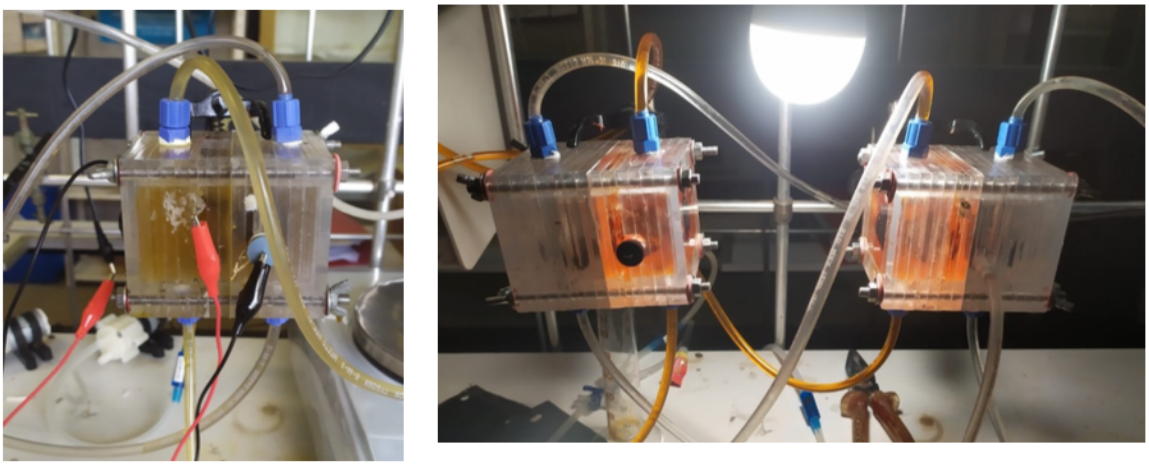


Figure 5.2 a) NF-MFC system and b) under light conditions

As a comparison system, cubic MFCs exposed to air (100 mL volume) were made of Plexiglas (Figure 5.2) and doped with nafion membranes (Fuel cell store, USA). Carbon cloth (ELAT- Hydrophilic, Fuel Cell Store., USA) with 25 cm^2 apparent surface area was used as the anode electrode, while in the air-cathode chamber carbon cloth (0.5 mg Pt-cm^{-2}, 60% Platinum at Vulcan Fuel Cells Store, USA) was used as the cathode (25 cm^2). Both electrodes were connected through Ni-Ti wires (0.016, Fresmile).

5.2.6 Inoculation

The composition of the synthetic wastewater (feed solution) was a modified M9 medium containing 6 g L^{-1} of Na_2HPO_4, 3 g L^{-1} of KH_2PO_4, 0.5 g L^{-1} of NH_4Cl, 0.5 g L^{-1} of NaCl, 0.1 g L^{-1} of $MgSO_4$ $7H_2O$, 14.6 mg L^{-1} of $CaCl_2$ and 4 mL L^{-1} of a mixed solution of trace elements (Guo et al., 2017), subsequently adjusted to pH 8, to remove oxygen from the system nitrogen gas was flushed through for 30 min. The anodic chamber had with 4 g L^{-1} (48 mM) of sodium acetate as electron donor and 100mg L^{-1} of methyl orange (MO) as dye. The anodic anode chamber was inoculated with 50 mL (8 vol%) of fresh anodic effluent from an existing acetate-fed bioelectrochemical system dominated by *Geobacter spp*. provided by Center for Microbial Ecology and Technology (Ghent University, Belgium). During the operation, each chamber was stirred gently using a magnetic bar at a speed of 250 rpm, and the temperatures were regulated at 35°C and 25°C for cathode and anode respectively. The draw solution for the cathodic chamber was a one mol L^{-1} solution of PBS containing 53 g KH_2PO_4 and 107 g K_2HPO_4 in 1 L DI water of deionized water. The anode was operated in a continuous mode with the HRT of 6.7 h. The cathode compartment was aerated with the air at a flow rate of 10 mL min^{-1} to provide oxygen for cathode reaction and create flow turbulence. The catholyte was recirculated at 21 mL min^{-1}. A 250-mL flask placed on a digital balance (VWR, LP-2102i, Italy) was used to measure the mass change in the draw solution. The feed and draw solutions were replaced every three days. A period of the NF-MFC operation from one solution replacement to the next replacement was defined as a single batch cycle.

5.2.7 Measurement and analysis

NF-MFC voltage was recorded using a data logger and Picolog 6beta software (ADC-24 Terminal Board, Pico Technology Co., Ltd., UK) and converted to current and power according to $V=IR_{ext}$ and $P=IV$. The power density curve was obtained from the measured

voltage as $P = V^2/R_{ext} A$, where P is the power density (mW m^2), R_{ext} is the external resistance and A is the Area of anode electrode in m^2.

The pH and conductivity of the extraction solution were measured with a portable meter (Metrohm Instruments, CH-9100 Herisau, Switzerland). The concentration of chemical oxygen demand (COD) in the influent and effluent of the feed solution was analyzed following standard methods with a DR/890 colorimeter (HACH Co., Ltd., USA) (Xue et al., 2021).

The change in anodic DO was observed using the DO probe (HACH, USA) and oxygen mass transfer coefficient *k*o (cm/s) was determined using the following equation:

$$ko = -\frac{v}{At} ln\left[\frac{Cc-Ca}{Cc}\right] \quad (1)$$

where, Cc is saturated DO concentration in the cathode chamber and Ca is the anode chamber DO concentration at determine time t (s), *v* is the volume of anode chamber (100 mL), A is the membrane effective area (25 cm^2). The oxygen diffusion coefficient Do (cm^2/s) was also calculated using Do= Im *k*o , where, Im is the thickness of the membrane.

Coulombic efficiency (CE), was determined following Eq (2):

$$CE = \frac{\sum(I \times \Delta t)}{F \times COD_{removed} \times 4} \times 100\% \quad (2)$$

Where, F is Faraday's constant (i.e., 96485 C mol^{-1}) and $COD_{removed}$ is the COD removed in a time interval (t), mol.

The change in water flux was evaluated by was calculated by the mass change in the draw solution reservoir versus time, the water flux (Jw, L m^{-2} h^{-1} as LMH)) was determined as follow (Eq 3):

$$J_w = \frac{\Delta V}{\Delta t\, A_m} \quad (3)$$

where, ΔV is the volume change of the draw solution, Δt is the time interval between two successive reading, A_m is the membrane surface area in m^2.

The reverse solute flux, RSF (g m^{-2} h^{-1}, or gMH), was determined by the net mass change of the feed solution per unit membrane area and unit time (Eq 4):

$$RSF = \frac{C_f V_f - C_i V_i}{A\,\Delta t} \qquad (4)$$

Where C_i y C_f are initial and final feed solution concentrations, and V_i and V_f are initial and final feed volumes over a predetermined time Δt (12h).

In order to evaluate the influence of pressure on water permeability and salt rejection ($MgSO_4$ and NaCl) in NF-MFCs, the membranes were studied separately using a transparent plastic dead-end cell (Figure 5.3, Amicon® Stirred Cells Merck-USA), whit active area of 31.6cm^2. All membranes were evaluated under visible light. To compare the performance of the modification, the membranes were tested before and after the modification. The dead-end cell was filled with 100mL of salty solution 1g L^{-1}($MgSO_4$ and NaCl) and tested at ambient temperature at 5 bar for limitation of cell. The permeate was collected when the system reached steady state. The water permeability (A_{wbar}) was calculated as follow: $A_{wbar} = J_w/\Delta P$ Where water flux (J_w) was calculated from (Eq. 3) and ΔP is the transmembrane pressure. In order to reduce concentration polarization, the stiring speed was established at 500rpm. The salt rejection (R) was calculated by conductivity measures of the permeate solution (Cp) and concentrated solution (Co) as follow: R= 1-Cp/Co.

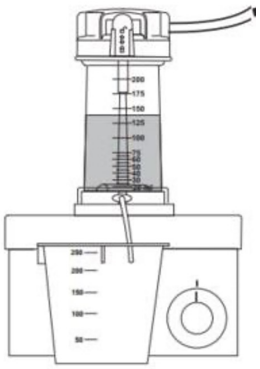


Figure 5.3. Transparent plastic dead-end cell (Amicon ® stirred, model UFSC20001, Merck USA)

5.2.8 Salt rejection under dark conditions

The salt rejection of the membranes was evaluated in a relative long-term condition, the salt rejection was carried out in a cross-flow devise (Armfield FT17-UK) (Figure 5.4) with 9.2cm of diameter membrane and effective filtration area of 0.0059m^2, the experiment was done in no light conditions. In order to test the pressure influence on the water flux and salt rejection, two pressures were evaluated 5 bar and 10 bar.

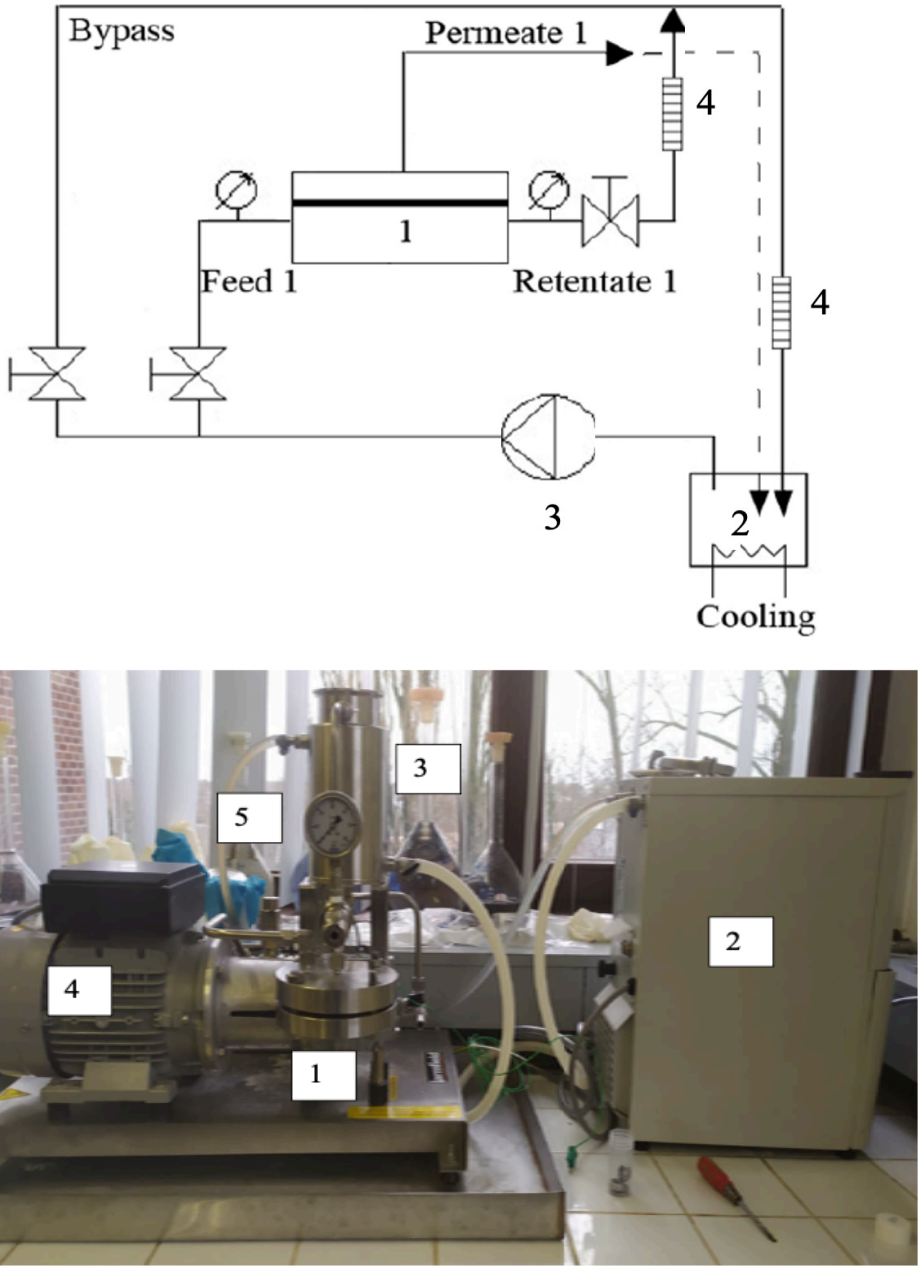


Figure 5.4. a) Schematic representation of cross-flow nanofiltration devise and b) real device, (1, module membrane, 2 cooling, 3 feed tank, 4 pump, and 5 flow meter).

5.3 Results and Discussions

5.3.1 MFC performances

Enrichment and adaptation of electrochemically active bacteria for NF-MFCs was previously performed in batch mode under a fixed external resistance of 10Ω for approximately 2 months. All MFCs reached peak power around the seventh or eighth batch, suggesting that the anode was enriched with electrochemically active bacteria. Subsequently, polarization curves were obtained for all NF-MFCs using various resistors (10Ω at 10 MΩ) with an interval of 20 min, necessary for voltage stabilization.

Figure 5.5 shows the performance of NF-MFCs with two different membranes. The power density measured in the cells with pristine membranes always showed a better power density (Figure 5.5 a and b) compared to the modified membranes. The Nafion membrane showed 25% and 50% higher performance than the pristine and modified membrane respectively. This result shows that the Nafion membrane has better ionic conduction than the nanofiltration membrane. However, it is necessary to emphasize that the Nafion cell was a single compartment cell and equipped with larger Pt doped cathodes, which may influence the better electrical production. For the nanofiltration fuel cells, a higher performance of the pristine nanofiltration membrane was observed compared to the Er-Al/ZnO membrane, showing a power density of 185 ± 11 and 117 ± 15 mW m^{-2}, respectively. This could be due to the fact that the photocatalyst present on the modified membrane surface may affect the bacterial growth of the anodic compartment, because the antibacterial activity of catalyst is raised as demonstrated in Chapter 4. In addition, the aggregates of these inorganic materials may reduce the ion mobility, yet our previous work showed that the use of a membrane with a mixture of catalysts (TiO_2:ZnO) on the surface had a positive effect on the power density, hence, presumably the new Er-Al/ZnO photocatalyst is activated more efficiently by visible light, thus, this catalyst may have a greater antibacterial effect than the mixture of catalysts. However, in the present work, the power density for all membranes was higher than some recent studies of osmotic fuel cells (Bhagat et al., 2021; Gangadharan et al., 2021; Xue et al., 2021). These results are promising due to the fact that this work is the first one carried out

with nanofiltration membranes, which opens the way to explore more types of nanofiltration membranes.

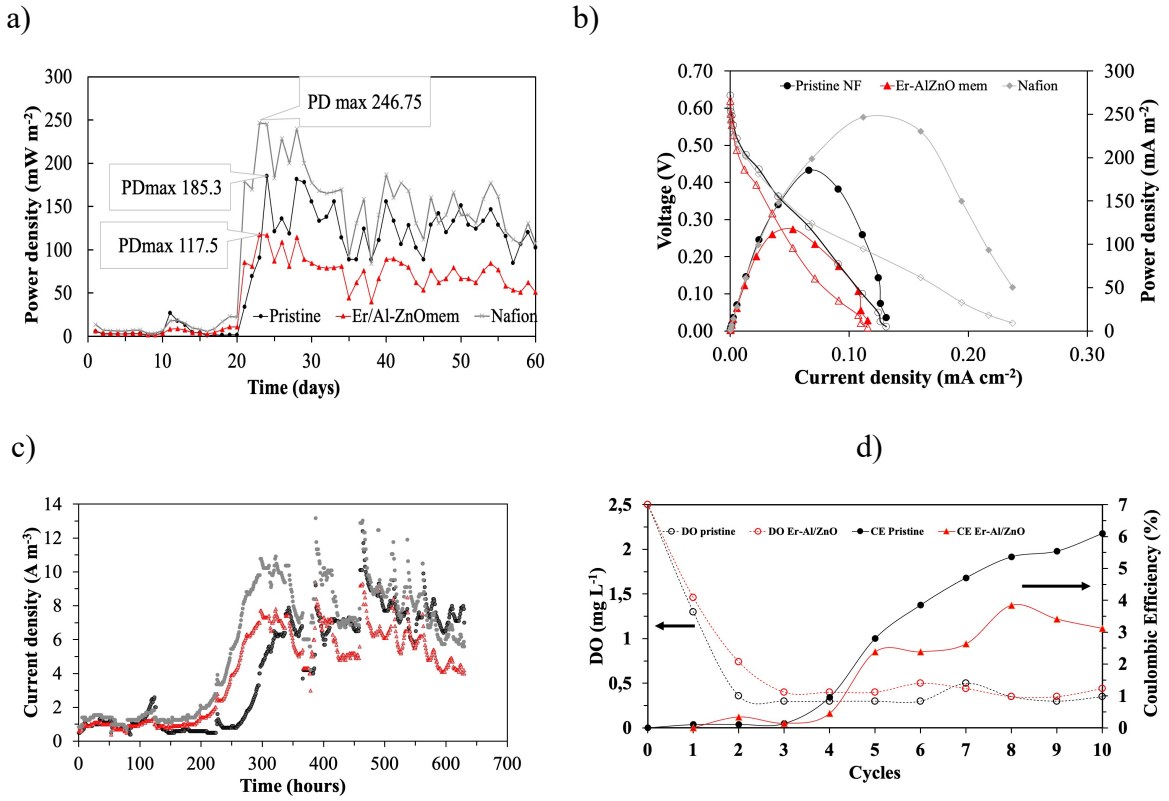


Figure 5.5. a) Polarization curves and b) power density per day, c) current and d) Oxygen diffusion through membranes and coulombic efficiency (%) for pristine and Er-Al/ZnO membranes with respect to time.

The current density generation of the NF-MFC with pristine membrane, Er-Al/ZnO and Nafion is illustrated in Figure 5.5c. In reactors, the current density increased after 200h of operation. The exponential increase of the potential from the 200th hour could be due to the fact that at this stage, there was a stable formation of biofilm growth at the anode electrode (Kandpal et al., 2021), where the biofilms were producing electrons from the organic degradation process more efficiently (Al-Mamun et al., 2017). The sequential replacement of the anolyte decreased the depletion of organic substrates in all cycles and every cell. It should be noted that the cell with Er-Al/ZnO membrane had higher current output in the period from 200 to 300 h, however, after 300 h the current was higher for the cell with pristine

membrane. Based on the previous results, the NF-MFC with pristine membrane showed better current generation than the Er-Al/ZnO NF-MFC in the long term, which is in agreement with the power output results of the cells.

The dissolved oxygen in the anode chamber was monitored during the operating cycles (Figure 5.5d). In order to determine the effect of dissolved oxygen in the anodic chamber and the ability of the membrane to maintain low DO levels. The first and second cycles were operated at relatively high DO (~2mg L^{-1}). As can be seen from the second cycle onwards, the DO remained stable in the range of 0.3 mg L-1 and did not vary throughout the operation of the cells, which shows that both the pristine and modified nanofiltration membranes had the ability to maintain low and stable oxygen concentration at the end of each cycle. This result shows that using nanofiltration membranes as separators in this type of BES can maintain stable oxygen diffusion over long periods of operation, which is promising since this work is one of the first to use this type of membranes as separators, and since there is a high variety of nanofiltration membranes, it opens a wide field of exploration.
In addition, it can be observed that the coulombic efficiency also increased from the 2nd cycle of operation, due to the fact that the coulombic efficiency is affected as a result of aerobic degradation of the substrate (Kim et al., 2007)

Furthermore, the coulombic efficiency obtained by the pristine membrane system showed higher efficiency (from 3 to 6%) than that obtained with the modified membrane (~3%). This result could be due to the antibacterial capacity of the catalyst used, as mentioned above. Even so, the efficiency shown by the pristine membrane is higher than a recent work on osmotic microbial fuel cells (Pardeshi and Mungray, 2021). Moreover, bacterial growth was visually observed on both sides of the pristine membrane separator, suggesting substrate and oxygen crossover. However, membranes such as Nafion normally used in BES are known to be permeable to both oxygen and acetate (Kim et al., 2007).

In addition, in order to understand the oxygen diffusion capacity of the membrane, the diffusion coefficient (Do) and mass transfer coefficient (Ko) of oxygen were evaluated for

pristine and modified membranes at room temperature. The pristine membranes and the modified membrane showed an oxygen mass transfer of (Ko) of 3.27 (± 0.50) × 10^{-4} cm s^{-1}, (Do = 5.23 (± 0.10) ×10^{-6} cm^2 s^{-1}) and 3.38 (± 0.70) × 10^{-4} cm s^{-1} (Do = 5.40 (± 0.12) × 10^{-6} cm^2 s^{-1}) respectively. Based on these results, the oxygen diffusion observed for both the pristine and modified membrane showed to be low compared to results from previous work for osmotic membranes (Pardeshi and Mungray, 2021), leading to speculation that nanofiltration membranes might be interesting candidates for further studies and other BES systems.

5.3.2 Influence of membrane modification on water flux

Transmembrane water flux was measured in the nanofiltration cells. The presence of an osmotic pressure difference across the nanofiltration membrane allowed the flow of water molecules from the anodic chamber to the cathodic chamber with an initial flux of 1.5 L m^{-2} h for both the pristine and modified membranes (Figure 5.6). A rapid drop in water flux was observed during the first few days of operation, where the water flux decreased to approximately 1.1 and 0.9 $Lm^{-2}h^{-1}$ for the Er-Al/ZnO and pristine membrane, respectively. Substitution of fresh extraction solution did not result in full water flux recovery. However, the modified membrane cell exhibited an improvement in water flux for each operating cycle compared to the pristine membrane. This could be due to the effects of the anti-fouling properties of the photocatalyst on the membrane, preventing the formation of membrane fouling. This is demonstrated in the microscopy analysis section.

As shown in Figure 5.6a, COD removal remained between 71% and 74% from the third cycle onwards and continued that way thereafter for cells with pristine membrane, for cells with Er-Al/ZnO membrane the removal range was slightly lower, between 65% and 68%. These data are in agreement with the results obtained in the power density section. The superior COD removal by cell with pristine membrane also produced a higher power density output, which produces more energy from the respiratory chain. Forcing the microorganisms to consume more carbon sources to maintain their metabolic rate (Li et al., 2010).

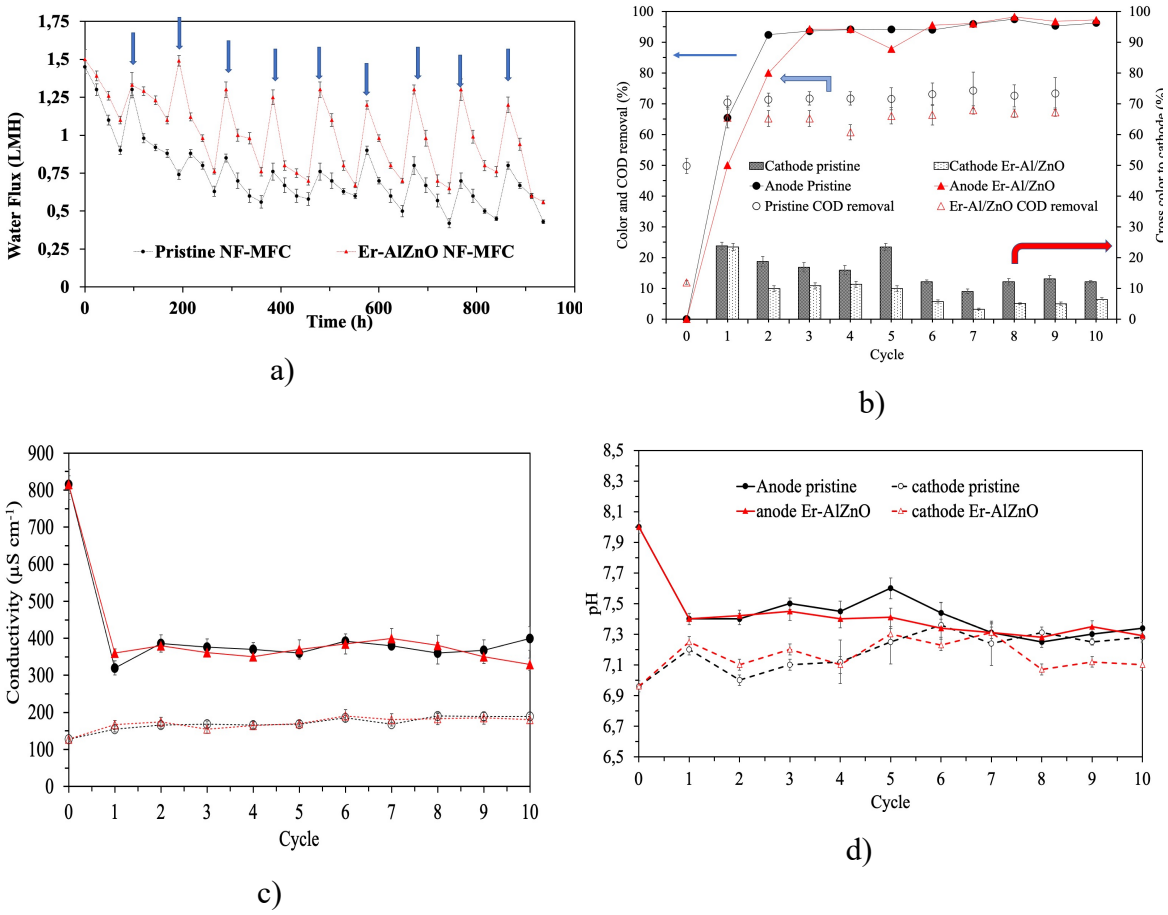


Figure 5.6. a) Comparison of transmembrane water flux (Jw) in NF-MFC with a pristine and Er-Al/ZnO modified membrane. The arrows indicate the change of extraction solution and comparison of final removal data for b) color and COD (MO= 100 mg L-1, 10 cycles) and crossover from color to cathode, c) pH and d) conductivity values in the anolyte and catholyte between NF-MFC with pristine membrane (black) and Er-Al/ZnO (red).

These results lead to the hypothesis that the density of microorganisms in the anode could be higher when using a virgin membrane than the catalyst-modified membrane, due to the anti-fouling character that the modified membrane showed. However, color removal was efficient in both cells at around 96% from the third cycle, which shows that the process was able to break -N=N- groups (Mu et al., 2009). This could be due to a good adaptation period of the bacteria with the previous textile wastewater (Hosseini and Ahadzadeh, 2013; Krithika et al., 2021; Q. Wang et al., 2019).

Additionally starting from the second cycle, the color crossover to the cathodic compartment at the end of each cycle ranged from 9% to 23% for the cell with pristine membrane and from 5% to 11% for the cell with modified membrane. Which shows that the membrane modified with the Er-Al/ZnO catalyst decreased the color transfer from the anodic to the cathodic compartment. These results could be due to the fact that the catalyst effectively activated with visible light (previous work) can help to remove the near color with the membrane surface (Bahamonde Soria et al., 2020). Which shows that membrane modification can have more benefits for future research.

During each cycle, the salinity in the anode compartment had a slight increase to the initial value, due to the rejection of the nanofiltration membrane used by the influent solutes and the reverse transport of solutes from the extraction solution, while it decreased in the cathode compartment due to the dilution of the permeate. However, the anolyte conductivity at the end of each cycle was in a low range of 164-193 $\mu S\ cm^{-1}$ (Figure 5.6b). This range of fluctuations was similar for both the pristine and modified membrane. This indicates that the modification did not alter the salt rejection. Furthermore, the pH change in the feed solution for all cycles changed from an initial pH of 8 to a range of 7.25 to 7.5 at the end of each cycle. In the case of the draw solution, values always fluctuated from 7 to 7.2 (Figure 5.6c)

5.3.3 Change in electrical resistance by fouling of the NF membrane

Figure 5.7a shows the change of surface electrical resistance of the pristine nanofiltration membrane and Er-Al/ZnO membrane in the electrodialysis unit. Over 1110 minutes, when BSA was used as the fouling material, the pristine membrane had an increase in the surface electrical resistance. In contrast, the Er-Al/ZnO membrane did not show an obvious elevation in electrical resistance, which showed that the modification improves the antifouling ability compared to the pristine membrane. After testing, the membranes were characterized by SEM. Figure 5.7b and c show the surface of the original pristine and Er-Al/ZnO membranes, respectively, before use. After testing, Figure 5.7 b’ and c’ show that BSA fouled the membranes after 1110 min.

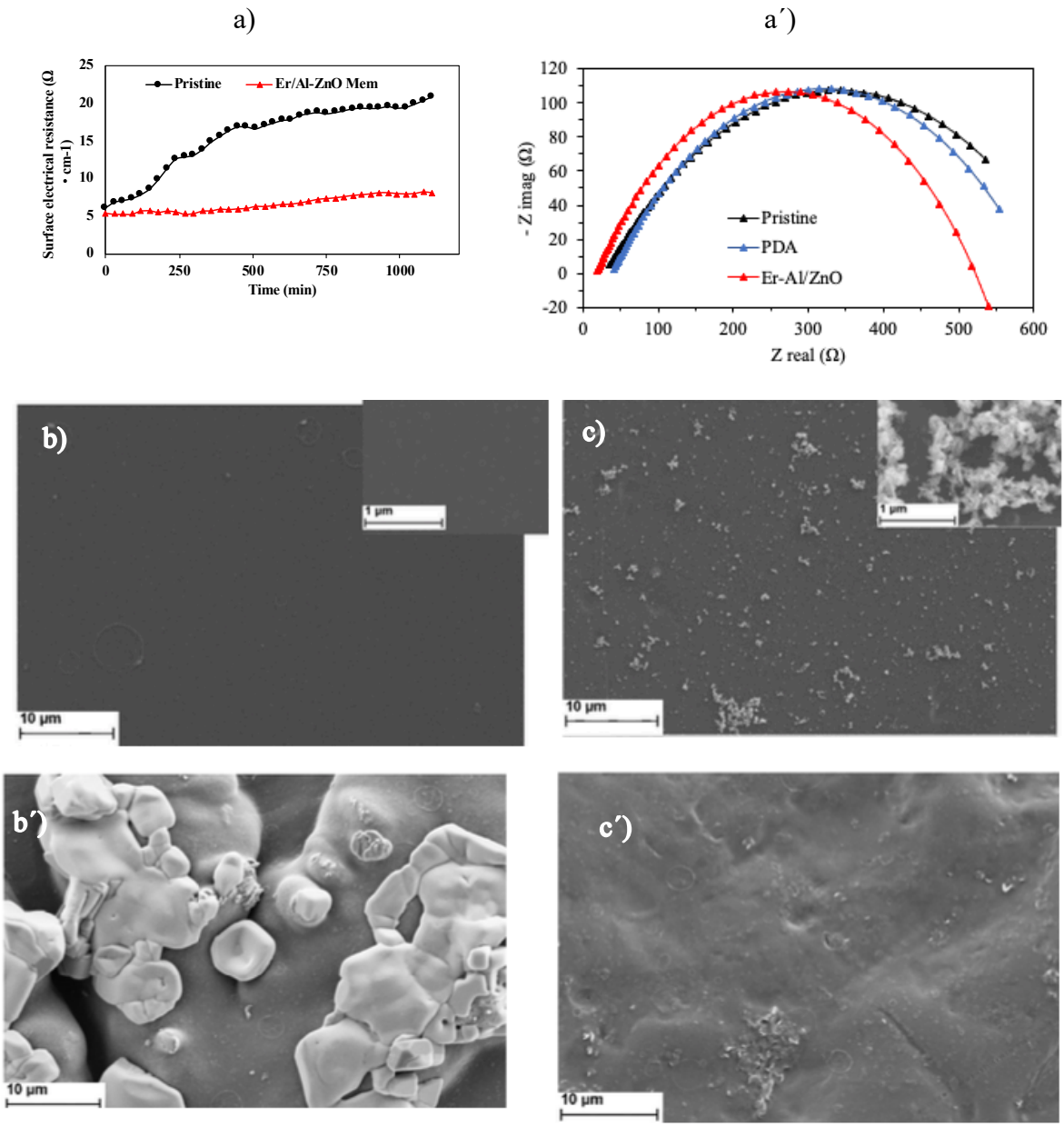


Figure 5.7. a) Surface electrical resistance change of the original pristine NF membrane and the modified Er-Al/ZnO membrane fouled by BSA under desalting conditions, and a´) Nyquist plot of pristine, PDA and Er-Al/ZnO membranes. SEM images of b) pristine and c) modified Er-Al/ZnO membrane before use and SEM images after evaluation for b') pristine and c') Er-Al/ZnO membranes

The fouling materials mostly adhered to the surface of the unmodified membrane (Figure 5.7b'). In comparison, the modified membrane kept its surface almost clean after contact

with BSA Figure 5.7 c′. Which confirms the antifouling ability of the modified membranes measured ’s change in surface electrical resistance.

The system studied is Ag/AgCl electrode/ Ag/AgCl electrode. The Nyquist plot for the membranes studied are presented in Figure. 5.7a`. Only one relaxation process (a semicircle in the Nyquist) is observed for all three membranes (Fortunato et al., 2006). The impedance spectra of the nanofiltration membranes are shown by the Nyquist plot, in which the real impedance (Zreal) is plotted against the imaginary impedance (-Zimag). The Nyquist plots show that the ohmic resistance of the pristine membranes was 35.7 Ω. For the PDA-decorated membrane, the ohmic resistance increased to 41.4 Ω. For the Er-Al/ZnO membranes the ohmic resistance was 19.2 Ω. This decrease in ohmic resistance is attributed to both the compact coating layer and the higher charge that ZnO provides on the surface of the membranes along with the PDA catechol groups. In addition, one would expect the monovalent selectivity to be increased by the Er-Al/ZnO co-deposition coating layer, because the monovalent selectivity increases with the increase of the total amount of charge on the membrane surface. These results were corroborated with the membrane resistivity cell of section 5.2.4 (Figure5.1). Which showed similar resistance to those presented by impedance, i.e.: 32.1Ω, 35.9Ω and 17.5Ω for pristine, PDA and Er-Al/ZnO membranes respectively.

5.3.4 Membrane fouling in NF-MFC

Compared to the pristine NF and modified membranes, a fouling layer could be observed on the membrane surface after 5 cycles of NF-MFC operation. Figure 5.8 a′ shows less density of microorganisms per optical field on the Er-Al/ZnO membrane compared to the NF membrane. This result confirms the antifouling activity produced by the membrane modification. After 20 consecutive running cycles, SEM images (Figure 5.8 b and b′) show that the density increased for both membranes. However, the cross-sectional photographs showed higher thickness of the microorganism layer on the nanofiltration pristine membrane (254±3.4 nm) compared to the Er-Al/ZnO membrane (107±2.7 nm) (Figure 5.8 c and c′), suggesting that the modification could slow down the membrane fouling process. However, the fouling layer could be easily removed by simply washing with tap water for both

membranes, indicating that the fouling of the pristine and modified nanofiltration membrane is reversible.

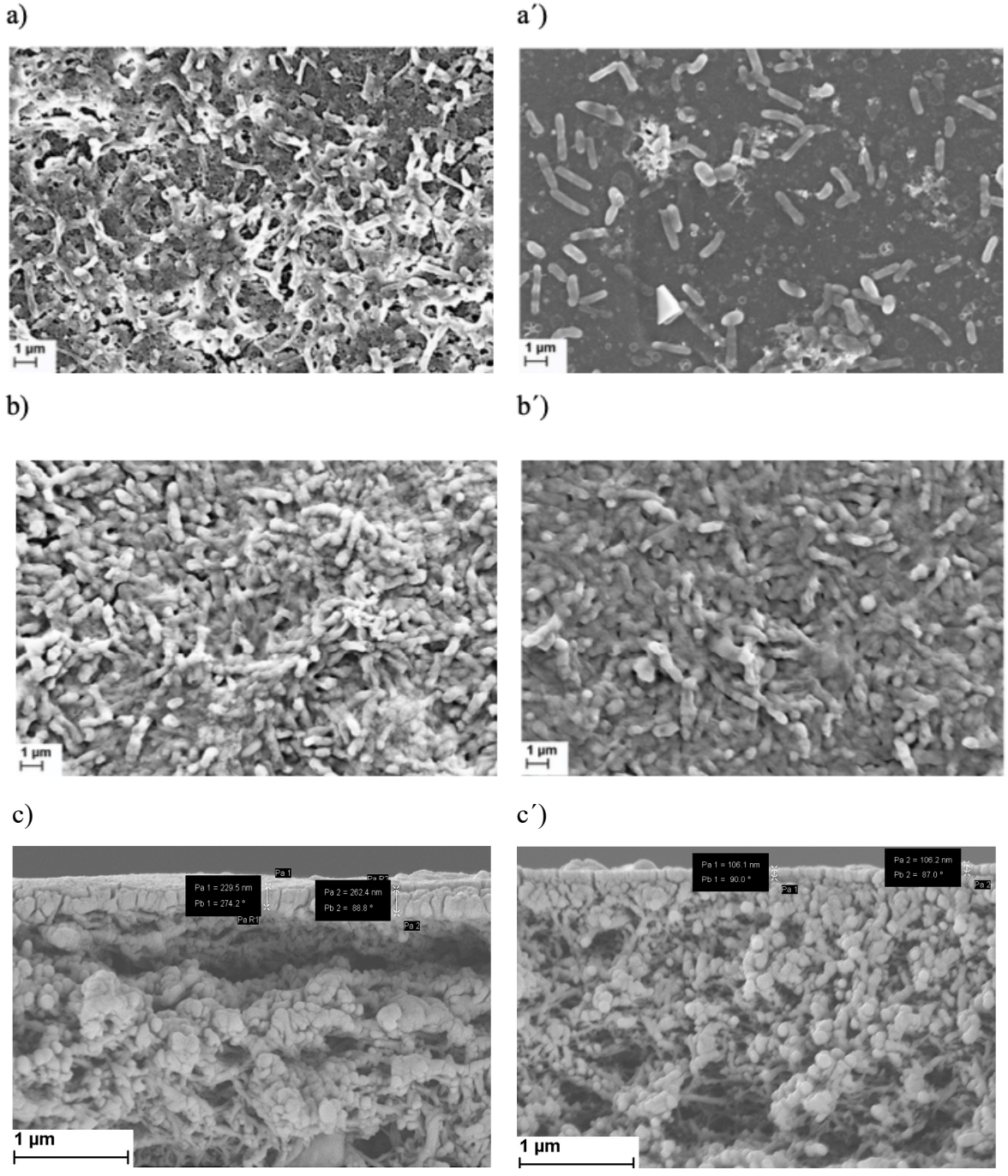


Figure 5.8. SEM image of fouling on pristine membrane after a) 5 cycles operation, b) 20 cycles operation, c) cross section after 20 cycles operation, and Er-Al/ZnO membrane after a´) 5 cycles operation, b´) 20 cycles operation and c´) cross section after 20 cycles operation.

5.3.5 Performance of membranes under light conditions and pressure

In order to test the membrane performance at higher pressures. The separation performance of the pristine and modified membrane was evaluated in light conditions and at 4 bar in a dead-end cell (Figure 5.9 A). For a 1 g L^{-1} aqueous solution of $MgSO_4$, both pristine and modified membranes showed no change in solute rejection (~98%). However, NaCl (1g L^{-1}) rejection showed a slight increase for the modified membrane, probably due to the fact that nanoparticles and nanometric polydopamine oligomers can block or grow in the larger defects or pores of the pristine membrane surfaces in the early stage (Bahamonde Soria et al., 2020). In the case of synthetic textile wastewater, salt and color rejection had a slight decrease compared to the pristine membrane, which could be due to the complexity of the matrix. However, the modified membranes maintained reasonable performance.

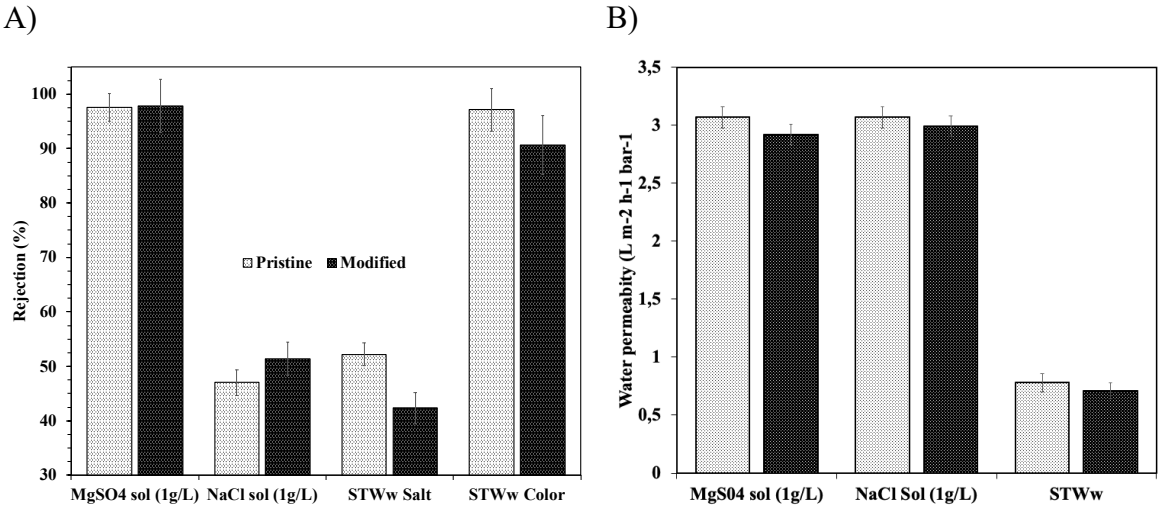


Figure 5.9. Filtration performance of the membranes pristine and modified membranes for solutions 1gL-1 of $MgSO_4$, NaCl and synthetic textile wastewater. A) Salt and color rejection, and B) Water permeability.

Figure 5.9B shows the average permeability to solutions (1g L^{-1}) of $MgSO_4$, NaCl and synthetic textile wastewater for the pristine and modified membrane. Upon modification of the membrane surface, the permeability value did not show a statistically significant change.

In turn, the permeability of synthetic textile wastewater was lower compared to the permeability of salt solutions. This decrease reveals that matrix complexity is an important factor to consider.

5.3.6 Filtration performance under Dark Conditions

In general, an additional layer could modify the hydraulic resistance of the modified membranes (Zhao et al, 2019), which could directly influence the filtration performance. Figure 5.10 shows the synthetic textile wastewater permeability and color rejection of the membranes before and after modification. In order to ensure that the differences in the performance of the modified membranes, all tests have been performed under the same conditions.

As can be seen in Figure 5.10a, the membrane modified with polydopamine and Er-Al/ZnO showed reduced flux compared to the pristine membrane at 4 bar, indicating that the modification layer produced a higher hydraulic resistance (Wang et al., 2020). This change could probably be mostly due to the blocking of the pores of the supporting membrane by the polydopamine in the polymerization process (R.-X. Zhang et al., 2017). In turn, the Er-Al/ZnO catalyst could also influence in pore blocking in its binding with polydopamine. As the evaluation time increased, the permeability of the membranes remained stable at around 0.9 LMHbar and 0.7 LMHbar for the pristine membrane and the modified membrane, respectively. In turn, the color rejection did not show a statistically significant change over the long test period compared to the pristine membrane. In contrast to the results obtained at lower pressure, the evaluation of the membrane modification at a higher pressure of 10 bar (Figure 5.10b) showed an increase in water permeability for the modified membrane (~23%), which was maintained throughout the experiment. In addition, MO rejection showed an increase from the 100th minute compared to the pristine membrane.

From these results, it can be speculated that the modification did not exhibit an improvement in membrane permeability or color rejection at low pressures. However, at a pressure of 10 bar, the modified membrane improved its performance. Indeed, this suggests that at lower pressures the tangential flow of the cross flow could remove the catalysts weakly bound to

dopamine from the surface of the modified membrane (Chowdhury et al., 2017; Trzaskus et al., 2017). Nevertheless, the higher pressure may have compacted the catalysts on the membrane surface. Therefore, higher pressure improved the performance of the membrane. For future experiments, the compaction process of the catalysts is suggested as a preliminary step in the use of the membranes.

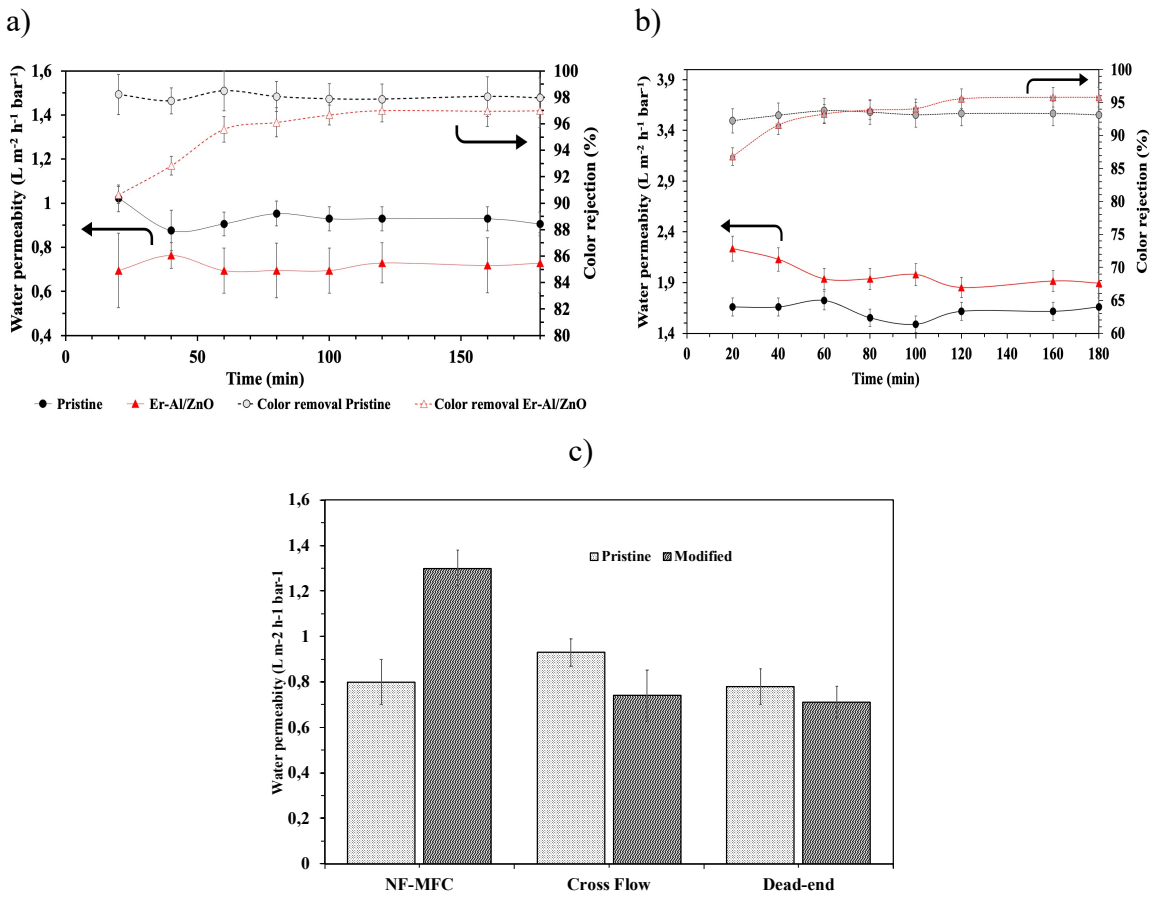


Figure 5.10. Filtration performance of the membranes before and after the modification, water permeability (L m^{-2} h^{-1} bar^{-1}), Color rejection (%) at a) 5 bar and b) 10 bars in a cross-flow device and drack conditions. C) comparison of water permeability in systems used NF-MFC, Cross flow and dead-end.

In order to have a better understanding of the performance of the membrane modification. Figure 5.10c compares the water permeability in the three established conditions: NF-MFC, cross flow and dead end, where it is possible to observe that the modified membrane

produced an improvement in the flux at NF-MFC conditions. This result shows that the modification had a positive effect on the flux at normal operating conditions of the nanofiltration microbial fuel cell, which is promising since no extra energy cost is required to drive the pressure filtration process.

5.4. Conclusions

In this work, a novel visible-light photosensitizing catalyst (Er-Al/ZnO) at 0.03 wt.% was successfully attached to the PDA layer by a bio-inspired method to the nanofiltration membrane. The Er-Al/ZnO composite membrane exhibited a higher antibiofouling capacity on the membrane surface, which kept the water permeability almost constant for long periods of NF-MFC operation. In addition, SEM analysis confirmed the hypothesis that the modification could minimize surface fouling. However, the modified membrane had lower energy production efficiency compared to the pristine membrane, presumably due to the efficiency of the membrane's antibacterial properties, even so, the power densities achieved were higher than recently published osmotic fuel cells. Finally, the modified membrane showed lower surface electrical resistance, which generated a good expectation for the use of membranes modified with this catalyst for future bioelectrochemical systems. In addition, because the catalyst used in the present work can be activated with visible (solar) light according to the previous chapter, the energy savings for the activation of the catalyst can be even higher.

Chapter 6.

General conclusions and Future work

6.1 **Main conclusions of the thesis**

Textile waste water is a source of environmental pollution. The analysis in Chapter 1 showed different treatment methods for textile wastewater, among which, the treatment by advanced oxidation methods – AOPs, membrane technology and biochemicals (microbial fuel cells – MFCs) proved to be effective methods for the degradation of textile dyes. However, textile wastewaters are far from ideal electrolytes for microbial fuel cells, due to their difficult degradability and membrane fouling. Membrane fouling in bioelectrochemical systems is a problem that crucially affects the efficiency of these systems. The development of antifouling membranes for water treatment using membrane technology has made great progress in recent years. Therefore, using the benefits of all three technologies (AOPs, membrane technology and MFCs) can be efficient in the development of antifouling membranes for microbial fuel cells. Furthermore, thanks to the literature review presented in this chapter, nanofiltration membrane properties, such as the very small pore size that prevents oxygen crossover and the low ion transfer resistance compared to the ion exchange membranes normally used in MFCs, showed promise for the use of nanofiltration membranes as efficient separators in these systems. In turn, from the analyzed antifouling membrane production methods, the bio-inspired modification method using polydopamine as bio glue provide the ability to bind photocatalysts on the surface of commercial membranes in a simple and efficient way, conferring the membranes self-cleaning and antifouling properties.

In Chapter 2, the effects of the type of bio-inspired modification and the catalyst used (TiO_2 or ZnO) on nanofiltration membranes were studied, as well as their impact on the hydrophobicity, performance, antifouling, antibacterial and self-cleaning properties of the membranes. The results showed that the two-step bio-inspired modification method was more efficient in supporting catalysts on the surface, while catalysts supported on PDA-modified surfaces by the two-step method improved hydrophilicity by 22% on average, monovalent salt rejection by 11% and maintained pristine membrane water flux. In addition, modification of the membranes with the mixture of catalysts proved to be extremely effective against *B. Subtilis*. Relative to the control sample, the modified membranes reduced 64%, 93.0%, 92.7% and 47.5% against *B. Subtilis* for ZnO-modified membranes and membranes

modified with ratios (TiO_2:ZnO 0.03 wt.%) 2:1, 1:2 and 1:1, respectively. Compared to literature reports, the results showed that the catalyst mixture provided the membranes both antibacterial and self-cleaning activity under sunlight exposure.

Thus, in Chapter 2, the 0.03 wt% TiO_2:ZnO (1:1) catalyst mixture was successfully attached to the PDA layer by a bio-inspired method on low-cost membranes. In chapter 3, the effects of the membrane modification were evaluated in terms of power density, open-circuit potential, coulombic efficiency, antibiofouling properties, color removal and COD removal efficiency in MFCs. The results showed that the use of the modified membrane with PDA and a mixture of catalysts facilitated the transfer of cations released during the oxidation process in the anodic compartment of the MFC. The modified membranes increased the energy generation in the MFC by 2.5 times and 5.7 times the current compared to pristine membranes. In addition, the modified membranes decreased the MFC wastewater degradation time from 5 to 3 days and doubled the lifetime of the low-cost membranes. Thus, Cel-PDA/TiO_2:ZnO composite cation exchange membranes with higher physical stability than the original ones were obtained. The SEM and AFM analyses confirmed the hypothesis that the modification could minimize surface fouling. Finally, the highest COD removal of 60% and 75% was obtained for synthetic and real textile wastewater, respectively, with color removal of 90%. Considering its physicochemical and electrochemical properties, good antifouling property, simple preparation process and lower cost make this modification method a promising alternative for the formation of antifouling membranes for microbial fuel cells. In addition, visible light (artificial and natural) was used to activate the membrane catalysts rather than ultraviolet light, which lowers operating costs and avoids violent activation of the catalysts, preventing undesirable damage to the membrane.

Apart from controlling environmental pollution, part of this work was focused on developing an efficient photocatalyst activated with visible light (artificial and solar) able to act as an effective barrier against textile dyes in wastewater. Based on the results presented in Chapter 3, the ZnO catalyst was selected as the most promising catalyst for further doping. The set of tests showed that the doping of ZnO with Er and Al improved 98% of the dye degradation efficiency under artificial light and 84% under sunlight, showing that the doping

of the catalyst maximizes the formation of •OH ·radicals. In Chapter 4, doping served to conclude that visible light activates the catalyst with higher energy efficiency than ZnO. Chapter 4 also showed that the new catalyst was able to maintain the high antibacterial activity (94%) against *B. Subtilis,* and also increased the activity against *E. coli* 16% increasing it to 95%. Which showed that the new catalyst was efficient both to efficiently remove dyes from textile wastewater and to be used as a more efficient catalyst to provide anti-fouling characteristics to modified membranes.

In Chapter 5, a novel 0.03 % visible light photosensitive catalyst (Er-Al/ZnO) was successfully binded to the PDA layer on the nanofiltration membrane. The Er-Al/ZnO membrane showed excellent antibiofouling capacity on the membrane surface, which kept the water permeability almost constant during long (>900hours) periods of NF-MFC operation. In addition, SEM analysis confirmed that the modification minimised surface fouling by 47% after 20 consecutive cycles of operation. Furthermore, the modified membranes in these systems were able to maintain limited oxygen crossover from the cathodic compartment to the anodic compartment. However, the modified membrane showed lower energy production efficiency compared to the pristine membrane fuel cell, presumably due to the efficiency of the membrane's antibacterial properties. Unfortunately, the nanofiltration microbial fuel cells did not surpass the electrical efficiency obtained by the single-chamber fuel cells equipped with Nafion membranes, however, it should be noted that the single-chamber MFCs were not osmotic. Even so, the power densities achieved were higher than those of recently published osmotic fuel cells. Finally, the modified membrane showed a lower surface electrical resistance, which generated a good expectation for the use of membranes modified with this catalyst for future bioelectrochemical systems. Moreover, since the catalyst used in the present work can be activated with visible (solar) light according to the previous chapter, the energy savings for catalyst activation can be even higher.

The idea of using the benefit of three technologies (membrane technology, advanced oxidation processes and microbial fuel cells) to develop a process to treat textile wastewater using anti-fouling and self-cleaning membranes as efficient separators (as nanofiltration microbial fuel cells) has been technically demonstrated. The membranes had direct impacts

on both electrical and textile wastewater treatment efficiencies, demonstrating that the membrane modification method has a direct influence on this class of bioelectrochemical systems.

However, the formation of toxic by-products during treatment trials can be a drawback due to possible ecotoxicity. Therefore, future experiments should be conducted to understand the mechanisms of toxic by-product formation and their origins during oxidation processes. Furthermore, it is important to elaborate the necessary engineering for the proposal of textile water purification installations with different toxicity tests adapted to the pollution in presence.

In conclusion, this work provided new insights into the impact of modifying commercial membranes by bio-inspired methods as efficient, anti-fouling and sunlight-activated separators in both microbial fuel cell systems and a new generation of nanofiltration microbial fuel cells. This research opens up an interesting line for future research since the vast range of nanofiltration membrane types and their efficiency in water treatment can greatly improve the development of efficient separators for microbial fuel cells and other bioelectrochemical systems.

6.2 Recommendations for future research

6.2.1 Surface chemistry in the formation of antifouling membranes.

Currently, most separator evaluation studies focused on improving the performance of microbial cells with anodic microbial processes. Recently, cathodic microbial processes have attracted increasing interest, as they are essential for different bioelectrochemical processes such as the bioelectrosynthesis of valuable chemicals. In contrast to the case of anodic processes, the bacteria are located in the anodic compartment. Therefore, elaboration and/or modification of membrane surface characteristics is probably one of the effective strategies to promote efficient processes.

Consequently, it is of great importance to use the knowledge we have gained on membrane surface chemical modifications to improve the performance of new bioelectrochemical systems.

6.2.2 Topography in surface modification and biofilm formation

From the results obtained and based on other investigations of membrane surface biofilm formation, it is known that surface topography not only affects bacterial adhesion and biofilm formation, but also influences biofilm structure and function (Bahamonde Soria et al., 2020). Therefore, it is very likely that increased attention on topography (homogeneity of catalyst decortication) at the macro-, micro- and nano-scale will also influence biofilm formation and antifouling properties of membranes. However, the impact of surface topography on bacterial adhesion and biofilm formation on membranes in BES systems is still unknown. In addition, the effects of size, heights and density of membrane surface topographical features on antifouling properties have not been extensively investigated. Therefore, great potential for decreasing bacterial adhesion and biofilm formation by optimizing membrane surface topographical properties is anticipated.

6.2.3 Expansion of photocatalysts in membranes

The application of photocatalysts has shown great potential and possibilities for scale-up. However, the mixture of TiO_2:ZnO catalysts activated with a weak UV radiation source showed a considerable increase in the efficiency of low-cost air-cathode and membrane MFC, which was not the case with the use of an efficient solar visible light activated catalyst (Er-Al/ZnO) for NF-MFC. Therefore, it is suggested to test the performance of this mixture (TiO_2:ZnO) as a membrane modifier for NF-MFC in order to further increase its efficiency. In addition, different cell and membrane configurations can be used as tubular cells (Guo et al., 2017). Additionally, in order to improve ion transfer, modifications currently used in membrane technology, such as the use of graphene (Anand et al., 2018), metal organic frameworks (MOFs) and covalent organic frameworks (COFs) can be replicated (Jun et al., 2020a; Zhu et al., 2020). Therefore, it would be very interesting to further research other

modifications developed for efficient and antifouling filtration processes in membrane technology, which could improve to power density production in microbial fuel cells (MFCs) and other BES.

Finally, the development of membrane technology for CO_2 capture can be used for CO_2 fixation and subsequent production of new products in electrosynthesis BES reactors.

6.2.4 Nanofiltration membranes as separator in BES

In addition to high resistance to biofouling, maintenance of low oxygen transfer levels and recovery and maintenance of water permeability, modified nanofiltration membranes have also proven to be an interesting candidate as new separators for BES systems. Therefore, it offers a great opportunity to extend applications to microbial electrolysis cells (MEC) or desalination cells (MDC).

6.3 Perspectives

The present thesis firstly elucidated the impact of membrane surface chemical modification, and then determined a simple and effective method to modify membrane surfaces to obtain the antifouling, anti-biofouling and self-cleaning properties. The fundamental insights acquired on membrane surface modifications can also be useful for other surface modifications, which contributes to other areas of materials science for the control of fouling and biofouling on other materials. Both the novel surface modification methods and the catalysts synthesized and used in this study could also be applicable to other surface modifications of materials such as sunlight-activated antimicrobial coated clothing.

6.3.1 Surface modification for biofilm control

The main goal of this study was to improve the reduction of bacterial adhesion and biofilm formation on membranes of bioelectrochemical systems by chemical modification of the surface. The results showed that surfaces decorated with both commercial catalysts (TiO_2

and ZnO) as well as with a more efficient Er-Al/ZnO catalyst exhibited antibiofouling characteristics. Also, we found that membrane roughness dramatically affects bioadhesion. These results can be extended to the design of materials to reduce biofilm formation. For example, decreasing biofilm formation in biomedical materials, such as artificial teeth, medical material or medical surfaces. In the field of other bioelectrochemical systems, the formation of biofilms on commonly used membranes, such as nafion, considerably increases the internal resistance, so the look for new modification materials is an interesting challenge.

6.3.2 Surface modifications for other applications

Both effective methods of membrane surface modification could also be used for the modification of enzymes on membranes, i.e. it is known that the immobilisation of carbonic anhydrase on membranes for CO_2 capture is a novel line of research. Therefore, if it is possible to bind enzymes for CO_2 fixation on membranes (Molina-Fernández and Luis, 2021), enzymes could be bonded on either anodes or cathodes to perform electrosynthesis of compounds. These modified surfaces could be used to catalyze specific electrochemical reactions.

Using the same method, immobilization of conductive polymers on new hydrophobic electrodes could also be performed, due to the fact that polydopamine has the ability to adhere to hydrophobic surfaces such as graphene, giving it a better hydrophilic character. These modified surfaces could be used for improved adhesion of electroactive biofilms.

6.3.3 Scale-up of NF-MFCs in the treatment of textile wastewater.

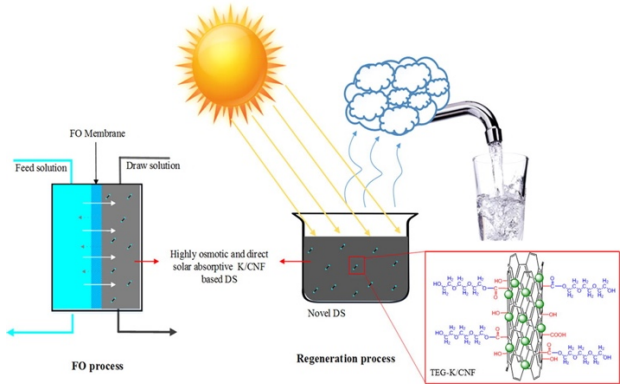
In this study, the effect of membrane modification on the treatment of synthetic and real textile wastewater was evaluated. Both the low-cost membrane cell and the nanofiltration cells were able to treat the applied wastewater, however, due to the high stability of the dyes and their difficult degradability, a secondary treatment is suggested after the treatment used here, in order to prevent the production of secondary products that could be more toxic than the dyes perse (Li et al., 2010; Mu et al., 2009). The finalized thesis was not focused on the

scale-up of the proposed system, it was focused on the development of anti-fouling membranes for microbial fuel cells. For this reason, in order to solve this drawback and due to the promising results of the antifouling effect of the membranes, a new project will be proposed between the Renewable Energies Laboratory - Central University of Ecuador and the group Membrane Technology for a Sustainable World at UCLouvain to develop a scale-up system for MFC-NF.

6.3.4 New approach based on BES for organic wastewater treatment

In the last decade, the current/power density of BES has improved considerably in osmotic systems (Os-MFC). Since our tested system evaluated the level of osmotic flux in the NF-MFC, the high cost of clean water extraction and salt concentration from the cathodic compartment in the NF-MFC could make this technology less competitive with respect to traditional wastewater treatment techniques. However, novel technologies and energy efficient materials have been proposed as complements to the draw solution (DS), e.g. highly sunlight absorbing potassium functionalized carbon nanofibers (K/CNF)(Amjad et al., 2018). These have two functions, to generate high osmotic pressure and to absorb solar energy efficiently for the regeneration phase of DS (Figure 6.1).

a)



b)

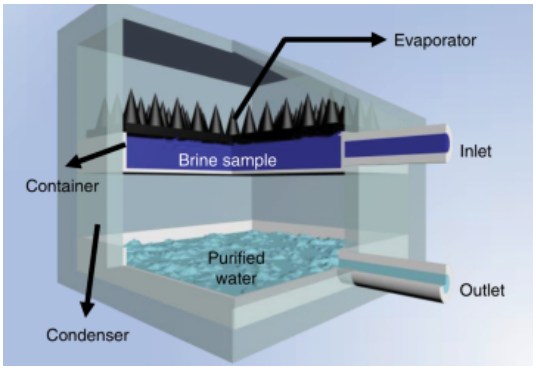


Figure 6.1. a) Setup for photothermal performance and draw solution regeneration (Amjad et al., 2018), b) schematic of the prototype 3D evaporator for solar water purification(L. Wu et al., 2020).

In addition, solar water evaporation represents an environmentally friendly method to purify and desalinate water. However, many evaporators have low efficiency due to increased concentration and accumulation of salts. Therefore, new evaporators such as 3D biomimetic based evaporators have the ability to fully reuse the energy input (solar) through the Marangoni effect and result in localized salt crystallization (Philip et al, 2013; Wu et al, 2020). Additionally, the energy efficiency and water evaporation in these evaporators are not influenced by salt accumulation, indicating their potential for sustainable and practical applications both osmotic and in this new NF-MFC line. Finally, these solar evaporators could be efficiently applicable to the reality of Ecuador due to the high level of solar irradiation.

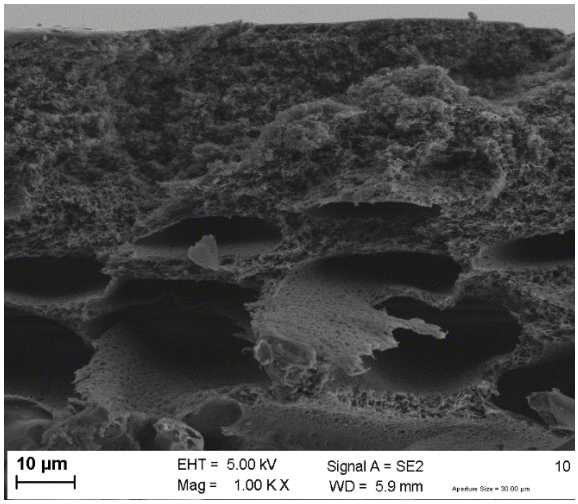
7. Appendices

Appendix 1. chapter 2

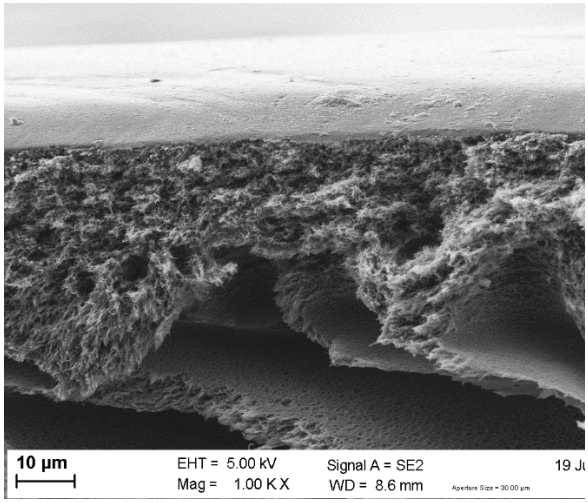
Chapter 3. Effect of (TiO_2:ZnO) ratio on the anti-fouling properties of bio-inspired nanofiltration membranes

1. Transversal section and Morphology

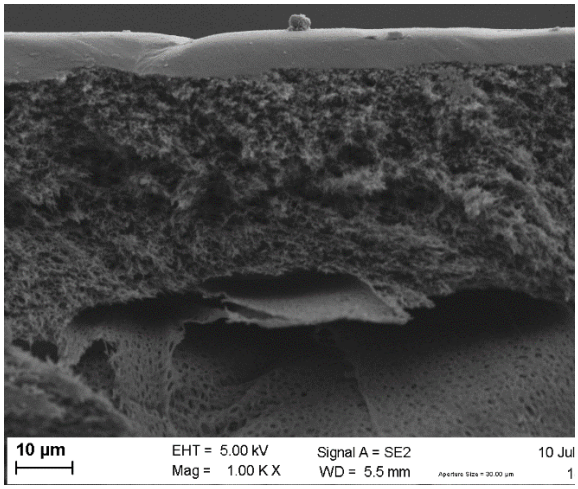
a



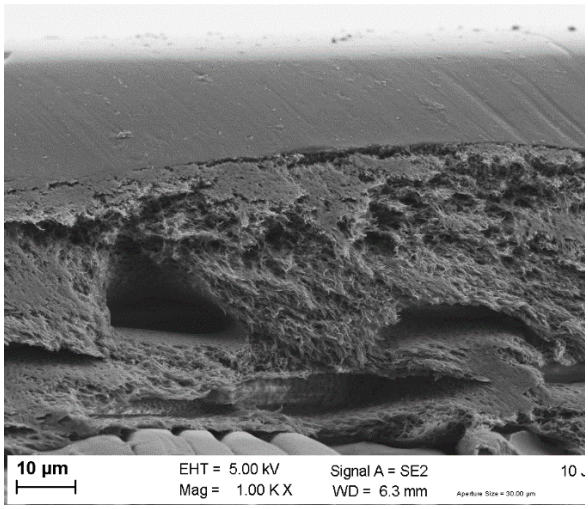
b



c

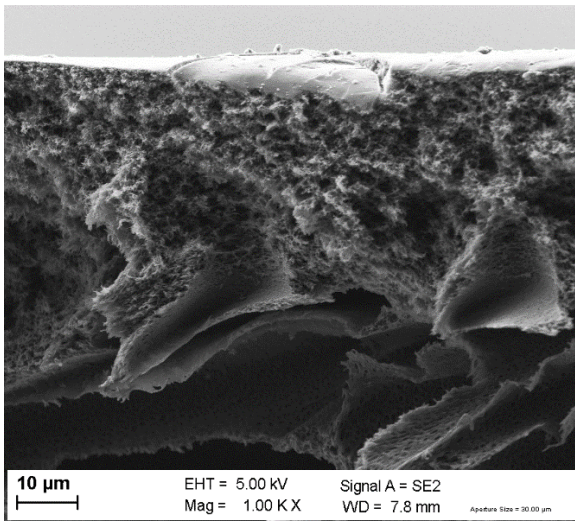


d

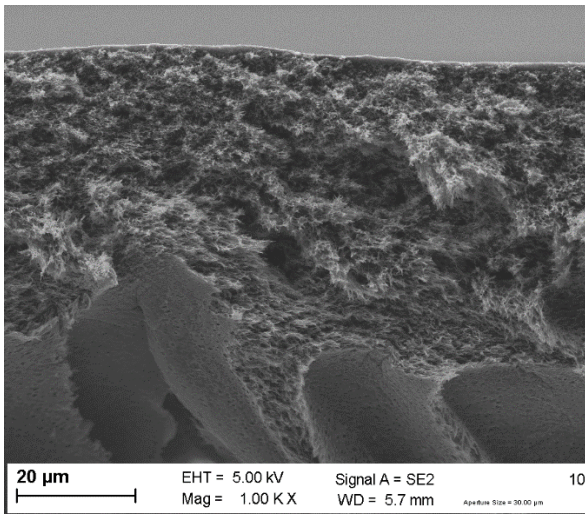


e

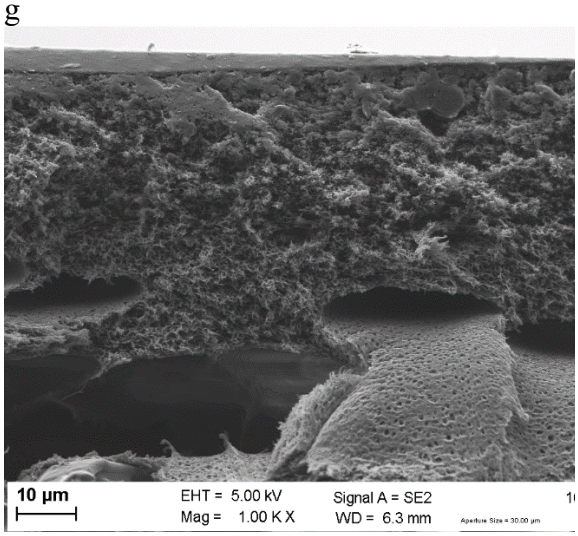
f


10 µm
EHT = 5.00 kV
Mag = 1.00 K X
Signal A = SE2
WD = 7.8 mm

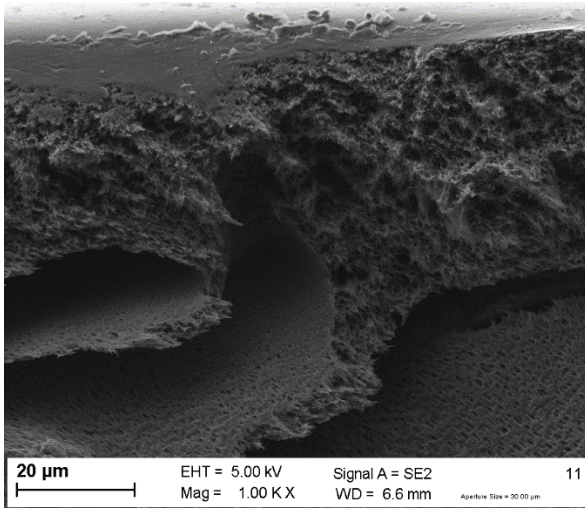
g


20 µm
EHT = 5.00 kV
Mag = 1.00 K X
Signal A = SE2
WD = 5.7 mm

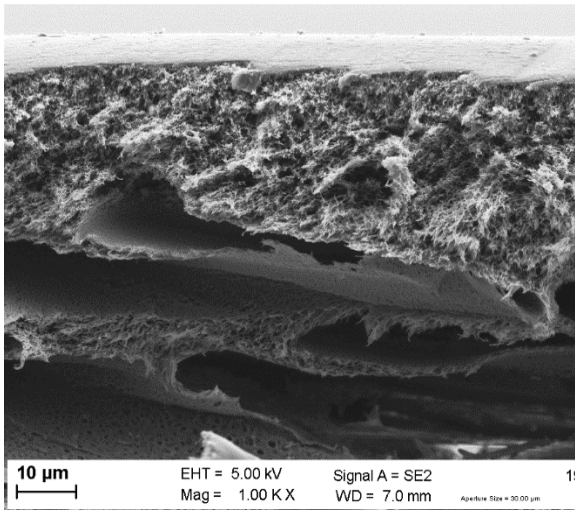
h

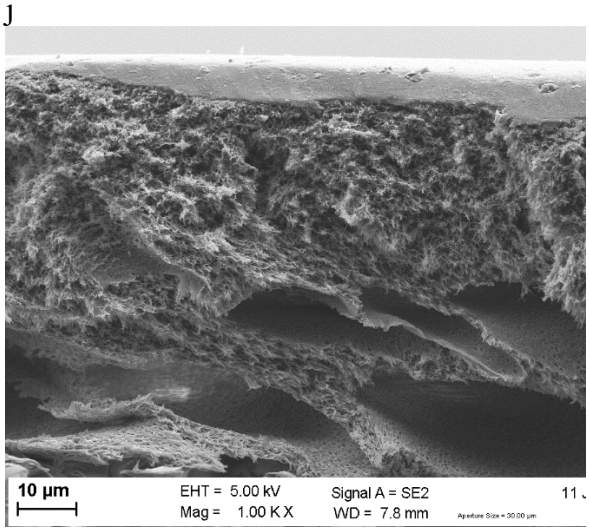

10 µm
EHT = 5.00 kV
Mag = 1.00 K X
Signal A = SE2
WD = 6.3 mm

i

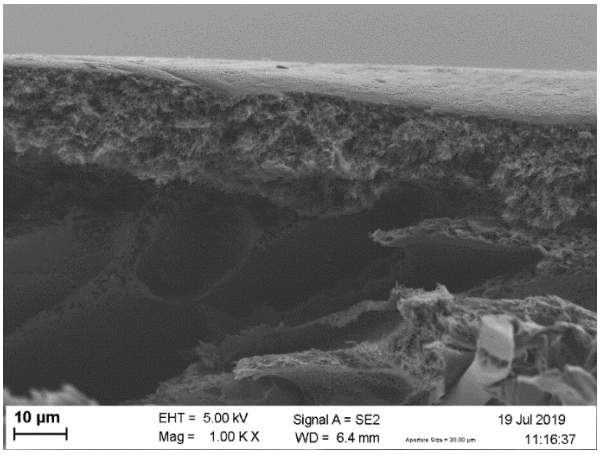

20 µm
EHT = 5.00 kV
Mag = 1.00 K X
Signal A = SE2
WD = 6.6 mm

j

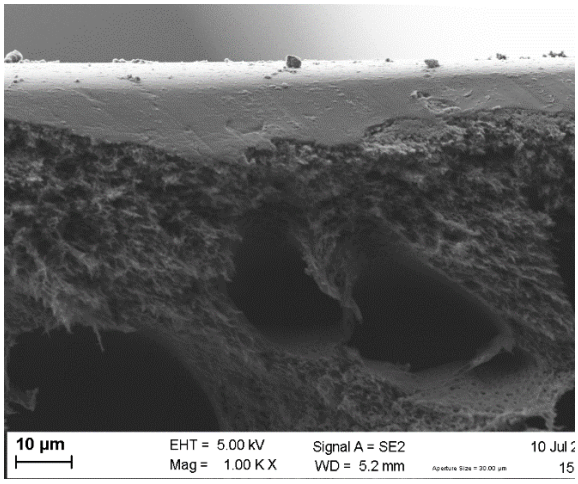

10 µm
EHT = 5.00 kV
Mag = 1.00 K X
Signal A = SE2
WD = 7.0 mm


10 µm
EHT = 5.00 kV
Mag = 1.00 K X
Signal A = SE2
WD = 7.8 mm

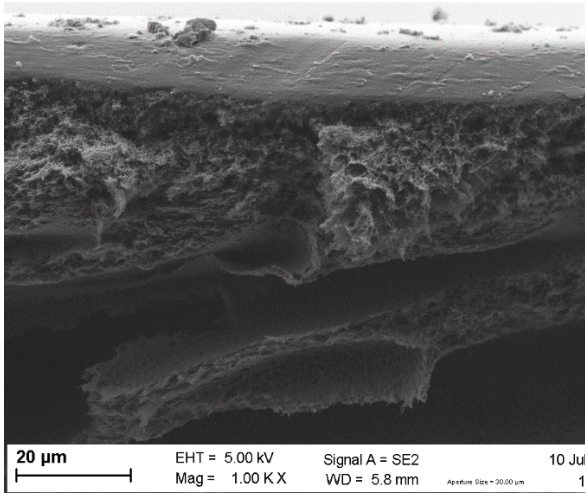
k


10 µm
EHT = 5.00 kV
Mag = 1.00 K X
Signal A = SE2
WD = 6.4 mm
19 Jul 2019
11:16:37

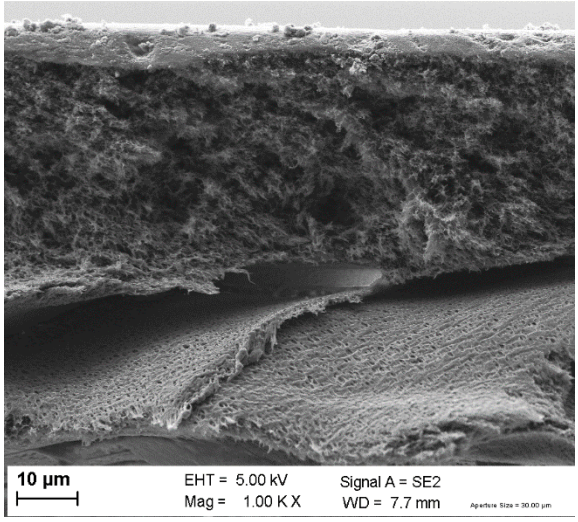
l


10 µm
EHT = 5.00 kV
Mag = 1.00 K X
Signal A = SE2
WD = 5.2 mm

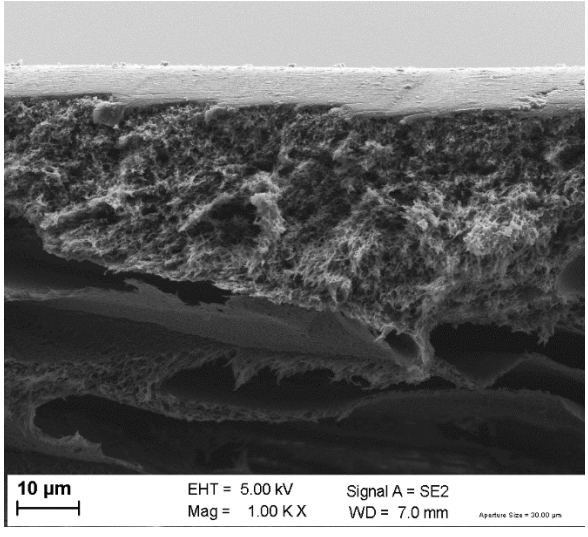
m


20 µm
EHT = 5.00 kV
Mag = 1.00 K X
Signal A = SE2
WD = 5.8 mm

n


10 µm
EHT = 5.00 kV
Mag = 1.00 K X
Signal A = SE2
WD = 7.7 mm

o


10 µm
EHT = 5.00 kV
Mag = 1.00 K X
Signal A = SE2
WD = 7.0 mm

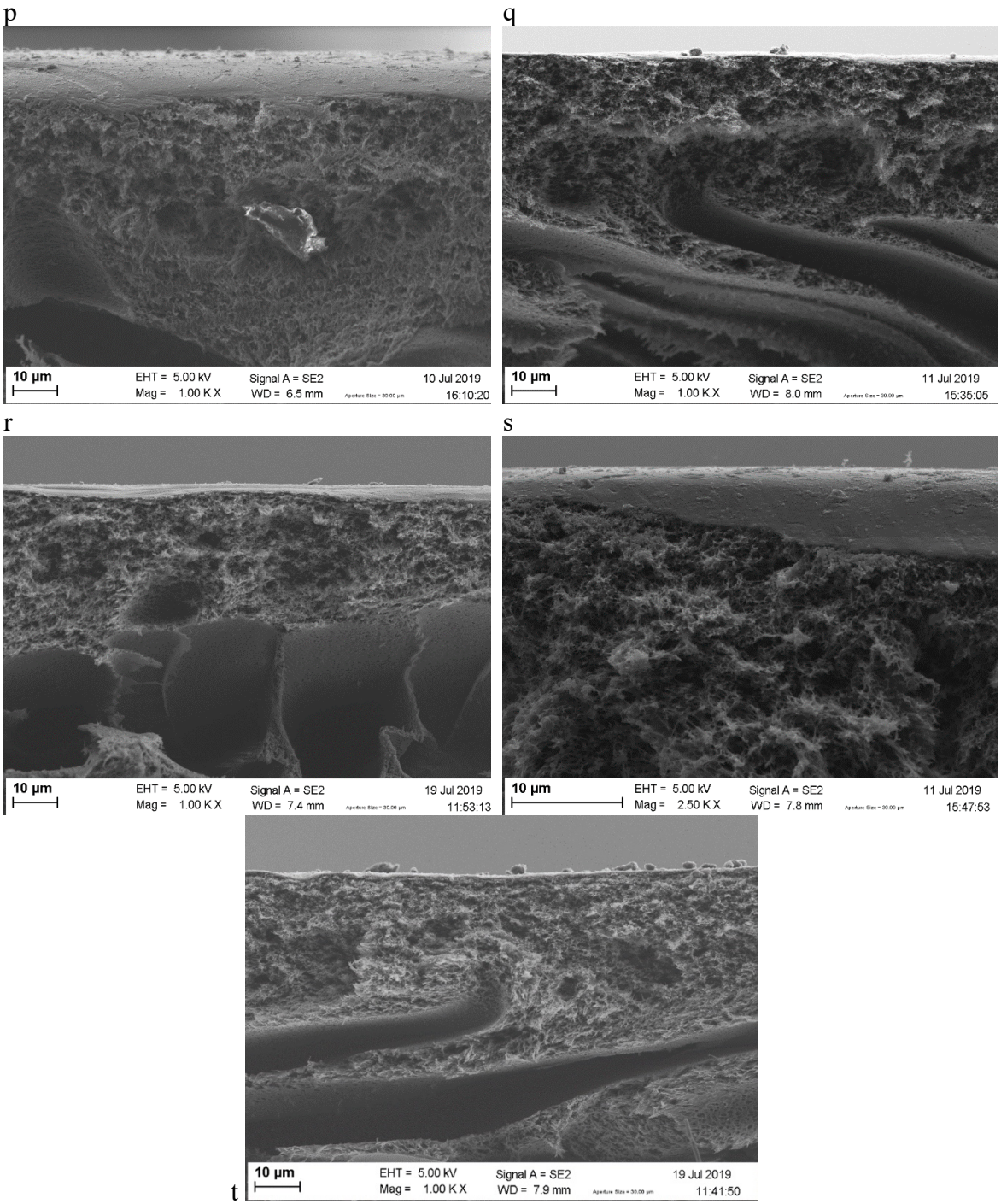


Figure A2.1. Transversal SEM images of modified membranes, using co-deposition method (one-step): (a) Pristine, (b) NF-PDA, (c) NF-1a, (d) NF-2a, (e) NF-3a, f) NF-4a, g) NF-5a, h) NF-6a, i) NFX-1a, j) NFX-2a, k)NFX-3a and using binding method (two steps): (l) NF-1b, (m) NF-2b, (n) NF-3b, o) NF-4b, p) NF-5b, q) NF-6b, r) NFX-1b, s) NFX-2b, t)NFX-3b

2.- Antibacterial activity of modified membranes

Iso Sensitest

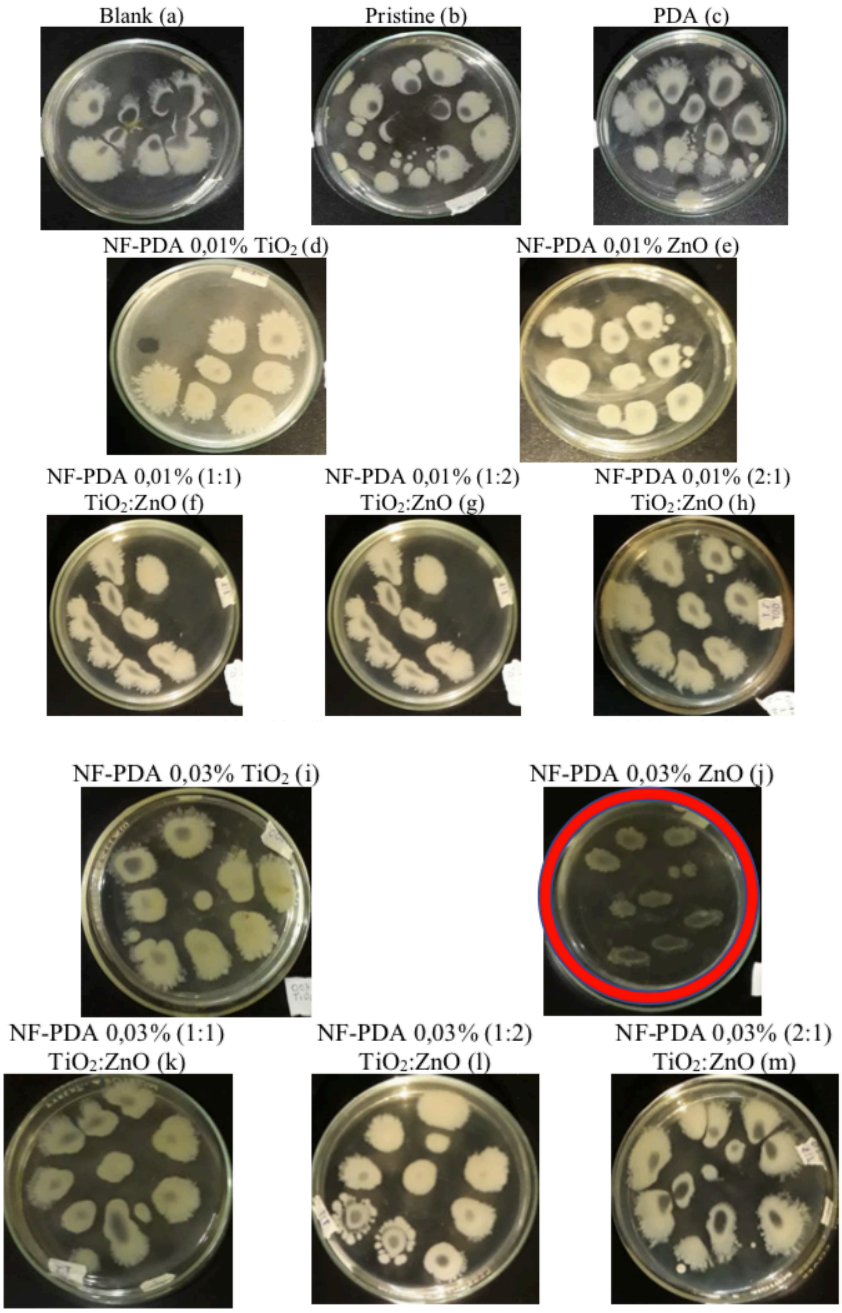
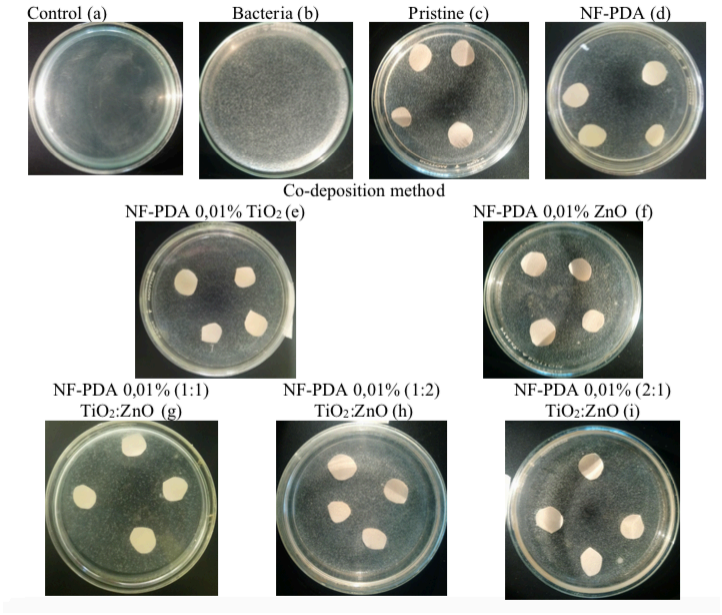


Figure A2.2. Images of the *B. Subtilis* colonies formed in the plate of UV-treated (a) blank, (b) Pristine, (c) NF-PDA, (d) NF-1a (e) NF-4a, (f) NFX-1a, (g) NFX-2a, (h) NFX-3a, (i) NF2b, (j) NF-5b. (k) NFX-1b, (l) NFX-2b, (m) NFX-3b, membranes after 30 minutes of UV irradiation

Disk diffusion technique

A) Co-deposition method



B) Binding method

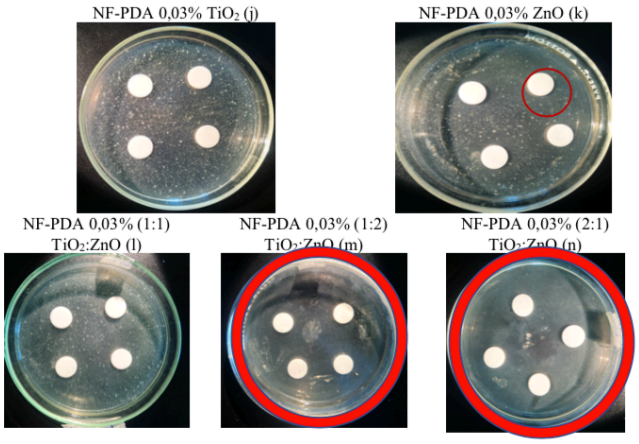
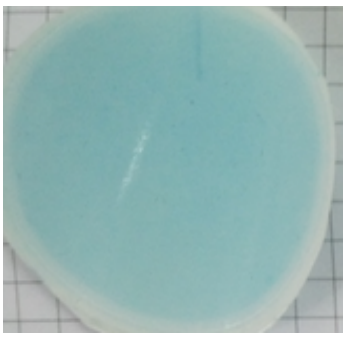
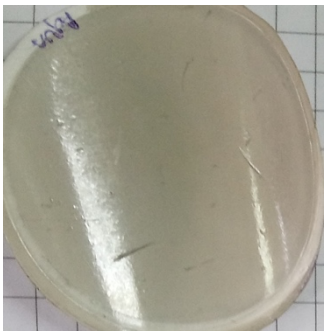


Figure A2.3. Photograph of inhibitory effect of the Nanoparticles on membrane surface against *B, Subtilis* (a) control, (b) blank, (c) Pristine, (d) NF-PDA, modified membranes by co-deposition method, (e) NF-1a (f) NF-4a and (g) NFX-1a, (h) NFX-2a, (i) NFX-3a, and by binding method (j) NF2b, (k) NF5b., (l) NFX-1b, (m) NFX-2b, (n) NFX-3b, membranes after 30 minutes of UV irradiation

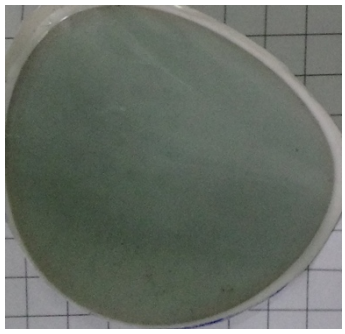
Pristine before use



PDA

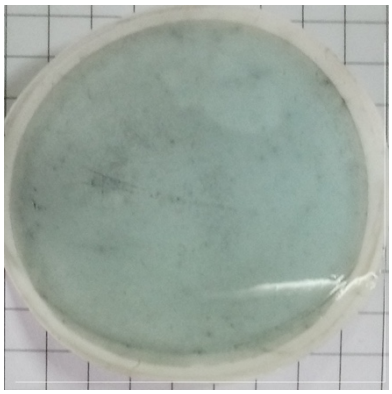


TiO_2

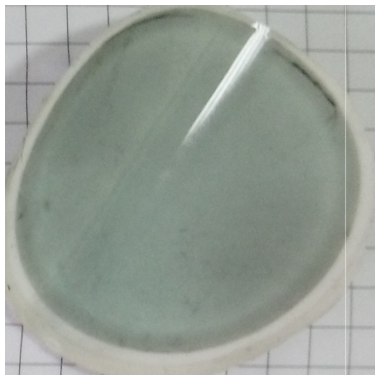


ZnO

After use membrane- 0,01%wt one step

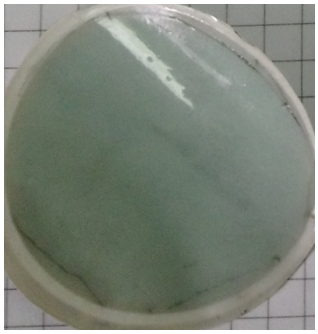


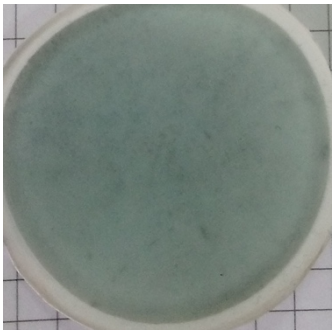
1:2

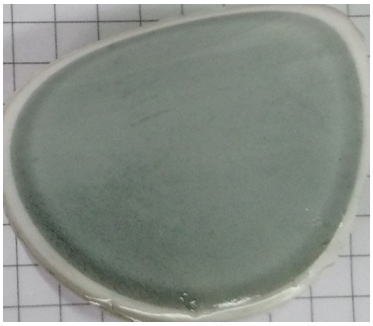


1:1

2:1







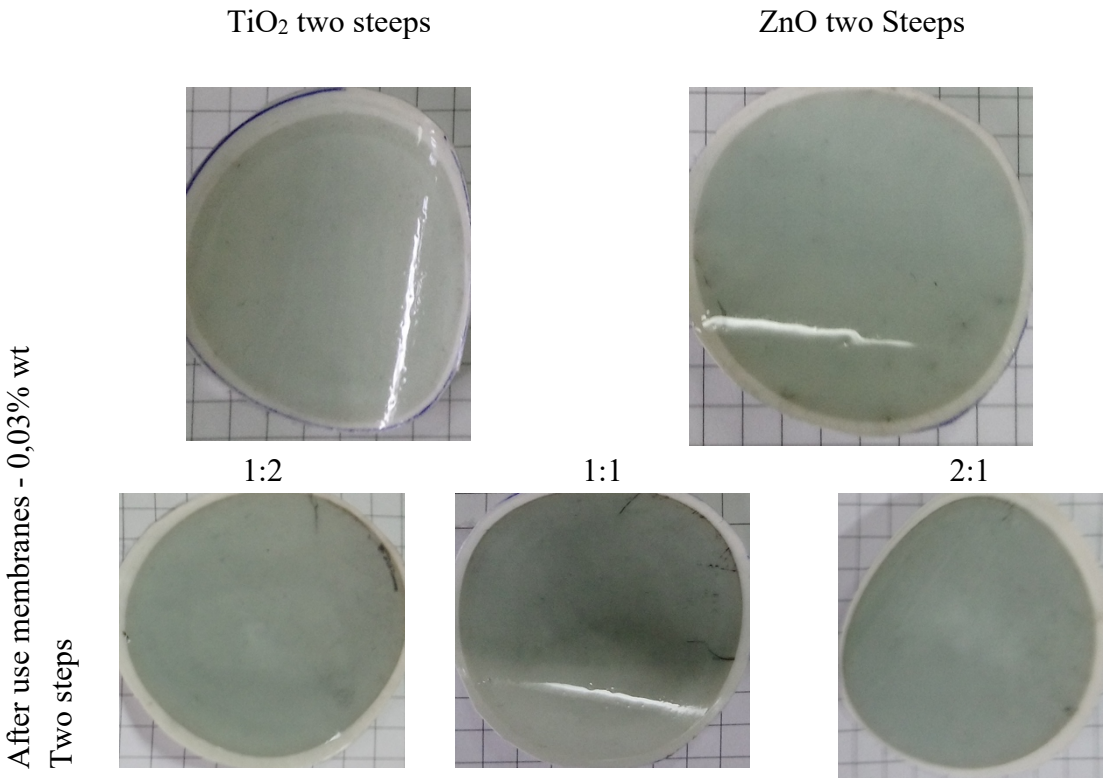


Figure **A2.4** shows the modified membranes after being in contact for 5 hours with methylene blue solution (10 mg L^{-1}) and under solar irradiation

Appendix 2. chapter 3

Chapter 3. TiO_2:ZnO modified low-cost membranes with mussel-inspired polydopamine binding as microbial fuel cell membranes

1.- Membrane ruptures

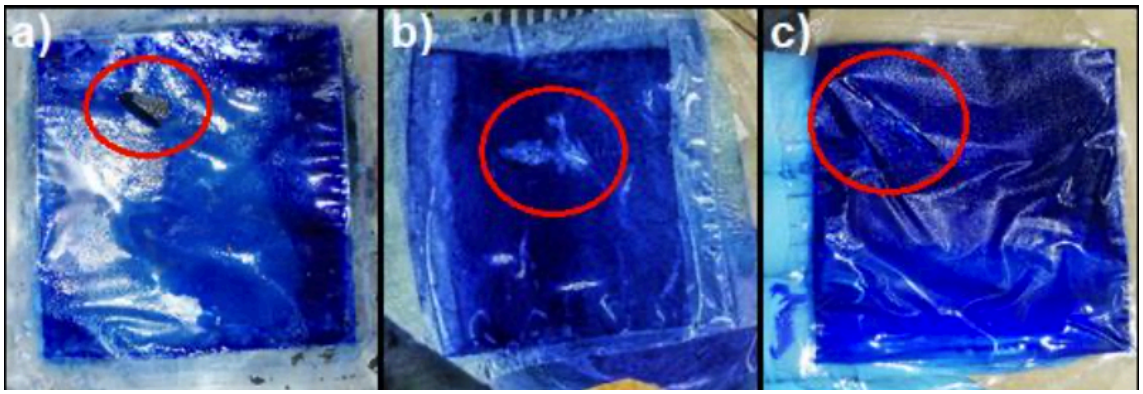


Figure A3.1. Membrane ruptures, a) pristine after 5 cycles, and b) Cel-PDA and c) Cel-PDA/TiO2:ZnO after 10 cycles

2.- Power density of the MFC with catalysts and without catalysts

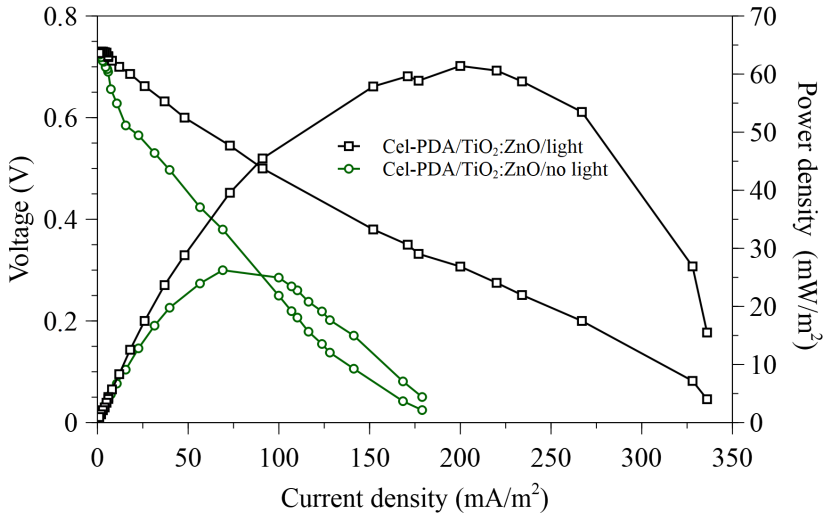
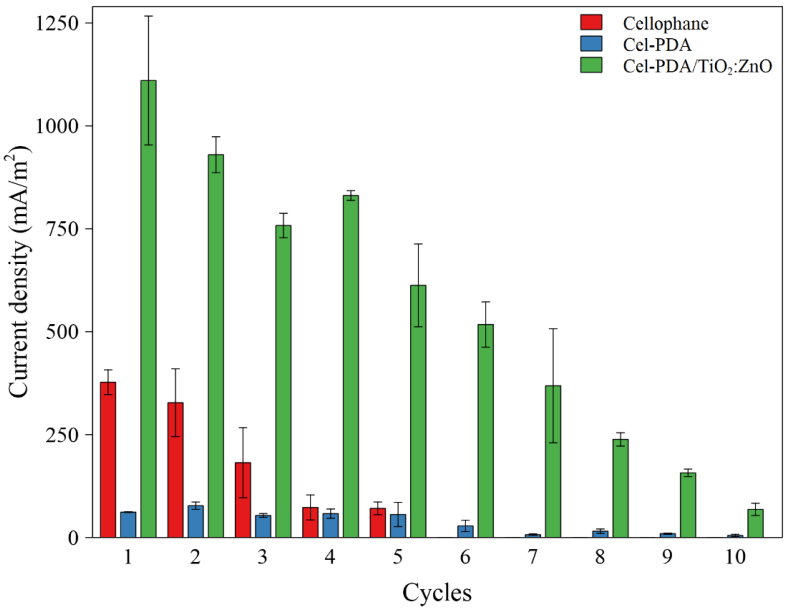


Figure A3.2. Polarization curves of MFCs with Cel-PDA/TiO_2:ZnO composite membranes with light and without light.

3.- Power density and internal resistance of every cycle of MFCs

a)



b)

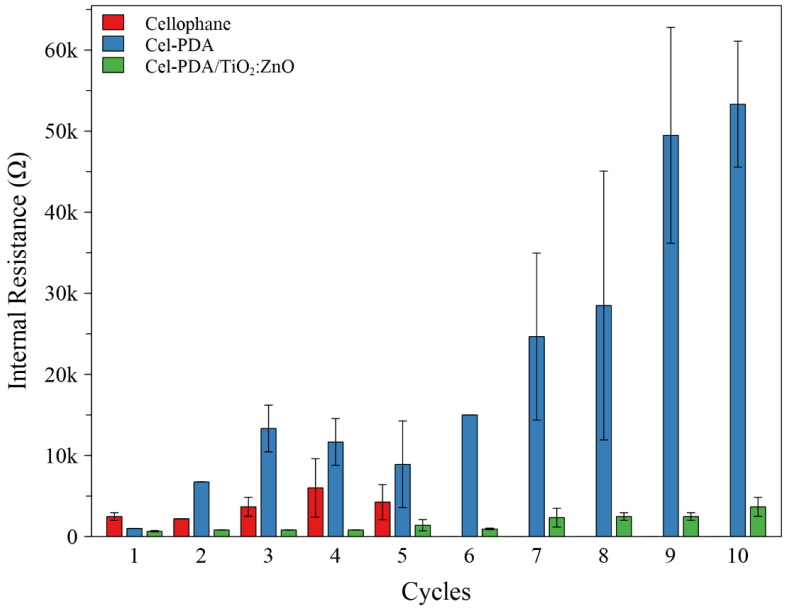


Figure A3.3 a) power density of MFC with Cel-PDA/TiO_2:ZnO was higher than that of the other membranes in all operating cycles and b) internal resistance

Appendix 3. chapter 4

Chapter 4 Effect od Er, Al and Er/Al dopants on the photocatalytic and antibacterial properties of ZnO nanoparticles

Effect of Type of light on MO degradation

The useful life of a fluorescent is 5000h while an LED is 15000h. The white LEDs have higher luminous efficacy that fluorescent lamp.

Highly efficient warm-white all-nitride phosphor-converted light emitting diode (LED) use GaN based quantum well blue LED and novel nitrogen containing luminescent materials as Eu^{2+}(Jandt et al., 2000; Mueller-Mach et al., 2005; Narukawa et al., 2010). It has an excellent color quality (correlated color temperature CCT = 4000 K) and the highest color stability. Thus, these LEDs are superior to both incandescent and fluorescent lamps (UV Blacklight lamp)(Narukawa et al., 2010).

For all reasons the studies were continued with LED light but at 18W to ensure the degradation of dyes.

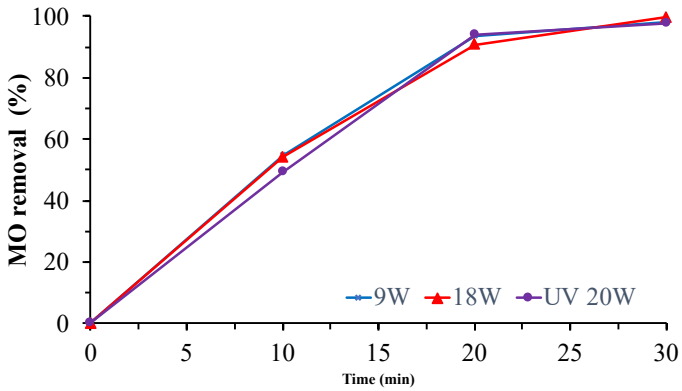


Figure A4.1. Effect of the lamp used for MO removal with ZnO-Er/Al. (10 mg/L initial MO concentration of solution 0,3g/L catalyst).

Effect of initial concentration MO on the photodegradation.

In order to study the effect of azo dye initial concentrations on the photodegradation activity, the initial concentrations of MO were changed from 10 to 50 mg/ L. The results of the comparison of removal rates of the dyes after 30 min of reaction time are shown inFigure. S2. The removal rates of MO showed the same removal. These preliminary tests showed the adsorption of O_2 and OH^- on the photocatalyst was not decreased for 10 and 25 mg/L. These concentrations did not decrease generation of radicals, due to, the photons were not blocked before reaching the photocatalyst surface; hence, the adsorption of photons was maintained by the photo- catalyst. However, for the concentration of 50, a 18% decline was observed.

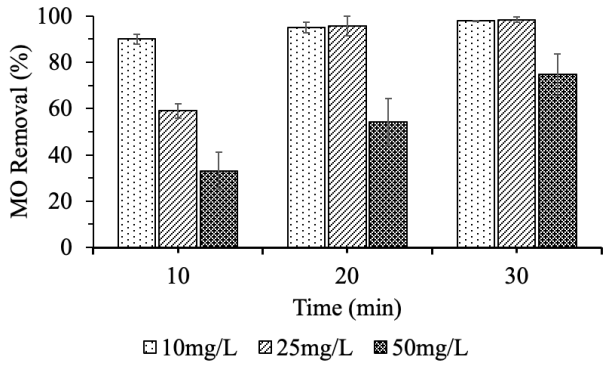


Figure A4.2. Effect of initial concentration MO on the photodegradation activities of 1Er/5Al ZnO (18W visible light).

8. References

Abid, H.S., Johnson, D.J., Hashaikeh, R., Hilal, N., 2017. A review of efforts to reduce membrane fouling by control of feed spacer characteristics. Desalination 420, 384–402. https://doi.org/10.1016/j.desal.2017.07.019

Adams, L.K., Lyon, D.Y., Alvarez, P.J.J., 2006. Comparative eco-toxicity of nanoscale TiO2, SiO2, and ZnO water suspensions. Water Res. 40, 3527–3532. https://doi.org/10.1016/j.watres.2006.08.004

Al-Mamun, A., Baawain, M.S., Dhar, B.R., Kim, I.S., 2017. Improved recovery of bioenergy and osmotic water in an osmotic microbial fuel cell using micro-diffuser assisted marine aerobic biofilm on cathode. Biochem. Eng. J. 128, 235–242. https://doi.org/10.1016/j.bej.2017.09.020

Al-Sahari, M., Al-Gheethi, A., Saphira, R.M., Mohamed, R., Noman, E., Naushad, M., Rizuan, B., Dai-Viet, , Vo, N., Ismail, N., 2021. Green approach and strategies for wastewater treatment using bioelectrochemical systems: A critical review of fundamental concepts, applications, mechanism, and future trends. Chemosphere 285, 131373. https://doi.org/10.1016/j.chemosphere.2021.131373

Alklaibi, A.M., Lior, N., 2005. Membrane-distillation desalination: Status and potential. Desalination 171, 111–131. https://doi.org/10.1016/j.desal.2004.03.024

Almatouq, A., Babatunde, A.O., Khajah, M., Webster, G., Alfodari, M., 2020. Microbial community structure of anode electrodes in microbial fuel cells and microbial electrolysis cells. J. Water Process Eng. 34, 101140. https://doi.org/10.1016/j.jwpe.2020.101140

Alventosa-Delara, E., Barredo-Damas, S., Alcaina-Miranda, M.I., Iborra-Clar, M.I., 2014. Study and optimization of the ultrasound-enhanced cleaning of an ultrafiltration ceramic membrane through a combined experimental-statistical approach. Ultrason. Sonochem. 21, 1222–1234. https://doi.org/10.1016/j.ultsonch.2013.10.022

Alzahrani, S., Mohammad, A.W., 2014. Challenges and trends in membrane technology implementation for produced water treatment: A review. J. Water Process Eng. 4,

107–133. https://doi.org/10.1016/j.jwpe.2014.09.007

Ambient secretary government of Quito Ecuador, 2020. Ambient secretary government of Quito Ecuador [WWW Document].

Ambient Secretary, Q.E., 2018. Ambient secretary government of Quito Ecuador [WWW Document].

Amjad, M., Gardy, J., Hassanpour, A., Wen, D., 2018. Novel draw solution for forward osmosis based solar desalination. Appl. Energy 230, 220–231. https://doi.org/10.1016/j.apenergy.2018.08.021

Anand, A., Unnikrishnan, B., Mao, J.Y., Lin, H.J., Huang, C.C., 2018. Graphene-based nanofiltration membranes for improving salt rejection, water flux and antifouling–A review. Desalination 429, 119–133. https://doi.org/10.1016/j.desal.2017.12.012

Anandan, S., Kumar Ponnusamy, V., Ashokkumar, M., 2020. A review on hybrid techniques for the degradation of organic pollutants in aqueous environment. Ultrason. Sonochem. 67. https://doi.org/10.1016/j.ultsonch.2020.105130

Andrade, J. de L., Oliveira, A.G., Mariucci, V.V.G., Bento, A.C., Companhoni, M.V., Nakamura, C.V., Lima, S.M., Andrade, L.H. da C., Moraes, J.C.G., Hechenleitner, A.A.W., Pineda, E.A.G., de Oliveira, D.M.F., 2017. Effects of Al3+ concentration on the optical, structural, photocatalytic and cytotoxic properties of Al-doped ZnO. J. Alloys Compd. 729, 978–987. https://doi.org/10.1016/j.jallcom.2017.09.128

Ang, M.B.M.Y., Trilles, C.A., De Guzman, M.R., Pereira, J.M., Aquino, R.R., Huang, S.H., Hu, C.C., Lee, K.R., Lai, J.Y., 2019. Improved performance of thin-film nanocomposite nanofiltration membranes as induced by embedded polydopamine-coated silica nanoparticles. Sep. Purif. Technol. 224, 113–120. https://doi.org/10.1016/j.seppur.2019.05.018

Atmaca, S., Gül, K., Çiçek, R., 2998. The Effect of Zinc On Microbial Growth. Tr. J. Med. Sci. 28, 595–597.

Bagheri, M., Akbari, A., Mirbagheri, S.A., 2019. Advanced control of membrane fouling in filtration systems using artificial intelligence and machine learning techniques: A critical review. Process Saf. Environ. Prot. 123, 229–252. https://doi.org/10.1016/j.psep.2019.01.013

Bahamonde Soria, R., Luis, P., 2021. Effect of Er, Al and Er/Al dopants on the

photocatalytic and antibacterial properties of ZnO nanoparticles. Ind. Eng. Chem. Res.

Bahamonde Soria, R., Zhu, J., Gonza, I., Van der Bruggen, B., Luis, P., 2020. Effect of (TiO2: ZnO) ratio on the anti-fouling properties of bio-inspired nanofiltration membranes. Sep. Purif. Technol. 251. https://doi.org/10.1016/j.seppur.2020.117280

Bajracharya, S., Yuliasni, R., Vanbroekhoven, K., Buisman, C.J.N., Strik, D.P.B.T.B., Pant, D., 2017. Long-term operation of microbial electrosynthesis cell reducing CO2 to multi-carbon chemicals with a mixed culture avoiding methanogenesis. Bioelectrochemistry 113, 26–34. https://doi.org/10.1016/j.bioelechem.2016.09.001

Baker, R.W., 2012. Membrane Technology and Research, Inc, 3rd ed. Wiley, Newark, California.

Bakonyi, P., Koók, L., Kumar, G., Tóth, G., Rózsenberszki, T., Nguyen, D.D., Chang, S.W., Zhen, G., Bélafi-Bakó, K., Nemestóthy, N., 2018. Architectural engineering of bioelectrochemical systems from the perspective of polymeric membrane separators: A comprehensive update on recent progress and future prospects. J. Memb. Sci. 564, 508–522. https://doi.org/10.1016/j.memsci.2018.07.051

Ball, V., 2018. Polydopamine films and particles with catalytic activity. Catal. Today 301, 196–203. https://doi.org/10.1016/j.cattod.2017.01.031

Balta, S., Sotto, A., Luis, P., Benea, L., Van der Bruggen, B., Kim, J., 2012. A new outlook on membrane enhancement with nanoparticles: The alternative of ZnO. J. Memb. Sci. 389, 155–161. https://doi.org/10.1016/j.memsci.2011.10.025

Banat, I.M., Nigam, P., Singh, D., Marchant, R., 1996. Microbial decolorization of textile-dye-containing effluents: A review. Bioresour. Technol. 58, 217–227. https://doi.org/10.1016/S0960-8524(96)00113-7

Barclay, T.G., Hegab, H.M., Clarke, S.R., Ginic-Markovic, M., 2017. Versatile Surface Modification Using Polydopamine and Related Polycatecholamines: Chemistry, Structure, and Applications. Adv. Mater. Interfaces 4, 1–38. https://doi.org/10.1002/admi.201601192

Bazrgar Bajestani, M., Mousavi, S.A., 2016. Effect of casting solvent on the characteristics of Nafion/TiO2 nanocomposite membranes for microbial fuel cell application. Int. J. Hydrogen Energy 41, 476–482. https://doi.org/10.1016/j.ijhydene.2015.11.036

Bellona, C., Drewes, J.E., Xu, P., Amy, G., 2004. Factors affecting the rejection of organic

solutes during NF/RO treatment - A literature review. Water Res. 38, 2795–2809. https://doi.org/10.1016/j.watres.2004.03.034

Bernsmann, F., Ball, V., Addiego, F., Ponche, A., Michel, M., Gracio, J.J. de A., Toniazzo, V., Ruch, D., 2011. Dopamine−Melanin Film Deposition Depends on the Used Oxidant and Buffer Solution. Langmuir 27, 2819–2825. https://doi.org/10.1021/la104981s

Bhagat, M.S., Mungray, A.K., Mungray, A.A., 2021. Effect of sound waves and inclination of membrane on the performance of the osmotic microbial fuel cell. Water-Energy Nexus 4, 113–122. https://doi.org/10.1016/j.wen.2021.07.003

Bhushan, B., 2012. Bioinspired structured surfaces. Langmuir 28, 1698–1714. https://doi.org/10.1021/la2043729

Bi, L., Ci, S., Cai, P., Li, H., Wen, Z., 2018. One-step pyrolysis route to three dimensional nitrogen-doped porous carbon as anode materials for microbial fuel cells. Appl. Surf. Sci. 427, 10–16. https://doi.org/10.1016/j.apsusc.2017.08.030

Bououdina, M., Azzaza, S., Ghomri, R., Shaikh, M.N., Dai, J.H., Song, Y., Song, W., Cai, W., Ghers, M., 2017. Structural and magnetic properties and DFT analysis of ZnO:(Al,Er) nanoparticles. RSC Adv. 7, 32931–32941. https://doi.org/10.1039/c7ra01015j

Brady, R.F., Singer, I.L., 2000. Mechanical factors favoring release from fouling release coatings. Biofouling 15, 73–81. https://doi.org/10.1080/08927010009386299

Brooms, T.J., Otieno, B., Onyango, M.S., Ochieng, A., 2018. Photocatalytic degradation of P-Cresol using TiO2/ZnO hybrid surface capped with polyaniline. J. Environ. Sci. Heal. - Part A Toxic/Hazardous Subst. Environ. Eng. 53, 99–107. https://doi.org/10.1080/10934529.2017.1377583

Cavallos-Sierra, J., Ramos-Martin, J., 2018. Spatial assessment of the potential of renewable energy: The case of Ecuador. Renew. Sustain. Energy Rev. 81, 1154–1165. https://doi.org/10.1016/J.RSER.2017.08.015

Chae, K.J., Choi, M., Ajayi, F., Park, W., Chang, I.S., Kim, I.S., 2016. Mass Transport through a Proton Exchange Membrane (Nafion) in Microbial Fuel Cells. Energy & Fuels 22, 169–176. https://doi.org/10.1021/ef700308u

Chen, X., Wu, Z., Liu, D., Gao, Z., 2017. Preparation of ZnO Photocatalyst for the Efficient

and Rapid Photocatalytic Degradation of Azo Dyes. Nanoscale Res. Lett. 12, 4–13. https://doi.org/10.1186/s11671-017-1904-4

Choi, M.J., Chae, K.J., Ajayi, F.F., Kim, K.Y., Yu, H.W., Kim, C. won, Kim, I.S., 2011. Effects of biofouling on ion transport through cation exchange membranes and microbial fuel cell performance. Bioresour. Technol. 102, 298–303. https://doi.org/10.1016/j.biortech.2010.06.129

Chong, M.N., Jin, B., Chow, C.W.K., Saint, C., 2010. Recent developments in photocatalytic water treatment technology: a review. Water Res. 44, 2997–3027. https://doi.org/10.1016/j.watres.2010.02.039

Choudhury, R.R., Gohil, J.M., Mohanty, S., Nayak, S.K., 2018. Antifouling, fouling release and antimicrobial materials for surface modification of reverse osmosis and nanofiltration membranes. J. Mater. Chem. A 6, 313–333. https://doi.org/10.1039/c7ta08627j

Chowdhury, M.R., Ren, J., Reimund, K., McCutcheon, J.R., 2017. A hybrid dead-end/cross-flow forward osmosis system for evaluating osmotic flux performance at high recovery of produced water. Desalination 421, 127–134. https://doi.org/10.1016/j.desal.2016.08.021

Christodoulou, X., Okoroafor, T., Parry, S., Velasquez-Orta, S.B., 2017. The use of carbon dioxide in microbial electrosynthesis: Advancements, sustainability and economic feasibility. J. CO2 Util. 18, 390–399. https://doi.org/10.1016/j.jcou.2017.01.027

Cui, J., Zhou, Z., Xie, A., Meng, M., Cui, Y., Liu, S., Lu, J., Zhou, S., Yan, Y., Dong, H., 2019. Bio-inspired fabrication of superhydrophilic nanocomposite membrane based on surface modification of SiO2 anchored by polydopamine towards effective oil-water emulsions separation. Sep. Purif. Technol. 209, 434–442. https://doi.org/10.1016/j.seppur.2018.03.054

Daghrir, R., Drogui, P., Robert, D., 2013. Modified TiO2 for environmental photocatalytic applications: A review. Ind. Eng. Chem. Res. 52, 3581–3599. https://doi.org/10.1021/ie303468t

Dalsin, J.L., Lin, L., Tosatti, S., Vo, J., Textor, M., Messersmith, P.B., 2005. Protein Resistance of Titanium Oxide Surfaces Modified by Biologically Inspired mPEG - DOPA. Langmuir 21, 640–646.

Darbi, A., Viraraghavan, T., Jin, Y.C., Braul, L., Corkal, D., 2003. Sulfate removal from water. Water Qual. Res. J. Canada 38, 169–182. https://doi.org/10.2166/wqrj.2003.011

De Aragão Umbuzeiro, G., Freeman, H.S., Warren, S.H., De Oliveira, D.P., Terao, Y., Watanabe, T., Claxton, L.D., 2005. The contribution of azo dyes to the mutagenic activity of the Cristais River. Chemosphere 60, 55–64. https://doi.org/10.1016/j.chemosphere.2004.11.100

De Filpo, G., Pantuso, E., Armentano, K., Formoso, P., Di Profio, G., Poerio, T., Fontananova, E., Meringolo, C., Mashin, A.I., Nicoletta, F.P., 2018. Chemical vapor deposition of photocatalyst nanoparticles on PVDF membranes for advanced oxidation processes. Membranes (Basel). 8, 35. https://doi.org/10.3390/membranes8030035

De Vrieze, J., Arends, J.B.A., Verbeeck, K., Gildemyn, S., Rabaey, K., 2018. Interfacing anaerobic digestion with (bio)electrochemical systems: Potentials and challenges. Water Res. 146, 244–255. https://doi.org/10.1016/j.watres.2018.08.045

Dědková, K., Kuzníková, Pavelek, L., Matějová, K., Kupková, J., Čech Barabaszová, K., Váňa, R., Burda, J., Vlček, J., Cvejn, D., Kukutschová, J., 2017. Daylight induced antibacterial activity of gadolinium oxide, samarium oxide and erbium oxide nanoparticles and their aquatic toxicity. Mater. Chem. Phys. 197, 226–235. https://doi.org/10.1016/j.matchemphys.2017.05.039

Deepti, Sinha, A., Biswas, P., Sarkar, S., Bora, U., Purkait, M.K., 2020. Separation of chloride and sulphate ions from nanofiltration rejected wastewater of steel industry. J. Water Process Eng. 33, 101108. https://doi.org/10.1016/j.jwpe.2019.101108

Delsouz Khaki, M.R., Shafeeyan, M.S., Raman, A.A.A., Daud, W.M.A.W., 2018. Evaluating the efficiency of nano-sized Cu doped TiO2/ZnO photocatalyst under visible light irradiation. J. Mol. Liq. 258, 354–365. https://doi.org/10.1016/j.molliq.2017.11.030

Desgupta, J., Sikder, J., Chakraborty, S., Curcio, S., Drioli, E., 2015. Remediation of textile effluents by membrane based treatment techniques: A state of the art review. J. Environ. Manage. 147, 55–72.

Di Palma, L., Bavasso, I., Sarasini, F., Tirillò, J., Puglia, D., Dominici, F., Torre, L., 2018. Synthesis, characterization and performance evaluation of Fe3O4/PES nano composite membranes for microbial fuel cell. Eur. Polym. J. 99, 222–229.

https://doi.org/10.1016/j.eurpolymj.2017.12.037

Ding, Y.H., Floren, M., Tan, W., 2016. Mussel-inspired polydopamine for bio-surface functionalization. Biosurface and Biotribology 2, 121–136. https://doi.org/10.1016/j.bsbt.2016.11.001

Divya, N.K., Pradyumnan, P.P., 2016. Solid state synthesis of erbium doped ZnO with excellent photocatalytic activity and enhanced visible light emission. Mater. Sci. Semicond. Process. 41, 428–435.

Dong, S., Xu, K., Liu, J., Cui, H., 2011. Photocatalytic performance of ZnO:Fe array films under sunlight irradiation. Phys. B Condens. Matter 406, 3609–3612. https://doi.org/10.1016/j.physb.2011.06.053

Duay, J., Kelly, M., Lambert, T.N., 2018. Evaluation of a ceramic separator for use in rechargeable alkaline Zn/MnO2 batteries. J. Power Sources 395, 430–438. https://doi.org/10.1016/j.jpowsour.2018.05.072

Fane, A.G., Xi, W., Rong, W., 2006. Membrane filtration processes and fouling, in: Interface Science in Drinking Water Treatmen. Elsevier Ltd., pp. 109–132. https://doi.org/10.1016/S1573-4285(06)80076-1

Fang, J., Deng, B., 2014. Rejection and modeling of arsenate by nanofiltration: Contributions of convection, diffusion and electromigration to arsenic transport. J. Memb. Sci. 453, 42–51. https://doi.org/10.1016/j.memsci.2013.10.056

Fatima, M., Farooq, R., Lindström, R.W., Saeed, M., 2017. A review on biocatalytic decomposition of azo dyes and electrons recovery. J. Mol. Liq. 246, 275–281. https://doi.org/10.1016/j.molliq.2017.09.063

Feris, K., Otto, C., Tinker, J., Wingett, D., Punnoose, A., Thurber, A., Kongara, M., Sabetian, M., Quinn, B., Hanna, C., Pink, D., 2010. Electrostatic interactions affect nanoparticle-mediated toxicity to gram-negative bacterium pseudomonas aeruginosa PAO1. Langmuir 26, 4429–4436. https://doi.org/10.1021/la903491z

Firdaus, C.M., Shah Rizam, M.S.B., Rusop, M., Rahmatul Hidayah, S., 2012. Characterization of ZnO and ZnO: TiO2 thin films prepared by sol-gel spray-spin coating technique. Procedia Eng. 41, 1367–1373. https://doi.org/10.1016/j.proeng.2012.07.323

Flimban, S.G.A., Hassan, S.H.A., Rahman, M.M., Oh, S.E., 2018. The effect of Nafion

membrane fouling on the power generation of a microbial fuel cell. Int. J. Hydrogen Energy. https://doi.org/10.1016/j.ijhydene.2018.02.097

Forgacs, E., Cserháti, T., Oros, G., 2004. Removal of synthetic dyes from wastewaters: a review. Environ. Int. 30, 953–71. https://doi.org/10.1016/j.envint.2004.02.001

Fortunato, R., Branco, C., Afonso, C.A.M., Benavente, J., Crespo, G., 2006. Electrical impedance spectroscopy characterisation of supported ionic liquid membranes. J. Memb. Sci. 270, 42–49. https://doi.org/10.1016/j.memsci.2005.06.040

Freguia, S., Masuda, M., Tsujimura, S., Kano, K., 2009. Lactococcus lactis catalyses electricity generation at microbial fuel cell anodes via excretion of a soluble quinone. Bioelectrochemistry 76, 14–18. https://doi.org/10.1016/j.bioelechem.2009.04.001

Freguia, S., Tsujimura, S., Kano, K., 2010. Electron transfer pathways in microbial oxygen biocathodes. Electrochim. Acta 55, 813–818. https://doi.org/10.1016/j.electacta.2009.09.027

Fu, F., Wang, Q., 2011. Removal of heavy metal ions from wastewaters: a review. J. Environ. Manage. 92, 407–18. https://doi.org/10.1016/j.jenvman.2010.11.011

Fu, M., Li, Y., Wu, S., Lu, P., Liu, J., Dong, F., 2011. Sol-gel preparation and enhanced photocatalytic performance of Cu-doped ZnO nanoparticles. Appl. Surf. Sci. 258, 1587–1591. https://doi.org/10.1016/j.apsusc.2011.10.003

Gangadharan, P., Vadekeetil, A., Sibi, R., Sheelam, A., 2021. Concentrating nutrients and recovering water and energy from source separated urine using osmotic microbial fuel cell. Chemosphere 285, 131548. https://doi.org/10.1016/j.chemosphere.2021.131548

Ge, Z., Ping, Q., Xiao, L., He, Z., 2013. Reducing effluent discharge and recovering bioenergy in an osmotic microbial fuel cell treating domestic wastewater. Desalination 312, 52–59. https://doi.org/10.1016/j.desal.2012.08.036

Ghasemi, M., Wan Daud, W.R., Ismail, M., Rahimnejad, M., Ismail, A.F., Leong, J.X., Miskan, M., Ben Liew, K., 2013. Effect of pre-treatment and biofouling of proton exchange membrane on microbial fuel cell performance. Int. J. Hydrogen Energy 38, 5480–5484. https://doi.org/10.1016/j.ijhydene.2012.09.148

Ghomri, R., Shaikh, M.N., Ahmed, M.I., Song, W., Cai, W., Bououdina, M., Ghers, M., 2018. Pure and (Er, Al) co-doped ZnO nanoparticles: synthesis, characterization, magnetic and photocatalytic properties. J. Mater. Sci. Mater. Electron. 29, 10677–

10685. https://doi.org/10.1007/s10854-018-9136-7

Gimkiewicz, C., Harnisch, F., 2013. Waste water derived electroactive microbial biofilms: growth, maintenance, and basic characterization. J. Vis. Exp. 50800. https://doi.org/10.3791/50800

Gomez-Solís, C., Ballesteros, J.C., Torres-Martínez, L.M., Juárez-Ramírez, I., Díaz Torres, L.A., Elvira Zarazua-Morin, M., Lee, S.W., 2015. Rapid synthesis of ZnO nano-corncobs from Nital solution and its application in the photodegradation of methyl orange. J. Photochem. Photobiol. A Chem. 298, 49–54. https://doi.org/10.1016/j.jphotochem.2014.10.012

Guo, K., Prévoteau, A., Rabaey, K., 2017. A novel tubular microbial electrolysis cell for high rate hydrogen production. J. Power Sources 356, 484–490. https://doi.org/10.1016/j.jpowsour.2017.03.029

Guvendiren, M., Messersmith, P.B., Shull, K.R., 2008. Self-assembly and adhesion of DOPA-modified methacrylic triblock hydrogels. Biomacromolecules 9, 122–128. https://doi.org/10.1021/bm700886b

Haghighi, N., Abdi, Y., Haghighi, F., 2011. Light-induced antifungal activity of TiO 2 nanoparticles/ZnO nanowires. Appl. Surf. Sci. 257, 10096–10100. https://doi.org/10.1016/j.apsusc.2011.06.145

Hairom, N.H.H., Mohammad, A.W., Kadhum, A.A.H., 2014. Effect of various zinc oxide nanoparticles in membrane photocatalytic reactor for Congo red dye treatment. Sep. Purif. Technol. 137, 74–81. https://doi.org/10.1016/j.seppur.2014.09.027

Hajipour, M.J., Fromm, K.M., Akbar Ashkarran, A., Jimenez de Aberasturi, D., Larramendi, I.R. de, Rojo, T., Serpooshan, V., Parak, W.J., Mahmoudi, M., 2012. Antibacterial properties of nanoparticles. Trends Biotechnol. 30, 499–511. https://doi.org/10.1016/j.tibtech.2012.06.004

Han, T.H., Khan, M.M., Kalathil, S., Lee, J., Cho, M.H., 2013. Simultaneous enhancement of methylene blue degradation and power generation in a microbial fuel cell by gold nanoparticles. Ind. Eng. Chem. Res. 52, 8174–8181. https://doi.org/10.1021/ie4006244

He, L., Du, P., Chen, Y., Lu, H., Cheng, X., Chang, B., Wang, Z., 2017. Advances in microbial fuel cells for wastewater treatment. Renew. Sustain. Energy Rev. 71, 388–

403. https://doi.org/10.1016/j.rser.2016.12.069

Heggo, D., Ookawara, S., 2017. Multiphase photocatalytic microreactors. Chem. Eng. Sci. 169, 67–77. https://doi.org/10.1016/j.ces.2017.01.019

Heidrich, E.S., Dolfing, J., Wade, M.J., Sloan, W.T., Quince, C., Curtis, T.P., 2018. Temperature, inocula and substrate: Contrasting electroactive consortia, diversity and performance in microbial fuel cells. Bioelectrochemistry 119, 43–50. https://doi.org/10.1016/j.bioelechem.2017.07.006

Heinlaan, M., Ivask, A., Blinova, I., Dubourguier, H.C., Kahru, A., 2008. Toxicity of nanosized and bulk ZnO, CuO and TiO2 to bacteria Vibrio fischeri and crustaceans Daphnia magna and Thamnocephalus platyurus. Chemosphere 71, 1308–1316. https://doi.org/10.1016/j.chemosphere.2007.11.047

Hernandez-Fernandez, F.J., de Los Rios, A.P., Salar-Garcia, M.J., Ortiz-Martinez, V.M., Lozano-Blanco, L.J., Godinez, C., Tomas-Alonso, F., Quesada-Medina, J., 2015. Recent progress and perspectives in microbial fuel cells for bioenergy generation and wastewater treatment. Fuel Process. Technol. 138, 284–297. https://doi.org/10.1016/j.fuproc.2015.05.022

Herzberg, M., Elimelech, M., 2007. Biofouling of reverse osmosis membranes: Role of biofilm-enhanced osmotic pressure. J. Memb. Sci. 295, 11–20. https://doi.org/10.1016/j.memsci.2007.02.024

Hołda, A.K., Vankelecom, I.F.J., 2015. Understanding and guiding the phase inversion process for synthesis of solvent resistant nanofiltration membranes. J. Appl. Polym. Sci. 132, 1–17. https://doi.org/10.1002/app.42130

Holkar, C.R., Jadhav, A.J., Pinjari, D. V., Mahamuni, N.M., Pandit, A.B., 2016. A critical review on textile wastewater treatments: Possible approaches. J. Environ. Manage. 182, 351–366. https://doi.org/10.1016/j.jenvman.2016.07.090

Homayoonfal, M., Mehrnia, M.R., Mojtahedi, Y.M., Ismail, A.F., 2013. Effect of metal and metal oxide nanoparticle impregnation route on structure and liquid filtration performance of polymeric nanocomposite membranes: A comprehensive review. Desalin. Water Treat. 51, 3295–3316. https://doi.org/10.1080/19443994.2012.749055

Hong, S., Na, Y.S., Choi, S., Song, I.T., Kim, W.Y., Lee, H., 2012. Non-covalent self-assembly and covalent polymerization co-contribute to polydopamine formation. Adv.

Funct. Mater. 22, 4711–4717. https://doi.org/10.1002/adfm.201201156

Hosseini, M.G., Ahadzadeh, I., 2013. Electrochemical impedance study on methyl orange and methyl red as power enhancing electron mediators in glucose fed microbial fuel cell. J. Taiwan Inst. Chem. Eng. 44, 617–621. https://doi.org/10.1016/j.jtice.2013.01.004

Husain, Q., 2010. Peroxidase mediated decolorization and remediation of wastewater containing industrial dyes: A review. Rev. Environ. Sci. Biotechnol. 9, 117–140. https://doi.org/10.1007/s11157-009-9184-9

Ivnitsky, H., Katz, I., Minz, D., Shimoni, E., Chen, Y., Tarchitzky, J., Semiat, R., Dosoretz, C.G., 2005. Characterization of membrane biofouling in nanofiltration processes of wastewater treatment. Desalination 185, 255–268. https://doi.org/10.1016/j.desal.2005.03.081

Ivnitsky, H., Minz, D., Kautsky, L., Preis, A., Ostfeld, A., Semiat, R., Dosoretz, C.G., 2010. Biofouling formation and modeling in nanofiltration membranes applied to wastewater treatment. J. Memb. Sci. 360, 165–173. https://doi.org/10.1016/j.memsci.2010.05.007

Jabeen, G., Farooq, R., 2017. Microbial Fuel Cells and Their Applications for Cost Effective Water Pollution Remediation. Proc. Natl. Acad. Sci. India Sect. B - Biol. Sci. 87, 625–635. https://doi.org/10.1007/s40011-015-0683-x

Jandt, K.D., Mills, R.W., Blackwell, G.B., Ashworth, S.H., 2000. Depth of cure and compressive strength of dental composites cured with blue light emitting diodes (LEDs). Dent. Mater. 16, 41–47. https://doi.org/10.1016/S0109-5641(99)00083-4

Jhaveri, J.H., Murthy, Z.V.P., 2016. A comprehensive review on anti-fouling nanocomposite membranes for pressure driven membrane separation processes. Desalination 379, 137–154. https://doi.org/10.1016/j.desal.2015.11.009

Jiang, J.-H., Zhu, L.-P., Li, X.-L., Xu, Y.-Y., Zhu, B.-K., 2010. Surface modification of PE porous membranes based on the strong adhesion of polydopamine and covalent immobilization of heparin. J. Memb. Sci. 364, 194–202. https://doi.org/https://doi.org/10.1016/j.memsci.2010.08.017

Jin, Y., Zhao, Y., Liu, H., Sotto, A., Gao, C., Shen, J., 2018. A durable and antifouling monovalent selective anion exchange membrane modified by polydopamine and

sulfonated reduced graphene oxide. Sep. Purif. Technol. 207, 116–123. https://doi.org/10.1016/j.seppur.2018.06.053

Jun, B.M., Al-Hamadani, Y.A.J., Son, A., Park, C.M., Jang, M., Jang, A., Kim, N.C., Yoon, Y., 2020a. Applications of metal-organic framework based membranes in water purification: A review. Sep. Purif. Technol. 247, 116947. https://doi.org/10.1016/j.seppur.2020.116947

Jun, B.M., Cho, J., Jang, A., Chon, K., Westerhoff, P., Yoon, Y., Rho, H., 2020b. Charge characteristics (surface charge vs. zeta potential) of membrane surfaces to assess the salt rejection behavior of nanofiltration membranes. Sep. Purif. Technol. 247, 117026. https://doi.org/10.1016/J.SEPPUR.2020.117026

Jung, S., Lee, J., Park, Y.K., Kwon, E.E., 2020. Bioelectrochemical systems for a circular bioeconomy. Bioresour. Technol. 300, 122748. https://doi.org/10.1016/j.biortech.2020.122748

Kandpal, R., Nara, S., Shahadat, M., Ansari, M.O., Alshahrie, A., Ali, W., Ziauddin Ahammad, S., Dhar Malhotra, B., 2021. Impedance spectroscopic study of biofilm formation on pencil lead graphite anode in microbial fuel cell. J. Taiwan Inst. Chem. Eng. 000, 1–10. https://doi.org/10.1016/j.jtice.2021.09.002

Karkhanechi, H., Takagi, R., Matsuyama, H., 2014. Enhanced antibiofouling of RO membranes via polydopamine coating and polyzwitterion immobilization. Desalination 337, 23–30. https://doi.org/10.1016/j.desal.2014.01.007

Kasemset, S., Lee, A., Miller, D.J., Freeman, B.D., Sharma, M.M., 2013. Effect of polydopamine deposition conditions on fouling resistance, physical properties, and permeation properties of reverse osmosis membranes in oil/water separation. J. Memb. Sci. 425–426, 208–216. https://doi.org/10.1016/j.memsci.2012.08.049

Kesting, R.E., 1985. Phase Inversion Membranes. ACS Symp. Ser. 131–164. https://doi.org/10.1021/bk-1985-0269.ch007

Khanzada, N.K., Rehman, S., Leu, S.Y., An, A.K., 2020. Evaluation of anti-bacterial adhesion performance of polydopamine cross-linked graphene oxide RO membrane via in situ optical coherence tomography. Desalination 479, 114339. https://doi.org/10.1016/j.desal.2020.114339

Khorshidi, B., Biswas, I., Ghosh, T., Thundat, T., Sadrzadeh, M., 2018. Robust fabrication

of thin film polyamide-TiO2 nanocomposite membranes with enhanced thermal stability and anti-biofouling propensity. Sci. Rep. 8, 1–10. https://doi.org/10.1038/s41598-017-18724-w

Khulbe, K.C., Matsuura, T., 2000. Characterization of synthetic membranes by Raman spectroscopy, electron spin resonance, and atomic force microscopy; a review. Polymer (Guildf). 41, 1917–1935. https://doi.org/10.1016/S0032-3861(99)00359-6

Kim, J., Van Der Bruggen, B., 2010. The use of nanoparticles in polymeric and ceramic membrane structures: Review of manufacturing procedures and performance improvement for water treatment. Environ. Pollut. 158, 2335–2349. https://doi.org/10.1016/j.envpol.2010.03.024

Kim, J.H., Park, C.H., Kim, C.S., Joshi, M.K., Lee, J., 2017. Polydopamine-assisted immobilization of hierarchical zinc oxide nanostructures on electrospun nanofibrous membrane for photocatalysis and antimicrobial activity. J. Colloid Interface Sci. 513, 566–574. https://doi.org/10.1016/j.jcis.2017.11.061

Kim, J.R., Cheng, S., Oh, S.-E., Logan, B.E., 2007. Membranes in Microbial Fuel Cells 41, 1004–1009.

Kim, J.R., Min, B., Logan, B.E., 2005. Evaluation of procedures to acclimate a microbial fuel cell for electricity production. Appl. Microbiol. Biotechnol. 68, 23–30. https://doi.org/10.1007/s00253-004-1845-6

Kim, K.-Y., Yang, E., Lee, M.-Y., Chae, K.-J., Kim, C.-M., Kim, I.S., 2014. Polydopamine coating effects on ultrafiltration membrane to enhance power density and mitigate biofouling of ultrafiltration microbial fuel cells (UF-MFCs). Water Res. 54, 62–68. https://doi.org/10.1016/j.watres.2014.01.045

Kim, K.Y., Yang, E., Lee, M.Y., Chae, K.J., Kim, C.M., Kim, I.S., 2014. Polydopamine coating effects on ultrafiltration membrane to enhance power density and mitigate biofouling of ultrafiltration microbial fuel cells (UF-MFCs). Water Res. 54, 62–68. https://doi.org/10.1016/j.watres.2014.01.045

Koch, K., Barthlott, W., 2009. Superhydrophobic and superhydrophilic plant surfaces: An inspiration for biomimetic materials. Philos. Trans. R. Soc. A Math. Phys. Eng. Sci. 367, 1487–1509. https://doi.org/10.1098/rsta.2009.0022

Kodali, M., Santoro, C., Herrera, S., Serov, A., Atanassov, P., 2017. Bimetallic platinum

group metal-free catalysts for high power generating microbial fuel cells. J. Power Sources 366, 18–26. https://doi.org/10.1016/j.jpowsour.2017.08.110

Kolesnyk, I., Konovalova, V., Kharchenko, K., Burban, A., Kujawa, J., Kujawski, W., 2020. Enhanced transport and antifouling properties of polyethersulfone membranes modified with α-amylase incorporated in chitosan-based polymeric micelles. J. Memb. Sci. 595. https://doi.org/10.1016/j.memsci.2019.117605

Kondaveeti, S., Lee, J., Kakarla, R., Kim, H.S., Min, B., 2014. Low-cost separators for enhanced power production and field application of microbial fuel cells (MFCs), Electrochimica Acta. https://doi.org/10.1016/j.electacta.2014.03.046

Konstantinou, I.K., Albanis, T.A., 2004. TiO2-assisted photocatalytic degradation of azo dyes in aqueous solution: Kinetic and mechanistic investigations: A review. Appl. Catal. B Environ. 49, 1–14. https://doi.org/10.1016/j.apcatb.2003.11.010

Koók, L., Kaufer, B., Bakonyi, P., Rózsenberszki, T., Rivera, I., Buitrón, G., Bélafi-Bakó, K., Nemestóthy, N., 2019. Supported ionic liquid membrane based on [bmim][PF6] can be a promising separator to replace Nafion in microbial fuel cells and improve energy recovery: A comparative process evaluation. J. Memb. Sci. 570–571, 215–225. https://doi.org/10.1016/j.memsci.2018.10.063

Krithika, T., Kavitha, R., Dinesh, M., Angayarkanni, J., 2021. Assessment of ligninolytic bacterial consortium for the degradation of azo dye with electricity generation in a dual-chambered microbial fuel cell. Environ. Challenges 4, 100093. https://doi.org/10.1016/j.envc.2021.100093

Labarca, F., Bórquez, R., 2020. Comparative study of nanofiltration and ion exchange for nitrate reduction in the presence of chloride and iron in groundwater. Sci. Total Environ. 723, 137809. https://doi.org/10.1016/j.scitotenv.2020.137809

Lakhotia, S.R., Mukhopadhyay, M., Kumari, P., 2019. Iron oxide (FeO) nanoparticles embedded thin-film nanocomposite T nanofiltration (NF) membrane for water treatment 211, 98–107.

Lakshmi Prasanna, V., Vijayaraghavan, R., 2017. Chemical manipulation of oxygen vacancy and antibacterial activity in ZnO. Mater. Sci. Eng. C 77, 1027–1034. https://doi.org/10.1016/j.msec.2017.03.280

Laohaprapanon, S., Matahum, J., Tayo, L., You, S., 2015. Photodegradation of Reactive

Black 5 in a ZnO / UV slurry membrane reactor. J. Taiwan Inst. Chem. Eng. 49, 136–141.

Lau, W.J., Gray, S., Matsuura, T., Emadzadeh, D., Paul Chen, J., Ismail, A.F., 2015. A review on polyamide thin film nanocomposite (TFN) membranes: History, applications, challenges and approaches. Water Res. 80, 306–324. https://doi.org/10.1016/j.watres.2015.04.037

Lau, W.J., Ismail, A.F., Misdan, N., Kassim, M.A., 2012. A recent progress in thin film composite membrane: A review. Desalination 287, 190–199. https://doi.org/10.1016/j.desal.2011.04.004

Layek, A., Banerjee, S., Manna, B., Chowdhury, A., 2016. Synthesis of rare-earth doped ZnO nanorods and their defect-dopant correlated enhanced visible-orange luminescence. RSC Adv. 6, 35892–35900. https://doi.org/10.1039/c6ra02278b

Le, N.L., Nunes, S.P., 2016. Materials and membrane technologies for water and energy sustainability. Sustain. Mater. Technol. 7, 1–28. https://doi.org/10.1016/j.susmat.2016.02.001

Lee, H., Dellatore, S.M., Miller, W.M., Messersmith, P.B., 2007. Mussel-Inspired Surface Chemistry for Multifunctional Coatings. Science (80-.). 318, 426–430. https://doi.org/10.1126/science.1147241.Mussel-Inspired

Lee, H.J., Choi, J.H., Cho, J., Moon, S.H., 2002. Characterization of anion exchange membranes fouled with humate during electrodialysis. J. Memb. Sci. 203, 115–126. https://doi.org/10.1016/S0376-7388(01)00792-X

Lee, K.M., Lai, C.W., Ngai, K.S., Juan, J.C., 2016. Recent developments of zinc oxide based photocatalyst in water treatment technology: A review. Water Res. 88, 428–448. https://doi.org/10.1016/j.watres.2015.09.045

Li, C., Song, Y., Wang, X., Zhang, Q., 2020. Synthesis, characterization and application of S-TiO2/PVDF-g-PSSA composite membrane for improved performance in MFCs. Fuel 264, 116847. https://doi.org/10.1016/j.fuel.2019.116847

Li, H., Ohdaira, E., Ide, M., 1996. Effect of ultrasonic irradiation on permeability of dialysis membrane. Japanese J. Appl. Physics, Part 1 Regul. Pap. Short Notes Rev. Pap. 35, 3255–3258. https://doi.org/10.1143/jjap.35.3255

Li, J., Yuan, S., Wang, J., Zhu, J., Shen, J., Van der Bruggen, B., 2018. Mussel-inspired

modification of ion exchange membrane for monovalent separation. J. Memb. Sci. 553, 139–150. https://doi.org/10.1016/j.memsci.2018.02.046

Li, W.W., Sheng, G.P., Liu, X.W., Yu, H.Q., 2011. Recent advances in the separators for microbial fuel cells. Bioresour. Technol. 102, 244–252. https://doi.org/10.1016/j.biortech.2010.03.090

Li, Ya, Bi, R., Su, Y., Li, Yafei, Yang, C., You, X., Shen, J., Yuan, J., Zhang, R., Jiang, Z., 2021. Tuning the pore size of graphene quantum dots composite nanofiltration membranes by P-aminobenzoic acid for enhanced dye/salt separation. Sep. Purif. Technol. 263, 118372. https://doi.org/10.1016/J.SEPPUR.2021.118372

Li, Z., Zhang, X., Lin, J., Han, S., Lei, L., 2010. Azo dye treatment with simultaneous electricity production in an anaerobic-aerobic sequential reactor and microbial fuel cell coupled system. Bioresour. Technol. 101, 4440–4445. https://doi.org/10.1016/j.biortech.2010.01.114

Liebscher, J., Mrówczyński, R., Scheidt, H.A., Filip, C., Haìdade, N.D., Turcu, R., Bende, A., Beck, S., 2013. Structure of polydopamine: A never-ending story? Langmuir 29, 10539–10548. https://doi.org/10.1021/la4020288

Liu, L., Shao, B., Yang, F., 2013. Polydopamine coating - Surface modification of polyester filter and fouling reduction. Sep. Purif. Technol. 118, 226–233. https://doi.org/10.1016/j.seppur.2013.07.003

Liu, X., Qi, S., Li, Y., Yang, L., Cao, B., Tang, C.Y., 2013. Synthesis and characterization of novel antibacterial silver nanocomposite nanofiltration and forward osmosis membranes based on layer-by-layer assembly. Water Res. 47, 3081–3092. https://doi.org/10.1016/j.watres.2013.03.018

Liu, Z., Hu, Y., Liu, C., Zhou, Z., 2016. Surface-independent one-pot chelation of copper ions onto filtration membranes to provide antibacterial properties. Chem. Commun. 52, 12245–12248. https://doi.org/10.1039/c6cc06015c

Logan, B., Rabaey, K., 2013. Conversion of Wastes into Bioelectricity and Chemicals by Using Microbial Electrochemical Technologies. Science (80-.). 337, 686–690.

Logan, B.E., 2009. Exoelectrogenic bacteria that power microbial fuel cells. Nat. Rev. Microbiol. 7, 375–381. https://doi.org/10.1038/nrmicro2113

Logan, B.E., Hamelers, B., Rozendal, R., Schröder, U., Keller, J., Freguia, S., Aelterman,

P., Verstraete, W., Rabaey, K., 2006a. Microbial fuel cells: Methodology and technology. Environ. Sci. Technol. 40, 5181–5192. https://doi.org/10.1021/es0605016

Logan, B.E., Hamelers, B., Rozendal, R., Schröder, U., Keller, J., Freguia, S., Aelterman, P., Verstraete, W., Rabaey, K., 2006b. Critical Review Microbial Fuel Cells : Methodology and Technology. Environ. Sci. Technol. 40, 5181–5192. https://doi.org/10.1021/es0605016

Logan, B.E., Hamelers, B., Rozendal, R., Schröder, U., Keller, J., Freguia, S., Aelterman, P., Verstraete, W., Rabaey, K., 2006c. Microbial fuel cells: Methodology and technology. Environ. Sci. Technol. 40, 5181–5192. https://doi.org/10.1021/es0605016

Logan, B.E., Rabaey, K., 2012. Conversion of wastes into bioelectricity and chemicals by using microbial electrochemical technologies. Science (80-.). 337, 686–690. https://doi.org/10.1126/science.1217412

Logroño, W., Pérez, M., Urquizo, G., Kadier, A., Echeverría, M., Recalde, C., Rákhely, G., 2017. Single chamber microbial fuel cell (SCMFC) with a cathodic microalgal biofilm: A preliminary assessment of the generation of bioelectricity and biodegradation of real dye textile wastewater. Chemosphere 176, 378–388. https://doi.org/10.1016/j.chemosphere.2017.02.099

Long, X., Li, X., Wang, H., Pan, Q., Wang, C., Li, H., 2017. Microbial fuel cell-photoelectrocatalytic cell combined system for the removal of azo dye wastewater. Bioresour. Technol. 244, 182–191. https://doi.org/10.1016/j.biortech.2017.07.088

Lu, P., Liang, S., Zhou, T., Xue, T., Mei, X., Wang, Q., 2017. Layered double hydroxide nanoparticle modified forward osmosis membranes via polydopamine immobilization with significantly enhanced chlorine and fouling resistance. Desalination 421, 99–109. https://doi.org/10.1016/j.desal.2017.04.030

Lu, X., Boo, C., Ma, J., Elimelech, M., 2014. Bidirectional diffusion of ammonium and sodium cations in forward osmosis: Role of membrane active layer surface chemistry and charge. Environ. Sci. Technol. 48, 14369–14376. https://doi.org/10.1021/es504162v

Lu, Y., Qin, M., Yuan, H., Abu-Reesh, I.M., He, Z., 2015. When bioelectrochemical systems meet forward osmosis: Accomplishing wastewater treatment and reuse through synergy. Water (Switzerland) 7, 38–50. https://doi.org/10.3390/w7010038

Lu, Y., Wang, W. yan, Xue, F., Yang, J. hui, Qi, X. dong, Zhou, Z. wan, Wang, Y., 2018. Bio-inspired polydopamine-assisted graphene oxide coating on tetra-pod zinc oxide whisker for dielectric composites. Chem. Eng. J. 345, 353–363. https://doi.org/10.1016/j.cej.2018.03.188

MacLean, L.C.W., Martinez, R.E., Fowle, D.A., 2004. Experimental studies of bacteria-iodide adsorption interactions. Chem. Geol. 212, 229–238. https://doi.org/10.1016/j.chemgeo.2004.08.014

Mahdavi, R., Talesh, S.S.A., 2017. Sol-gel synthesis , structural and enhanced photocatalytic performance of Al doped ZnO nanoparticles 28, 1418–1425.

Makuła, P., Pacia, M., Macyk, W., 2018. How To Correctly Determine the Band Gap Energy of Modified Semiconductor Photocatalysts Based on UV-Vis Spectra. J. Phys. Chem. Lett. 9, 6814–6817. https://doi.org/10.1021/acs.jpclett.8b02892

Manawi, Y., Kochkodan, V., Hussein, M.A., Khaleel, M.A., Khraisheh, M., Hilal, N., 2016. Can carbon-based nanomaterials revolutionize membrane fabrication for water treatment and desalination? Desalination 391, 69–88. https://doi.org/10.1016/j.desal.2016.02.015

Mansouri, J., Harrisson, S., Chen, V., 2010. Strategies for controlling biofouling in membrane filtration systems: Challenges and opportunities. J. Mater. Chem. 20, 4567–4586. https://doi.org/10.1039/b926440j

Mathew, M.L., Gopalakrishnan, A., Aravindakumar, C.T., Aravind, U.K., 2019. Low – cost multilayered green fiber for the treatment of textile industry waste water. J. Hazard. Mater. 365, 297–305. https://doi.org/10.1016/j.jhazmat.2018.11.014

McCloskey, B.D., Park, H.B., Ju, H., Rowe, B.W., Miller, D.J., Freeman, B.D., 2012. A bioinspired fouling-resistant surface modification for water purification membranes. J. Memb. Sci. 413–414, 82–90. https://doi.org/10.1016/j.memsci.2012.04.021

Miller, D.J., Araújo, P.A., Correia, P.B., Ramsey, M.M., Kruithof, J.C., van Loosdrecht, M.C.M., Freeman, B.D., Paul, D.R., Whiteley, M., Vrouwenvelder, J.S., 2012. Short-term adhesion and long-term biofouling testing of polydopamine and poly(ethylene glycol) surface modifications of membranes and feed spacers for biofouling control. Water Res. 46, 3737–3753. https://doi.org/10.1016/j.watres.2012.03.058

Miller, D.J., Kasemset, S., Wang, L., Paul, D.R., Freeman, B.D., 2014. Constant flux

crossflow filtration evaluation of surface-modified fouling-resistant membranes. J. Memb. Sci. 452, 171–183. https://doi.org/10.1016/j.memsci.2013.10.037

Misdan, N., Ismail, A.F., Hilal, N., 2016. Recent advances in the development of (bio)fouling resistant thin film composite membranes for desalination. Desalination 380, 105–111. https://doi.org/10.1016/j.desal.2015.06.001

Miskan, M., Ismail, M., Ghasemi, M., Md Jahim, J., Nordin, D., Abu Bakar, M.H., 2016. Characterization of membrane biofouling and its effect on the performance of microbial fuel cell. Int. J. Hydrogen Energy 41, 1–10. https://doi.org/10.1016/j.ijhydene.2015.09.037

Mohammad, A.W., Ali, N., 2002. Understanding the steric and charge contributions in NF membranes using increasing MWCO polyamide membranes. Desalination 147, 205–212. https://doi.org/10.1016/S0011-9164(02)00535-0

Mohammad, A.W., Teow, Y.H., Ang, W.L., Chung, Y.T., Oatley-Radcliffe, D.L., Hilal, N., 2015. Nanofiltration Membranes Review: Recent Advances and Future Prospects. Desalination 356, 226–254.

Molina-Fernández, C., Luis, P., 2021. Immobilization of carbonic anhydrase for CO2capture and its industrial implementation: A review. J. CO2 Util. 47. https://doi.org/10.1016/j.jcou.2021.101475

Moqsud, M.A., Omine, K., Yasufuku, N., Hyodo, M., Nakata, Y., 2013. Microbial fuel cell (MFC) for bioelectricity generation from organic wastes. Waste Manag. 33, 2465–2469. https://doi.org/10.1016/j.wasman.2013.07.026

Moradi, S., Aberoomand-azar, P., Raeis-farshid, S., Abedini-Khorrami, S., Givianrad, M.H., 2016. The effect of different molar ratios of ZnO on characterization and photocatalytic activity of TiO 2 / ZnO nanocomposite. J. Saudi Chem. Soc. 20, 373–378.

Mu, Y., Rabaey, K., Rozendal, R.A., Yuan, Z., Keller, J., 2009. Decolorization of azo dyes in bioelectrochemical systems. Environ. Sci. Technol. 43, 5137–5143. https://doi.org/10.1021/es900057f

Mueller-Mach, R., Mueller, G., Krames, M.R., Höppe, H.A., Stadler, F., Schnick, W., Juestel, T., Schmidt, P., 2005. Highly efficient all-nitride phosphor-converted white light emitting diode. Phys. Status Solidi Appl. Mater. Sci. 202, 1727–1732.

https://doi.org/10.1002/pssa.200520045

Munawar, T., Yasmeen, S., Mukhtar, F., Nadeem, M.S., Mahmood, K., Saqib Saif, M., Hasan, M., Ali, A., Hussain, F., Iqbal, F., 2020. Zn0.9Ce0.05M0.05O (M = Er, Y, V) nanocrystals: Structural and energy bandgap engineering of ZnO for enhancing photocatalytic and antibacterial activity. Ceram. Int. 46, 14369–14383. https://doi.org/10.1016/j.ceramint.2020.02.232

Narayanaswamy Venkatesan, P., Dharmalingam, S., 2015. Effect of cation transport of SPEEK - Rutile TiO2 electrolyte on microbial fuel cell performance. J. Memb. Sci. 492, 518–527. https://doi.org/10.1016/j.memsci.2015.06.025

Narukawa, Y., Ichikawa, M., Sanga, D., Sano, M., Mukai, T., 2010. White light emitting diodes with super-high luminous efficacy. J. Phys. D. Appl. Phys. 43, 354002. https://doi.org/10.1088/0022-3727/43/35/354002

Nasrollahi, N., Ghalamchi, L., Vatanpour, V., Khataee, A., 2021. Photocatalytic-membrane technology: a critical review for membrane fouling mitigation. J. Ind. Eng. Chem. 93, 101–116. https://doi.org/10.1016/j.jiec.2020.09.031

Ng, L.Y., Mohammad, A.W., Leo, C.P., Hilal, N., 2013. Polymeric membranes incorporated with metal/metal oxide nanoparticles: A comprehensive review. Desalination 308, 15–33. https://doi.org/10.1016/j.desal.2010.11.033

Noshirvani, N., Ghanbarzadeh, B., Reza, M., Hashemi, M., Coma, V., 2017. Preparation and characterization of active emulsified films based on chitosan-carboxymethyl cellulose containing zinc oxide nano particles. Int. J. Biol. Macromol. 99, 530–538. https://doi.org/.1037//0033-2909.I26.1.78

Nunes, S.P., Culfaz-Emecen, P.Z., Ramon, G.Z., Visser, T., Koops, G.H., Jin, W., Ulbricht, M., 2020. Thinking the future of membranes: Perspectives for advanced and new membrane materials and manufacturing processes. J. Memb. Sci. 598, 117761. https://doi.org/10.1016/j.memsci.2019.117761

Oliot, Manon, Galier, S., Roux de Balmann, H., Bergel, A., 2016. Ion transport in microbial fuel cells: Key roles, theory and critical review. Appl. Energy 183, 1682–1704. https://doi.org/10.1016/j.apenergy.2016.09.043

Oliot, M., Galier, S., Roux de Balmann, H., Bergel, A., 2016. Ion transport in microbial fuel cells: Key roles, theory and critical review. Appl. Energy 183, 1682–1704.

https://doi.org/10.1016/j.apenergy.2016.09.043

Oturan, M.A., Aaron, J.J., 2014. Advanced oxidation processes in water/wastewater treatment: Principles and applications. A review. Crit. Rev. Environ. Sci. Technol. 44, 2577–2641. https://doi.org/10.1080/10643389.2013.829765

Ou, J., Wang, J., Zhang, D., Zhang, P., Liu, S., Yan, P., Liu, B., Yang, S., 2010. Fabrication and biocompatibility investigation of TiO 2 films on the polymer substrates obtained via a novel and versatile route. Colloids Surfaces B Biointerfaces 76, 123–127. https://doi.org/10.1016/j.colsurfb.2009.10.024

Pardeshi, P.M., Mungray, A.A., 2021. Performance of photopolymerized active layer forward osmosis membrane in the osmotic microbial fuel cell. Environ. Technol. Innov. 23, 101669. https://doi.org/10.1016/j.eti.2021.101669

Park, S.G., Rajesh, P.P., Hwang, M.H., Chu, K.H., Cho, S., Chae, K.J., 2021. Long-term effects of anti-biofouling proton exchange membrane using silver nanoparticles and polydopamine on the performance of microbial electrolysis cells. Int. J. Hydrogen Energy 46, 11345–11356. https://doi.org/10.1016/j.ijhydene.2020.04.059

Pellegrin, M.-L., Greiner, A.D., Aguinaldo, J., Diamond, J., Gluc, S., Burbano, M.S., Arabi, S., Wert, J., McCandless, R., Padhye, L.P., Shoaf, R., 2012. Membrane processes, Water Environment Research. https://doi.org/10.1007/978-3-319-20475-8_1

Peyravi, M., Jahanshahi, M., Rahimpour, A., Javadi, A., Hajavi, S., 2014. Novel thin film nanocomposite membranes incorporated with functionalized TiO2 nanoparticles for organic solvent nanofiltration. Chem. Eng. J. 241, 155–166. https://doi.org/10.1016/j.cej.2013.12.024

Philip, L., Reddy, K.S., Kumar, B., Bhallamudi, S.M., Kannan, A., 2013. Performance evaluation of a solar and wind aided cross-flow evaporator for RO reject management. Desalination 317, 1–10. https://doi.org/10.1016/j.desal.2013.02.008

Potter, M.C., 1911. Electrical Effects Accompanying the Decomposition of Organic Compounds. Proc. R. Soc. B Biol. Sci. 84, 260–276. https://doi.org/10.1098/rspb.1911.0073

Prasannalakshmi, P., Shanmugam, N., 2017. Fabrication of TiO2/ZnO nanocomposites for solar energy driven photocatalysis. Mater. Sci. Semicond. Process. 61, 114–124.

https://doi.org/10.1016/j.mssp.2017.01.008

Prasert, A., Sontikaew, S., Sriprapai, D., Chuangchote, S., 2020. Polypropylene/ZnO Nanocomposites: Mechanical Properties, Photocatalytic Dye Degradation, and Antibacterial Property. Materials (Basel). 13, 914. https://doi.org/10.3390/ma13040914

Qin, M., Ping, Q., Lu, Y., Abu-Reesh, I.M., He, Z., 2015. Understanding electricity generation in osmotic microbial fuel cells through integrated experimental investigation and mathematical modeling. Bioresour. Technol. 195, 194–201. https://doi.org/10.1016/j.biortech.2015.06.013

Rabaey, K., Verstraete, W., 2005. Microbial fuel cells: Novel biotechnology for energy generation. Trends Biotechnol. 23, 291–298. https://doi.org/10.1016/j.tibtech.2005.04.008

Radke, L., Hahn, B., Wagner, D., Sohnle, P., 1994. Effect of abscess fluid supernatants on the kinetics of Candida albicans growth. Clin. Immunol. Immunopathol. 73, 344–349.

Ragab, M., Elawwad, A., Abdel-Halim, H., 2019. Evaluating the performance of Microbial Desalination Cells subjected to different operating temperatures. Desalination 462, 56–66. https://doi.org/10.1016/j.desal.2019.04.008

Raghupathi, K.R., Koodali, R.T., Manna, A.C., 2011. Size-dependent bacterial growth inhibition and mechanism of antibacterial activity of zinc oxide nanoparticles. Langmuir 27, 4020–4028. https://doi.org/10.1021/la104825u

Raizada, P., Singh, P., Kumar, A., Sharma, G., Pare, B., Jonnalagadda, S.B., Thakur, P., 2014. Solar photocatalytic activity of nano-ZnO supported on activatedcarbon or brick grain particles: Role of adsorption in dye degradation. Appl. Catal. A Gen. 486, 159–169. https://doi.org/10.1016/j.apcata.2014.08.043

Rajamanickam, D., Shanthi, M., 2012. Photocatalytic degradation of an organic pollutant, 4-nitrophenol by zinc oxide - UV process. Res. J. Chem. Environ. 9, S1858–S1868.

Rajeshwar, K., Osugi, M.E., Chanmanee, W., Chenthamarakshan, C.R., Zanoni, M.V.B., Kajitvichyanukul, P., Krishnan-Ayer, R., 2008. Heterogeneous photocatalytic treatment of organic dyes in air and aqueous media. J. Photochem. Photobiol. C Photochem. Rev. 9, 171–192. https://doi.org/10.1016/j.jphotochemrev.2008.09.001

Rajh, T., Chen, L.X., Lukas, K., Liu, T., Thurnauer, M.C., Tiede, D.M., 2002. Surface

restructuring of nanoparticles: An efficient route for ligand-metal oxide crosstalk. J. Phys. Chem. B 106, 10543–10552. https://doi.org/10.1021/jp021235v

Ran, J., He, M., Li, W., Cheng, D., Wang, X., 2018. Growing ZnO nanoparticles on polydopamine-templated cotton fabrics for durable antimicrobial activity and UV protection. Polymers (Basel). 10, 495. https://doi.org/10.3390/polym10050495

Rani, M., Shanker, U., 2018. Sun-light driven rapid photocatalytic degradation of methylene blue by poly(methyl methacrylate)/metal oxide nanocomposites. Colloids Surfaces A Physicochem. Eng. Asp. 559, 136–147. https://doi.org/10.1016/j.colsurfa.2018.09.040

Rittmann, B.E., 2008. Opportunities for renewable bioenergy using microorganisms. Biotechnol. Bioeng. 100, 203–212. https://doi.org/10.1002/bit.21875

Rodenstein, M., Zürcher, S., Tosatti, S.G.P., Spencer, N.D., 2010. Fabricating chemical gradients on oxide surfaces by means of fluorinated, catechol-based, self-assembled monolayers. Langmuir 26, 16211–16220. https://doi.org/10.1021/la100805z

Ryou, M.H., Lee, D.J., Lee, J.N., Lee, Y.M., Park, J.K., Choi, J.W., 2012. Excellent cycle life of lithium-metal anodes in lithium-ion batteries with mussel-inspired polydopamine-coated separators. Adv. Energy Mater. 2, 645–650. https://doi.org/10.1002/aenm.201100687

Sakai, H., Nakagawa, T., Tokita, Y., Hatazawa, T., Ikeda, T., Tsujimura, S., Kano, K., 2009. A high-power glucose/oxygen biofuel cell operating under quiescent conditions. Energy Environ. Sci. 2, 133–138. https://doi.org/10.1039/b809841g

Saleh, T.A., Gupta, V.K., 2016. Membrane Fouling and Strategies for Cleaning and Fouling Control, in: Nanomaterial and Polymer Membranes. Elsevier, Amsterdam - Netherlands, pp. 25–53. https://doi.org/10.1016/b978-0-12-804703-3.00002-4

Santoro, C., Abad, F.B., Serov, A., Kodali, M., Howe, K.J., Soavi, F., Atanassov, P., 2017. Supercapacitive microbial desalination cells: New class of power generating devices for reduction of salinity content. Appl. Energy 208, 25–36. https://doi.org/10.1016/j.apenergy.2017.10.056

Saratale, G.D., Saratale, R.G., Shahid, M.K., Zhen, G., Kumar, G., Shin, H.S., Choi, Y.G., Kim, S.H., 2017. A comprehensive overview on electro-active biofilms, role of exo-electrogens and their microbial niches in microbial fuel cells (MFCs). Chemosphere

178, 534–547. https://doi.org/10.1016/j.chemosphere.2017.03.066

Sathe, P., Myint, M.T.Z., Dobretsov, S., Dutta, J., 2016. Removal and regrowth inhibition of microalgae using visible light photocatalysis with ZnO nanorods: A green technology. Sep. Purif. Technol. 162, 61–67. https://doi.org/10.1016/j.seppur.2016.02.007

Saxena, V., Pandey, L.M., 2019. Synthesis, characterization and antibacterial activity of aluminum doped zinc oxide. Mater. Today Proc. 18, 1388–1400. https://doi.org/10.1016/j.matpr.2019.06.605

Schneider, J., Matsuoka, M., Takeuchi, M., Zhang, J., Horiuchi, Y., Anpo, M., Bahnemann, D.W., 2014. Understanding TiO2photocatalysis: Mechanisms and materials. Chem. Rev. 114, 9919–9986. https://doi.org/10.1021/cr5001892

Senthilraja, A., Krishnakumar, B., Hariharan, R., Sobral, A.J.F.N., Surya, C., John, N.A.A., Shanthi, M., 2018. Synthesis and characterization of bimetallic nanocomposite and its photocatalytic, antifungal and antibacterial activity. Sep. Purif. Technol. 202, 373–384. https://doi.org/10.1016/j.seppur.2018.04.015

Shabani, Z., Zarghami, S., Mohammadi, T., 2020. Nanomaterials for fouling-resistant RO membranes, Nanotechnology in the Beverage Industry. Elsevier Inc. https://doi.org/10.1016/b978-0-12-819941-1.00006-7

Sirelkhatim, A., Mahmud, S., Seeni, A., Kaus, N.H.M., Ann, L.C., Bakhori, S.K.M., Hasan, H., Mohamad, D., 2015. Review on zinc oxide nanoparticles: Antibacterial activity and toxicity mechanism. Nano-Micro Lett. 7, 219–242. https://doi.org/10.1007/s40820-015-0040-x

Slokar, Y.M., Majcen Le Marechal, A., 1998. Methods of decoloration of textile wastewaters. Dye. Pigment. 37, 335–356. https://doi.org/10.1016/S0143-7208(97)00075-2

Solanki, K., Subramanian, S., Basu, S., 2013a. Microbial fuel cells for azo dye treatment with electricity generation: A review. Bioresour. Technol. 131, 564–571. https://doi.org/10.1016/j.biortech.2012.12.063

Solanki, K., Subramanian, S., Basu, S., 2013b. Microbial fuel cells for azo dye treatment with electricity generation: A review. Bioresour. Technol. 131, 564–571. https://doi.org/10.1016/j.biortech.2012.12.063

Soleymani Lashkenari, A., Hamed Mosavian, M.T., Peyravi, M., Jahanshahi, M., 2019. Biofouling mitigation of bilayer polysulfone membrane assisted by zinc oxide-polyrhodanine couple nanoparticle. Prog. Org. Coatings 129, 147–158. https://doi.org/10.1016/j.porgcoat.2018.12.012

Soltani, T., Entezari, M.H., 2013. Photolysis and photocatalysis of methylene blue by ferrite bismuth nanoparticles under sunlight irradiation. J. Mol. Catal. A Chem. 377, 197–203. https://doi.org/10.1016/j.molcata.2013.05.004

Soria, R.B., Chinchin, B.D., Arboleda, D., Zhao, Y., Bonilla, P., Van der Bruggen, B., Luis, P., 2021. Effect of the bio-inspired modification of low-cost membranes with TiO2:ZnO as microbial fuel cell membranes. Chemosphere 132840. https://doi.org/10.1016/j.chemosphere.2021.132840

Sotto, A., Boromand, A., Zhang, R., Luis, P., Arsuaga, J.M., Kim, J., Van der Bruggen, B., 2011. Effect of nanoparticle aggregation at low concentrations of TiO 2 on the hydrophilicity, morphology, and fouling resistance of PES-TiO 2 membranes. J. Colloid Interface Sci. 363, 540–550. https://doi.org/10.1016/j.jcis.2011.07.089

Štrbac, D., Aggelopoulos, C.A., Štrbac, G., Dimitropoulos, M., Novaković, M., Ivetić, T., Yannopoulos, S.N., 2018. Photocatalytic degradation of Naproxen and methylene blue: Comparison between ZnO, TiO2 and their mixture. Process Saf. Environ. Prot. 113, 174–183. https://doi.org/10.1016/j.psep.2017.10.007

Sugarman, B., 1983. Zinc and infection. Rev. Infect. Dis. 5, 137–147. https://doi.org/10.1093/clinids/5.1.137

Sun, M., Mu, Z.X., Sheng, G.P., Shen, N., Tong, Z.H., Wang, H.L., Yu, H.Q., 2010. Hydrogen production from propionate in a biocatalyzed system with in-situ utilization of the electricity generated from a microbial fuel cell. Int. Biodeterior. Biodegrad. 64, 378–382. https://doi.org/10.1016/j.ibiod.2010.04.004

Suresh, R., Rajendran, S., Kumar, P.S., Dutta, K., Vo, D.V.N., 2022. Current advances in microbial fuel cell technology toward removal of organic contaminants – A review. Chemosphere 287, 132186. https://doi.org/10.1016/j.chemosphere.2021.132186

Susanto, H., Robbani, M.H., Istirokhatun, T., Firmansyah, A.A., Rhamadhan, R.N., 2020. Preparation of low-fouling polyethersulfone ultrafiltration membranes by incorporating high-molecular-weight chitosan with the help of a surfactant. South

African J. Chem. Eng. 33, 133–140. https://doi.org/10.1016/j.sajce.2020.07.003

Suzuki, M., Suzuki, Y., Uzuka, K., Kawase, Y., 2020. Biological treatment of non-biodegradable azo-dye enhanced by zero-valent iron (ZVI) pre-treatment. Chemosphere 259, 12470. https://doi.org/10.1016/j.chemosphere.2020.127470

Talebian, N., Matin, S., Doudi, M., 2013. Journal of Photochemistry and Photobiology B : Biology Controllable synthesis of ZnO nanoparticles and their morphology-dependent antibacterial and optical properties 120, 66–73.

Tang, C.Y., Zhao, Y., Wang, R., Hélix-Nielsen, C., Fane, A.G., 2013. Desalination by biomimetic aquaporin membranes: Review of status and prospects. Desalination 308, 34–40. https://doi.org/10.1016/j.desal.2012.07.007

Tang, Y., Lin, Y., Ford, D.M., Qian, X., Cervellere, M.R., Millett, P.C., Wang, X., 2021. A review on models and simulations of membrane formation via phase inversion processes. J. Memb. Sci. 640, 119810. https://doi.org/10.1016/j.memsci.2021.119810

Tekin, D., Kiziltas, H., Ungan, H., 2020. Kinetic evaluation of ZnO/TiO2 thin film photocatalyst in photocatalytic degradation of Orange G. J. Mol. Liq. 306. https://doi.org/10.1016/j.molliq.2020.112905

Tian, J., Chen, L., Yin, Y., Wang, X., Dai, J., Zhu, Z., Liu, X., Wu, P., 2009. Photocatalyst of TiO2/ZnO nano composite film: Preparation, characterization, and photodegradation activity of methyl orange. Surf. Coatings Technol. 204, 205–214. https://doi.org/10.1016/j.surfcoat.2009.07.008

Tobajas, M., Belver, C., Rodriguez, J.J., 2017. Degradation of emerging pollutants in water under solar irradiation using novel TiO2-ZnO/clay nanoarchitectures. Chem. Eng. J. 309, 596–606. https://doi.org/10.1016/j.cej.2016.10.002

Tomé, L.C., Gonalves, C.M.B., Boaventura, M., Brandão, L., Mendes, A.M., Silvestre, A.J.D., Neto, C.P., Gandini, A., Freire, C.S.R., Marrucho, I.M., 2011. Preparation and evaluation of the barrier properties of cellophane membranes modified with fatty acids. Carbohydr. Polym. 83, 836–842. https://doi.org/10.1016/j.carbpol.2010.08.060

Torres, C.I., Krajmalnik-Brown, R., Parameswaran, P., Marcus, A.K., Wanger, G., Gorby, Y.A., Rittmann, B.E., 2009. Selecting anode-respiring bacteria based on anode potential: Phylogenetic, electrochemical, and microscopic characterization. Environ. Sci. Technol. 43, 9519–9524. https://doi.org/10.1021/es902165y

Trzaskus, K.W., Lee, S.L., de Vos, W.M., Kemperman, A., Nijmeijer, K., 2017. Fouling behavior of silica nanoparticle-surfactant mixtures during constant flux dead-end ultrafiltration. J. Colloid Interface Sci. 506, 308–318. https://doi.org/10.1016/j.jcis.2017.07.043

Vakili, M.R., Gholami, M., Mosallaei, Z., Ghasemi, A.M., 2020. Modification of regenerated cellulose membrane by impregnation of silver nanocrystal clusters. J. Appl. Polym. Sci. 137, 1–9. https://doi.org/10.1002/app.48292

Van Der Bruggen, B., Koninckx, A., Vandecasteele, C., 2004. Separation of monovalent and divalent ions from aqueous solution by electrodialysis and nanofiltration. Water Res. 38, 1347–1353. https://doi.org/10.1016/j.watres.2003.11.008

Vaselbehagh, M., Karkhanechi, H., Mulyati, S., Takagi, R., Matsuyama, H., 2014. Improved antifouling of anion-exchange membrane by polydopamine coating in electrodialysis process. Desalination 332, 126–133. https://doi.org/10.1016/j.desal.2013.10.031

Viezbicke, B.D., Patel, S., Davis, B.E., Birnie, D.P., 2015. Evaluation of the Tauc method for optical absorption edge determination: ZnO thin films as a model system. Phys. Status Solidi Basic Res. 252, 1700–1710. https://doi.org/10.1002/pssb.201552007

Vrijenhoek, E.M., Hong, S., Elimelech, M., 2001. Influence of membrane properties, solution chemistry, and hydrodynamics on colloidal fouling of reverse osmosis and nanofiltration membranes. J. Memb. Sci. 188, 115–128.

Wang, J., Xie, Y., Zhang, Z., Li, J., Chen, X., Zhang, L., 2009. Solar Energy Materials & Solar Cells Photocatalytic degradation of organic dyes with Er 3 + : YAlO 3 / ZnO composite under solar light 93, 355–361. https://doi.org/10.1016/j.solmat.2008.11.017

Wang, P., Wang, F., Jiang, H., Zhang, Y., Zhao, M., Xiong, R., Ma, J., 2020. Strong improvement of nanofiltration performance on micropollutant removal and reduction of membrane fouling by hydrolyzed-aluminum nanoparticles. Water Res. 175, 115649. https://doi.org/10.1016/j.watres.2020.115649

Wang, Q., Huang, L., Quan, X., Li Puma, G., 2019. Sequential anaerobic and electro-Fenton processes mediated by W and Mo oxides for degradation/mineralization of azo dye methyl orange in photo assisted microbial fuel cells. Appl. Catal. B Environ. 245, 672–680. https://doi.org/10.1016/j.apcatb.2019.01.026

Wang, X., Chen, G.Q., Zhang, W., Deng, H., 2019. Surface-modified anion exchange membranes with self-cleaning ability and enhanced antifouling properties. J. Taiwan Inst. Chem. Eng. 105, 8–16. https://doi.org/10.1016/j.jtice.2019.09.026

Wang, Y.K., Sheng, G.P., Li, W.W., Huang, Y.X., Yu, Y.Y., Zeng, R.J., Yu, H.Q., 2011. Development of a novel bioelectrochemical membrane reactor for wastewater treatment. Environ. Sci. Technol. 45, 9256–9261. https://doi.org/10.1021/es2019803

Wang, Y.P., Liu, X.W., Li, W.W., Li, F., Wang, Y.K., Sheng, G.P., Zeng, R.J., Yu, H.Q., 2012. A microbial fuel cell-membrane bioreactor integrated system for cost-effective wastewater treatment. Appl. Energy 98, 230–235. https://doi.org/10.1016/j.apenergy.2012.03.029

Wang, Z., Lim, B., 2017a. Mixed cellulose ester filter as a separator for air-diffusion cathode microbial fuel cells. Environ. Technol. (United Kingdom) 38, 979–984. https://doi.org/10.1080/09593330.2016.1215353

Wang, Z., Lim, B., 2017b. Mixed cellulose ester filter as a separator for air-diffusion cathode microbial fuel cells. Environ. Technol. (United Kingdom) 38, 979–984. https://doi.org/10.1080/09593330.2016.1215353

Wang, Z.X., Lau, C.H., Zhang, N.Q., Bai, Y.P., Shao, L., 2015. Mussel-inspired tailoring of membrane wettability for harsh water treatment. J. Mater. Chem. A 3, 2650–2657. https://doi.org/10.1039/c4ta05970k

Watanabe, T., Nakajima, A., Wang, R., Minabe, M., Koizumi, S., Fujishima, A., Hashimoto, K., 1999. Photocatalytic activity and photoinduced hydrophilicity of titanium dioxide coated glass. Thin Solid Films 351, 260–263. https://doi.org/10.1016/s0040-6090(99)00205-9

Wei, Y., Kong, J., Yang, L., Ke, L., Tan, H.R., Liu, H., Huang, Y., Sun, X.W., Lu, X., Du, H., 2013. Polydopamine-assisted decoration of ZnO nanorods with Ag nanoparticles: An improved photoelectrochemical anode. J. Mater. Chem. A 1, 5045–5052. https://doi.org/10.1039/c3ta10499k

Weldegebrieal, G.K., 2020. Synthesis method, antibacterial and photocatalytic activity of ZnO nanoparticles for azo dyes in wastewater treatment: A review. Inorg. Chem. Commun. 120. https://doi.org/10.1016/j.inoche.2020.108140

Werber, J.R., Osuji, C.O., Elimelech, M., 2016. Materials for next-generation desalination

and water purification membranes. Nat. Rev. Mater. 1. https://doi.org/10.1038/natrevmats.2016.18

Wu, L., Dong, Z., Cai, Z., Ganapathy, T., Fang, N.X., Li, C., Yu, C., Zhang, Y., Song, Y., 2020. Highly efficient three-dimensional solar evaporator for high salinity desalination by localized crystallization. Nat. Commun. 11, 1–12. https://doi.org/10.1038/s41467-020-14366-1

Wu, L.C., Chen, C.Y., Lin, T.K., Su, Y.Y., Chung, Y.C., 2020. Highly efficient removal of victoria blue R and bioelectricity generation from textile wastewater using a novel combined dual microbial fuel cell system. Chemosphere 258, 127326. https://doi.org/10.1016/j.chemosphere.2020.127326

Wu, T.F., Hong, J.D., 2015. Dopamine-melanin nanofilms for biomimetic structural coloration. Biomacromolecules 16, 660–666. https://doi.org/10.1021/bm501773c

Xiang, Y., Liu, F., Xue, L., 2015. Under seawater superoleophobic PVDF membrane inspired by polydopamine for efficient oil/seawater separation, Journal of Membrane Science. Elsevier. https://doi.org/10.1016/j.memsci.2014.11.052

Xie, Y., Ren, L., Zhu, X., Gou, X., Chen, S., 2018. Physical and chemical treatments for removal of perchlorate from water–A review. Process Saf. Environ. Prot. 116, 180–198. https://doi.org/10.1016/j.psep.2018.02.009

Xu, A.W., Gao, Y., Liu, H.Q., 2002. The preparation, characterization, and their photocatalytic activities of rare-earth-doped TiO2 nanoparticles. J. Catal. 207, 151–157. https://doi.org/10.1006/jcat.2002.3539

Xu, J., Sheng, G.P., Luo, H.W., Li, W.W., Wang, L.F., Yu, H.Q., 2012a. Fouling of proton exchange membrane (PEM) deteriorates the performance of microbial fuel cell. Water Res. 46, 1817–1824. https://doi.org/10.1016/j.watres.2011.12.060

Xu, J., Sheng, G.P., Luo, H.W., Li, W.W., Wang, L.F., Yu, H.Q., 2012b. Fouling of proton exchange membrane (PEM) deteriorates the performance of microbial fuel cell. Water Res. 46, 1817–1824. https://doi.org/10.1016/j.watres.2011.12.060

Xue, W., He, Y., Yumunthama, S., Udomkittayachai, N., Hu, Y., Tabucanon, A.S., Zhang, X., Kurniawan, T.A., 2021. Membrane cleaning and performance insight of osmotic microbial fuel cell. Chemosphere 285, 131549. https://doi.org/10.1016/j.chemosphere.2021.131549

Yalcinkaya, F., Lubasova, D., 2017a. Quantitative evaluation of antibacterial activities of nanoparticles (ZnO, TiO2, ZnO/TiO2, SnO2, CuO, ZrO2, and AgNO3) incorporated into polyvinyl butyral nanofibers. Polym. Adv. Technol. 28, 137–140. https://doi.org/10.1002/pat.3883

Yalcinkaya, F., Lubasova, D., 2017b. Quantitative evaluation of antibacterial activities of nanoparticles (ZnO, TiO2, ZnO/TiO2, SnO2, CuO, ZrO2, and AgNO3) incorporated into polyvinyl butyral nanofibers. Polym. Adv. Technol. 28, 137–140. https://doi.org/10.1002/pat.3883

Yan, Z., Zhang, Y., Yang, H., Fan, G., Ding, A., Liang, H., Li, G., Ren, N., Van der Bruggen, B., 2020. Mussel-inspired polydopamine modification of polymeric membranes for the application of water and wastewater treatment: A review. Chem. Eng. Res. Des. 157, 195–214. https://doi.org/10.1016/j.cherd.2020.03.011

Yang, E., Chae, K.-J., Kim, I.S., 2016a. Comparison of different semipermeable membranes for power generation and water flux in osmotic microbial fuel cells. J chem technol Biotechnol 91, 2305–2312. https://doi.org/10.1002/jctb.4817

Yang, E., Chae, K.J., Alayande, A.B., Kim, K.Y., Kim, I.S., 2016b. Concurrent performance improvement and biofouling mitigation in osmotic microbial fuel cells using a silver nanoparticle-polydopamine coated forward osmosis membrane. J. Memb. Sci. 513, 217–225. https://doi.org/10.1016/j.memsci.2016.04.028

Yang, E., Chae, K.J., Choi, M.J., He, Z., Kim, I.S., 2019. Critical review of bioelectrochemical systems integrated with membrane-based technologies for desalination, energy self-sufficiency, and high-efficiency water and wastewater treatment. Desalination 452, 40–67. https://doi.org/10.1016/j.desal.2018.11.007

Yang, E., Chae, K.J., Kim, I.S., 2016c. Comparison of different semipermeable membranes for power generation and water flux in osmotic microbial fuel cells. J. Chem. Technol. Biotechnol. 91, 2305–2312. https://doi.org/10.1002/jctb.4817

Yang, H.C., Liao, K.J., Huang, H., Wu, Q.Y., Wan, L.S., Xu, Z.K., 2014. Mussel-inspired modification of a polymer membrane for ultra-high water permeability and oil-in-water emulsion separation. J. Mater. Chem. A 2, 10225. https://doi.org/10.1039/c4ta00143e

Yang, Y., Qin, M., Yang, X., He, Z., 2017. Sustainable operation of osmotic microbial fuel

cells through effective reproduction of polyelectrolyte draw solutes facilitated by cathodic pH increase. J. Clean. Prod. 168, 1143–1149. https://doi.org/10.1016/j.jclepro.2017.09.107

Yang, Z., Wu, Y., Wang, J., Cao, B., Tang, C.Y., 2016. In situ reduction of silver by polydopamine: A novel antimicrobial modification of a thin-film composite polyamide membrane. Environ. Sci. Technol. 50, 9543–9550. https://doi.org/10.1021/acs.est.6b01867

Ye, Q., Zhou, F., Liu, W., 2011. Bioinspired catecholic chemistry for surface modification. Chem. Soc. Rev. 40, 4244–4258. https://doi.org/10.1039/c1cs15026j

Yoon, J., Oh, S.-G., 2021. Synthesis of amine modified ZnO nanoparticles and their photocatalytic activities in micellar solutions under UV irradiation. J. Ind. Eng. Chem. 96, 390–396. https://doi.org/10.1016/j.jiec.2021.01.043

Yu, B., Liu, J., Liu, S., Zhou, F., 2010. Pdop layer exhibiting zwitterionicity: A simple electrochemical interface for governing ion permeability. Chem. Commun. 46, 5900–5902. https://doi.org/10.1039/c0cc00596g

Yun, S.H., Ingole, P.G., Kim, K.H., Choi, W.K., Kim, J.H., Lee, H.K., 2014. Properties and performances of polymer composite membranes correlated with monomer and polydopamine for flue gas dehydration by water vapor permeation. Chem. Eng. J. 258, 348–356. https://doi.org/10.1016/j.cej.2014.07.038

Zangeneh, H., Akbar, A., Zinadini, S., Feyzi, M., Bahnemann, D.W., 2018. A novel photocatalytic self-cleaning PES nano fi ltration membrane incorporating triple metal-nonmetal doped TiO 2 (K-B-N-TiO 2) for post treatment of biologically treated palm oil mill e ffl uent. React. Funct. Polym. 127, 139–152.

Zangmeister, R.A., Morris, T.A., Tarlov, M.J., 2013. Characterization of polydopamine thin films deposited at short times by autoxidation of dopamine. Langmuir 29, 8619–8628. https://doi.org/10.1021/la400587j

Zhang, C., Li, H.N., Du, Y., Ma, M.Q., Xu, Z.K., 2017. CuSO4/H2O2-Triggered Polydopamine/Poly(sulfobetaine methacrylate) Coatings for Antifouling Membrane Surfaces. Langmuir 33, 1210–1216. https://doi.org/10.1021/acs.langmuir.6b03948

Zhang, L., Jia, H., Wang, J., Wen, H., Li, J., 2020. Characterization of fouling and concentration polarization in ion exchange membrane by in-situ electrochemical

impedance spectroscopy. J. Memb. Sci. 594, 117443. https://doi.org/10.1016/j.memsci.2019.117443

Zhang, L., Jiang, Y., Ding, Y., Povey, M., York, D., 2007. Investigation into the antibacterial behaviour of suspensions of ZnO nanoparticles (ZnO nanofluids). J. Nanoparticle Res. 9, 479–489. https://doi.org/10.1007/s11051-006-9150-1

Zhang, Q., Hu, J., Lee, D., 2016. Bioresource Technology Microbial fuel cells as pollutant treatment units : Research updates. Bioresour. Technol. 217, 121–128. https://doi.org/10.1016/j.biortech.2016.02.006

Zhang, R.-X., Braeken, L., Liu, T., Luis, P., Wang, X.-L., Van der Bruggen, B., 2017. Remarkable Anti-Fouling performance of TiO2-modified TFC membranes with mussel-inspired polydopamine binding. Appl. Sci. 7, 81.

Zhang, R., Liu, Y., He, M., Su, Y., Zhao, X., Elimelech, M., Jiang, Z., 2016. Antifouling membranes for sustainable water purification: Strategies and mechanisms. Chem. Soc. Rev. https://doi.org/10.1039/c5cs00579e

Zhang, R.X., Braeken, L., Luis, P., Wang, X.L., Van der Bruggen, B., 2013. Novel binding procedure of TiO2 nanoparticles to thin film composite membranes via self-polymerized polydopamine. J. Memb. Sci. 437, 179–188. https://doi.org/10.1016/j.memsci.2013.02.059

Zhang, T.C., Surampalli, R.Y., Vigneswaran, S., Ong, S.L., Kao, C.M., 2012. Membrane Technology and Environmental Aplications. American Society of Civil Engineers, Reston, VA.

Zhang, W., Rittmann, B., Chen, Y., 2011. Size effects on adsorption of hematite nanoparticles on E. coli cells. Environ. Sci. Technol. 45, 2172–2178. https://doi.org/10.1021/es103376y

Zhang, X., Chen, Y., Zhang, S., Qiu, C., 2017. High photocatalytic performance of high concentration Al-doped ZnO nanoparticles. Sep. Purif. Technol. 172, 236–241. https://doi.org/10.1016/j.seppur.2016.08.016

Zhang, X., Cheng, S., Wang, X., Huang, X., Logan, B.E., 2009. Separator characteristics for increasing performance of microbial fuel cells. Environ. Sci. Technol. 43, 8456–8461. https://doi.org/10.1021/es901631p

Zhang, X., Dong, S., Zhou, X., Yan, L., Chen, G., Zhou, D., 2015. A facile one-pot

synthesis of Er-Al co-doped ZnO nanoparticles with enhanced photocatalytic performance under visible light. Mater. Lett. 143, 312–314. https://doi.org/10.1016/j.matlet.2014.12.094

Zhao, C.E., Gai, P., Song, R., Chen, Y., Zhang, J., Zhu, J.J., 2017. Nanostructured material-based biofuel cells: Recent advances and future prospects. Chem. Soc. Rev. 46, 1545–1564. https://doi.org/10.1039/c6cs00044d

Zhao, G., Lyu, X., Lee, J., Cui, X., Chen, W.N., 2019. Biodegradable and transparent cellulose film prepared eco-friendly from durian rind for packaging application. Food Packag. Shelf Life 21, 100345. https://doi.org/10.1016/j.fpsl.2019.100345

Zhao, Q., Yu, H., Zhang, W., Kabutey, F.T., Jiang, J., Zhang, Y., Wang, K., Ding, J., 2017. Microbial fuel cell with high content solid wastes as substrates: a review. Front. Environ. Sci. Eng. 11. https://doi.org/10.1007/s11783-017-0918-6

Zhao, X., Su, Y., Liu, Y., Zhang, R., Jiang, Z., 2015. Multiple antifouling capacities of hybrid membranes derived from multifunctional titania nanoparticles. J. Memb. Sci. 495, 226–234. https://doi.org/10.1016/j.memsci.2015.08.026

Zhao, X., Zhang, R., Liu, Y., He, M., Su, Y., Gao, C., Jiang, Z., 2018. Antifouling membrane surface construction: Chemistry plays a critical role. J. Memb. Sci. 551, 145–171. https://doi.org/10.1016/j.memsci.2018.01.039

Zhao, Y., Gao, C., Van Der Bruggen, B., 2019. Technology-driven layer-by-layer assembly of a membrane for selective separation of monovalent anions and antifouling. Nanoscale 11, 2264–2274. https://doi.org/10.1039/c8nr09086f

Zhao, Y., Liu, Y., Wang, C., Ortega, E., Wang, X., Xie, Y.F., Shen, J., Gao, C., Van Der Bruggen, B., 2020. Electric field-based ionic control of selective separation layers. J. Mater. Chem. A 8, 4244–4251. https://doi.org/10.1039/c9ta13247c

Zhao, Y., Zhu, J., Li, J., Zhao, Z., Charchalac Ochoa, S.I., Shen, J., Gao, C., Van Der Bruggen, B., 2018. Robust Multilayer Graphene-Organic Frameworks for Selective Separation of Monovalent Anions. ACS Appl. Mater. Interfaces 10, 18426–18433. https://doi.org/10.1021/acsami.8b03839

Zhu, H., Jiang, R., Fu, Y., Guan, Y., Yao, J., Xiao, L., Zeng, G., 2012. Effective photocatalytic decolorization of methyl orange utilizing TiO 2/ZnO/chitosan nanocomposite films under simulated solar irradiation. Desalination 286, 41–48.

https://doi.org/10.1016/j.desal.2011.10.036

Zhu, J., Tilahun, M., Wang, J., Uliana, A., Tian, M., Yuan, S., Li, J., Zhang, Y., Volodin, A., Bruggen, B. Van Der, 2018a. A rapid deposition of polydopamine coatings induced by iron (III) chloride / hydrogen peroxide for loose nanofiltration. J. Colloid Interface Sci. 523, 86–97. https://doi.org/10.1016/j.jcis.2018.03.072

Zhu, J., Uliana, A., Wang, J., Yuan, S., Li, J., Tian, M., Simoens, K., Volodin, A., Lin, J., Bernaerts, K., Zhang, Y., Van Der Bruggen, B., 2016. Elevated salt transport of antimicrobial loose nanofiltration membranes enabled by copper nanoparticles: Via fast bioinspired deposition. J. Mater. Chem. A 4, 13211–13222. https://doi.org/10.1039/c6ta05661j

Zhu, J., Yuan, S., Uliana, A., Hou, J., Li, J., Li, X., Tian, M., Chen, Y., Volodin, A., Bruggen, B. Van Der, 2018b. High- flux thin film composite membranes for nano filtration mediated by a rapid co-deposition of polydopamine / piperazine. J. Memb. Sci. 554, 97–108. https://doi.org/https://doi.org/10.1016/j.memsci.2018.03.004

Zhu, J., Yuan, S., Uliana, A., Hou, J., Li, J., Li, X., Tian, M., Chen, Y., Volodin, A., der Bruggen, B. Van, 2018c. High-flux thin film composite membranes for nanofiltration mediated by a rapid co-deposition of polydopamine/piperazine. J. Memb. Sci. 554, 97–108. https://doi.org/10.1016/j.memsci.2018.03.004

Zhu, J., Yuan, S., Wang, J., Zhang, Y., Tian, M., Van der Bruggen, B., 2020. Microporous organic polymer-based membranes for ultrafast molecular separations. Prog. Polym. Sci. 110, 101308. https://doi.org/10.1016/j.progpolymsci.2020.101308

Zhu, X.-Z., Zhang, F., Li, W.-W., Liu, H.-Q., Wang, Y.-K., Huang, M.-S., 2015. Forward osmosis membrane favors an improved proton flux and electricity generation in microbial fuel cells. Desalination 372, 26–31. https://doi.org/10.1016/j.desal.2015.06.011

Zhu, X.Z., Zhang, F., Li, W.W., Li, J., Li, L.L., Yu, H.Q., Huang, M.S., Huang, T.Y., 2016a. Insights into enhanced current generation of an osmotic microbial fuel cell under membrane fouling condition. J. Memb. Sci. 504, 40–46. https://doi.org/10.1016/j.memsci.2015.12.050

Zhu, X.Z., Zhang, F., Li, W.W., Li, J., Li, L.L., Yu, H.Q., Huang, M.S., Huang, T.Y., 2016b. Insights into enhanced current generation of an osmotic microbial fuel cell

under membrane fouling condition. J. Memb. Sci. 504, 40–46.
https://doi.org/10.1016/j.memsci.2015.12.050

Curriculum Vitae (with publication list)

Raúl Bahamonde Soria

PERSONAL INFORMATION

Date of Birth: July 12th, 1984
Nationality: Ecuadorian

CONTACT

Université catholique de Louvain, Belgium
SST/IMMC - Institute of Mechanics, Materials and Civil Engineering (iMMC)
IMAP - Materials and process engineering (IMAP)
Place Sainte Barbe 2, 1348 Louvain-la-Neuve, Belgium

Universidad Central del Ecuador,
Renewable Energy Laboratory, Chemical Sciences Faculty.
Quito 170129, Ecuador
E-mail : r.bahamonde@uclouvain.be; rabahamonde@uce.edu.ec
Tel: +593 992707137

EDUCATION

February. 2018 – 2022 PhD candidate in Science of Engineering and Technology
Université catholique de Louvain, Belgium

Sept. 2008 – Sept. 2010 Master of Chemistry Science
Universidad Autónoma de México

Sept 2002 – Sept. 2007 Chemist
Central University of Ecuador

LIST OF PUBLICATIONS

Approved review chapter book. 01/07/2021.**Raúl Bahamonde Soria**, Luis Patricia. Chapter 9. Current Trends and Future Developments on (Bio-) Membranes: Membrane technologies in Environmental Protection and Public Health, Elsevier, Chapter 9, Antifouling membranes for polluted solvents treatments,

Raúl Bahamonde Soria, Junyong Zhu, IrmaGonza, BartVan der Bruggen and Patricia Luis. Effect of (TiO2: ZnO) ratio on the anti-fouling properties of bio-inspired nanofiltration membranes. *Separation and Purification Technology,* 251, (2020), 117280

Raúl Bahamonde Soria, Billy Daniel Chinchin, Daniel Arboleda, Yan Zhao, Pablo Bonilla Bart Van der Bruggen and Patricia Luis. Effect of the bio-inspired modification of low-cost membranes with TiO2:ZnO as microbial fuel cell membranes, *Chemosphere,* 291, (2022), 132840.

Yi Li, Jian Li, **Raul Bahamonde Soria**, Alexander Volodine, Bart Van der Bruggen. Aramid nanofiber and modified ZIF-8 constructed porous nanocomposite membrane for organic solvent nanofiltration. *Journal of Membrane Science.* 603 (2020) 118002.

Mar Garcia Alvarez, Vida Sang Sefidi, Marine Beguin, Alexandre Collet, **Raul Bahamonde Soria** and Patricia Luis. Osmotic Membrane Distillation Crystallization of $NaHCO_3$. *Energies* 2022.

Submitted research paper

Research paper in preparation: **Raúl Bahamonde Soria,** Jefferson Estupiñan, Irma Gonza, Monserrat Naranjo, Billy Chinchina, Patricia Luis. Research paper submitted on 03/11/2021 to Industrial & Engineering Chemistry Research Journal. Effect of Er, Al and Er/Al dopants on the photocatalytic and antibacterial properties of ZnO nanoparticles.

Research paper in preparation: **Raúl Bahamonde Soria** and Patricia Luis. Influence of Er-Al-ZnO photocatalyst in the antifouling performance of new nanofiltration Microbial fuel cells.

INTERNATIONAL CONFERENCES

Raúl Bahamonde, Patricia Luis, Magnetic field in MFC, Green Win Chemistry 2018, July 23rd – 24th, 2018, Louvain la Neuve - Belgium. (Poster presentation)

Raúl Bahamonde, Patricia Luis, Influence of different photocatalytic dopants in the antifouling performance of a new generation of MFC membranes, MELPRO 2018, May 13th – 16th, 2018, Prague -Czech Republic (Oral presentation)

Raúl Bahamonde, Bart Van der Bruggen, Patricia Luis; Different photocatalytic dopants (ZnO/TiO2) in nanofiltration membrane antifouling. V Latin American Congress of Students of Chemistry. November 21st 2018, Quito-Ecuador. (Oral presentation)

Raúl Bahamonde, Bart Van der Bruggen, Patricia Luis, Effect of different photocatalytic dopants in bioinspired antifouling membranes for NF-MFC, 4th Green and Sustainable Chemistry Conference 2019, May 5th – 8th, Dresden Germany. (Poster presentation)

Raúl Bahamonde, Patricia Luis, Different photocatalytic (Vis) Er/Al doped ZnO in a new generation of NF-MFC in antifouling membranes, ANQUE 2019, Juny 19th – 21st, Santander - Spain. (Oral presentation)

Raúl Bahamonde, Patricia Luis, Influence of different photocatalytic dopants in the antifouling performance of Nanofiltration Microbial fuel cells, UE-ISMET 2021, Sep 13th – 15th, Girona- Spain. (Oral presentation)

Raúl Bahamonde, Billy Chinchin, Patricia Luis, TiO_2:ZnO-modified low-cost membranes with mussel-inspired polydopamine binding as microbial fuel cell membranes, Euromembrane 2021, Nov 28th – dec 2nd, Copenhagen- Denmark. (Poster presentation)